SAPIENZA
UNIVERSITÀ DI ROMA

Department of Drug Chemistry and Technologies

# NEW PYRROLE AND PYRAZOLE BASED COMPOUNDS ACTIVE AS ANTI-INFLAMMATORY AND ANTIMALARIAL DRUGS

XXXV Cycle

PhD program in "Molecular design and characterization for the promotion of health and well-being: from drug to food"

Supervisor:

Prof. Giovanna Poce

PhD candidate:

Federico Appetecchia

Director of PhD program:

Luisa Mannina

# ABSTRACT

This thesis addresses the urgent requirement for novel anti-inflammatory drugs and antimalarial interventions:

The beneficial effects of carbon monoxide (CO) gained much interest in research and offer new potential treatments of vascular- and inflammatory-related diseases. However, the medical application of this gas has been hampered by the complexity of the administration route. This problem has been overcome with the discovery of CO-releasing molecules (CORMs), which are an effective tool to deliver CO safely and precisely to the target locations. Particularly, metal-based CORMs are emerging for their striking anti-inflammatory properties that are amplified by the transition metal and are being progressively improved in view of novel future applications.
We developed novel dual-active metal-based CORMs with the potential to be used as therapeutic agents in tendon-derived diseases. Specifically, we designed and synthesized dicobalt(0)hexacarbonyl (DCH)-CORMs containing structural fragments of COX-2 selective inhibitors and tested them for the CO release kinetic (myoglobin release assay) and anti-inflammatory/cytoprotective effects on hydrogen peroxide-stimulated human primary-derived tenocytes by taking in account the PGE2 secretion as a readout.

Malaria drug research and development efforts have recently resurged in the last decade following deceleration rate of mortality and malaria cases in endemic regions. Inefficiency of malaria interventions are largely driven by the spreading resistance of the *Plasmodium falciparum* parasite to the current drug regimens and from the malaria vector – mosquito *Anopheles* – to insecticides. In response to the new eradication agenda, the development of drugs that act by breaking the malaria transmission cycle (transmission-blocking drugs) has been recognized as an important and additional target for intervention. These drugs take advantage of the susceptibility of *Plasmodium* population bottlenecks before transmission (gametocytes) and in the mosquito vector (gametes, zygotes, ookinetes, oocysts,

sporozoites). In this context, we sought to address the urgent requirement for novel antimalarial interventions by developing and aiding future discovery of transmission-blocking drugs.

We designed and synthesized analogues of the pyrazole MMV1580843, recently discovered in a high-throughput screening as a potent and selective gametocytocidal compound. SAR studies of these compounds hold promise for improved chemical modifications to progress to a hit-to-lead campaign. Particularly, we found that the pyrazole core allows a variety of substitutions that maintain potent activity towards late-stage gametocytes along with favorable physicochemical and safety profiles.

In parallel, from a phenotypic screening of compounds belonging to an in-house library, we discovered new pyrazole- and pyrrole-based compounds endowed with selective activity towards ring and trophozoite stages in the *P. falciparum* asexual cycle and potential activity against sporogonic stages in mosquitoes. The transmission-blocking potential was assessed by performing topical exposure assays on females *Anopheles Gambiae* mosquitoes of selected hits and found compound **19** and **12** to significantly decrease the parasite development in the mosquito midgut.

# List of Figures

**FIGURE 1.1.** MOLECULAR ORBITAL DIAGRAM OF THE CO MOLECULE, EXCLUDING 1S ATOMIC ORBITAL CONTRIBUTIONS. 16

**FIGURE 1.2.** SCHEMATIC OVERVIEW OF HEME DEGRADATION PATHWAY LEADING TO CO PRODUCTION. 19

**FIGURE 1.3.** MAIN SIGNALING PATHWAYS REGULATED BY CO. 22

**FIGURE 1.4**. CHEMICAL STRUCTURES OF CORM-1, CORM-2, AND CORM-3. 27

**FIGURE 1.5.** SCHEMATIC REPRESENTATION OF METAL-BASED CORMS 27

**FIGURE 3.1.** GLOBAL DISTRIBUTION OF MALARIA IN 2020. 81

**FIGURE 3.2.** GENERAL CELLULAR STRUCTURE OF *PLASMODIUM* PARASITES. 84

**FIGURE 3.3.** MALARIA PARASITE LIFE CYCLE. 88

**FIGURE 3.4.** CHEMICAL STRUCTURE OF ANTIMALARIA DRUGS USED IN THERAPY. 90

**FIGURE 3.5.** CHEMICAL STRUCTURES OF COMPOUNDS WITH TRANSMISSION-BLOCKING ACTIVITY IN TRANSLATIONAL AND PRODUCT DEVELOPMENT PHASES. 103

**FIGURE 4.1.** SCHEMATIC REPRESENTATION OF TRANSMISSION-BLOCKING ACTIVITY OF **MMV843** AND **ATQ**. 132

**FIGURE 4.2.** PRELIMINARY SAR CHARACTERIZATION AROUND **MMV843**. 137

**FIGURE 4.3.** GENERAL STRUCTURES OF THE 127 SELECTED COMPOUNDS. 139

**FIGURE 4.5**. ABS-SPECIFICITY ASSAY OF COMPOUNDS **16** AND **19**. 146

**FIGURE 4.6**. ISMFA USING COMPOUND **3** WITH 24 AND 48 HOURS OF EXPOSURE. 147

**FIGURE 4.7**. TOPICAL EXPOSURE ASSAY OF COMPOUNDS **3**, **12**, **16**, **18 – 20**. 149

**FIGURE 4.8**. RESISTANT PARASITE SELECTIONS USING COMPOUND **16**. 151

# List of Tables

**TABLE 1.1.** INTERNAL AND EXTERNAL STIMULI FOR CO RELEASE FROM METAL-BASED CORMS. 29

**TABLE 3.1.** TARGET CANDIDATE PROFILES (TCPS) DESCRIPTION AND THEIR COMBINATION FOR OBTAINING IDEAL TARGET PRODUCT PROFILES (TPPS). 94

**TABLE 4.1.** ACTIVITY OF **MMV843** AGAINST ASEXUAL AND LATE-STAGE GC OF *P. FALCIPARUM* PARASITES AND STRUCTURE. 130

**TABLE 4.2.** CHEMICAL STRUCTURES OF COMPOUNDS **1-15**. 133

**TABLE 4.3.** ACTIVITY AGAINST *PF*NF54 ABS AND LATE-STAGES OF GC (IV/V), PHYSICO-CHEMICAL PROPERTIES, CYTOTOXICITY ON HEPG2 CELLS AND HERG INTERACTIONS OF COMPOUNDS **1 - 15** AND **MMV843**, COMPARED TO TCP-5 HIT/EARLY LEAD CRITERIA. 136

**TABLE 4.4.** ACTIVITY AGAINST *PF*NF54 ABS, PHYSICO-CHEMICAL PROPERTIES, **3**, **6**, **11**, **12**, AND **19-23**. 141

# List of Abbreviations

3-MST: 3-mercaptopyruvate sulfurtransferase; 12
ABS: asexual blood stages; 4; 5; 6; 58; 64; 66; 69; 70; 71; 72; 73; 100; 101; 106; 107; 111; 112; 113; 117; 119; 121; 123; 124; 126; 144; 145; 146
AcAS: acetyl-CoA synthase; 72
ACT: artemisinin-based combination therapy; 60
ACTs: artemisinin-based combination therapies; 59; 60; 62; 63; 65; 77
AMA-1: apical membrane antigen-1; 54; 55
AO: acridine orange; 75
ARDS: acute respiratory distress syndrome; 25; 43
ATQ: Atovaquone; 4; 67; 78; 102; 103; 111; 113; 119; 125; 126
CBS: cystathionine-synthase; 12
CDC: Centers for Disease Control and Prevention; 51
CETSA: conditional knockdown and cellular thermal shift assay; 72
cGMP: cyclic guanosine monophosphate; 20; 56
CNVs: copy number variations; 63
CO: carbon monoxide; 2; 4; 6; 9; 10; 11; 12; 13; 14; 15; 16; 17; 18; 19; 20; 21; 22; 23; 24; 25; 26; 27; 28; 29; 30; 31; 32; 33; 36; 37; 42; 43; 44; 45; 46; 47; 48
CoA: Coenzyme-A; 69; 72
COHb: carbonmonoxy hemoglobin; 17
COVID-19: coronavirus disease 2019; 23; 41; 52; 80
CPR: Cytochrome P450 reductase; 17
CSE: cystathionine-lyase; 12
CSP: circumsporozoite protein; 54; 57; 62
DDT: dichlorodiphenyltrichloroethane; 51; 61
DGFA: Dual Gamete Formation Assay; 75; 76; 118; 120; 125; 145; 148; 159; 161
DHA: dihydroartemisin; 60; 146; 147
DMSO: dimethyl sulfoxide; 5; 117; 118; 121; 132; 146; 147; 148; 149; 150; 161; 162
DOX: doxorubicin; 25
EBL: erythrocyte-binding-like; 55
eCO: exhaled CO; 23
ECP1: egress cysteine protease 1; 57
EDGs: electron donating groups; 104; 112
EMA: European Medicines Agency; 14; 52
ENOG: European Network on Gasotransmitters; 14
ER: endoplasmic reticulum; 4; 5; 52; 58; 69
ET-CORMs: enzyme-triggered carbon releasing molecules; 29; 31; 46; 47
EWG: electron withdrawing group; 107
EWGs: electron withdrawing groups; 104; 112; 124
**FC**: fold change; 101; 106; 107; 122
FV: food vacuole; 53
GC: gametocytes; 4; 6; 100; 101; 103; 105; 106; 107; 144; 145; 146; 148; 149
GDV1: gametocyte development 1; 56
GI: gastrointestinal; 25
GMEP: Global Malaria Eradication Program; 51
GNF: Genomics Institute of the Novartis Research Foundation; 69
GTP: guanosine triphosphate; 20
GTS: Global technical strategy; 52
$H_2S$: hydrogen sulfide; 11; 12; 13; 15; 36
HDA2: histone deacetylase 2; 56
hERG: human ether-a-go-go-related gene; 6; 104; 107; 123
HO: heme oxygenase; 14; 17; 18; 20; 23; 24; 25; 37
HP1: heterochromatin protein 1; 56
HYCO: hybrid carbon monoxide-releasing molecule; 22
iCO: inhaled CO; 22; 23; 24; 25; 26
IMC: inner membrane complex; 52; 54; 56
IRS: indoor residual spraying; 59; 61; 77
iSMFA: indirect SMFA; 5; 117; 118; 119; 120; 125; 145; 149; 159; 161
ISS: Istituto Superiore di Sanita'; 75
ITNs: insecticide-treated mosquito bed nets; 61
IVIEWGA: in vitro assays such as evolution and whole-genome analysis; 72
LLINs: long-lasting insecticide-treated bed nets; 59; 61; 77; 85
LPS: lipopolysaccharides; 21; 23; 45
MAPK: mechanism involving mitogen activated protein kinases; 21; 39
MB: Methylene Blue; 5; 70; 71; 117; 118; 148; 161
MbCO: carbonmonoxy myoglobin; 32
MCC: metal carbonyl complex; 26; 27; 30

Mmpl3: mycobacterial membrane protein large 3; 100
MMV: Medicines for Malaria Venture; 63; 68; 70; 71; 72; 95; 100; 152
MoA: mechanism of action; 100
MSPs: merozoite surface proteins; 55
MW: molecular weight; 15; 107; 112; 113
NEK: NIMA (never-in-mitosis gene A)-related kinase; 57
NF-κB: nuclear factor kappa-light-chain-enhancer of activated B cells; 21
NIR: near-infrared; 28
NO: Nitric oxide; 11; 12; 13; 14; 15; 18; 20; 23
NOSs: NO synthases; 12; 20
Nox family: NADPH oxidase family; 20
ODA: ookinete development assay; 76
PanAm: pantothenamide; 72
*PfCRT*: Plasmodium falciparum chloroquine resistance transporter; 63; 86; 155
*Pf*DGFA: Plasmodium falciparum Dual Gamete Formation Assay; 148
*PfDHFR*: Plasmodium falciparum dihydrofolate reductase; 63
*Pfk13*: Plasmodium falciparum of the Kelch protein 13 gene; 63
*Pf*LDH: Plasmodium falciparum lactate dehydrogenase; 74
*PfMDR1*: Plasmodium falciparum multidrug resistance protein 1; 63; 155
pIBM: post infected-blood meal; 76; 117; 119; 149; 150
PKG: cGMP-dependent protein kinase; 56
PLC: phospholipase C; 56
PQ: primaquine; 66; 77
PRB: Pandemic Response Box; 100
PV: parasitophorous vacuole; 55; 56
RBCs: red blood cells; 55; 114; 147; 148
RBL: reticulocyte-binding-like; 55
RDTs: rapid diagnostic tests; 61
RON2: rhoptry neck protein 2; 55
ROS: reactive oxygen species; 17; 20; 21; 28; 30; 39; 40; 46
SaLSSA: Saponin-lysis Sexual Stage Assay; 74
SAR: structure-activity relationship; 3; 4; 78; 102; 105; 108; 111; 119; 123; 124; 126; 127
scavenger receptor B1: scavenger receptor B1; 55
sGC: soluble guanylate cyclase; 20
SMFA: standard membrane feeding assay; 75; 76; 101; 117; 126
SNVs: single nucleotide variations; 63
SP: sulfadoxine–pyrimethamine; 4; 58; 60; 61
TBVs: transmission-blocking vaccines; 66
TCPs: target candidate profiles; 6; 63; 64
TLR: toll-like receptor; 21; 40
TNF-α: tumor necrosis factor alpha; 21; 24; 38
TPPs: target product profiles; 6; 63; 64
tPSA: topological polar surface area; 108; 111; 119; 128; topologicalpolar surface area; 101
TRA: transmission reducing activity; 101
TRAP: thrombospondin-related adhesive protein; 54
WGS: whole genome sequencing; 121; 126
WHO: World Health Organization; 51; 52; 59; 61; 62; 66; 79; 85; 86
XA: xanthurenic acid; 56

# Table of Contents

**ABSTRACT** **3**

**List of Figures** **5**

**List of Tables** **6**

**List of Abbreviations** **7**

**Chapter 1 – An Overview of Carbon Monoxide and its Therapeutic Uses** **12**

*1.1 Gasotransmitters family* *12*

*1.2 Carbon Monoxide: A Brief Historical Account* *14*

*1.3 General Chemistry of CO* *15*

*1.4 Biosynthesis of CO in Human Physiology* *17*

*1.5 Signaling Pathways Mediated by CO* *19*

*1.6 Therapeutic Potential of CO* *22*

*1.7 CO Delivery Systems* *25*

*1.8 Objectives of Our Study* *33*

*References* *34*

**Chapter 2 – Article: A Novel Class of Dual-Active DCH-CORMs Counteracts Oxidative Stress-Induced Inflammation in Human Primary Tenocytes** **50**

**Chapter 3 – Malaria: Current Status and Key Interventions to Block Transmission** **80**

*3.1 Malaria* *80*

*3.2 Plasmodium Biology and Malaria Life Cycle* *82*

*3.3 Current Malaria Control - Elimination Strategies and Challenges* *89*

*3.4 Antimalarial Drug Resistance and New Target Candidate Profiles* *92*

*3.5 Transmission-Blocking Compounds* *95*

*3.6 The Global Antimalarial Pipeline* *98*

*3.7 The Transmission-blocking Screening Landscape* *103*

*3.8 Conclusions and Objectives of Our Study* *107*

*References* *109*

**Chapter 4 - Discovery of Novel Pyrazole- and Pyrrole- Based Compounds as Potential Transmission-Blocking Compounds** **129**

*4.1 Introduction* *129*

*4.2 Results* *133*

*4.3 Discussion* *151*

*4.4 Materials and Methods* *156*

*References* *181*

**LIST OF PUBLICATIONS AND CONFERENCES** **193**

# Chapter 1 – An Overview of Carbon Monoxide and its Therapeutic Uses

## 1.1 Gasotransmitters family

Gasotransmitters are a class of small signaling molecules that exist as natural gas or dissolved in circulation and include nitric oxide (NO), carbon monoxide (CO), and hydrogen sulfide ($H_2S$). Evidences suggest that these gases had a role in the start of life when $O_2$ concentration was scarce.[1] These gases were once assumed to be only smelly (the case of $H_2S$) and poisonous for human beings. It was, nonetheless, later discovered their biological role in living organisms at low concentrations with significant pharmacological, therapeutic, and physiological effects.[2–4]

Thus, the pharmacological responses triggered by the interaction of these gaseous molecules to their targets gained much interest in research. A comprehensive knowledge of the pharmacological characteristics of these gasotransmitters is essential to establish the clinical use, however some modes of action are complex and that makes it an uphill battle.

Gasotransmitters may have different functions but share some characteristics such as:

1. Permeable in cellular membranes. Although some efforts have been made to find any transportation mechanism, there is no evidence that confirms that gasotransmitters need specific channels to pass across cellular membranes.[5,6]
2. Endogenous production. Gasotransmitters can be produced in human cells by specific enzymes. NO is generated by NO-synthases (NOSs), CO is produced by heme oxygenases (HOs) during heme breakdown and $H_2S$ is created during the metabolism of L-cysteine by four enzymes: cystathionine-synthase (CBS), cystathionine-lyase (CSE or CTH), and 3-mercaptopyruvate sulfurtransferase (3-MST) and D-amino acid oxidase.[7–9]
3. Activity-concentration dependency. A concentration-dependent mechanism is used to mediate a variety of physiological processes. For instance, NO acts through the activation of guanylate cyclase with different physiological responses at certain

concentrations. Apoptosis or antimicrobial responses are induced by high NO concentrations, whereas angiogenesis is induced by low NO circulation.[10]

4. Gasotransmitters' functions can be duplicated by exogenously administered analogues. There is evidences that gasotransmitters, delivered both endogenously and exogenously, can lead to the same therapeutic effects.[11,12]

Following these requirements, NO, CO, and $H_2S$ are the most well-known molecules classified as gasotransmitters but, similarly, new molecules, including their derivatives, are currently under investigation and may join this family in the future.[13] While these molecules are involved in signaling pathways, the majority of their biochemical and biological impacts do not happen while they are gaseous but only when they are solutes. As solutes, they may freely penetrate and move across aqueous and hydrophobic environments because to their low molecular weight and minor polarity. Gasotransmitters are generally Lewis bases, nucleophiles, or ligands because due to the presence of lone pairs of electrons in their structure. NO and $H_2S$ have a high inherent reactivity (short half-life), allowing them to react with a wide range of biological targets (organic cofactors, lipids, and nucleic acids, as well as change protein amino acid side chains). CO is a very stable naturally occurring and metabolically inactive molecule, interacting mostly with ferrous ion complexes in mammalians and then it targets a variety of proteins, each with its own set of physiological effects. Both NO and $H_2S$ can take part in redox processes and interact with one another and their metabolites, and all three gasotransmitters can interact with heme to generate coordination chemistries, with NO and CO interacting with iron (II) and $H_2S$ connecting with iron (III), respectively. Because $O_2$ is necessary for NO and CO synthesis and $H_2S$ metabolism, each gasotransmitter relies on it.[14,15]

Gasotransmitters possess unique features. Unlike neurotransmitters, gasotransmitters are not stored in vesicles, thus they must be generated quickly in response to stimuli. Unlike other signaling molecules, gasotransmitters do not bind receptors and do not operate on G protein or tyrosine kinases that trigger a series of signaling events, culminating in a change in cell function. By contrast, they act directly on intracellular proteins with chemical modifications, impacting synthesis, their downstream molecular targets, and their chemical

interaction. The large spectrum of action allows gasotransmitters to regulate many intracellular functions such as cytoprotection, apoptosis, proliferation, inflammation, and gene transcription. Therefore, they play a role in a wide range of physiological activities, including cardiovascular, neurological, gastrointestinal, excretory, and immune system regulation. As a result, all three gases have a significant impact on human health and potential value as a therapeutic target (cardioprotective, antihypertensive, antithrombotic, antitumor, smooth muscle relaxant).[15]

Our knowledge of gasotransmitters' physiological relevance and targeted strategies is fast advancing, but more understanding of the intricate molecular processes of gasotransmitters will be crucial in accelerating the development of directed action techniques to regulate these signaling systems for their clinical use.

Fundamental research is progressing on the future application of CO in therapy. In this chapter, the biosynthesis, pharmacological use, and therapeutic value of the gaseous molecule CO will be then discussed.

## 1.2 Carbon Monoxide: A Brief Historical Account

Traces of carbon monoxide have been linked to have prehistoric origins, originating mostly from thermal combustion with some reported evidence of CO's psychoactive effects in the context of fire exposures.[16] However, it remains still debated the actual discovery of CO molecule and as denoted by the American Chemical Society, it should be attributed to Priestley during his experiments in 1796.[16] CO characterization began in the nineteenth century starting with the observations of William Cruikshank who enclosed the molecule formula by inducing incomplete combustion in conditions with less $O_2$ and no hydrogen source.[17] CO physiological effects and toxicity's mechanism was discovered over a long period of time and, thanks to Claude Bernard's and F. Hoppe-Seyler's research in the mid-century it was demonstrated that CO molecule displaces $O_2$ within the body that results in hypoxia and asphyxiation.[16] Despite the multitude of hypothesized processes, only in the twentieth century it was proven the existence of endogenous CO in human blood by the HO metabolism of heme, and since the 1990s, after NO, CO has been recognized as a

physiologically important signaling molecule showing neurotransmitter qualities (coined as "gasotransmitter" later).[18,19] Following a considerable amount of work to study the protective benefits of CO, since 2000 enormous improvements in the physiological (mainly in nervous and cardiovascular systems) and pharmacological functions for medicinal application of CO have been made and more must be done to reach an approval from medical agencies such as FDA and EMA. The large amounts of research and projects on gasotransmitters that was growing rapidly gave rise to the foundation of the European Network on Gasotransmitters (ENOG) on 2011 to "to boost the quality, competitiveness and impact of European biomedical research in the field of gasotransmitter molecules (NO, CO and $H_2S$) and to translate the progress made into potential therapies".[20]

## 1.3 General Chemistry of CO

Under atmospheric temperature and pressure CO is a colorless, odorless, tasteless, and ubiquitous residual gas (M.P., −205 °C; B.P., −191.5 °C; density, 1.250 g/l at 0 °C) created by incomplete combustion of organic molecules in the environment and it can be used in synthesis for the creation of the corresponding esters and aldehydes, despite its poisonous reputation. CO is a linear diatomic species where a triple bond connects carbon (oxidation state +2) and oxygen (bond length: 1.128 Å) representing one of the strongest chemical bonds yet discovered (bond dissociation energy of 1072 kJ/mol). Like all gaseous signaling molecules, CO does not possess a charge, is soluble in water (2.6mL/100mL) and has a small molecular weight (MW 28.01). Among the triad of gasotransmitter (NO, CO, and $H_2S$), CO is the most physiologically stable molecule due to the lack of free electrons and thus, it does not react with water in physiological conditions, but it dissolves, and it may be capable of exerting its physiological effects in longer time periods.[13,21]

The molecular orbital diagram of CO is reported in Figure 1.1. CO possesses ten valence electrons (carbon atom has four valence electrons, oxygen has six valence electrons) that occupy 2s and 2p orbitals. Because oxygen has a higher electronegative charge than carbon, its orbitals are more stabilized and have a lower energy than carbon's orbitals and a high interaction occurs. As a result, two 2p orbitals combine to give two σ molecular orbitals, one

energetically higher (antibonding orbital) and empty and the other one with lower energy (bonding orbital) that contains two electrons. Similarly, the other four 2p orbitals (2py, 2pz) will join to give four π-type molecular orbitals where also in this case the bonding orbitals are occupied by two electrons each and the antibonding orbitals are empty. In this scenario, three bonding orbitals are occupied, but no p-antibonding orbitals contain electrons. σ* antibonding orbital is much more energetic than the other two π* antibonding orbitals, which are accessible for back donation with a low oxidation number metal. This property renders CO an ideal binder to the heme iron ($Fe^{+2}$) that can displace the oxygen from hemoglobin nearly in an irreversible manner, which represents the primary cause of toxicity in human organism. [22]

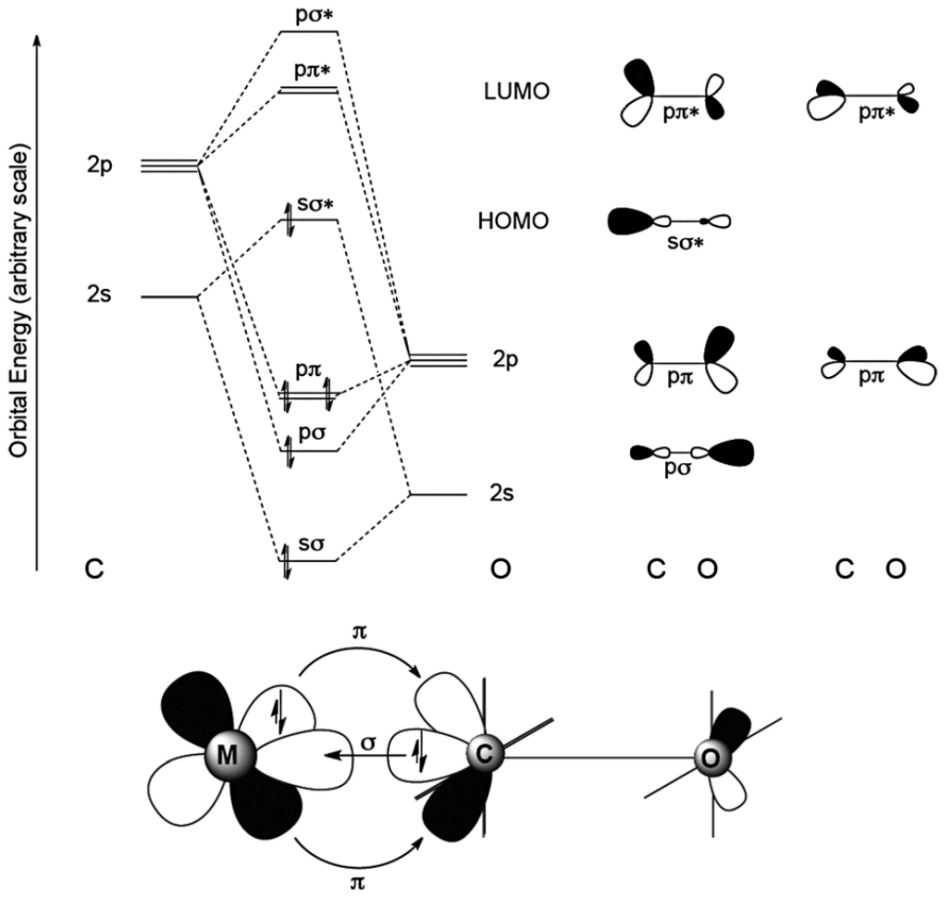


**Figure 1.1.** Molecular orbital diagram of the CO molecule, excluding 1s atomic orbital contributions. Adapted from Romão et al.[22]

CO has good donor and acceptor properties. When CO meets a low oxidation state metal, donation of two electrons from the carbon atom lone pair to the metal's d-orbital occurs (σ bond) but, to relieve the extra electron density, part of the electrons of the metal may be moved to the lowest-energy unoccupied molecular orbitals of CO, which is a π* antibonding orbital, that shares similar energy and symmetry to the metal's d orbitals resulting in system stability. The latter mechanism of interaction is mostly known as "backbonding" or "backdonation" and it has a synergistic nature since strength of the bond increases with electron-rich the metals and the amount of carbonyl donated on the metal center. This property of CO makes it an important ligand (carbonyl) in organometallic chemistry to form the corresponding transition-metal carbonyl complexes that proved to have important industrial applications as catalyst and can be exploited also in therapeutics. [14,22]

## 1.4 Biosynthesis of CO in Human Physiology

As in other mammals, in the human body there are continuous CO production and elimination that are regulated by critical cellular processes.

Endogenous production of CO is possible from different metabolic mechanisms and the amount of CO bonded to the hemoglobin (COHb) in the bloodstream determines how much CO is generated through these processes. Heme degradation is the primary source of CO, indeed its metabolism accounts for at least 86% of CO production and the remaining portion coming from xenobiotics or lipid oxidation mechanisms (Figure 1.2).[23] Cellular heme serves as a vital cofactor in oxygen transport proteins, such as hemoglobin and myoglobin but it is also a known stimulator of reactive oxygen species (ROS) production and rapid heme breakdown is crucial for protecting cells from its cytotoxic effects. The enzyme heme oxygenase (HO) is the main responsible for the elimination of heme since it catalyzes the rate-limiting step through the production of CO, biliverdin (then quickly transformed to bilirubin) and free ferrous iron in a stoichiometric manner. Three moles of oxygen and seven electrons supplied by NADPH cytochrome P450 reductase (CPR) are needed in this reaction to enable the binding of oxygen and to reduce iron.[7,24] In humans there are three isoforms of HO, HO-1 that is inducible from oxidative stress and the constitutively expressed HO-2 and

HO-3. HO-1 and HO-2 appear to be the only functional enzymes and they have a heme-regulatory domain but while the HO-1 gene is expressed mostly in the spleen where erythrocyte breakdown occurs, HO-2 is predominant in brain and testis.[25] Heme degradation plays an important role for response to ROS stimuli in inflammatory or disease-like circumstances thanks to the anti-oxidative and cytoprotective actions of bilirubin and CO.[26,27] After a complete reaction, iron is reused, bilirubin is expelled from the body through the urine and CO will either be bonded to hemoglobin and circulate in the blood as carboxyhemoglobin or be sequestered in cells connected to proteins that contain heme. CO may also promote HO-1 expression, creating a cycle that feeds on itself. However, to avoid the harmful heme-CO bonding, heme production is regulated by negative feedback mechanism from the amount of heme and hemin (oxidized form of heme) synthesized, thus indirectly restricting CO supply.[28]

While heme catabolism is the primary source of endogenously generated CO, other processes, such as the induction of CYP450[29–31] and lipid peroxidation seem also to be involved.[32,33]

Contrary to other gasotransmitters such as NO, elimination of endogenous CO occurs in a slow process (half time of around 4h) and is mostly excreted from lungs.[34] It also appears that the mitochondrial cytochrome c oxidase is able to remove CO through oxidation to $CO_2$, but to our knowledge this assumption has never been validated.[35]

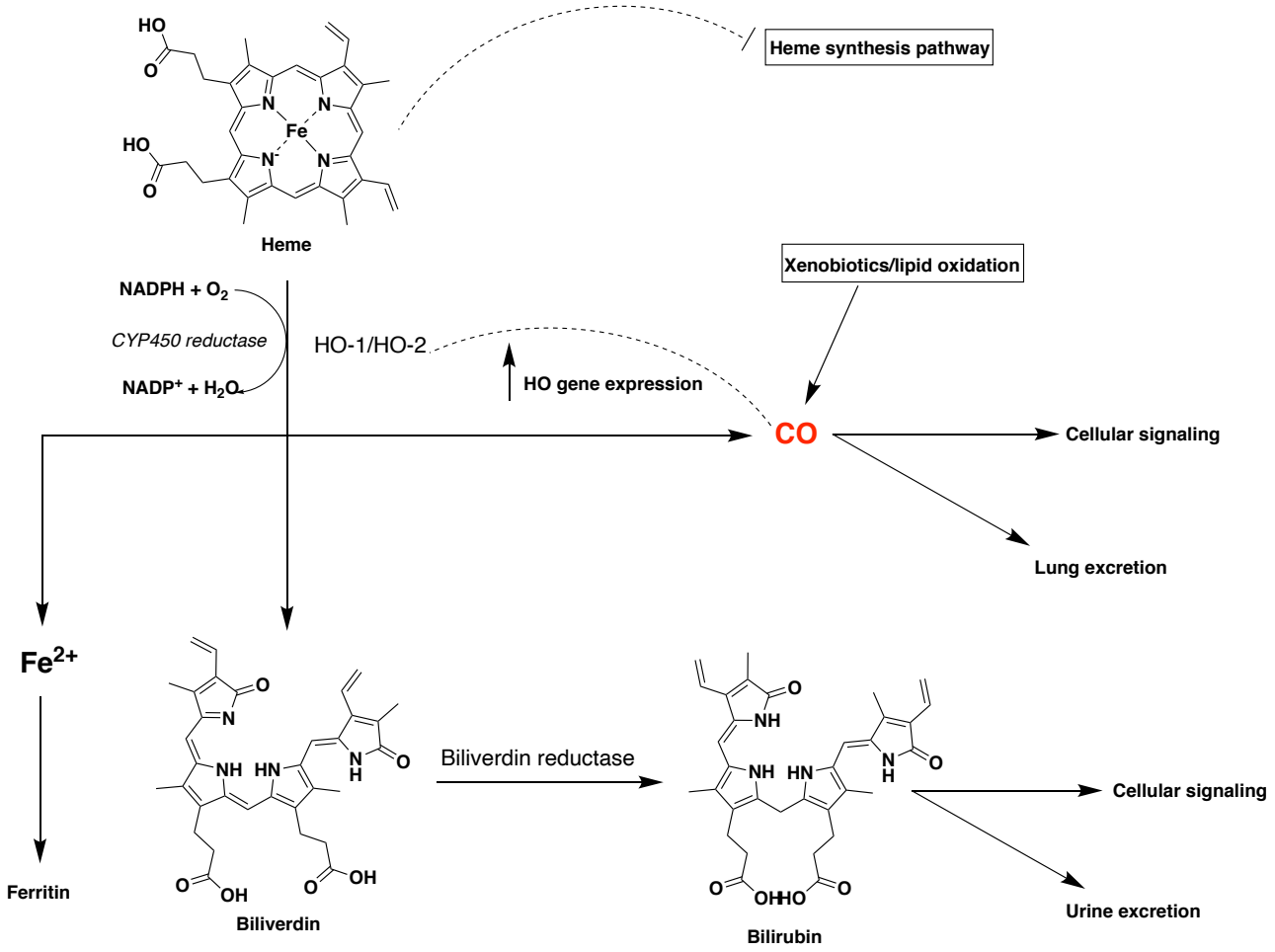


**Figure 1.2.** Schematic overview of heme degradation pathway leading to CO production.

## 1.5 Signaling Pathways Mediated by CO

CO may affect a variety of physiological activities in cells as it can interact with a vast array of proteins determining a somewhat ambiguous biological action and involving nearly every organ and regulatory system. CO may act as both anti- and pro-inflammatory, pro- and anti-apoptotic, and pro- and antiproliferative agent and thus, it controls cell proliferation and survival[36], the immunological response[37] and tissue[38]. Moreover, as it happens for other gasotransmitters, the biological activity and selectivity of CO are dependent on the concentration, timing and tissue localization.[39] CO's targets that mediate cellular signaling can be divided into two main class: heme-containing proteins, also called "hemoproteins", and nonheme-containing proteins. In Figure 1.3 reports a schematic representation of the main molecular pathways validated for CO.

Hemoproteins such as hemoglobin, soluble guanylate cyclase (sGC), the mitochondria oxidases or enzymes needed for ROS generation are ubiquitous in cells and are the main target of CO due to the strong affinity with the heme iron ($Fe^{2+}$). The receptor protein sGC is a heterodimeric complex that catalyzes the transformation of guanosine triphosphate (GTP) into cyclic guanosine monophosphate (cGMP), a key regulator of cell proliferation, differentiation and apoptosis. Upon binding with CO at low concentrations, sGC produces more cGMP, although less effectively than binding with NO, and it induces vasorelaxation and inhibits platelet aggregation.[40] Vascular and organ protective functions of CO are partially indirect since are mediated through NO. CO at low concentration enhances NOSs activity, a hemoprotein family that catalyze the production of NO from L-arginine and NAD(P)H. On the other hand, the catalytic activity of NOSs is limited to high concentrations of CO that acts as a negative regulator by interacting with the heme moiety.[7,41,42] The latter mechanism is thought to limit the damage caused during CO poisoning or oxidative stress where NO, as a free radical, is highly reactive and a strong oxidant that can cause cell damage, while CO is more stable.[14] Noteworthy, HO-1 function is also induced by NO, thereby increasing CO levels that in turn can regulate NO production. This feedback system is important in particular conditions and cell types where one of the gasotransmitters is more needed than the other.[39] CO-mediated vasorelaxation has been attributed also to the direct activation of calcium ($Ca^{2+}$)-dependent potassium ($K^{+}$) channels.[43,44] CO can also regulate ROS generation through a number of mechanisms. The interaction with NADPH oxidase family (Nox family), which play a critical role in the generation of ROS, and other hemoproteins in mitochondria have significant consequences in different defensive signal mechanisms. For instance, CO inhibition of Nox4 activation led to reduced oxidative stress in endothelial brain cells with increased survival.[45] The binding of CO with cytochrome c oxidase of the mitochondrial electron transport chain (also implicated in the generation of ROS) happens because of its property of binding metalloproteins and because heme is generated in the mitochondrial compartment. Cytochrome c oxidase contributes on danger cellular signaling *via* the generation of ROS that operate on gene regulation influencing cellular ultimate responses. The enzymatic activity of cytochrome c oxidase is regulated by

CO through a conversely mechanism. High amount of CO inhibits cytochrome c oxidase activity and mitochondrial respiration stopping the oxygen consumption and reducing ATP production coupled to increased ROS production and leading to further damage in cells and tissues. At low levels of CO, low amounts of ROS are produced by cytochrome c oxidase activity promoting beneficial effects to the cell since they act as important signaling molecules in different functions such as cytoprotection, anti-inflammatory, mitochondrial metabolism induction.[46,47] Traumas caused during organ damage lead to the breakdown of CYP, a large group of hemoproteins, that can be prevented following CYP-CO stabilization. This mechanism was exploited to prevent adverse CYP450 degradation during kidney transplantation.[48]

Along with these main heme-containing target structures, CO also affects indirectly a wide range of targets that lack heme structures which confer for the major part the anti-inflammatory and anti-apoptotic effects of this gasotransmitter.

The previously discussed cytochrome c oxidase inhibition may eventually induce to the activation PPAR-$\gamma$ that favour anti-inflammatory responses and the nuclear translocation of nuclear factor kappa-light-chain-enhancer of activated B cells (NF-κB) to induce antiapoptotic genes and pro-survival pathways.[49]

CO exerts anti-inflammatory, anti-proliferative and anti-apoptotic effect also through a mechanism involving mitogen activated protein kinases (MAPK). CO has been shown to activate the MKK3/p38β MAPK pathway that, combined to the downregulation of JNK or ERK1/2, increase the production of the anti-inflammatory factor IL-10 and decrease pro-inflammatory factors such as IL-1β, tumor necrosis factor alpha (TNF-$\alpha$), IL-6 and also of anti-apoptotic factors (e.g., Bcl-2, Bcl-$X_L$).[50–53]

CO-related suppression of TLR-4 trafficking by at the outer plasma membrane by increasing the interaction between TLR-4 and Caveolin-1, a downstream target of CO and an important regulator of MAPK inflammatory signaling processes, was also shown to contribute to the anti-inflammatory regulation in LPS-induced inflammation.[54–56]

Taken together, CO controls a number and heterogeneous of cellular process for the modulation of inflammation, apoptosis, pro-survival signaling and vasoactive responses.

Noteworthy, herein we described only the main mechanisms that lead to these effects and, while research is still ongoing, more reviews reported CO signaling pathway in detail given the complexity and specificity of these molecular mechanisms.[39,57,58]

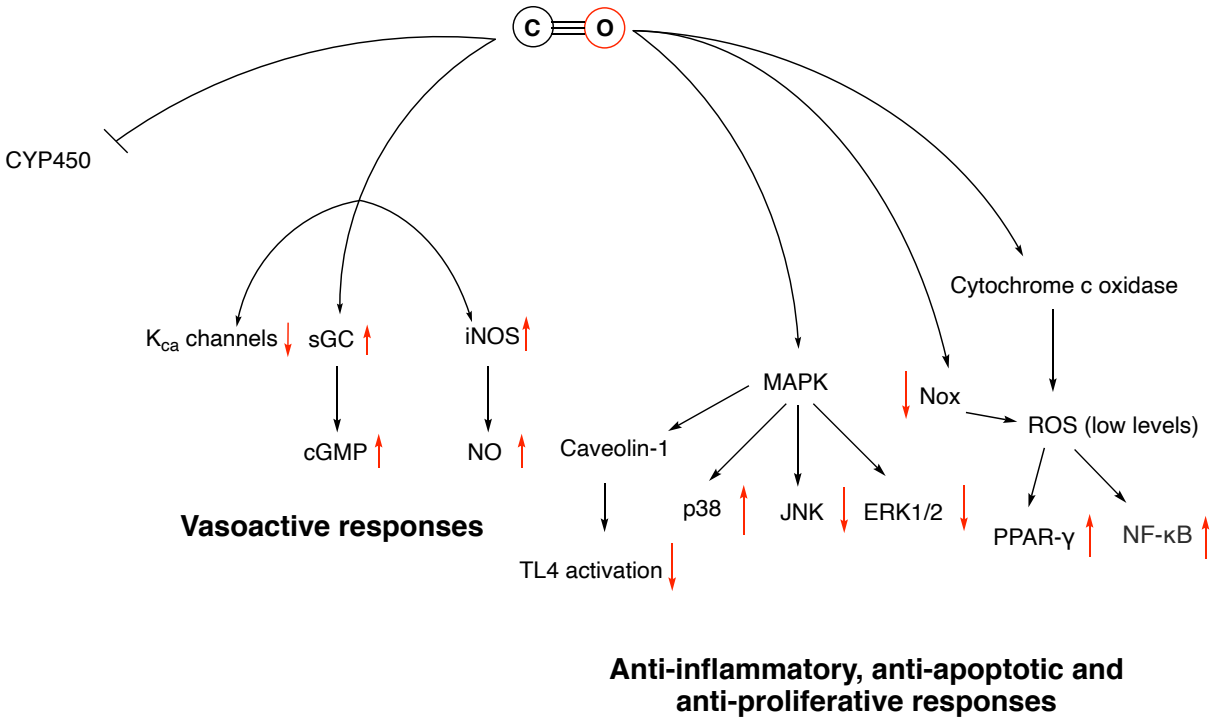


**Figure 1.3.** Main signaling pathways regulated by CO.

## 1.6 Therapeutic Potential of CO

Extensive studies are being done on the crucial function of heme oxygenase and endogenous CO generation given the regulation of an abundance of physiological processes of this system supporting a therapeutic role for CO. The latter has gathered widespread attention but there are some limitations that need to be overcome before the clinical application of CO becomes a real fact. The use of CO is hampered from the intrinsic chemical characteristics of this gas and toxicity that makes it difficult to deliver and not specific. Currently, different forms of treatment involving CO include inhaled CO (iCO), carbon monoxide-releasing molecules (CORMs), and hybrid carbon monoxide-releasing molecules (HYCOs). CO-delivery systems will be discussed in the section 2.6.

Generally, in the cardiovascular system CO is a vasodilator with moderate potency and it was also found to inhibit aggregation and adhesion of platelets and the activation of

monocytes.[59,60] In the respiratory system, CO can induce bronchodilation via a NO-independent, cyclic GMP-related mechanism.[61]

CO can even play a role in gastroprotection[62] All these functions, together with the anti-inflammatory, anti-apoptotic and antioxidant properties of CO can be exploited in various settings including neurodegenerative disorders, microbial infections, organ transplantation, ischemia, vascular injury, cancer, kidney disease and, more remarkably, in many inflammatory disorders.[63–68] Recently, also the treatment of COVID-19 symptoms through CO administration is receiving considerable attention.[69]

CO has been extensively studies as a modulator of immunosuppression and inflammation in a variety of diseases thus, herein we revisit some applications.

### 1.6.1 Therapeutic Application of CO in Inflammatory Diseases

The expression of the HO inducible isoform (HO-1) is triggered by cell responses toward oxidative stress and inflammation and results in cyto- and tissue protection. HO-1 metabolites, including CO, are important in restoring redox homeostasis and resolution of inflammation, and it has been widely demonstrated that the HO-1/CO axis can help to prevent cellular and tissue damage. Therefore, the manipulation of the HO-1/CO system is an attractive strategy to treat conditions linked to oxidative-stress-induced inflammation, such as lung hyper-inflammation in cystic fibrosis, sepsis and modulation of chronic pain.[57]

Due to the importance of CO in certain inflammatory diseases exhaled CO (eCO) has been used as a marker to detect pathophysiological conditions.[28,70–74]

The protective effect of CO alone was first shown in 1999 in rodents with hyperoxia-induced where iCO reduced the volume of pleural effusion and the protein concentration and neutrophil recruitment in the airways.[75]

Later, Mazzola et al. [76] researched on the effects of pretreatment with iCO on many acute pathological cases in animals induced by LPS, including stroke and disseminated intravascular coagulation, and they showed that CO dramatically decreased lung inflammatory response and avoided respiratory derangement. The anti-inflammatory protection of CO against LPS-induced organ injury was found to be mainly due to the

inhibition of iNOS expression and activity in the lung and iNOS expression and activity in the liver.[77] Similar anti-inflammatory activities of CO have also been established in mouse model of cerebral malaria where brain inflammation is the primary cause of morbidity and mortality, and CO could prevent this neuroinflammation.[64] It was also shown that an advanced application of iCO could prevent the establishment of inflammatory disorders during an organ transplant. For instance, nephropathies derived from kidney transplantation were prevented using at low doses of iCO that also improved the graft function.[78] Numerous studies have linked the positive benefits of CO on sepsis, a life-threatening organ dysfunction that arises from the host's inability to handle invasive infection. For example, Lee et al.[79] found that iCO increase the survival of mice injured by cecal ligation and puncture-induced polymicrobial sepsis enhancing autophagy and phagocytosis. Similar protective effects were obtained during the administration of exogenous CO by CORM-2 (CO-releasing molecule-2) against sepsis-induced acute kidney damage both *in vitro* and *in vivo*[80] indicating a possible alternative to gas inhalation for sepsis treatment. However, the active HO-1/CO pathway was associated with liver dysfunction in rats subjected to CLP-induced sepsis[81] and when it comes to human patients with sepsis-induced acute respiratory distress syndrome and idiopathic pulmonary fibrosis, CO showed no beneficial effects on phases I and II clinical trials.[82,83] Anti-inflammatory effects of CO have also been demonstrated in the treatment of pain derived from rheumatoid arthritis and osteoarthritis. Proinflammatory mediators including IL-1, IL-6, TNF-$\alpha$, inducible nitric oxide synthase (NOS2), PGE2, and bradykinin, which sensitize nociceptors and cause allodynia and the hypersensitive state that goes along with inflammation, are what cause inflammation-related pain. The intraperitoneal administration of CORM-3 (CO-releasing molecule-3), which inhibits expression of pro-inflammatory factors, alleviated the related symptoms to mice with collagen-induced arthritis and minimized the breakdown of cartilage.[84] Based on these studies, recently Berrino et al.[85] reported the synthesis of new hybrid molecules able to release CO and to inhibit carbonic anhydrases, which play a central role in inflammatory disorders with significant pain-relieving effects.

CO could also represent an alternative for treatment of inflammatory diseases regarding the digestive system such as gastric ulcers, inflammatory bowel disease, and postoperative ileus.[86,87] Interestingly, a recent study in this area exploited the capacity to deliver CO directly and safely to the gastrointestinal (GI) tract to treat inflammatory disorders with the development of safe gas-entrapping materials that reduced injury and inflammation in rodent models of colitis.[88]

Other inflammation settings in which CO gas and CORMs are effective, include side effects observed with other treatments. For instance, treatment with CORM-2 (30 mg/kg) of acute doxorubicin (DOX)-induced cardiotoxicity was significantly reduced in part because of CO's anti-apoptotic and anti-inflammatory effects.[67]

## 1.7 CO Delivery Systems

Even if in the past CO was hardly seen as a therapeutic substance, today considering that the great potentials of CO in therapy have been disclosed, researchers are trying to develop innovative, safe and effective strategies to deliver this gas to human bodies in clinic. Carbon monoxide may be administered to the human body mainly using three different methods: HO-1 inducers, iCO and CORMs. While the induction of HO-1 is limited by the need to identify safer and better-tolerated HO-1 inducers to currently available sources[89] the inhalation of CO and development of CORMs have found a faster access to clinical studies. Due to the inherent toxicity of CO, only low doses of this gas (20 – 500 ppm) can be safely inhaled in the human body. The inhalation of CO has brought promising results for its clinical use and has shown cytoprotective and anti-inflammatory effects *in vivo* models in lung disease.[90] To date, iCO has been tested in phase I-II clinical trials that seek to support the data generated so far for the protective effects toward sepsis-induced acute respiratory distress syndrome (ARDS).[91] For the delivery of iCO the Covox DS (Inkaria, Clinton, NJ, USA) was specifically designed for CO safe administration in investigational studies but there are no published guidelines for indications. Moreover, the use of iCO should always follow an approval from an institutional entity in human-subject research.[92] Nonetheless, the inhalation of CO has some disadvantages owing to the lack of specificity, risk of toxicity

and difficulty to implement. Indeed, the use of iCO is limited to lung injures and related diseases since a huge amount of CO would be needed to reach other target sites. To get around these issues, the use of a pharmaceutical formulation for delivery in a safe and controllable manner is required. Therefore, CORMs were formulated by scientists to meet the requirements of tissue specificity, low toxicity and prompt release at the site of action.[93]

### 1.7.1 Carbon Monoxide Releasing Molecules (CORMs)

An essential need for targeted CO delivery is a stable CO donor that only releases CO when triggered by an internal or external stimulation. For this purpose, CORMs were first reported in 2002 by Motterlini et al.[93] and turned out to be a safer and attractive therapeutic strategy to deliver a controlled amount of CO to cells.[94,95] Thus far, different generation of CORMs have been developed and can be categorized as metallic or non-metallic CORMs based on the type of CO controlled-release methods. Although a number of organic compounds have been explored for their potential as CORMs, to date, most of the developed CORMs are metal carbonyl complexes (MCCs) since provided the most relevant biological results and the greatest freedom for molecular design. Indeed, considering the preferential reactivity of CO for transition metals in a low oxidation state, organometallic complexes have emerged as suitable models to safely deliver CO *in vivo* and generate innovative therapeutic agents with reasonable pharmacological properties. CORMs that contain transition metals can include both essential trace elements such as manganese, iron and cobalt, and nonphysiological metals such as ruthenium, tungsten and rhenium.[94–96]

$Mn_2CO_{10}$ (CORM-1) was the first CORM to be described but, mainly due to Mn (I) toxicity, it was shortly abandoned for ruthenium-based compounds such as tricarbonyldichlororuthenium-(II)-dimer (CORM-2) and the water-soluble tricarbonylchoro(glycinato)-ruthenium (II) (CORM-3), which are currently the most frequently used CORMs for investigating physiological functions of CO release both *in vitro* and *in vivo*. Particularly, CORM-3 contains a glycinate auxiliary ligand and it appears to be more biocompatible for *in vivo* studies due to higher water solubility.[22,94,96]

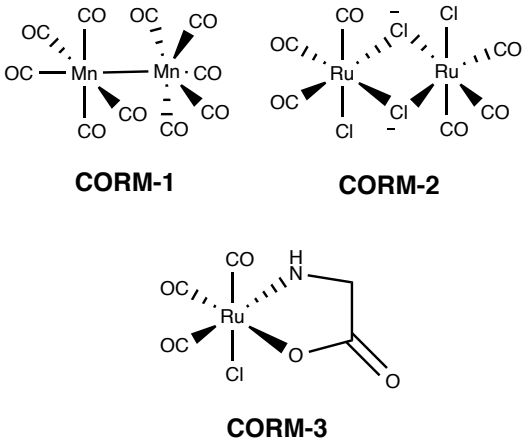


**Figure 1.4**. Chemical structures of CORM-1, CORM-2, and CORM-3.

More recently, Romão et al.[22] introduced a conceptual model (Figure 1.5) to rationalize and improve the design of MCCs with appropriate pharmaceutical properties. This model comprises three portions: (i) a metal core, which accounts for toxicity and the main properties of the MCC; (ii) a coordination-sphere, which influences the electronic density around the metal, tuning the stability and the chemical behavior of the whole complex and triggering CO release under specific conditions; and (iii) a drug-sphere, obtained through modulation of the distal sites of the metal complexes and accounting for pharmacological properties and drug-likeness. For drug design purposes, has not yet been established whether there are key requirements on the carbonyl (CO) number bonded on the transition metal and if a fast or slow kinetics is favorable and these properties might be more or less advantageous based on the medical target. For higher selectivity and also additional activity the drug-sphere plays a central role as reported in recent literature.[4,97]

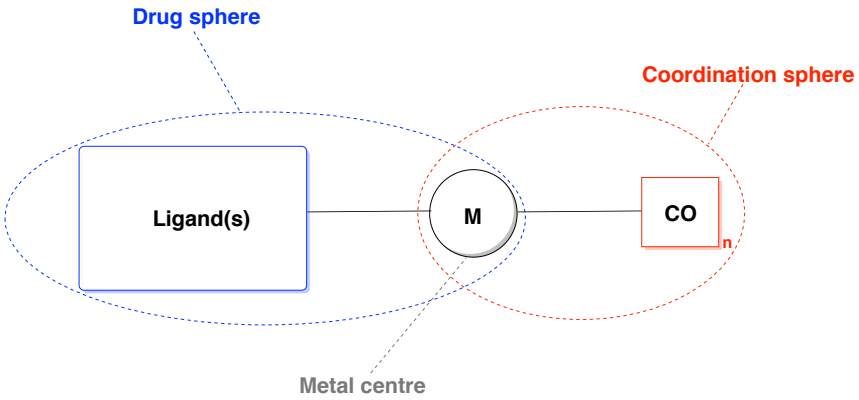


**Figure 1.5.** Schematic representation of metal-based CORMs adapted from Romão et al.[22]

As mentioned before, to enable a controlled CO release from the molecules there are different approaches. They can be differentiated in external and internal stimuli. External stimuli allow us to have a higher control of the starting point of action and avoid any spontaneous CO liberation, which is one of the key requirements in the design of CORMs. Examples of external stimuli used to trigger the release of CO are light, magnetic heating or ultrasound.[98–100] Among these, the use of light to release CO was more brought into attention of scientists and led to the development of photosensitive compounds called photoCORMs. The vast majority of photoCORMs are activated by UV light irradiation, but due to the scarce light penetration at such low wavelengths and related tissue toxicity, research has evolved into the development of systems showing controlled CO-release upon visible light (red light) and near-infrared (NIR) light irradiation. This could be possible mainly by tuning the drug sphere directed ligated to the metal center and through the incorporation of photoCORMs into amphiphilic nanoparticles, respectively.[101–103] Topical application might be a promising clinical application route but, despite the advances, it remains difficult to develop biocompatible photoCORMs that meet all the requirements for clinical development due to ligand exchange reactivity or redox reactivity of the metal byproducts. To date, most CORMs are spontaneous CO donors where CO liberation happens by ligand exchange reactions with the ligand in the medium or upon internal stimuli, which are physiological triggers such as pH, oxidants, and thiol- or enzyme-mediated reactivity.[93,103–106] Ph-sensitive and oxidation-sensitive CO donors change the kinetic of CO release following a pH change or a molecular oxidant (e.g., $O_2$, $H_2O$, ROS), respectively. While several diseases are associated with elevated levels of ROS, the design of CORMs containing ROS-sensitive groups is still a low explored area, indeed besides studies conducted on CORM-1[107] and non-metal CORMs[108] not much has been done to our knowledge. Also, CORMs sensitive to the presence of thiols- such as glutathione is an area that deserves to be explored. Interestingly a recent study from Gao et al.[109] demonstrated that using [$Fe_2${μ-$SCH_2CH(OH)CH_2(OH)$}2$(CO)_6$] (TG-FeCORM), a water-soluble and biocompatible organometallic diiron hexacarbonyl compound, the CO release was augmented in tumor

environment, where cancer cells have around fivefold more glutathione in concentration than normal cells. A class of CORMs known as enzyme-triggered CO-releasing molecules (ET-CORMs) release CO by the enzymatic breakage of chemical bonds. This family of CORMs promises strong tissue specificity CO delivery owing to their enzyme selectivity and different enzyme expression rates. For example, Romanski et al.[110] designed metal carbonyl compounds in which an organometallic ligand is either O-phosphorylated or esterified into one of two potential tautomeric forms. These CO prodrugs undergo hapticity changes when exposed to esterases or phosphatases, which increases their sensitivity to dioxygen and causes them to release CO.

**Table 1.1.** Internal and external stimuli for CO release from metal-based CORMs.

| TYPE OF CORM | DESCRIPTION | EXAMPLE | REFERENCE |
|---|---|---|---|
| **PHOTOCORM** | Photo-induced CO release from dark-stable metal-carbonyl complex prodrugs | 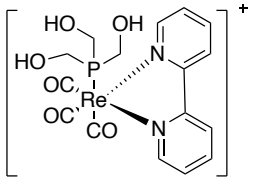 | 103 |
| **MAGNETIC-HEATED CORM** | Conjugated iron oxide nanoparticle with CORM that release CO under the application of an alternating magnetic field | 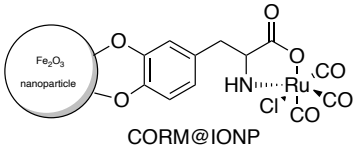 CORM@IONP | 111 |
| **ULTRASOUND-TRIGGERED CORM** | Low-intensity ultrasound application for CO release on sensitive CORMs | 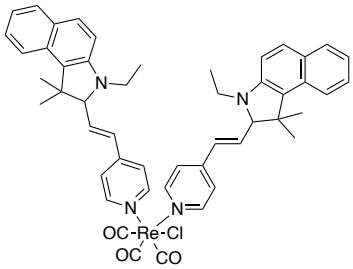 | 98 |
| **PH-SENSITIVE CORM** | Spontaneous CO donors that exhibit changes in the kinetic of CO release rate as a function of pH | 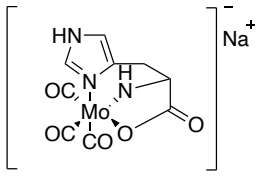 ALF186 | 112 |

| | | | |
|---|---|---|---|
| **THIOL-SENSITIVE CORM** | Spontaneous CO donors that exhibit changes in the kinetic of CO release rate as a function of of thiols concentration (e.g., GSH) | 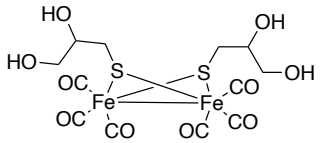 TG-FeCORM | 109 |
| **OXIDANT-SENSITIVE CORM** | CO donors that are oxidation-sensitive and release CO after being exposed to a molecular oxidant (e.g., $O_2$, $H_2O_2$, or ROS) | 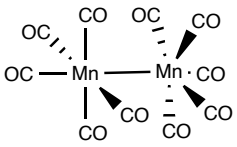 CORM-1 | 107 |
| **ET-CORM** | CO release prodrugs activated following enzyme catalyzed reactions (e.g., hydrolysis catalyzed by esterases) | 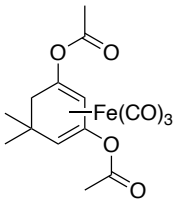 *rac*-9 | 113 |

In summary, the broad focus of scientists on MCC is due to their chemistry that allows the generation of a wide range of CORMs and a variety of CO release strategies useful in different biological settings. Noteworthy, when designing CORMs, some set of requirements must be met to be tested *in vivo* and later stages. CORMs should be soluble and stable enough at room temperature and aqueous solutions. Moreover, they should be active only in their target sites releasing CO in a controlled manner and in correct amounts, they should not degrade too quickly in circulation and should not produce toxic metabolites after CO release.[114]

## 1.7.2 Challenges and Future Perspective of Metallic CORMs

Metallic CORMs offer several advantages owing to their tunable and versatile chemistry of the coordination and drug spheres and because of the presence of the metal center, which brings important variations in the molecule by only changing from a metal to another or in oxidation state. These advantages are consistent with the number of metallic CORMs that were used for *in vitro*/*in vivo* studies in many biological settings and resulted promising in preclinical data. Despite having various biological activities, metallic CORMs are hardly used in clinical phases because of few challenges. Common challenges include (i) difficulty

in targeted delivery to specific biological sites for limited cellular uptake or CO controlled release; (ii) lack of drug-like properties (low toxicity, appropriate ADME properties [absorption, distribution, metabolism, elimination]); (iii) solubility and stability in aqueous media and biocompatibility in blood; (iv) contradictory CORM toxicity and efficacy profile in analytical assays. To use CORMs as pharmaceutical drugs, it is crucial to address all these issues and robust studies are required for a full assessment.[115–117] In CORMs design, fine-tuning of the coordination and drug sphere is always desirable. By doing so, ADME and kinetic profile of CO release can be modified based on the type of study or biological target. Moreover, a controlled release of CO can be reached by using the techniques already reported in Table 1.1. Yet, a metal carbonyl CORMs that meet all set of parameters for their applicability as therapeutics in clinic has never been reached and researchers are looking for more biocompatible formulations. The work on encapsulated CORMs showed a big improvement in terms of solubility, bioavailability, low toxicity and site-specific drug uptake. Indeed, metal CORMs can be bonded (covalent bond, electrostatic force, hydrogen bond, hydrophobic force exc.) to macromolecular carriers such as micelles, nanoparticles, copolymer, proteins and dendrimers[67,96] These systems overtake a traditional metal CORM especially when a long-term application is needed and allow a precise control of delivery in a specific tissue especially when linked to prodrugs such as ET-CORMs or photoCORMs. For example, it was shown that CORM-2 instability and solubility in blood circulation and off-target release can be fixed using CORM-2-loaded micelles composed of styrene-maleic acid copolymer.[118] In another study, Fernandes et al.[119] improved the cellular uptake, stability and solubility of CORM-3 by conjugation with gold nanoparticles. By doing so, the wound-healing and anti-inflammatory effects of CORM-3 were increased due a higher amount of CO released inside the cell. The use of encapsulation may reduce the toxicity related to the transition metal contained in CORMs. Overall, the introduction of macromolecular carriers can prevent CO diffusion, improve the stability of CORMs and carry CORMs to the act of site. Another key characteristic is their ability to avoid the liver's rapid metabolism. However, there is still some uncertainty on the biological effects of these carriers towards cells and how affected is the mechanism of CO release of CORMs.[117]

Noteworthy, metal CORMs toxicity should not be considered only relative to the metal center since toxicological assays give contradictory results. Indeed, other metal-based formulations are being developed or are currently in use in clinic.[120] The potential toxicity of the metal has been questioned as, like for other factors, is dependent on the dose and time of exposure.[58] However, there is no doubt that the presence of a transition metal put constraints to their pharmaceutical development due to some uncertainty to long-term effects. In order to avoid metal-related concerns there is a strong urge to create further CORMs. The creation of organic CO-prodrugs devoid of metals would fall under this category. Generally, the use of metals already physiologically present in the human body such as Fe, Mn, Co, Cr and Ru is ideal in metal CORMs design and it is crucial to fully investigate the toxicity profile of metal-base CORMs to see if the toxicity derives from the metal itself or other factors (e.g., unspecific release of CO).[121]

Fine tuning of CO release from metal CORMs is required but quantifying it both *in vitro* and *in vivo* is also an important task. *In vitro*, the deoxymyoglobin carbonylation assay has been widely used and is the first procedure of choice for initial screening of CORM activity. In this experiment, reduced deoxymyoglobin combines with CO from CORMs to generate carbonmonoxy myoglobin, which absorbs light at 557 nm in absorbance spectroscopy (MbCO). While the old absorbance at 557 nm declines and finally vanishes, two new absorption bands of MbCO rise at 540 and 577 nm. Therefore, spectrophotometers may be used to track and measure this process. For this test to be accurate the use of sodium dithionite is needed, which then it must be removed before reduced deoxymyoglobin is incubated with the CORM solution since it may trigger CO release.[94,122] There is still considerable doubt regarding the interaction of myoglobin with CO, whether it occurs with free CO released in solution or in a coupled process upon myoglobin-metal-CORM interaction. An additional challenge may show up during the use of this method on photoCORMs, which could give an overlap of absorption bands with complicated spectra to solve.[123] For detection of CO *in vivo*, fluorescent probes are available. They can detect low amount of CO but are not suitable for short-term measurements.[124] Although other sensing methods have been used (e.g., electrochemical sensors, gas chromatography and gas-phase

IR spectroscopy), there is still an urgent need for further improvement in CO detection to enable a more predictable behavior of metal CORMs in the human body.[116]

Taken together, many challenges hamper metal carbonyl CORMs clinical application and they vary from the CO release rates to the various physicochemical characteristics, such as permeability and solubility. These days, along with medicinal chemistry efforts to improve these characteristics, research is proceeding towards conjugated CORMs system since so far has brought many benefits in terms of CO delivery, toxicity and biocompatibility. However, there are still some concerns to be addressed concerning sensitivity of prodrugs upon stimulus (e.g., photoCORMs) and their efficacy along with the unknown biological effects of these carriers. Then, also role of the metal center after CO release needs more in-depth exploration. The determination of the kinetics of CO release is also of great importance to facilitate CORM clinical usage and understand better CORM biology. But despite the progress made in precise quantification and imaging of CO release in cells and tissues, there is still some to be settled, which require further investigations.

## 1.8 Objectives of Our Study

Tendinopathies are common musculoskeletal conditions characterized by persistent low-grade inflammation and tissue degradation. They account for a significant portion of the worldwide healthcare burden in chronic inflammatory disorders and there is an urgent need for the development of an effective treatment. Evidence suggests that $PGE_2$ expression plays a crucial role in maintaining inflammation and pain.[125,126] The anti-inflammatory potential of CO can potentially improve the therapeutic management of tendinopathies, and therefore it offers a valid alternative to the current treatments.[97] In this context, aim of our study is to develop new dual-active CORMs where the cytoprotective effect of released CO is accompanied by $PGE_2$ reduction following COX inhibition.

## References


(1) Olson, K. R.; Donald, J. A.; Dombkowski, R. A.; Perry, S. F. Evolutionary and Comparative Aspects of Nitric Oxide, Carbon Monoxide and Hydrogen Sulfide. *Respir Physiol Neurobiol* **2012**, *184* (2), 117–129. https://doi.org/10.1016/j.resp.2012.04.004.

(2) Gantner, B. N.; LaFond, K. M.; Bonini, M. G. Nitric Oxide in Cellular Adaptation and Disease. *Redox Biol* **2020**, *34*, 101550. https://doi.org/10.1016/j.redox.2020.101550.

(3) Xiao, Q.; Ying, J.; Xiang, L.; Zhang, C. The Biologic Effect of Hydrogen Sulfide and Its Function in Various Diseases. *Medicine* **2018**, *97* (44), e13065. https://doi.org/10.1097/MD.0000000000013065.

(4) Adach, W.; Błaszczyk, M.; Olas, B. Carbon Monoxide and Its Donors - Chemical and Biological Properties. *Chem Biol Interact* **2020**, *318*, 108973. https://doi.org/10.1016/j.cbi.2020.108973.

(5) Lee, C. T.; Comer, J.; Herndon, C.; Leung, N.; Pavlova, A.; Swift, R. v.; Tung, C.; Rowley, C. N.; Amaro, R. E.; Chipot, C.; Wang, Y.; Gumbart, J. C. Simulation-Based Approaches for Determining Membrane Permeability of Small Compounds. *J Chem Inf Model* **2016**, *56* (4), 721–733. https://doi.org/10.1021/acs.jcim.6b00022.

(6) Riahi, S.; Rowley, C. N. Why Can Hydrogen Sulfide Permeate Cell Membranes? *J Am Chem Soc* **2014**, *136* (43), 15111–15113. https://doi.org/10.1021/ja508063s.

(7) Ryter, S. W.; Alam, J.; Choi, A. M. K. Heme Oxygenase-1/Carbon Monoxide: From Basic Science to Therapeutic Applications. *Physiol Rev* **2006**, *86* (2), 583–650. https://doi.org/10.1152/physrev.00011.2005.

(8) Rőszer, T. Nitric Oxide Signaling and Nitrosative Stress in the Musculoskeletal System. In *Systems Biology of Free Radicals and Antioxidants*; Springer Berlin Heidelberg: Berlin, Heidelberg, 2014; pp 2895–2926. https://doi.org/10.1007/978-3-642-30018-9_1.

(9) Roy, B.; Garthwaite, J. Nitric Oxide Activation of Guanylyl Cyclase in Cells Revisited. *Proceedings of the National Academy of Sciences* **2006**, *103* (32), 12185–12190. https://doi.org/10.1073/pnas.0602544103.

(10) Chen, Y.; Yuan, S.; Cao, Y.; Kong, G.; Jiang, F.; Li, Y.; Wang, Q.; Tang, M.; Zhang, Q.; Wang, Q.; Liu, L. Gasotransmitters: Potential Therapeutic Molecules of Fibrotic Diseases. *Oxid Med Cell Longev* **2021**, *2021*, 1–18. https://doi.org/10.1155/2021/3206982.

(11) Hsu, C.-N.; Tain, Y.-L. Gasotransmitters for the Therapeutic Prevention of Hypertension and Kidney Disease. *Int J Mol Sci* **2021**, *22* (15), 7808. https://doi.org/10.3390/ijms22157808.

(12) Wang, L.; Xie, X.; Ke, B.; Huang, W.; Jiang, X.; He, G. Recent Advances on Endogenous Gasotransmitters in Inflammatory Dermatological Disorders. *J Adv Res* **2022**, *38*, 261–274. https://doi.org/10.1016/j.jare.2021.08.012.

(13) Mir, J. M.; Maurya, R. C. A Gentle Introduction to Gasotransmitters with Special Reference to Nitric Oxide: Biological and Chemical Implications. *Reviews in Inorganic Chemistry* **2018**, *38* (4), 193–220. https://doi.org/10.1515/revic-2018-0011.

(14) Nowaczyk, A.; Kowalska, M.; Nowaczyk, J.; Grześk, G. Carbon Monoxide and Nitric Oxide as Examples of the Youngest Class of Transmitters. *Int J Mol Sci* **2021**, *22* (11), 6029. https://doi.org/10.3390/ijms22116029.

(15) Wang, R. Chapter 1. Overview of Gasotransmitters and the Related Signaling Network; 2018; pp 1–28. https://doi.org/10.1039/9781788013000-00001.

(16) Hopper, C. P.; Zambrana, P. N.; Goebel, U.; Wollborn, J. A Brief History of Carbon Monoxide and Its Therapeutic Origins. *Nitric Oxide* **2021**, *111–112*, 45–63. https://doi.org/10.1016/j.niox.2021.04.001.

(17) Qiao, L.; Zhang, N.; Huang, J.; Yang, X. Carbon Monoxide as a Promising Molecule to Promote Nerve Regeneration after Traumatic Brain Injury. *Med Gas Res* **2017**, *7* (1), 45. https://doi.org/10.4103/2045-9912.202909.

(18) Wang, R. Two's Company, Three's a Crowd: Can H2S Be the Third Endogenous Gaseous Transmitter? *The FASEB Journal* **2002**, *16* (13), 1792–1798. https://doi.org/10.1096/fj.02-0211hyp.

(19) Wang, R. Gasotransmitters: Growing Pains and Joys. *Trends Biochem Sci* **2014**, *39* (5), 227–232. https://doi.org/10.1016/j.tibs.2014.03.003.

(20) European Network on Gasotransmitters. *Objectives*.

(21) Kim, H.; Doan, V. D.; Cho, W. J.; Valero, R.; Aliakbar Tehrani, Z.; Madridejos, J. M. L.; Kim, K. S. Intriguing Electrostatic Potential of CO: Negative Bond-Ends and Positive Bond-Cylindrical-Surface. *Sci Rep* **2015**, *5* (1), 16307. https://doi.org/10.1038/srep16307.

(22) Romão, C. C.; Blättler, W. A.; Seixas, J. D.; Bernardes, G. J. L. Developing Drug Molecules for Therapy with Carbon Monoxide. *Chem Soc Rev* **2012**, *41* (9), 3571. https://doi.org/10.1039/c2cs15317c.

(23) Slebos, D.-J.; Ryter, S. W.; Choi, A. M. Heme Oxygenase-1 and Carbon Monoxide in Pulmonary Medicine. *Respir Res* **2003**, *4* (1), 7. https://doi.org/10.1186/1465-9921-4-7.

(24) Rivera, M.; Rodríguez, J. C. The Dual Role of Heme as Cofactor and Substrate in the Biosynthesis of Carbon Monoxide. In *Metal-Carbon Bonds in Enzymes and Cofactors*; DE GRUYTER, 2015; pp 241–294. https://doi.org/10.1515/9783110436587-012.

(25) Siracusa, R.; Schaufler, A.; Calabrese, V.; Fuller, P. M.; Otterbein, L. E. Carbon Monoxide: From Poison to Clinical Trials. *Trends Pharmacol Sci* **2021**, *42* (5), 329–339. https://doi.org/10.1016/j.tips.2021.02.003.

(26) Ryter, S. W. Significance of Heme and Heme Degradation in the Pathogenesis of Acute Lung and Inflammatory Disorders. *Int J Mol Sci* **2021**, *22* (11), 5509. https://doi.org/10.3390/ijms22115509.

(27) Osiak, W.; Wątroba, S.; Kapka-Skrzypczak, L.; Kurzepa, J. Two Faces of Heme Catabolic Pathway in Newborns: A Potential Role of Bilirubin and Carbon Monoxide in Neonatal Inflammatory Diseases. *Oxid Med Cell Longev* **2020**, *2020*, 1–14. https://doi.org/10.1155/2020/7140496.

(28) di Pietro, C.; Öz, H. H.; Murray, T. S.; Bruscia, E. M. Targeting the Heme Oxygenase 1/Carbon Monoxide Pathway to Resolve Lung Hyper-Inflammation and Restore a Regulated Immune Response in Cystic Fibrosis. *Front Pharmacol* **2020**, *11*. https://doi.org/10.3389/fphar.2020.01059.

(29) Stewart, R. D.; Fisher, T. N.; Hosko, M. J.; Peterson, J. E.; Baretta, E. D.; Dodd, H. C. Carboxyhemoglobin Elevation after Exposure to Dichloromethane. *Science (1979)* **1972**, *176* (4032), 295–296. https://doi.org/10.1126/science.176.4032.295.

(30) Takehito, T.; Yoshifumi, M. Metabolism of Dichloromethane and the Subsequent Binding of Its Product, Carbon Monoxide, to Cytochrome P-450 in Perfused Rat Liver. *Toxicol Lett* **1988**, *40* (1), 93–96. https://doi.org/10.1016/0378-4274(88)90187-7.

(31) Amsel, J.; Soden, K. J.; Sielken, R. L.; Valdez-Flora, C. Observed versus Predicted Carboxyhemoglobin Levels in Cellulose Triacetate Workers Exposed to Methylene Chloride. *Am J Ind Med* **2001**, *40* (2), 180–191. https://doi.org/10.1002/ajim.1086.

(32) Thom, S. R. Carbon Monoxide-Mediated Brain Lipid Peroxidation in the Rat. *J Appl Physiol* **1990**, *68* (3), 997–1003. https://doi.org/10.1152/jappl.1990.68.3.997.

(33) Archakov, A. I.; Karuzina, I. I.; Petushkova, N. A.; Lisitsa, A. V.; Zgoda, V. G. Production of Carbon Monoxide by Cytochrome P450 during Iron-Dependent Lipid Peroxidation. *Toxicology in Vitro* **2002**, *16* (1), 1–10. https://doi.org/10.1016/S0887-2333(01)00094-7.

(34) Zavorsky, G. S.; Tesler, J.; Rucker, J.; Fedorko, L.; Duffin, J.; Fisher, J. A. Rates of Carbon Monoxide Elimination in Males and Females. *Physiol Rep* **2014**, *2* (12), e12237. https://doi.org/10.14814/phy2.12237.

(35) Luomanmaki, K.; Coburn, R. Effects of Metabolism and Distribution of Carbon Monoxide on Blood and Body Stores. *American Journal of Physiology-Legacy Content* **1969**, *217* (2), 354–363. https://doi.org/10.1152/ajplegacy.1969.217.2.354.

(36) Loboda, A.; Jozkowicz, A.; Dulak, J. HO-1/CO System in Tumor Growth, Angiogenesis and Metabolism — Targeting HO-1 as an Anti-Tumor Therapy. *Vascul Pharmacol* **2015**, *74*, 11–22. https://doi.org/10.1016/j.vph.2015.09.004.

(37) Taylor, C. T.; Colgan, S. P. Regulation of Immunity and Inflammation by Hypoxia in Immunological Niches. *Nat Rev Immunol* **2017**, *17* (12), 774–785. https://doi.org/10.1038/nri.2017.103.

(38) Jung, E.; Koh, S.-H.; Yoo, M.; Choi, Y. K. Regenerative Potential of Carbon Monoxide in Adult Neural Circuits of the Central Nervous System. *Int J Mol Sci* **2020**, *21* (7), 2273. https://doi.org/10.3390/ijms21072273.

(39) Motterlini, R.; Foresti, R. Biological Signaling by Carbon Monoxide and Carbon Monoxide-Releasing Molecules. *American Journal of Physiology-Cell Physiology* **2017**, *312* (3), C302–C313. https://doi.org/10.1152/ajpcell.00360.2016.

(40) Lu, W.; Yang, X.; Wang, B. Carbon Monoxide Signaling and Soluble Guanylyl Cyclase: Facts, Myths, and Intriguing Possibilities. *Biochem Pharmacol* **2022**, *200*, 115041. https://doi.org/10.1016/j.bcp.2022.115041.

(41) Choi, Y. K.; Kim, Y.-M. Regulation of Endothelial and Vascular Functions by Carbon Monoxide via Crosstalk With Nitric Oxide. *Front Cardiovasc Med* **2021**, *8*. https://doi.org/10.3389/fcvm.2021.649630.

(42) Hartsfield, C. L. Cross Talk Between Carbon Monoxide and Nitric Oxide. *Antioxid Redox Signal* **2002**, *4* (2), 301–307. https://doi.org/10.1089/152308602753666352.

(43) Wang, R.; Wang, Z.; Wu, L. Carbon Monoxide-Induced Vasorelaxation and the Underlying Mechanisms. *Br J Pharmacol* **1997**, *121* (5), 927–934. https://doi.org/10.1038/sj.bjp.0701222.

(44) Zhang, D.; Krause, B. M.; Schmalz, H.-G.; Wohlfart, P.; Yard, B. A.; Schubert, R. ET-CORM Mediated Vasorelaxation of Small Mesenteric Arteries: Involvement of Kv7 Potassium Channels. *Front Pharmacol* **2021**, *12*. https://doi.org/10.3389/fphar.2021.702392.

(45) Basuroy, S.; Tcheranova, D.; Bhattacharya, S.; Leffler, C. W.; Parfenova, H. Nox4 NADPH Oxidase-Derived Reactive Oxygen Species, via Endogenous Carbon Monoxide, Promote Survival of Brain Endothelial Cells during TNF-$\alpha$-Induced Apoptosis. *American Journal of Physiology-Cell Physiology* **2011**, *300* (2), C256–C265. https://doi.org/10.1152/ajpcell.00272.2010.

(46) Choi, Y. K.; Por, E. D.; Kwon, Y.-G.; Kim, Y.-M. Regulation of ROS Production and Vascular Function by Carbon Monoxide. *Oxid Med Cell Longev* **2012**, *2012*, 1–17. https://doi.org/10.1155/2012/794237.

(47) Alonso, J.-R.; Cardellach, F.; López, S.; Casademont, J.; Miró, Ò. Carbon Monoxide Specifically Inhibits Cytochrome C Oxidase of Human Mitochondrial Respiratory Chain. *Pharmacol Toxicol* **2003**, *93* (3), 142–146. https://doi.org/10.1034/j.1600-0773.2003.930306.x.

(48) Nakao, A.; Faleo, G.; Shimizu, H.; Nakahira, K.; Kohmoto, J.; Sugimoto, R.; Choi, A. M. K.; McCurry, K. R.; Takahashi, T.; Murase, N. Ex Vivo Carbon Monoxide Prevents Cytochrome P450 Degradation and Ischemia/Reperfusion Injury of Kidney Grafts. *Kidney Int* **2008**, *74* (8), 1009–1016. https://doi.org/10.1038/ki.2008.342.

(49) Korbecki, J.; Bobiński, R.; Dutka, M. Self-Regulation of the Inflammatory Response by Peroxisome Proliferator-Activated Receptors. *Inflammation Research* **2019**, *68* (6), 443–458. https://doi.org/10.1007/s00011-019-01231-1.

(50) Morse, D.; Pischke, S. E.; Zhou, Z.; Davis, R. J.; Flavell, R. A.; Loop, T.; Otterbein, S. L.; Otterbein, L. E.; Choi, A. M. K. Suppression of Inflammatory Cytokine Production by Carbon Monoxide Involves the JNK Pathway and AP-1. *Journal of Biological Chemistry* **2003**, *278* (39), 36993–36998. https://doi.org/10.1074/jbc.M302942200.

(51) Ning, W.; Choi, A. M. K.; Li, C. Carbon Monoxide Inhibits IL-17-Induced IL-6 Production through the MAPK Pathway in Human Pulmonary Epithelial Cells. *American Journal of Physiology-Lung Cellular and Molecular Physiology* **2005**, *289* (2), L268–L273. https://doi.org/10.1152/ajplung.00168.2004.

(52) Otterbein, L. E.; Bach, F. H.; Alam, J.; Soares, M.; Tao Lu, H.; Wysk, M.; Davis, R. J.; Flavell, R. A.; Choi, A. M. K. Carbon Monoxide Has Anti-Inflammatory Effects Involving the Mitogen-Activated Protein Kinase Pathway. *Nat Med* **2000**, *6* (4), 422–428. https://doi.org/10.1038/74680.

(53) Ryter, S. W.; Ma, K. C.; Choi, A. M. K. Carbon Monoxide in Lung Cell Physiology and Disease. *American Journal of Physiology-Cell Physiology* **2018**, *314* (2), C211–C227. https://doi.org/10.1152/ajpcell.00022.2017.

(54) Rocuts, F.; Ma, Y.; Zhang, X.; Gao, W.; Yue, Y.; Vartanian, T.; Wang, H. Carbon Monoxide Suppresses Membrane Expression of TLR4 via Myeloid Differentiation Factor-2 in BTC3 Cells. *The Journal of Immunology* **2010**, *185* (4), 2134–2139. https://doi.org/10.4049/jimmunol.0902782.

(55) Scandura, G.; Giallongo, C.; Puglisi, F.; Romano, A.; Parrinello, N. L.; Zuppelli, T.; Longhitano, L.; Giallongo, S.; di Rosa, M.; Musumeci, G.; Motterlini, R.; Foresti, R.; Palumbo, G. A.; Li Volti, G.; di Raimondo, F.; Tibullo, D. TLR4 Signaling and Heme Oxygenase-1/Carbon Monoxide Pathway Crosstalk Induces Resiliency of Myeloma Plasma Cells to Bortezomib Treatment. *Antioxidants* **2022**, *11* (4), 767. https://doi.org/10.3390/antiox11040767.

(56) Nakahira, K.; Kim, H. P.; Geng, X. H.; Nakao, A.; Wang, X.; Murase, N.; Drain, P. F.; Wang, X.; Sasidhar, M.; Nabel, E. G.; Takahashi, T.; Lukacs, N. W.; Ryter, S. W.; Morita, K.; Choi, A. M. K. Carbon Monoxide Differentially Inhibits TLR Signaling Pathways by Regulating ROS-Induced Trafficking of TLRs to Lipid Rafts. *Journal of Experimental Medicine* **2006**, *203* (10), 2377–2389. https://doi.org/10.1084/jem.20060845.

(57) Ryter, S. Therapeutic Potential of Heme Oxygenase-1 and Carbon Monoxide in Acute Organ Injury, Critical Illness, and Inflammatory Disorders. *Antioxidants* **2020**, *9* (11), 1153. https://doi.org/10.3390/antiox9111153.

(58) Stucki, D.; Stahl, W. Carbon Monoxide – beyond Toxicity? *Toxicol Lett* **2020**, *333*, 251–260. https://doi.org/10.1016/j.toxlet.2020.08.010.

(59) Bilska-Wilkosz, A.; Górny, M.; Iciek, M. Biological and Pharmacological Properties of Carbon Monoxide: A General Overview. *Oxygen* **2022**, *2* (2), 130–151. https://doi.org/10.3390/oxygen2020012.

(60) Chhikara, M.; Wang, S.; Kern, S. J.; Ferreyra, G. A.; Barb, J. J.; Munson, P. J.; Danner, R. L. Carbon Monoxide Blocks Lipopolysaccharide-Induced Gene Expression by Interfering with Proximal TLR4 to NF-KB Signal Transduction in Human Monocytes. *PLoS One* **2009**, *4* (12), e8139. https://doi.org/10.1371/journal.pone.0008139.

(61) Deshmukh, R.; Harwansh, R. K.; Bandyopadhyay, N.; Bandopadhyay, S.; Kumar, P. Pharmacology of Gasotransmitters (Nitric Oxide and Carbon Monoxide) and Their Action. In *Frontiers in Pharmacology of Neurotransmitters*; Springer Singapore: Singapore, 2020; pp 579–617. https://doi.org/10.1007/978-981-15-3556-7_17.

(62) Koka Yildiz, D. S.; Eroglu, E.; Koka, H. B.; Erol, K. Gastroprotective Effects of Hydrogen Sulfide, Carbon Monoxide and Nitric Oxide on an Experimental Ulcer Model in Rats. *Journal of Surgery and Medicine* **2021**, *5* (10), 1024–1028. https://doi.org/10.28982/josam.885628.

(63) Queiroga, C. S. F.; Vercelli, A.; Vieira, H. L. A. Carbon Monoxide and the CNS: Challenges and Achievements. *Br J Pharmacol* **2015**, *172* (6), 1533–1545. https://doi.org/10.1111/bph.12729.

(64) Pena, A. C.; Pamplona, A. Heme Oxygenase-1, Carbon Monoxide, and Malaria – The Interplay of Chemistry and Biology. *Coord Chem Rev* **2022**, *453*, 214285. https://doi.org/10.1016/j.ccr.2021.214285.

(65) Dugbartey, G. J. Carbon Monoxide as an Emerging Pharmacological Tool to Improve Lung and Liver Transplantation Protocols. *Biochem Pharmacol* **2021**, *193*, 114752. https://doi.org/10.1016/j.bcp.2021.114752.

(66) Chu, L. M.; Shaefi, S.; Byrne, J. D.; Alves de Souza, R. W.; Otterbein, L. E. Carbon Monoxide and a Change of Heart. *Redox Biol* **2021**, *48*, 102183. https://doi.org/10.1016/j.redox.2021.102183.

(67) Zhou, Y.; Yu, W.; Cao, J.; Gao, H. Harnessing Carbon Monoxide-Releasing Platforms for Cancer Therapy. *Biomaterials* **2020**, *255*, 120193. https://doi.org/10.1016/j.biomaterials.2020.120193.

(68) Yang, X.; Caestecker, M.; Otterbein, L. E.; Wang, B. Carbon Monoxide: An Emerging Therapy for Acute Kidney Injury. *Med Res Rev* **2020**, *40* (4), 1147–1177. https://doi.org/10.1002/med.21650.

(69) Kwong, K. K.; Chan, S. The Role of Carbon Monoxide and Heme Oxygenase-1 in COVID-19. *Toxicol Rep* **2020**, *7*, 1170–1171. https://doi.org/10.1016/j.toxrep.2020.08.027.

(70) Ryter, S. W.; Choi, A. M. K. Heme Oxygenase-1/Carbon Monoxide. *Am J Respir Cell Mol Biol* **2009**, *41* (3), 251–260. https://doi.org/10.1165/rcmb.2009-0170TR.

(71) Constantin, M.; Choi, A. J. S.; Cloonan, S. M.; Ryter, S. W. Therapeutic Potential of Heme Oxygenase-1/Carbon Monoxide in Lung Disease. *Int J Hypertens* **2012**, *2012*, 1–19. https://doi.org/10.1155/2012/859235.

(72) Motterlini, R.; Haas, B.; Foresti, R. Emerging Concepts on the Anti-Inflammatory Actions of Carbon Monoxide-Releasing Molecules (CO-RMs). *Med Gas Res* **2012**, *2* (1), 28. https://doi.org/10.1186/2045-9912-2-28.

(73) Castruccio Castracani, C.; Longhitano, L.; Distefano, A.; di Rosa, M.; Pittalà, V.; Lupo, G.; Caruso, M.; Corona, D.; Tibullo, D.; Li Volti, G. Heme Oxygenase-1 and Carbon Monoxide Regulate Growth and Progression in Glioblastoma Cells. *Mol Neurobiol* **2020**, *57* (5), 2436–2446. https://doi.org/10.1007/s12035-020-01869-7.

(74) Pol, O. The Role of Carbon Monoxide, Heme Oxygenase 1, and the Nrf2 Transcription Factor in the Modulation of Chronic Pain and Their Interactions with Opioids and Cannabinoids. *Med Res Rev* **2021**, *41* (1), 136–155. https://doi.org/10.1002/med.21726.

(75) Otterbein, L. E.; Mantell, L. L.; Choi, A. M. K. Carbon Monoxide Provides Protection against Hyperoxic Lung Injury. *American Journal of Physiology-Lung Cellular and Molecular Physiology* **1999**, *276* (4), L688–L694. https://doi.org/10.1152/ajplung.1999.276.4.L688.

(76) Mazzola, S.; Forni, M.; Albertini, M.; Bacci, M. L.; Zannoni, A.; Gentilini, F.; Lavitrano, M.; Bach, F. H.; Otterbein, L. E.; Clement, M. G. Carbon Monoxide Pretreatment Prevents Respiratory Derangement and Ameliorates Hyperacute Endotoxic Shock in Pigs. *The FASEB Journal* **2005**, *19* (14), 2045–2047. https://doi.org/10.1096/fj.05-3782fje.

(77) Sarady, J. K.; Zuckerbraun, B. S.; Bilban, M.; Wagner, O.; Usheva, A.; Liu, F.; Ifedigbo, E.; Zamora, R.; Choi, A. M. K.; Otterbein, L. E. Carbon Monoxide Protection against Endotoxic Shock Involves Reciprocal Effects on INOS in the Lung and Liver. *The FASEB Journal* **2004**, *18* (7), 854–856. https://doi.org/10.1096/fj.03-0643fje.

(78) Dugbartey, G. J.; Alornyo, K. K.; Luke, P. P. W.; Sener, A. Application of Carbon Monoxide in Kidney and Heart Transplantation: A Novel Pharmacological Strategy for a Broader Use of Suboptimal Renal and Cardiac Grafts. *Pharmacol Res* **2021**, *173*, 105883. https://doi.org/10.1016/j.phrs.2021.105883.

(79) Lee, S.; Lee, S.-J.; Coronata, A. A.; Fredenburgh, L. E.; Chung, S. W.; Perrella, M. A.; Nakahira, K.; Ryter, S. W.; Choi, A. M. K. Carbon Monoxide Confers Protection in Sepsis by Enhancing Beclin 1-Dependent Autophagy and Phagocytosis. *Antioxid Redox Signal* **2014**, *20* (3), 432–442. https://doi.org/10.1089/ars.2013.5368.

(80) Wang, P.; Huang, J.; Li, Y.; Chang, R.; Wu, H.; Lin, J.; Huang, Z. Exogenous Carbon Monoxide Decreases Sepsis-Induced Acute Kidney Injury and Inhibits NLRP3 Inflammasome Activation in Rats. *Int J Mol Sci* **2015**, *16* (9), 20595–20608. https://doi.org/10.3390/ijms160920595.

(81) Iwasashi, H.; Suzuki, M.; Unno, M.; Utiyama, T.; Oikawa, M.; Kondo, N.; Matsuno, S. Inhibition of Heme Oxygenase Ameliorates Sepsis-Induced Liver Dysfunction in Rats. *Surg Today* **2003**, *33* (1), 30–38. https://doi.org/10.1007/s005950300005.

(82) Fredenburgh, L. E.; Perrella, M. A.; Barragan-Bradford, D.; Hess, D. R.; Peters, E.; Welty-Wolf, K. E.; Kraft, B. D.; Harris, R. S.; Maurer, R.; Nakahira, K.; Oromendia, C.; Davies, J. D.; Higuera, A.; Schiffer, K. T.; Englert, J. A.; Dieffenbach, P. B.; Berlin, D. A.; Lagambina, S.; Bouthot, M.; Sullivan, A. I.; Nuccio, P. F.; Kone, M. T.; Malik, M. J.; Porras, M. A. P.; Finkelsztein, E.; Winkler, T.; Hurwitz, S.; Serhan, C. N.; Piantadosi, C. A.; Baron, R. M.; Thompson, B. T.; Choi, A. M. K. A Phase I Trial of Low-Dose Inhaled Carbon Monoxide in Sepsis-Induced ARDS. *JCI Insight* **2018**, *3* (23). https://doi.org/10.1172/jci.insight.124039.

(83) Rosas, I. O.; Goldberg, H. J.; Collard, H. R.; El-Chemaly, S.; Flaherty, K.; Hunninghake, G. M.; Lasky, J. A.; Lederer, D. J.; Machado, R.; Martinez, F. J.; Maurer, R.; Teller, D.; Noth, I.; Peters, E.; Raghu, G.; Garcia, J. G. N.; Choi, A. M. K. A Phase II Clinical Trial of Low-Dose Inhaled Carbon Monoxide in Idiopathic Pulmonary Fibrosis. *Chest* **2018**, *153* (1), 94–104. https://doi.org/10.1016/j.chest.2017.09.052.

(84) Ferrandiz, M. L.; Maicas, N.; Garcia-Arnandis, I.; Terencio, M. C.; Motterlini, R.; Devesa, I.; Joosten, L. A. B.; van den Berg, W. B.; Alcaraz, M. J. Treatment with a CO-Releasing Molecule (CORM-3) Reduces Joint Inflammation and Erosion in Murine Collagen-Induced Arthritis. *Ann Rheum Dis* **2007**, *67* (9), 1211–1217. https://doi.org/10.1136/ard.2007.082412.

(85) Berrino, E.; Milazzo, L.; Micheli, L.; Vullo, D.; Angeli, A.; Bozdag, M.; Nocentini, A.; Menicatti, M.; Bartolucci, G.; di Cesare Mannelli, L.; Ghelardini, C.; Supuran, C. T.; Carta, F. Synthesis and Evaluation of Carbonic Anhydrase Inhibitors with Carbon Monoxide Releasing Properties for the Management of Rheumatoid Arthritis. *J Med Chem* **2019**, *62* (15), 7233–7249. https://doi.org/10.1021/acs.jmedchem.9b00845.

(86) Bakalarz, D.; Surmiak, M.; Yang, X.; Wójcik, D.; Korbut, E.; Śliwowski, Z.; Ginter, G.; Buszewicz, G.; Brzozowski, T.; Cieszkowski, J.; Głowacka, U.; Magierowska, K.; Pan, Z.; Wang, B.; Magierowski, M. Organic Carbon Monoxide Prodrug, BW-CO-111, in Protection against Chemically-Induced Gastric Mucosal Damage. *Acta Pharm Sin B* **2021**, *11* (2), 456–475. https://doi.org/10.1016/j.apsb.2020.08.005.

(87) Damasceno, R. O. S.; Soares, P. M. G.; Barbosa, A. L. dos R.; Nicolau, L. A. D.; Medeiros, J.-V. R.; Souza, M. H. L. P. Modulatory Role of Carbon Monoxide on the Inflammatory

Response and Oxidative Stress Linked to Gastrointestinal Disorders. *Antioxid Redox Signal* **2022**, *37* (1–3), 98–114. https://doi.org/10.1089/ars.2020.8223.

(88) Byrne, J. D.; Gallo, D.; Boyce, H.; Becker, S. L.; Kezar, K. M.; Cotoia, A. T.; Feig, V. R.; Lopes, A.; Csizmadia, E.; Longhi, M. S.; Lee, J. S.; Kim, H.; Wentworth, A. J.; Shankar, S.; Lee, G. R.; Bi, J.; Witt, E.; Ishida, K.; Hayward, A.; Kuosmanen, J. L. P.; Jenkins, J.; Wainer, J.; Aragon, A.; Wong, K.; Steiger, C.; Jeck, W. R.; Bosch, D. E.; Coleman, M. C.; Spitz, D. R.; Tift, M.; Langer, R.; Otterbein, L. E.; Traverso, G. Delivery of Therapeutic Carbon Monoxide by Gas-Entrapping Materials. *Sci Transl Med* **2022**, *14* (651). https://doi.org/10.1126/scitranslmed.abl4135.

(89) Campbell, N. K.; Fitzgerald, H. K.; Dunne, A. Regulation of Inflammation by the Antioxidant Haem Oxygenase 1. *Nat Rev Immunol* **2021**, *21* (7), 411–425. https://doi.org/10.1038/s41577-020-00491-x.

(90) Ryter, S. W. Carbon Monoxide in Lung Injury and Disease. In *Carbon Monoxide in Drug Discovery*; Wiley, 2022; pp 360–376. https://doi.org/10.1002/9781119783435.ch20.

(91) National Institutes of Health. *ClinicalTrials.gov*. ClinicalTrials.gov.

(92) Gentile, M. A. Inhaled Medical Gases: More to Breathe Than Oxygen. *Respir Care* **2011**, *56* (9), 1341–1359. https://doi.org/10.4187/respcare.01442.

(93) Motterlini, R.; Clark, J. E.; Foresti, R.; Sarathchandra, P.; Mann, B. E.; Green, C. J. Carbon Monoxide-Releasing Molecules. *Circ Res* **2002**, *90* (2). https://doi.org/10.1161/hh0202.104530.

(94) Kautz, A. C.; Kunz, P. C.; Janiak, C. CO-Releasing Molecule (CORM) Conjugate Systems. *Dalton Transactions* **2016**, *45* (45), 18045–18063. https://doi.org/10.1039/C6DT03515A.

(95) Cavicchioli, F.; Cesarotti, I. M.; Fangman, M.; Lua, J.; Hautamaki, R.; Doré, S. Carbon Monoxide Therapy Using Hybrid Carbon Monoxide-Releasing/Nrf2-Inducing Molecules through a Neuroprotective Lens. *Chemistry (Easton)* **2021**, *3* (3), 800–817. https://doi.org/10.3390/chemistry3030057.

(96) Faizan, M.; Muhammad, N.; Niazi, K. U. K.; Hu, Y.; Wang, Y.; Wu, Y.; Sun, H.; Liu, R.; Dong, W.; Zhang, W.; Gao, Z. CO-Releasing Materials: An Emphasis on Therapeutic Implications, as Release and Subsequent Cytotoxicity Are the Part of Therapy. *Materials* **2019**, *12* (10), 1643. https://doi.org/10.3390/ma12101643.

(97) Berrino, E.; Carradori, S.; Angeli, A.; Carta, F.; Supuran, C. T.; Guglielmi, P.; Coletti, C.; Paciotti, R.; Schweikl, H.; Maestrelli, F.; Cerbai, E.; Gallorini, M. Dual Carbonic Anhydrase IX/XII Inhibitors and Carbon Monoxide Releasing Molecules Modulate LPS-Mediated Inflammation in Mouse Macrophages. *Antioxidants* **2021**, *10* (1), 56. https://doi.org/10.3390/antiox10010056.

(98) Zhu, J.; Ouyang, A.; He, J.; Xie, J.; Banerjee, S.; Zhang, Q.; Zhang, P. An Ultrasound Activated Cyanine-Rhenium(i) Complex for Sonodynamic and Gas Synergistic Therapy. *Chemical Communications* **2022**, *58* (20), 3314–3317. https://doi.org/10.1039/D1CC06769A.

(99) Lazarus, L. S.; Benninghoff, A. D.; Berreau, L. M. Development of Triggerable, Trackable, and Targetable Carbon Monoxide Releasing Molecules. *Acc Chem Res* **2020**, *53* (10), 2273–2285. https://doi.org/10.1021/acs.accounts.0c00402.

(100) Kunz, P. C.; Meyer, H.; Barthel, J.; Sollazzo, S.; Schmidt, A. M.; Janiak, C. Metal Carbonyls Supported on Iron Oxide Nanoparticles to Trigger the CO-Gasotransmitter Release by Magnetic Heating. *Chemical Communications* **2013**, *49* (43), 4896. https://doi.org/10.1039/c3cc41411f.

(101) Kottelat, E.; Fabio, Z. Visible Light-Activated PhotoCORMs. *Inorganics (Basel)* **2017**, *5* (2), 24. https://doi.org/10.3390/inorganics5020024.

(102) Wright, M. A.; Wright, J. A. PhotoCORMs: CO Release Moves into the Visible. *Dalton Transactions* **2016**, *45* (16), 6801–6811. https://doi.org/10.1039/C5DT04849D.

(103) Schatzschneider, U. PhotoCORMs: Light-Triggered Release of Carbon Monoxide from the Coordination Sphere of Transition Metal Complexes for Biological Applications. *Inorganica Chim Acta* **2011**, *374* (1), 19–23. https://doi.org/10.1016/j.ica.2011.02.068.

(104) Nielsen, V. G.; Kirklin, J. K.; George, J. F. Carbon Monoxide Releasing Molecule-2 Increases the Velocity of Thrombus Growth and Strength in Human Plasma. *Blood Coagulation & Fibrinolysis* **2009**, *20* (5), 377–380. https://doi.org/10.1097/MBC.0b013e32832ca3a3.

(105) Pfeiffer, H.; Rojas, A.; Niesel, J.; Schatzschneider, U. Sonogashira and "Click" Reactions for the N-Terminal and Side-Chain Functionalization of Peptides with [Mn(CO)3(Tpm)]+-Based CO Releasing Molecules (Tpm = Tris(Pyrazolyl)Methane). *Dalton Transactions* **2009**, No. 22, 4292. https://doi.org/10.1039/b819091g.

(106) Rimmer, R. D.; Richter, H.; Ford, P. C. A Photochemical Precursor for Carbon Monoxide Release in Aerated Aqueous Media. *Inorg Chem* **2010**, *49* (3), 1180–1185. https://doi.org/10.1021/ic902147n.

(107) Jin, Z.; Wen, Y.; Xiong, L.; Yang, T.; Zhao, P.; Tan, L.; Wang, T.; Qian, Z.; Su, B.-L.; He, Q. Intratumoral H2O2-Triggered Release of CO from a Metal Carbonyl-Based Nanomedicine for Efficient CO Therapy. *Chemical Communications* **2017**, *53* (40), 5557–5560. https://doi.org/10.1039/C7CC01576C.

(108) Pan, Z.; Zhang, J.; Ji, K.; Chittavong, V.; Ji, X.; Wang, B. Organic CO Prodrugs Activated by Endogenous ROS. *Org Lett* **2018**, *20* (1), 8–11. https://doi.org/10.1021/acs.orglett.7b02775.

(109) Gao, C.; Liang, X.; Guo, Z.; Jiang, B.-P.; Liu, X.; Shen, X.-C. Diiron Hexacarbonyl Complex Induces Site-Specific Release of Carbon Monoxide in Cancer Cells Triggered by Endogenous Glutathione. *ACS Omega* **2018**, *3* (3), 2683–2689. https://doi.org/10.1021/acsomega.8b00052.

(110) Romanski, S.; Rücker, H.; Stamellou, E.; Guttentag, M.; Neudörfl, J.-M.; Alberto, R.; Amslinger, S.; Yard, B.; Schmalz, H.-G. Iron Dienylphosphate Tricarbonyl Complexes as Water-Soluble Enzyme-Triggered CO-Releasing Molecules (ET-CORMs). *Organometallics* **2012**, *31* (16), 5800–5809. https://doi.org/10.1021/om300359a.

(111) Price, P. M.; Mahmoud, W. E.; Al-Ghamdi, A. A.; Bronstein, L. M. Magnetic Drug Delivery: Where the Field Is Going. *Front Chem* **2018**, *6*. https://doi.org/10.3389/fchem.2018.00619.

(112) Seixas, J. D.; Mukhopadhyay, A.; Santos-Silva, T.; Otterbein, L. E.; Gallo, D. J.; Rodrigues, S. S.; Guerreiro, B. H.; Gonçalves, A. M. L.; Penacho, N.; Marques, A. R.; Coelho, A. C.; Reis, P. M.; Romão, M. J.; Romão, C. C. Characterization of a Versatile Organometallic Pro-Drug (CORM) for Experimental CO Based Therapeutics. *Dalton Trans.* **2013**, *42* (17), 5985–5998. https://doi.org/10.1039/C2DT32174B.

(113) Romanski, S.; Stamellou, E.; Jaraba, J. T.; Storz, D.; Krämer, B. K.; Hafner, M.; Amslinger, S.; Schmalz, H. G.; Yard, B. A. Enzyme-Triggered CO-Releasing Molecules (ET-CORMs): Evaluation of Biological Activity in Relation to Their Structure. *Free Radic Biol Med* **2013**, *65*, 78–88. https://doi.org/10.1016/j.freeradbiomed.2013.06.014.

(114) Ling, K.; Men, F.; Wang, W.-C.; Zhou, Y.-Q.; Zhang, H.-W.; Ye, D.-W. Carbon Monoxide and Its Controlled Release: Therapeutic Application, Detection, and Development of Carbon

Monoxide Releasing Molecules (CORMs). *J Med Chem* **2018**, *61* (7), 2611–2635. https://doi.org/10.1021/acs.jmedchem.6b01153.

(115) Inaba, H.; Fujita, K.; Ueno, T. Design of Biomaterials for Intracellular Delivery of Carbon Monoxide. *Biomater Sci* **2015**, *3* (11), 1423–1438. https://doi.org/10.1039/C5BM00210A.

(116) Ling, K.; Men, F.; Wang, W.-C.; Zhou, Y.-Q.; Zhang, H.-W.; Ye, D.-W. Carbon Monoxide and Its Controlled Release: Therapeutic Application, Detection, and Development of Carbon Monoxide Releasing Molecules (CORMs). *J Med Chem* **2018**, *61* (7), 2611–2635. https://doi.org/10.1021/acs.jmedchem.6b01153.

(117) Yan, H.; Du, J.; Zhu, S.; Nie, G.; Zhang, H.; Gu, Z.; Zhao, Y. Emerging Delivery Strategies of Carbon Monoxide for Therapeutic Applications: From CO Gas to CO Releasing Nanomaterials. *Small* **2019**, *15* (49), 1904382. https://doi.org/10.1002/smll.201904382.

(118) Yin, H.; Fang, J.; Liao, L.; Nakamura, H.; Maeda, H. Styrene-Maleic Acid Copolymer-Encapsulated CORM2, a Water-Soluble Carbon Monoxide (CO) Donor with a Constant CO-Releasing Property, Exhibits Therapeutic Potential for Inflammatory Bowel Disease. *Journal of Controlled Release* **2014**, *187*, 14–21. https://doi.org/10.1016/j.jconrel.2014.05.018.

(119) Fernandes, A. R.; Mendonça-Martins, I.; Santos, M. F. A.; Raposo, L. R.; Mendes, R.; Marques, J.; Romão, C. C.; Romão, M. J.; Santos-Silva, T.; Baptista, P. v. Improving the Anti-Inflammatory Response via Gold Nanoparticle Vectorization of CO-Releasing Molecules. *ACS Biomater Sci Eng* **2020**, *6* (2), 1090–1101. https://doi.org/10.1021/acsbiomaterials.9b01936.

(120) Karges, J.; Stokes, R. W.; Cohen, S. M. Metal Complexes for Therapeutic Applications. *Trends Chem* **2021**, *3* (7), 523–534. https://doi.org/10.1016/j.trechm.2021.03.006.

(121) Winburn, I. C.; Gunatunga, K.; McKernan, R. D.; Walker, R. J.; Sammut, I. A.; Harrison, J. C. Cell Damage Following Carbon Monoxide Releasing Molecule Exposure: Implications for Therapeutic Applications. *Basic Clin Pharmacol Toxicol* **2012**, n/a-n/a. https://doi.org/10.1111/j.1742-7843.2012.00856.x.

(122) McLean, S.; Mann, B. E.; Poole, R. K. Sulfite Species Enhance Carbon Monoxide Release from CO-Releasing Molecules: Implications for the Deoxymyoglobin Assay of Activity. *Anal Biochem* **2012**, *427* (1), 36–40. https://doi.org/10.1016/j.ab.2012.04.026.

(123) Atkin, A. J.; Lynam, J. M.; Moulton, B. E.; Sawle, P.; Motterlini, R.; Boyle, N. M.; Pryce, M. T.; Fairlamb, I. J. S. Modification of the Deoxy-Myoglobin/Carbonmonoxy-Myoglobin UV-Vis Assay for Reliable Determination of CO-Release Rates from Organometallic Carbonyl Complexes. *Dalton Transactions* **2011**, *40* (21), 5755. https://doi.org/10.1039/c0dt01809k.

(124) Alday, J.; Mazzeo, A.; Suarez, S. Selective Detection of Gasotransmitters Using Fluorescent Probes Based on Transition Metal Complexes. *Inorganica Chim Acta* **2020**, *510*, 119696. https://doi.org/10.1016/j.ica.2020.119696.

(125) Millar, N. L.; Murrell, G. A. C.; McInnes, I. B. Inflammatory Mechanisms in Tendinopathy – towards Translation. *Nat Rev Rheumatol* **2017**, *13* (2), 110–122. https://doi.org/10.1038/nrrheum.2016.213.

(126) Bergqvist, F.; Carr, A. J.; Wheway, K.; Watkins, B.; Oppermann, U.; Jakobsson, P.-J.; Dakin, S. G. Divergent Roles of Prostacyclin and PGE2 in Human Tendinopathy. *Arthritis Res Ther* **2019**, *21* (1), 74. https://doi.org/10.1186/s13075-019-1855-5.

# Chapter 2 – Article:

*antioxidants*

MDPI

*Article*

# A Novel Class of Dual-Acting DCH-CORMs Counteracts Oxidative Stress-Induced Inflammation in Human Primary Tenocytes

**Federico Appetecchia [1,†], Sara Consalvi [1,†], Emanuela Berrino [1], Marialucia Gallorini [2], Arianna Granese [1], Cristina Campestre [2], Simone Carradori [2,*], Mariangela Biava [1,*] and Giovanna Poce [1,*]**

[1] Department of Chemistry and Technologies of Drug, Sapienza University of Rome, piazzale A. Moro 5, 00185 Rome, Italy; federico.appetecchia@uniroma1.it (F.A.); Sara.consalvi@uniroma1.it (S.C.); emanuela.berrino@uniroma1.it (E.B.); arianna.granese@uniroma1.it (A.G.)

[2] Department of Pharmacy, "G. d'Annunzio" University of Chieti-Pescara, Via dei Vestini 31, 66100 Chieti, Italy; marialucia.gallorini@unich.it (M.G.); cristina.campestre@unich.it (C.C.)

* Correspondence: simone.carradori@unich.it (S.C.); mariangela.biava@uniroma1.it (M.B.); giovanna.poce@uniroma1.it (G.P.)

† F. Appetecchia and S. Consalvi contributed equally to the work.

**Abstract:** Carbon monoxide (CO) can prevent cell and tissue damage by restoring redox homeostasis and counteracting inflammation. CO-releasing molecules (CORMs) can release a controlled amount of CO to cells and are emerging as a safer therapeutic alternative to delivery of CO in vivo. Sustained oxidative stress and inflammation can cause chronic pain and disability in tendon-related diseases, whose therapeutic management is still a challenge. In this light, we developed three small subsets of 1,5-diarylpyrrole and pyrazole dicobalt(0)hexacarbonyl (DCH)-CORMs to assess their potential use in musculoskeletal diseases. A myoglobin-based spectrophotometric assay showed that these CORMs act as slow and efficient CO-releasers. Five selected compounds were then tested on human primary-derived tenocytes before and after hydrogen peroxide stimulation to assess their efficacy in restoring cell redox homeostasis and counteracting inflammation in terms of $PGE_2$ secretion. The obtained results showed an improvement in tendon homeostasis and a cytoprotective effect, reflecting their activity as CO-releasers, and a reduction of $PGE_2$ secretion. As these compounds contain structural fragments of COX-2 selective inhibitors, we hypothesized that such a composite mechanism of action results from the combination of CO-release and COX-2 inhibition and that these compounds might have a potential role as dual-acting therapeutic agents in tendon-derived diseases.

**Keywords:** CO-releasing molecules; tenocytes; $PGE_2$; 1,5-diarylpyrrole; 1,5-diarylpyrazole; carbon monoxide



**Citation:** Appetecchia, F.; Consalvi, S.; Berrino, E.; Gallorini, M.; Granese, A.; Campestre, C.; Carradori, S.; Biava, M.; Poce, G. A Novel Class of Dual-Acting DCH-CORMs Counteracts Oxidative Stress-Induced Inflammation in Human Primary Tenocytes. *Antioxidants* **2021**, *10*, 1828. https://doi.org/10.3390/antiox10111828

Academic Editors: Elias Lianos and Maria G. Detsika

Received: 14 October 2021
Accepted: 16 November 2021
Published: 18 November 2021



## 1. Introduction

CO-releasing molecules (CORMs) can release carbon monoxide (CO) either spontaneously, enzymatically, or triggered by an external stimulus [1]. Their therapeutic potential relies on the release of a limited amount of CO. Along with NO and $H_2S$, CO is the third small signaling molecule and is produced endogenously by enzymes of the Heme Oxygenase (HO) class through heme oxidative degradation. The expression of the HO inducible isoform (HO-1) is triggered by cell responses toward oxidative stress and inflammation and results in cyto- and tissue protection. HO-1 metabolites, including CO, are important in restoring redox homeostasis and resolution of inflammation, and it has been widely demonstrated that the HO-1/CO axis can help to prevent cellular and tissue damage. Therefore, the manipulation of the HO-1/CO system is an attractive strategy to treat conditions linked to oxidative-stress-induced inflammation, such as lung hyper-inflammation in cystic fibrosis, sepsis and modulation of chronic pain [2–7]. The chemistry of CO is unique: unlike NO and $H_2S$ that react indiscriminately with intracellular targets, CO offers the advantage of binding only to transition metals in a low oxidation state. Such preferential reactivity,

along with its greater stability, makes it a more versatile candidate for the development of gaseous-based pharmaceuticals [8]. Indeed, gaseous CO has great potential as a therapeutic tool and has been found beneficial in the treatment of several inflammatory, cardiovascular, and neurological diseases [9–12]. For low-dose CO inhalation, the feasibility of the first clinical trials has been recently assessed [13]. However, the accurate delivery of gaseous CO to its molecular targets through inhalation is challenging, and inhalation therapy is hampered by CO low bioavailability and high affinity to hemoglobin, with consequent toxicity [14]. In this scenario, CORMs have emerged as a safer and attractive therapeutic strategy to deliver a controlled amount of CO to cells. To date, most of the developed CORMs are metal carbonyl complexes (MCCs) [15,16]. Indeed, considering the preferential reactivity of CO for transition metals in a low oxidation state, organometallic complexes have emerged as suitable models to safely deliver CO in vivo and generate innovative therapeutic agents with reasonable pharmacological properties. These molecules have an octahedral shape with six ligands around a central metal and can release CO spontaneously, mainly through hydrolysis in biological buffers. Romão and co-workers [17] introduced a conceptual model to rationalize and improve the design of MCCs with appropriate pharmaceutical properties. This model comprises three portions: (i) a metal core, which accounts for toxicity and the main properties of the MCC; (ii) a coordination-sphere, which influences the electronic density around the metal, tuning the stability and the chemical behavior of the whole complex and triggering CO release under specific conditions; and (iii) a drug-sphere, obtained through modulation of the distal sites of the metal complexes and accounting for pharmacological properties and drug-likeness.

The choice of the transition metal is crucial to design metal-based CORMs. CORMs containing an atom of cobalt (dicobalt(0)hexacarbonyl complexes, DCH) are innovative CO-releasing agents with interesting biological features and good CO-release kinetics [18–25]. The DCH metal core is a hexacarbonyl dicobalt moiety ($Co_2CO_6$) coordinated through an alkyne bond, which is in turn linked to the drug sphere. One of the main advantages of DCH-CORMs is their synthetic accessibility. Indeed, this highly versatile chemical scaffold is easy to synthesize, facilitating the chemical manipulation of the drug sphere. A series of dual acting DCH-CORMs-carbonic anhydrase inhibitors (CAI-CORMs) have very recently shown promising anti-inflammatory properties under oxidative-stress conditions in different oxidative-based disease models [22,23]. Interestingly, Gallorini et al. [26] demonstrated that some of these compounds were able to differentially modulate inflammation and counteract the $H_2O_2$-induced stress in rotator-cuff-derived human tenocytes, which activate the nuclear factor erythroid 2 [NF-E2]-related factor 2 (Nrf2)/HO-1/CO pathway to mitigate oxidative stress. It has also been reported that sustained oxidative stress causes aberrant cytokine secretion in a model of rotator cuff disease (RCD) in vitro [27]. Oxidative stress endurance and, consequently, inflammation occurrence, are considered the major factors causing the failure of tendon healing in clinical practice and can lead to chronic pain and disability. Moreover, the benefits of non-steroidal anti-inflammatory drug (NSAID)-based therapy in the acute phase are broadly accepted, but their use in chronic tendon-related diseases is still controversial [28]. Therefore, an innovative therapeutic approach for the treatment of tendon-derived diseases is urgently needed, as their therapeutic management remains a challenge.

In this light, we synthesized a small set of 1,5-diarylpyrrole and 1,5-diarylpyrazole-based DCH-CORMs linked through a propargylic chain (compounds **1**–**9**, Figure 1). According to the Romão model, the first aim of this study was to analyze the influence of different electronic and steric properties of the drug sphere on the CO release rate. Five selected compounds (**1**–**5**) were then tested on human primary tendon-derived cells stimulated with a low concentration of hydrogen peroxide ($H_2O_2$), using the NSAID Meloxicam as a reference compound. The present work aims to assess their efficacy in restoring cell redox homeostasis and counteracting inflammation in terms of $PGE_2$ secretion and at investigating their potential use in vitro to manage musculoskeletal diseases.

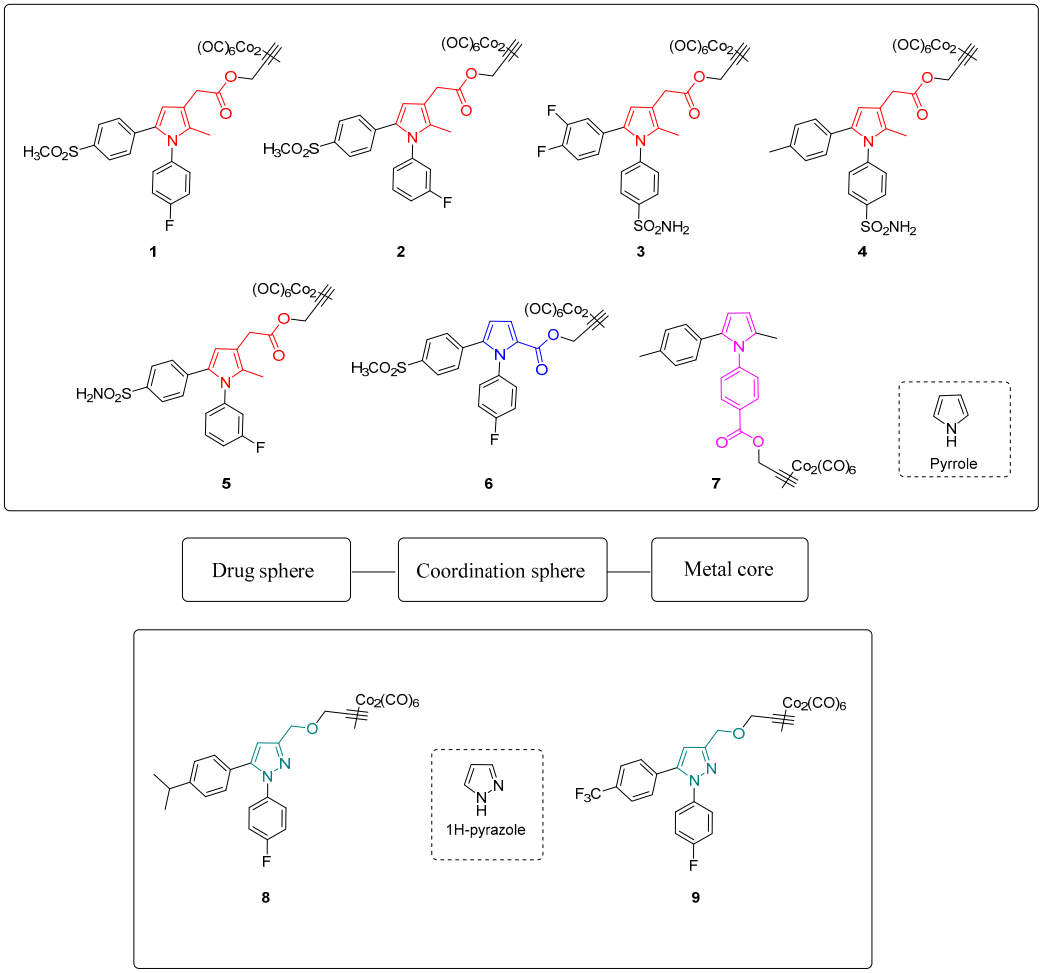


**Figure 1.** Chemical structures and conceptual model of compounds **1–9**.

## 2. Materials and Methods

### *2.1. Chemistry*

All chemicals used were obtained from commercial sources (Merck, Acros, Syngene) and were used as supplied without further purification. Merck silica gel 60 (230–400 mesh) and Merck aluminum oxide (activity II–III, according to Brockmann) were used for chromatographic columns with the indicated solvents. Merck TLC plates (silica gel 60 F254 and aluminum oxide F254) were used to monitor all operations, and then compounds were visualized under UV light (254 and 365 nm) and/or stained with the relevant reagents. The yields were not optimized and refer to the purified products. $^{13}$C NMR and $^{1}$H NMR spectra were recorded on a Bruker Avance III NMR 400 spectrometer with reference to tetramethylsilane (TMS) in the indicated solvent. Chemical shift values are expressed in parts per million (ppm). Coupling constants (*J*) are reported in hertz with signal multiplicities indicated as singlet (s), doublet (d), triplet (t), quadruplet (q) and multiplet (m). When specified, ChemDraw Professional 16.0 was used to generate systematic compound names following IUPAC conventions. Detailed synthetic procedures and spectroscopic data are reported in the Supplementary Materials.

### 2.2. CO-Release Assay

All reagents were of analytical grade and purchased from Merck. Gaseous CO was obtained from Rivoira (Milan, Italy). A Shimadzu UV1900 UV-Vis Spectrophotometer from 275 to 700 nm at the scanning rate of 200 nm/min was used to record UV-Vis absorption spectra in a disposable plastic cuvette (path length 0.44 cm). An Origin Lab software generated second derivative spectra, and the Savitzky–Golay method was applied using 25 data points for the differentiation process. Neither an increase nor a decrease in the number of points caused changes in the wavelength or in the bandwidth. Lyophilized horse heart Mb was dissolved in phosphate buffered saline flushed with $N_2$ (PBS, 0.01 M, pH 7.4 to a 20–22 μM final concentration). Two milliliters of this freshly prepared stock solution were placed in a cuvette to record the UV-Vis absorption spectrum of met-Mb. Next, the solutions were divided into two: 10 μL of sodium dithionite (30 mg/mL) were added to the first half (reference) and the UV-Vis spectrum of deoxy-Mb was registered. After that, the solution was flushed with CO gas, and the Mb-CO spectrum was acquired. Sodium dithionite was added to the second half (sample), and a spectrum was recorded. Afterwards, a CORM DMSO solution was added to a final CORM concentration of 3.33 μM and gently mixed. The solution was covered with 300 μL of light mineral oil to avoid CO escaping and oxygenation of Mb, and the absorption spectrum was recorded at t = 0. Spectra were acquired every 30 min for 210 min, keeping the sample at 37 °C. When necessary, a freshly prepared sodium dithionite solution was added. After 210 min, the total Mb concentration at the end of the assay was determined by flushing the sample with CO gas. Mb-CO concentration at each time point was determined as previously reported [23]. Each experiment was replicated three times, and the data were expressed as mean ± SEM.

### 2.3. Cell Culture

Human tenocytes (#TEN-F; ZenBio Inc.; Durham, NC, USA) were maintained in complete alpha-MEM (EuroClone, Milan, Italy) supplemented with 10% of heat-inactivated FBS (Gibco, ThermoFisher Scientific, Waltham, MA, USA) and 1% penicillin/streptomycin (EuroClone, Milan, Italy) at 37 °C and 5% $CO_2$ and used from passage 3 up to passage 6.

### 2.4. Cell Treatment

Cells were seeded in 96-well plates ($0.5 \times 10^4$/well) (ThermoFisher Scientific, Waltham, MA, USA) and left to adhere overnight at 37 °C and 5% $CO_2$. In a first set of experiments, tendon-derived cells were treated with increasing concentrations of compounds **1**–**5** in the range 0–100 μM for 24 and 72 h. Compounds were dissolved in DMSO to obtain a 200 mM stock solution, and they were afterwards diluted in complete alpha-MEM (DMSO final concentration = 0.1%) for further analyses. In a second set of experiments, tenocytes were pre-incubated with 100 μM $H_2O_2$ for 3 h. After that, the pre-incubation medium was discarded and replaced with a fresh one containing the proper CORM at increasing concentrations for 24 and 72 h. At the established time points, samples were processed for further analyses.

### 2.5. Cell Metabolic Activity

At the established time points (24 and 72 h), the incubation medium was harvested for further analyses, and complete alpha-MEM containing 0.5 mg/mL MTT (3-[4,5-dimethylthiazol-2-yl]-2,5-diphenyl tetrazolium bromide) (Sigma-Aldrich, St. Louis, MO, USA) was added to each well. Afterwards, cells were incubated for 5 h at 37 °C and cell metabolic activity was measured as already reported [29].

### 2.6. $PGE_2$ Secretion

Cell supernatants were collected from the 96-well plates used for the metabolic activity assay (MTT) after 24 and 72 h, and $PGE_2$ secretion was analyzed. A commercial ELISA kit (Enzo Life Sciences, Farmingdale, NY, USA) was used to measure the amount (pg/mL) of

$PGE_2$ in the culture media, according to the manufacturer's instructions. The $PGE_2$ concentration in each sample was determined following a previously reported procedure [30].

## 3. Results and Discussion

### *3.1. Chemistry*

Compounds **1-9** were easily synthesized in good yields by reacting the terminal alkyne of propargylic intermediates and dicobalt(0)carbonyl octacarbonyl in tetrahydrofuran (THF). Detailed synthetic procedures are reported in the Supporting Information.

### *3.2. CO Release Assay*

The CO releasing behaviors of compounds **1–9** were evaluated through a myoglobin (Mb)-based spectrophotometric assay, considered the gold standard to analyze the CO releasing kinetics and a key criterion to select CORM structures [17,31]. This method analyzes the release of CO from CORMs by following the conversion of deoxy-myoglobin (deoxy-Mb(II)) into CO-myoglobin (CO-Mb(II)) over time by UV-Vis spectroscopy. A 3.3 μM solution of compounds **1–9** was incubated with a 20 μM solution of deoxy-Mb (CORM/Mb 1:6 ratio), and a reducing agent (sodium dithionite) was added to prevent oxidation of deoxy-Mb(II) to Met-Mb(III). Changes in the absorption band in the Soret region of deoxy-Mb and Mb-CO were recorded every 30 min for 210 min, and a second derivative approach was applied to clearly discriminate between the three forms of Mb (deoxy-Mb, Mb-CO and Met-Mb). The relative amount of CO produced over time was calculated following a previously reported equation [23,32], and a correction factor was applied to account for Mb degradation induced by sodium dithionite. Concentration values of Mb-CO formed over time by compounds **1–9** are reported in Table 1. Their CO-release profiles are shown in Figure 2A–C, along with their $T_{1/10}$ values, defined as the time necessary for a CO-RM to produce a concentration of CO-Mb of 1/10 of the initial (Figure 2D). The number of CO units released by CORMs **1-9** after 210 min is reported in Table 2. For selected compounds, the assay was performed using a 1:1 CORM/Mb ratio (Figure 3A–D). The aim was to explore their ability to release CO in a less favored condition, considering that CO release from CORMs is stimulated by an excess of Mb.

**Table 1.** MbCO formed at each time point when compounds **1–9** were analyzed at 1:6 CORM:Mb ratio.

| Time (min) | MbCO Formed (μM) | | | | | | | | |
|---|---|---|---|---|---|---|---|---|---|
| | **1** | **2** | **3** | **4** | **5** | **6** | **7** | **8** | **9** |
| 0 | 0 | 0 | 0 | 0 | 0 | 0 | 0 | 0 | 0 |
| 30 | 0.56 | 0.58 | 0.50 | 0.52 | 0.63 | 0.82 | 0.57 | 0.56 | 0.08 |
| 60 | 0.88 | 1.03 | 1.01 | 1.15 | 1.09 | 1.46 | 0.91 | 0.77 | 0.45 |
| 90 | 1.49 | 1.59 | 1.50 | 1.42 | 1.35 | 2.09 | 1.27 | 0.95 | 0.59 |
| 120 | 1.90 | 1.76 | 1.90 | 1.86 | 1.57 | 2.45 | 1.52 | 1.24 | 0.74 |
| 150 | 2.32 | 2.06 | 2.07 | 2.37 | 1.72 | 3.12 | 1.68 | 1.37 | 0.99 |
| 180 | 2.28 | 2.20 | 2.31 | 2.35 | 1.85 | 3.08 | 1.88 | 1.57 | 1.09 |
| 210 | 2.25 | 2.22 | 2.48 | 2.51 | 2.12 | 3.05 | 2.00 | 1.75 | 1.22 |

**Table 2.** CO units released by compounds **1–9** after 210 min of incubation working at 1:6 CORM-Mb ratio and by compounds **1**, **5** and **6** at 1:1 CORM-Mb ratio.

| CO Units Released after 210 min | **1** | **2** | **3** | **4** | **5** | **6** | **7** | **8** | **9** |
|---|---|---|---|---|---|---|---|---|---|
| 3.33 μM (1:6) | 0.68 | 0.67 | 0.74 | 0.75 | 0.64 | 0.92 | 0.60 | 0.53 | 0.37 |
| 20 μM (1:1) | 0.11 | - | - | - | 0.11 | 0.12 | - | - | - |

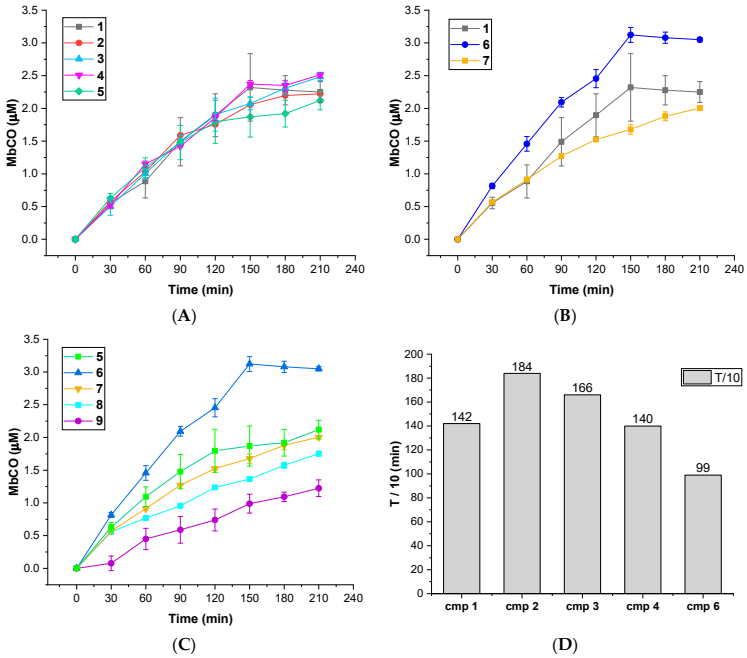


**Figure 2.** (**A**–**C**): CO-release profiles of compounds **1**–**9** as Mb-CO formed over time (1:6 CORM:Mb ratio); (**D**): $T_{1/10}$ values for compounds **1**–**4** and **6** (defined as the time necessary for a CORM solution to produce a Mb-CO concentration of 1/10 of the initial).

All the tested compounds were effective CO releasers, with CO release kinetics comparable to previously reported DCH-CORMs (slow CO release up to 210 min) [22,23,33]. The obtained data showed considerable differences among the analyzed compounds, depending on the heterocyclic nucleus and the different alkyne system linked to the DCH group (Table 1).

As shown in Figure 1, compounds **1**–**5** bear a propynyl-pyrrol-3-yl-acetate moiety, compound **6** a propynyl-pyrrole-2-carboxylate motif and compound **7** a propynyl benzoate group at position 1 of the pyrrole ring. Compounds **8** and **9** are characterized by a 3-((prop-2-yn-1-yloxy)methyl)-1*H*-pyrazole scaffold. Derivatives **1**–**5** showed comparable kinetics, with a sustained release of CO over time (Figure 2A). The kinetics of release were almost superimposable over the first 120 min, with negligible differences over the last 90 min. Despite slight differences in their $T_{1/10}$ (Figure 2D), the comparison of the units of CO released over time (Table 2) displayed a very similar behavior within the series, suggesting that the substitution pattern on the aryl rings only slightly impacts their CO-releasing abilities. In particular, compounds **1**, **2** and **5**, bearing a sulfonyl group on the aryl ring at C5, released almost the same amount of CO at the end of the assay (0.64–0.68 CO units, Table 2). Compounds **3** and **4**, both decorated with a sulfamoylphenyl moiety at position 1 of the pyrrole, displayed very similar behavior and released a comparable amount of CO after 210 min (0.74–0.75 CO units, Table 2). Pyrrole **6** showed a completely different CO releasing profile (Figure 2B,C) and was the fastest and most efficient CO-releaser of the series, with a $T_{1/10}$ value of 99.01 min (Figure 2D) and 0.92 CO units released after 210 min (Table 2). This compound showed a fast release of CO over the first 120 min, which reaches a maximum at 150 min and then slows down. When compared to its analogue **1**, compound **6** produced a 1.35-fold higher amount of Mb-CO at each time point until the end of the assay. These data suggest that the group bearing the DCH moiety and the chemical space around it strongly influences the CO release kinetic. The

CO releasing behavior of compound **7** supported this hypothesis: indeed, it releases CO slower than compounds **1**-**5**, although reaching almost the same amount of Mb-CO after 210 min of incubation (Figure 2B,C). Differently from compounds **1**-**6**, the DCH portion of this compound is linked to a propynyl benzoate group at position 1 of the pyrrole ring, suggesting that the electronic structure can induce different CO releasing properties. Pyrazoles **8** and **9** showed different CO releasing profiles (Figure 2C). At the end of the assay, these compounds produced much smaller values of Mb-CO (1.75 µM and 1.22 µM for **8** and **9**, respectively, Table 1) than compounds **1**–**7** at the same time point. Therefore, it is interesting to note that the 3-((prop-2-yn-1-yloxy)-methyl)-1-pyrazole moiety is probably detrimental in terms of CO releasing efficiency when compared to acetate, carboxylate or benzoate moieties decorating compounds **1**–**7**. Previous studies reported the impact of the group bearing the DCH moiety in determining the CO releasing properties [22,23]. The different CO release kinetics observed for compounds **1**–**9** confirm the influence of the drug sphere on CO releasing properties and suggest that both the electronic density around the pyrrole/pyrazole ring and the group bearing the DCH moiety strongly impact the rate of CO release, yet further studies are needed to better characterize this phenomenon. To further explore the releasing properties of these derivatives, we selected compounds **1**, **5** and **6** to be studied at different CO-RM:Mb ratios (Figure 3).

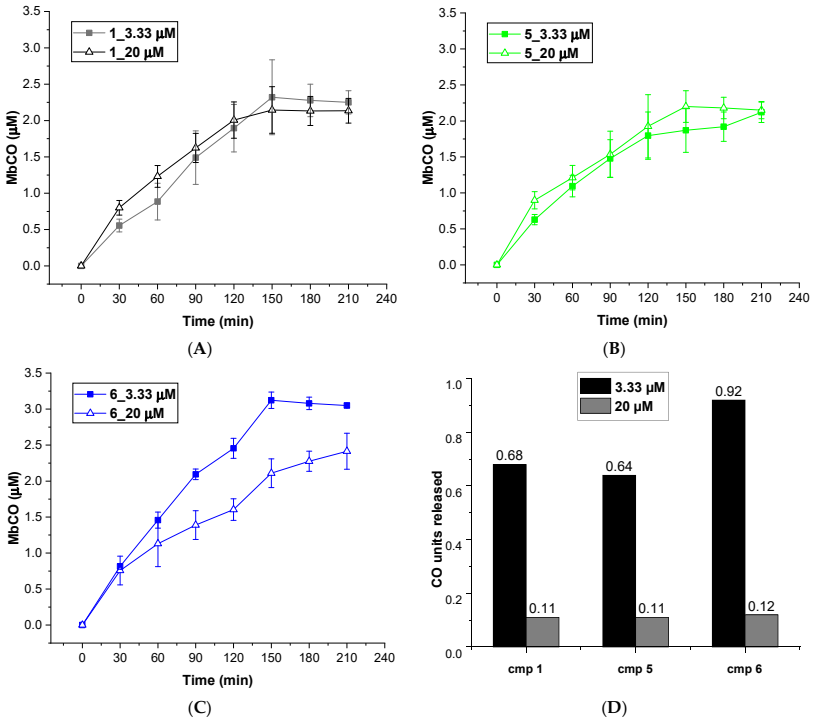


**Figure 3.** CO release profiles of compounds **1** (**A**), **5** (**B**) and **6** (**C**) analyzed at 1:6 (filled square) and 1:1 (empty triangles) CORM-Mb ratios; (**D**): CO units released by compounds **1**, **5** and **6** after 210 min of incubation working at 1:6 (blue columns) and 1:1 (orange columns) CORM-Mb ratios.

As mentioned above, an excess of the CO acceptor (Mb) stimulates the CO release from CORMs. Thus, we expected a decrease in CO release at 1:1 CO-RM:Mb ratio. As shown in Figure 3, after 210 min of incubation, compounds **1**, **5** and **6** released a lower amount of CO when compared to the one observed in 1:6 conditions (Figure 2). Moreover, all the compounds released the same CO units (0.11–0.12 CO units), regardless of their different

chemical structure. Therefore, disfavoring the CO release seems to reduce the differences in CO releasing efficiencies observed when Mb is present in excess (1:6/CO-RM:Mb).

### *3.3. Effects of Compounds* **1–5** *on Human Tenocytes*

Once the influence of electronic and steric properties on CO release has been established, a fine-tuning of the drug sphere should also focus on treating particular conditions and on the biological activity of the drug sphere itself [17,34]. Compounds **1-5** drug sphere belongs to a series of sulphone and sulfamoyl diarylpyrrole derivatives developed by our research group as COX-2 selective inhibitors [35–39]. This class of compounds showed promising in vitro and in vivo anti-nociceptive and anti-inflammatory properties and tolerates a wide range of substituents at position C3. As augmented $PGE_2$ levels are a marker of oxidative-stress inflammation, the modulation of $PGE_2$ secretion might be a valuable strategy for therapeutic intervention of tendon diseases [27,40]. We therefore speculated that the conjugation of a COX-2 inhibiting scaffold and a CO-releasing moiety could help to achieve promising CORM-candidates for the treatment of tendon inflammatory-based diseases, as COX-2 inhibition and CO release could act synergically to resolve inflammation and restore oxidative homeostasis. Moreover, the conjugation of structural fragments of anti-inflammatory drugs with metal carbonyl moieties is well documented in the literature [18,19,24], and the five selected compounds showed quite similar CO release profiles (Figure 2), allowing us to make a proper comparison and rationalization of the observed biological activities. To help to discriminate between COX-2 mediated and independent activities, the efficacies of these compounds against inflammation and oxidative cytotoxicity were studied through the analysis of different parameters: the metabolic activity of tenocytes before and after $H_2O_2$ stimulation and the quantification of $PGE_2$ secretion.

Tendinopathies are characterized by a higher level of tenocyte apoptosis and a decreased metabolic activity, which can reduce the resistance of tendon structures and lead to failure in healing [41,42]. Unstimulated tenocytes were therefore exposed to increasing concentrations of CORMs to evaluate their biocompatibility and effects under non-oxidative stress conditions (Figure 4). It is worth noting that Meloxicam exerted no significant effects on tenocytes when administered in the same experimental conditions [26].

On the other hand, compounds **1–5** significantly increased the metabolic activity of tendon-derived cells after 24 h, as observed for CAI-CORMs hybrids [26]. In more detail, all the tested compounds showed a dose-dependent rise up to 25–50 μM already after 24 h of exposure, which was particularly significant in the presence of compounds **3** and **5**. Interestingly, the tested compounds seemed less active after a 72 h exposure, as the metabolic activity was comparable to that of the control up to the concentration of 25 μM. This might be related to their slightly different CO release kinetics, but further studies are needed to corroborate this hypothesis.

### *3.4. Establishment of the Inflammatory Cell Model and Effects of Compounds* **1–5** *on Human Tenocytes under Oxidative Stress Conditions*

These preliminary results highlighted that compounds **1–5** have good proliferative effects on tendon-derived cells and provided a proof-of-concept that the biological features of these compounds are not only COX-2 mediated but also rely on CO release. As reported elsewhere [43], increasing cell metabolism and proliferation are particularly important for tendon tissue repair after the acute inflammatory phase. With this rationale, compounds **1–5** were tested in sub-toxic oxidative stress conditions in vitro [26] to investigate their ability to counteract $H_2O_2$-induced oxidative stress. After 3 h of incubation with 100 μM $H_2O_2$, human tenocytes were exposed to increasing concentrations of CORMs. As reported in Figure 5, all the tested compounds were more active than Meloxicam in increasing the cell metabolism of tenocytes. Notably, compounds **3–5** were the most active of the series. In particular, compound **3** showed an outstanding efficacy, being able to increase metabolic activity up to 166.2% after 72 h when administered at 25 μM. Unlike under non-oxidative stress conditions, the percentage of metabolically active tenocytes increases after 72 h. This observation suggests a composite mechanism of action, which

probably results from the combination of COX-2 inhibition and CO release. Consistent with previously obtained results, activities were maximum at 25 µM, then decreased at the higher concentrations tested.

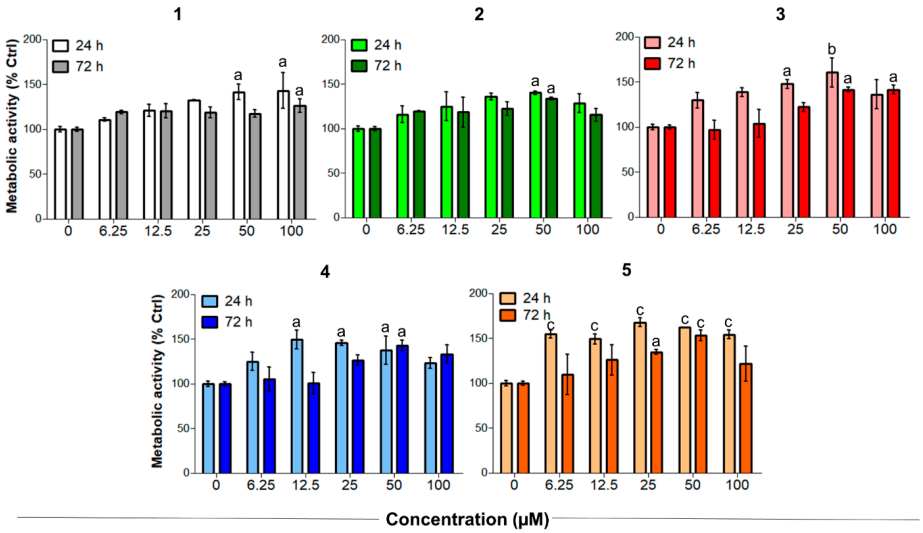


**Figure 4.** Metabolic activity of human primary tendon-derived cells exposed to increasing concentrations of CORMs (compounds **1**–**5**) after 24 and 72 h. The control sample (0 µM = cells treated with DMSO 0.1%) is set as 100%. a = $p < 0.01$; b = $p < 0.001$; c = $p < 0.0001$ between cells treated with CORMs and the control sample.

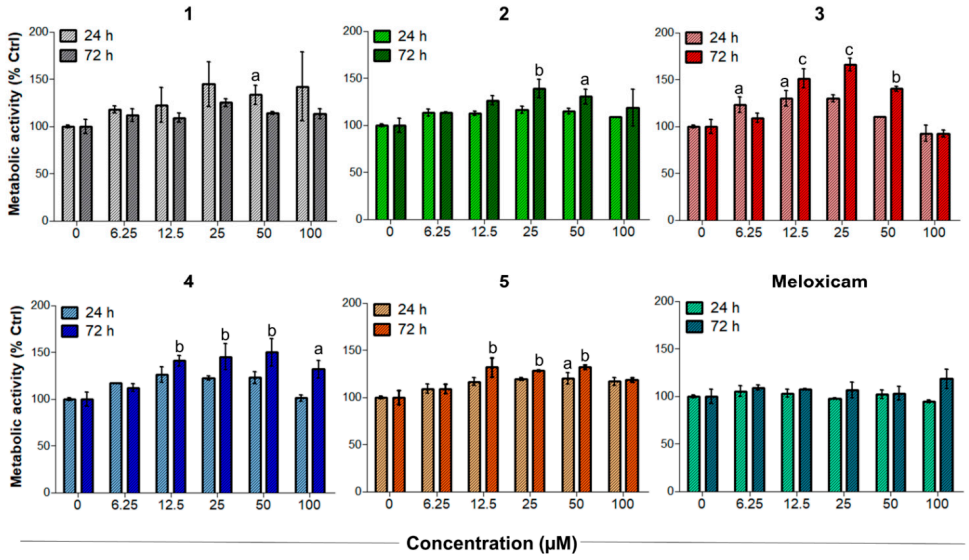


**Figure 5.** Metabolic activity of $H_2O_2$-pre-incubated human primary tendon-derived cells exposed to increasing concentrations of CORMs (compounds **1**–**5**) after 24 and 72 h. Cells were pre-incubated with $H_2O_2$ 100 µM for 3 h. The control sample (0 µM = cells pre-incubated with $H_2O_2$ and treated with DMSO 0.1%) is set as 100%. a = $p < 0.01$; b = $p < 0.001$; c = $p < 0.0001$ between cells treated with CORMs and the control sample.

### 3.5. *Effects of Compound* **1**–**5** *on* $PGE_2$ *Secretion*

Anti-inflammatory COX-related activities of compounds **1**–**5** were evaluated by quantifying $PGE_2$ secretion in the established oxidative stress conditions in vitro (Figure 6).

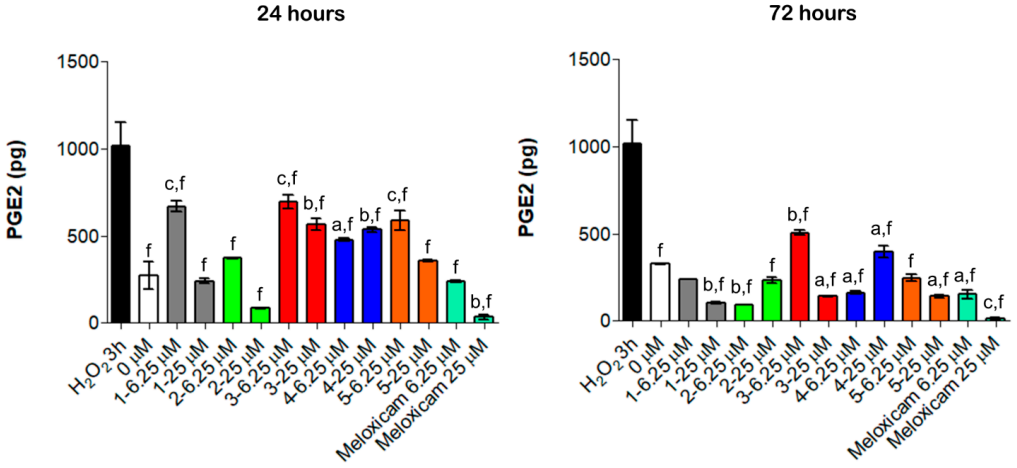


**Figure 6.** $PGE_2$ secretion from $H_2O_2$-pre-incubated human primary tendon-derived cells in the presence of increasing concentrations of CORMs after 24 and 72 h. Cells were pre-incubated with $H_2O_2$ 100 µM for 3 h. 0 µM = cells pre-incubated with $H_2O_2$ and treated with DMSO 0.1%. The amount of $PGE_2$ secreted (pg/mL) was normalized on cell metabolic activity data, resulting in the $PGE_2$ secreted from each sample (total picograms). a = $p < 0.01$; b = $p < 0.001$; c = $p < 0.0001$ between cells treated with CORMs and the control sample. f = $p < 0.0001$ between cells exposed to CORMs and cells pre-treated with $H_2O_2$ for 3 h.

Consistent with literature data [27], even a short exposure to $H_2O_2$ for 3 h increased $PGE_2$ secretion up to 1014.2 pg (Figure 6). Notably, all the tested compounds lowered the amount of $PGE_2$ compared to the $H_2O_2$ pre-incubation but were less effective than Meloxicam (Figure 6). Compared to our previous experiments, the obtained data revealed a different trend of activity: compounds **1**, **2** and **5** showed remarkable anti-inflammatory effects and considerably reduced $PGE_2$ secretion already at 24 h and mainly at 25 µM (240.5 pg, 84.8 pg and 357.1 pg, respectively), whereas compounds **3** and **4** were less efficient. Moreover, the modulation of $PGE_2$ is time-dependent, being that this cytokine decreased over the time. Actually, the amount of $PGE_2$ was almost halved with all the tested compounds after 72 h of exposure compared to 24 h treatment (Figure 6). These findings support the hypothesis that the observed anti-inflammatory effects rely on a COX-2 mediated mechanism of action and that the organometallic complexes retain the ability to inhibit COX-2.

Collectively, HO-1 expression and enzymatic activity are confirmed to influence positively and negatively both innate and adaptive immune responses; this dual action seems to be related to the stage of the inflammatory response or disease. The therapeutic potential of HO-1 may rely on limiting early inflammation, hampering successive tissue damage and modulating key pathways in most cell types of the immune system, given the complexity of heme catabolism and the role of HO-1 as a critical mediator of innate immune response. Immunomodulation is mostly related to higher demolition of the pro-inflammatory heme group, macrophage activation towards an anti-inflammatory macrophage profile with reduced secretion of pro-inflammatory cytokines and iNOS and interferon production by macrophages and dendritic cells. Indeed, T cells constitutively express HO-1, and their expansion regulatory is positively influenced by a tolerogenic phenotype sustained through HO-1 induction in dendritic cells. HO-1 modulation or application of low concentrations of CO to LPS-challenged macrophages reduced TNF-α and IL-1β expression and

simultaneously stimulated the anti-inflammatory IL-10 production through p38-MAPK activity [44–46].

This context was particularly evident in models of tendon-related diseases. In this light, the role of the macrophage is an area of emerging interest in tendinopathies and in general in the healing of tendons. In fact, inflammation appears to be driven by a high number of infiltrating macrophages at the inflamed tendon site [47]. Furthermore, damaged tendons from patients with tendinopathy show an abundance of $CD14^+$ and $CD68^+$ activated macrophages [48]. We have already reported that CORM hybrids exert their biological effects both on inflamed macrophages and tenocytes [22,26], disclosing a challenging field of application for molecules active on the HO-1/CO molecular axis not strictly related to the immune system. Finally, although once considered cells not involved in the immune-regulation and only related to tendon remodeling, tenocytes have been disclosed as active cells, secreting cytokines and expressing inflammation-related proteins [27].

## 4. Conclusions

We developed a novel series of DCH-CORMs based on a 1,5-diarylpyrrole scaffold. The screening of three small subsets of 1,5-diarylpyrroles and pyrazoles in a CO release assay allowed us to define the influence of the drug sphere electronic density on the kinetics of CO release. Based on these results, a series of 1,5-diarylpyrroles containing structural fragments of COX-2 selective inhibitors were selected for further biological studies on human primary tendon-derived cells. The observed results suggested the existence of different mechanisms of action and allowed us to conclude that the activities of these compounds result from the combination of COX-inhibition and CO release. Indeed, the obtained data suggest a multiple role for compounds **1**–**5** in tendon-derived diseases: a direct effect on tendon homeostasis and a cytoprotective effect in human tenocytes exposed to oxidative stress, reflecting their activity as CO-releasers, and a reduction of $PGE_2$ secretion, indicating a COX-2 mediated anti-inflammatory effect. Taken together, these findings indicate that these compounds could be potential double-acting therapeutic agents for the management of tendon-related diseases. Further studies are needed to better characterize their composite mechanism of action and the contribution of COX-2 inhibition to their biological activities.

**Supplementary Materials:** The following are available online at https://www.mdpi.com/article/10.3390/antiox10111828/s1, Scheme S1: Synthetic pathway for compounds **1**–**5**, Scheme S2: Synthetic pathway for compound **6**, Scheme S3: Synthetic pathway for compound **7**, Scheme S4: Synthetic pathway for compounds **8**,**9**.

**Author Contributions:** F.A., methodology, data curation and formal analysis; S.C. (Sara Consalvi), supervision, formal analysis, writing—original draft and writing—review and editing; S.C. (Simone Carradori), E.B., M.G. and A.G., methodology, data curation and formal analysis; C.C., supervision and formal analysis; S.C. (Simone Carradori) and M.B., conceptualization, funding acquisition, project administration and supervision; G.P., conceptualization, funding acquisition, project administration, supervision, data curation and writing—review and editing. All authors have read and agreed to the published version of the manuscript.

**Funding:** This work has been supported by the Italian Ministry of Education, Universities and Research—Dipartimenti di Eccellenza—L. 232/2016 and intramural grants to C.C. (FAR2019).

**Institutional Review Board Statement:** Not applicable.

**Informed Consent Statement:** Not applicable.

**Data Availability Statement:** Data are contained within the article.

**Conflicts of Interest:** The authors declare no conflict of interest.

## References


1. Zobi, F. CO and CO-Releasing Molecules in Medicinal Chemistry. *Future Med. Chem.* **2013**, *5*, 175–188. [CrossRef]
2. Ryter, S.W.; Choi, A.M.K. Heme Oxygenase-1/Carbon Monoxide. *Am. J. Respir. Cell. Mol. Biol.* **2009**, *41*, 251–260. [CrossRef] [PubMed]
3. Constantin, M.; Choi, A.J.S.; Cloonan, S.M.; Ryter, S.W. Therapeutic Potential of Heme Oxygenase-1/Carbon Monoxide in Lung Disease. *Int. J. Hypertens* **2012**, *2012*, e859235. [CrossRef]
4. Motterlini, R.; Haas, B.; Foresti, R. Emerging Concepts on the Anti-Inflammatory Actions of Carbon Monoxide-Releasing Molecules (CO-RMs). *Med. Gas. Res.* **2012**, *2*, 28. [CrossRef]
5. Castruccio Castracani, C.; Longhitano, L.; Distefano, A.; Di Rosa, M.; Pittalà, V.; Lupo, G.; Caruso, M.; Corona, D.; Tibullo, D.; Li Volti, G. Heme Oxygenase-1 and Carbon Monoxide Regulate Growth and Progression in Glioblastoma Cells. *Mol. Neurobiol.* **2020**, *57*, 2436–2446. [CrossRef]
6. Di Pietro, C.; Öz, H.H.; Murray, T.S.; Bruscia, E.M. Targeting the Heme Oxygenase 1/Carbon Monoxide Pathway to Resolve Lung Hyper-Inflammation and Restore a Regulated Immune Response in Cystic Fibrosis. *Front. Pharmacol.* **2020**, *11*, 1059. [CrossRef]
7. Pol, O. The Role of Carbon Monoxide, Heme Oxygenase 1, and the Nrf2 Transcription Factor in the Modulation of Chronic Pain and Their Interactions with Opioids and Cannabinoids. *Med. Res. Rev.* **2021**, *41*, 136–155. [CrossRef]
8. Motterlini, R.; Otterbein, L.E. The Therapeutic Potential of Carbon Monoxide. *Nat. Rev. Drug. Discov.* **2010**, *9*, 728–743. [CrossRef]
9. Foresti, R.; Bani-Hani, M.G.; Motterlini, R. Use of Carbon Monoxide as a Therapeutic Agent: Promises and Challenges. *Intensive Care Med.* **2008**, *34*, 649–658. [CrossRef]
10. Knauert, M.; Vangala, S.; Haslip, M.; Lee, P.J. Therapeutic Applications of Carbon Monoxide. *Oxid. Med. Cell. Longev.* **2013**, *2013*, e360815. [CrossRef]
11. Hess, D.R. Inhaled Carbon Monoxide: From Toxin to Therapy. *Respir. Care* **2017**, *62*, 1333–1342. [CrossRef] [PubMed]
12. Adach, W.; Błaszczyk, M.; Olas, B. Carbon Monoxide and Its Donors—Chemical and Biological Properties. *Chem. Biol. Interact* **2020**, *318*, 108973. [CrossRef] [PubMed]
13. Goebel, U.; Wollborn, J. Carbon Monoxide in Intensive Care Medicine—Time to Start the Therapeutic Application?! *Intensive Care Med. Exp.* **2020**, *8*, 2. [CrossRef] [PubMed]
14. Ling, K.; Men, F.; Wang, W.-C.; Zhou, Y.-Q.; Zhang, H.-W.; Ye, D.-W. Carbon Monoxide and Its Controlled Release: Therapeutic Application, Detection, and Development of Carbon Monoxide Releasing Molecules (CORMs). *J. Med. Chem.* **2018**, *61*, 2611–2635. [CrossRef]
15. Cavicchioli, F.; Cesarotti, I.M.; Fangman, M.; Lua, J.; Hautamaki, R.; Doré, S. Carbon Monoxide Therapy Using Hybrid Carbon Monoxide-Releasing/Nrf2-Inducing Molecules through a Neuroprotective Lens. *Chemistry* **2021**, *3*, 800–817. [CrossRef]
16. Kautz, A.C.; Kunz, P.C.; Janiak, C. CO-Releasing Molecule (CORM) Conjugate Systems. *Dalton Trans.* **2016**, *45*, 18045–18063. [CrossRef]
17. Romão, C.C.; Blättler, W.A.; Seixas, J.D.; Bernardes, G.J.L. Developing Drug Molecules for Therapy with Carbon Monoxide. *Chem. Soc. Rev.* **2012**, *41*, 3571–3583. [CrossRef]
18. Ott, I.; Kircher, B.; Bagowski, C.P.; Vlecken, D.H.W.; Ott, E.B.; Will, J.; Bensdorf, K.; Sheldrick, W.S.; Gust, R. Modulation of the Biological Properties of Aspirin by Formation of a Bioorganometallic Derivative. *Angew. Chem. Int. Ed. Engl.* **2009**, *48*, 1160–1163. [CrossRef]
19. Zanellato, I.; Bonarrigo, I.; Ravera, M.; Gabano, E.; Gust, R.; Osella, D. The Hexacarbonyldicobalt Derivative of Aspirin Acts as a CO-Releasing NSAID on Malignant Mesothelioma Cells. *Metallomics* **2013**, *5*, 1604–1613. [CrossRef]
20. Heffern, M.C.; Yamamoto, N.; Holbrook, R.J.; Eckermann, A.L.; Meade, T.J. Cobalt Derivatives as Promising Therapeutic Agents. *Curr. Opin. Chem. Biol.* **2013**, *17*, 189–196. [CrossRef]
21. Gong, Y.; Zhang, T.; Liu, H.; Zheng, Y.; Li, N.; Zhao, Q.; Chen, Y.; Liu, B. Synthesis, Toxicities and Cell Proliferation Inhibition of CO-Releasing Molecules Containing Cobalt. *Transit. Met. Chem.* **2015**, *40*, 413–426. [CrossRef]
22. Berrino, E.; Carradori, S.; Angeli, A.; Carta, F.; Supuran, C.T.; Guglielmi, P.; Coletti, C.; Paciotti, R.; Schweikl, H.; Maestrelli, F.; et al. Dual Carbonic Anhydrase IX/XII Inhibitors and Carbon Monoxide Releasing Molecules Modulate LPS-Mediated Inflammation in Mouse Macrophages. *Antioxidants* **2021**, *10*, 56. [CrossRef]
23. Berrino, E.; Milazzo, L.; Micheli, L.; Vullo, D.; Angeli, A.; Bozdag, M.; Nocentini, A.; Menicatti, M.; Bartolucci, G.; di Cesare Mannelli, L.; et al. Synthesis and Evaluation of Carbonic Anhydrase Inhibitors with Carbon Monoxide Releasing Properties for the Management of Rheumatoid Arthritis. *J. Med. Chem.* **2019**, *62*, 7233–7249. [CrossRef]
24. Li, J.; Zhang, J.; Zhang, Q.; Bai, Z.; Zhao, Q.; He, D.; Wang, Z.; Chen, Y.; Liu, B. Syntheses and Anti-Cancer Activity of CO-Releasing Molecules with Targeting Galactose Receptors. *Org. Biomol. Chem.* **2018**, *16*, 8115–8129. [CrossRef] [PubMed]
25. Perontsis, S.; Dimitriou, A.; Fotiadou, P.; Hatzidimitriou, A.G.; Papadopoulos, A.N.; Psomas, G. Cobalt(II) Complexes with the Non-Steroidal Anti-Inflammatory Drug Diclofenac and Nitrogen-Donor Ligands. *J. Inorg. Biochem.* **2019**, *196*, 110688. [CrossRef] [PubMed]
26. Gallorini, M.; Berardi, A.C.; Ricci, A.; Antonetti Lamorgese Passeri, C.; Zara, S.; Oliva, F.; Cataldi, A.; Carta, F.; Carradori, S. Dual Acting Carbon Monoxide Releasing Molecules and Carbonic Anhydrase Inhibitors Differentially Modulate Inflammation in Human Tenocytes. *Biomedicines* **2021**, *9*, 141. [CrossRef]
27. Oliva, F.; Gallorini, M.; Antonetti Lamorgese Passeri, C.; Gissi, C.; Ricci, A.; Cataldi, A.; Colosimo, A.; Berardi, A.C. Conjugation with Methylsulfonylmethane Improves Hyaluronic Acid Anti-Inflammatory Activity in a Hydrogen Peroxide-Exposed Tenocyte Culture In Vitro Model. *Int. J. Mol. Sci.* **2020**, *21*, 7956. [CrossRef]
28. Darrieutort-Laffite, C.; Soslowsky, L.J.; Le Goff, B. Molecular and Structural Effects of Percutaneous Interventions in Chronic Achilles Tendinopathy. *Int. J. Mol. Sci.* **2020**, *21*, 7000. [CrossRef] [PubMed]

29. Zara, S.; De Colli, M.; di Giacomo, V.; Zizzari, V.L.; Di Nisio, C.; Di Tore, U.; Salini, V.; Gallorini, M.; Tetè, S.; Cataldi, A. Zoledronic acid at subtoxic dose extends osteoblastic stage span of primary human osteoblasts. *Clin. Oral. Investig.* **2015**, *19*, 601–611. [CrossRef] [PubMed]
30. Marconi, G.D.; Gallorini, M.; Carradori, S.; Guglielmi, P.; Cataldi, A.; Zara, S. The Up-Regulation of Oxidative Stress as a Potential Mechanism of Novel MAO-B Inhibitors for Glioblastoma Treatment. *Molecules* **2019**, *24*, 2005. [CrossRef] [PubMed]
31. Atkin, A.J.; Lynam, J.M.; Moulton, B.E.; Sawle, P.; Motterlini, R.; Boyle, N.M.; Pryce, M.T.; Fairlamb, I.J.S. Modification of the Deoxy-Myoglobin/Carbonmonoxy-Myoglobin UV-Vis Assay for Reliable Determination of CO-Release Rates from Organometallic Carbonyl Complexes. *Dalton Trans.* **2011**, *40*, 5755–5761. [CrossRef]
32. Smulevich, G.; Droghetti, E.; Focardi, C.; Coletta, M.; Ciaccio, C.; Nocentini, M. A Rapid Spectroscopic Method to Detect the Fraudulent Treatment of Tuna Fish with Carbon Monoxide. *Food Chem.* **2007**, *101*, 1071–1077. [CrossRef]
33. Wilson, J.L.; Fayad Kobeissi, S.; Oudir, S.; Haas, B.; Michel, B.; Dubois Randé, J.-L.; Ollivier, A.; Martens, T.; Rivard, M.; Motterlini, R.; et al. Design and Synthesis of New Hybrid Molecules That Activate the Transcription Factor Nrf2 and Simultaneously Release Carbon Monoxide. *Chem. Eur. J.* **2014**, *20*, 14698–14704. [CrossRef] [PubMed]
34. García-Gallego, S.; Bernardes, G.J.L. Carbon-Monoxide-Releasing Molecules for the Delivery of Therapeutic CO in Vivo. *Angew. Chem. Int. Ed. Engl.* **2014**, *53*, 9712–9721. [CrossRef] [PubMed]
35. Biava, M.; Porretta, G.C.; Poce, G.; Supino, S.; Forli, S.; Rovini, M.; Cappelli, A.; Manetti, F.; Botta, M.; Sautebin, L.; et al. Cyclooxygenase-2 Inhibitors. 1,5-Diarylpyrrol-3-Acetic Esters with Enhanced Inhibitory Activity toward Cyclooxygenase-2 and Improved Cyclooxygenase-2/Cyclooxygenase-1 Selectivity. *J. Med. Chem.* **2007**, *50*, 5403–5411. [CrossRef] [PubMed]
36. Biava, M.; Porretta, G.C.; Poce, G.; Supino, S.; Manetti, F.; Forli, S.; Botta, M.; Sautebin, L.; Rossi, A.; Pergola, C.; et al. Synthesis, in Vitro, and in Vivo Biological Evaluation and Molecular Docking Simulations of Chiral Alcohol and Ether Derivatives of the 1,5-Diarylpyrrole Scaffold as Novel Anti-Inflammatory and Analgesic Agents. *Bioorg. Med. Chem.* **2008**, *16*, 8072–8081. [CrossRef]
37. Biava, M.; Porretta, G.C.; Poce, G.; Battilocchio, C.; Manetti, F.; Botta, M.; Forli, S.; Sautebin, L.; Rossi, A.; Pergola, C.; et al. Novel Ester and Acid Derivatives of the 1,5-Diarylpyrrole Scaffold as Anti-Inflammatory and Analgesic Agents. Synthesis and in Vitro and in Vivo Biological Evaluation. *J. Med. Chem.* **2010**, *53*, 723–733. [CrossRef]
38. Battilocchio, C.; Poce, G.; Alfonso, S.; Porretta, G.C.; Consalvi, S.; Sautebin, L.; Pace, S.; Rossi, A.; Ghelardini, C.; Di Cesare Mannelli, L.; et al. A Class of Pyrrole Derivatives Endowed with Analgesic/Anti-Inflammatory Activity. *Bioorg. Med. Chem.* **2013**, *21*, 3695–3701. [CrossRef]
39. Consalvi, S.; Alfonso, S.; Di Capua, A.; Poce, G.; Pirolli, A.; Sabatino, M.; Ragno, R.; Anzini, M.; Sartini, S.; La Motta, C.; et al. Synthesis, Biological Evaluation and Docking Analysis of a New Series of Methylsulfonyl and Sulfamoyl Acetamides and Ethyl Acetates as Potent COX-2 Inhibitors. *Bioorg. Med. Chem.* **2015**, *23*, 810–820. [CrossRef]
40. Bergqvist, F.; Carr, A.J.; Wheway, K.; Watkins, B.; Oppermann, U.; Jakobsson, P.-J.; Dakin, S.G. Divergent Roles of Prostacyclin and PGE2 in Human Tendinopathy. *Arthritis Res. Ther.* **2019**, *21*, 74. [CrossRef]
41. Osti, L.; Berardocco, M.; di Giacomo, V.; Di Bernardo, G.; Oliva, F.; Berardi, A.C. Hyaluronic Acid Increases Tendon Derived Cell Viability and Collagen Type I Expression in Vitro: Comparative Study of Four Different Hyaluronic Acid Preparations by Molecular Weight. *BMC Musculoskelet Disord.* **2015**, *16*, 284. [CrossRef] [PubMed]
42. Gallorini, M.; Petzel, C.; Bolay, C.; Hiller, K.-A.; Cataldi, A.; Buchalla, W.; Krifka, S.; Schweikl, H. Activation of the Nrf2-Regulated Antioxidant Cell Response Inhibits HEMA-Induced Oxidative Stress and Supports Cell Viability. *Biomaterials* **2015**, *56*, 114–128. [CrossRef]
43. Sharma, P.; Maffulli, N. Biology of Tendon Injury: Healing, Modeling and Remodeling. *J. Musculoskelet. Neuronal. Interact.* **2006**, *6*, 181–190. [PubMed]
44. Canesin, G.; Hejazi, S.M.; Swanson, K.D.; Wegiel, B. Heme-Derived Metabolic Signals Dictate Immune Responses. *Front. Immunol.* **2020**, *11*, 66. [CrossRef] [PubMed]
45. Fernández-Fierro, A.; Funes, S.C.; Rios, M.; Covián, C.; González, J.; Kalergis, A.M. Immune Modulation by Inhibitors of the HO System. *Int. J. Mol. Sci.* **2020**, *22*, 294. [CrossRef] [PubMed]
46. Campbell, N.K.; Fitzgerald, H.K.; Dunne, A. Regulation of Inflammation by the Antioxidant Haem Oxygenase 1. *Nat. Rev. Immunol.* **2021**, *21*, 411–425. [CrossRef] [PubMed]
47. Frich, L.H.; Fernandes, L.R.; Schrøder, H.D.; Hejbøl, E.K.; Nielsen, P.V.; Jørgensen, P.H.; Stensballe, A.; Lambertsen, K.L. The Inflammatory Response of the Supraspinatus Muscle in Rotator Cuff Tear Conditions. *J. Shoulder. Elbow. Surg.* **2021**, *30*, e261–e275. [CrossRef]
48. Dakin, S.G.; Newton, J.; Martinez, F.O.; Hedley, R.; Gwilym, S.; Jones, N.; Reid, H.A.B.; Wood, S.; Wells, G.; Appleton, L.; et al. Chronic Inflammation Is a Feature of Achilles Tendinopathy and Rupture. *Br. J. Sports. Med.* **2018**, *52*, 359–367. [CrossRef] [PubMed]

## Supporting information

# A novel class of dual-acting DCH-CORMs counteracts oxidative stress-induced inflammation in human primary tenocytes.

Federico Appetecchia[1†], Sara Consalvi[1†], Emanuela Berrino[1], Marialucia Gallorini[2], Arianna Granese[1], Cristina Campestre[2], Simone Carradori[2*], Mariangela Biava[1*] and Giovanna Poce[1*]

[1]Department of Chemistry and Technologies of Drug, Sapienza University of Rome, piazzale A. Moro 5, 00185 Rome, Italy.
[2]Department of Pharmacy, "G. d'Annunzio" University of Chieti-Pescara, via dei Vestini 31, 66100 Chieti, Italy.

[†]F. Appetecchia and S. Consalvi contributed equally to the work.

*Corresponding Authors. E-mail address: simone.carradori@unich.it (S. Carradori); mariangela.biava@uniroma1.it (M. Biava); giovanna.poce@uniroma1.it (G. Poce)

**Table of contents:**

**Chemistry** S3

**General procedures** S7

Full experimental details and $^{1}H$ NMR for all intermediates S10

Full experimental details and $^{1}H$ NMR and $^{13}C$ NMR for final compounds **1-9** S13

**References** S16

**Chemistry**

All chemicals used were obtained from commercial sources (Merck, Acros, Syngene) and were used as supplied without further purification. Compound **17** was commercially available and purchased from Syngene. Merck silica gel 60 (230–400 mesh) and Merck aluminum oxide (activity II-III, according to Brockmann) were used for chromatographic purifications with the indicated solvents. All operations were monitored by Merck TLC plates (silica gel 60 F 254 and Aluminium oxide F254) and then compounds were visualized under UV light (254 and 365 nm) and/or stained with the relevant reagent. The yields refer to the purified products, and they were not optimized. $^{13}C$ NMR and $^{1}H$ NMR spectra were recorded on a Bruker Avance III NMR 400 spectrometer in the indicated solvent with reference to tetramethylsilane (TMS). The values of the chemical shifts are expressed in parts per million (ppm) and the coupling constants (*J*) in hertz with signal multiplicities reported as singlet (s), doublet (d), triplet (t), quadruplet (q) and multiplet (m). When specified, systematic compound names were generated by ChemDraw Professional 16.0 following IUPAC conventions.

Compounds **1-5** were synthesized as reported in Scheme 1. Briefly, 1,5-diarylpyrroles **11a-d** were obtained through a reaction between 1,4-pentandiones **10a-c** and the suitable aniline according to Paal-Knorr conditions. Sulfamoylpyrrole **11e** was obtained as previously reported [1]. Pyrroles **11a-e** were then regioselectively acylated with ethoxalyl chloride and $TiCl_4$, affording ketoesters **12a-e**. The latter were reduced with triethylsilane and trifluoroacetic acid (TFA) to the ethyl esters **13a-e**, which were then hydrolized with NaOH, providing acids **14a-e** in very good yields. Propargylic derivatives **15a-b** were synthesized by reacting acids **14a-b** and propargyl bromide, using potassium carbonate as a base. To prevent side reactions, derivatives bearing a sulfamoyl moiety (**15c-e**) were synthesized by coupling acids **14c-e** and propargyl alcohol, using EDCI as activating agent and DMAP as covalent nucleophilic catalyst. The terminal alkyne of propargylic intermediates was then reacted with hexacarbonyl dicobalt providing compounds **1-5** in good yields.

**Scheme S1**: synthetic pathway for compounds **1-5**.

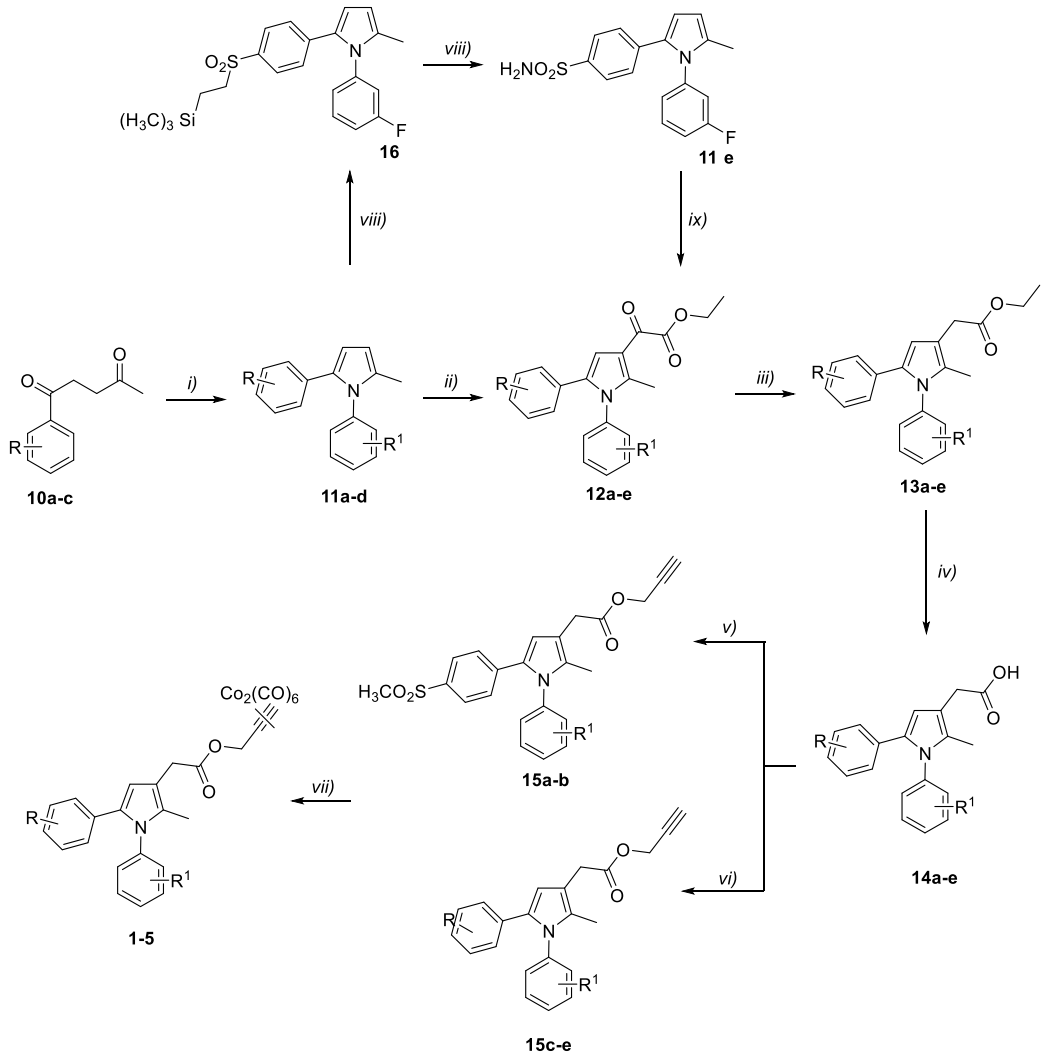


**Reagents and conditions**: *i)* $R^1PhNH_2$, PTSA, EtOH, reflux, 5h; *ii)* $CH_3CH_2OCOCOCl$, $TiCl_4$, $CH_2Cl_2$, room temperature, 4 h; *iii)* $Et_3SiH$, $CF_3COOH$, room temperature, 3h; *iv)* NaOH aq. 1N, EtOH, reflux, 1h; *v)* $BrCH_2CCH$, $K_2CO_3$, DMF, 40°C, 1h; *vi)* $OHCH_2CCH$, $NEt_3$, DMAP, EDCI, room temperature, 24h; *vii)* $Co_2(CO)_8$, THF, room temperature, 2h; *viii)* *n*-BuLi, $(Me_2CH)_2NH$, THF, -78°C, 1.5h, then $(CH_3)_3CH_2SiI$,room temperature, 24h; *ix)* $Bu_4NF$, THF, reflux, 1.5h, then $NH_2OSO_3H$, $CH_3COONa$, room temperature, 1h.

Derivative **6** was easily synthesized according to the synthetic pathway reported in Scheme 2: a reaction between the commercially available acid **17** and propargylic bromide afforded the propargylic ester **18**, which was then reacted with hexacarbonyl dicobalt to yield the DCH complex **6**.

**Scheme S2**: synthetic pathway for compound **6**.

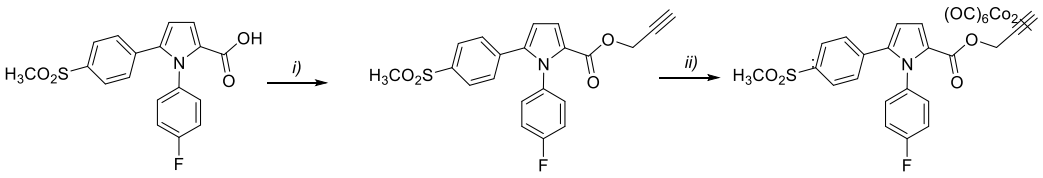


17 18 6

**Reagents and conditions**: *i)* $BrCH_2CCH$, $K_2CO_3$, DMF, 40°C, 1h; *ii)* $Co_2(CO)_8$, THF, room temperature, 2h.

Derivative **7** was prepared as shown in Scheme S3. A Paal-Knorr condensation of 1,4-pentandione **10c** and *p*-aminobenzoic acid gave pyrrole **19** which was in turn reacted with propargyl bromide in the presence of potassium carbonate. The so obtained propargylic ester **20** underwent a reaction with octacarbonyl dicobalt, affording final compound **7** in 70% yield.

**Scheme S3**: synthetic pathway for compound **7**.

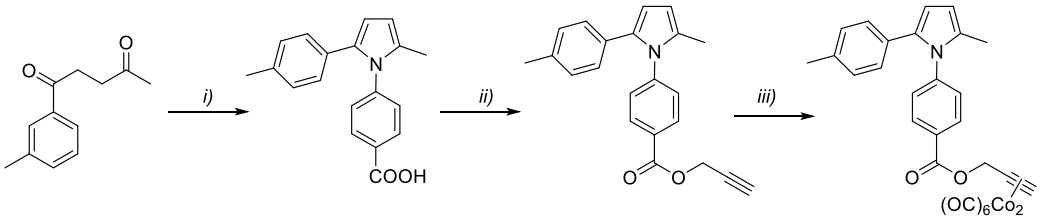


**10c** **19** **20** **7**

**Reagents and conditions**: *i)* $4\text{-}NH_2PhCOOH$, PTSA, EtOH, reflux, 5h; *ii)* $BrCH_2CCH$, $K_2CO_3$, DMF, 40°C, 1h; *iii)* $Co_2(CO)_8$, THF, room temperature, 2h.

1,5-diarylpyrazole alcohols **25a-b** were obtained according to a previously reported procedure [2] and then reacted with propargyl bromide using sodium hydride as a base. The so obtained propargylic ethers **26a-b** were then treated with hexacarbonyl dicobalt affording compounds **8-9** in satisfactory yields (Scheme S4).

**Scheme S4**: synthetic pathway for compounds **8-9**.

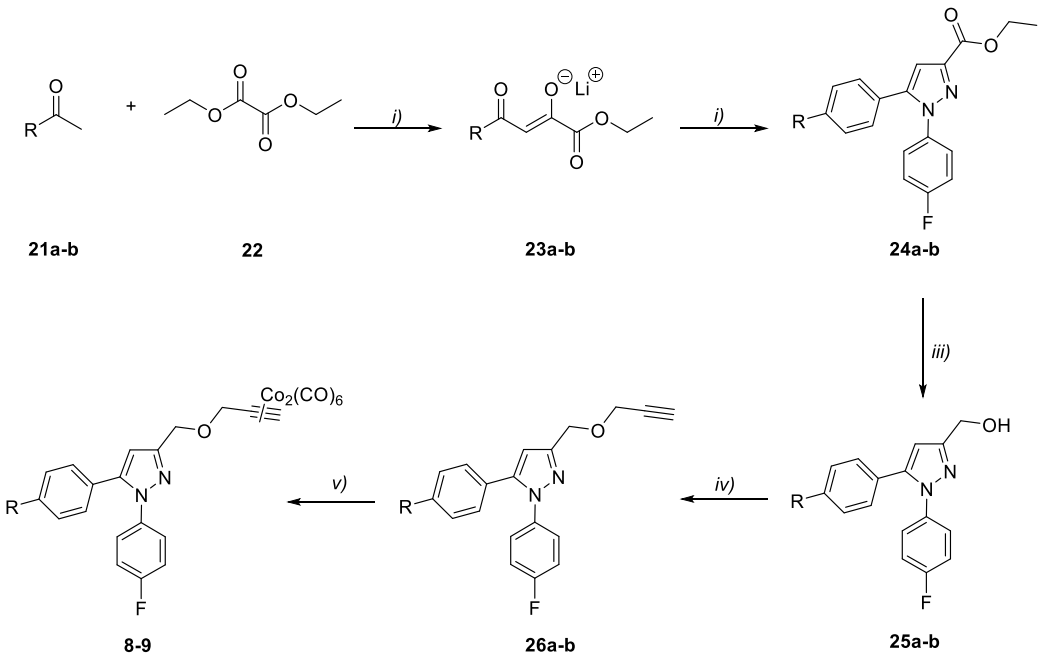


**Reagents and conditions**: *i)* $LiN(Si(CH_3)_3)_2$, THF, -78 °C and then room temperature, 24 h; *ii)* $FC_6H_4NHNH_2.HCl$, EtOH, reflux, 5h; *iii)* $LiAlH_4$, THF, 0°C, 1h, room temperature, 3h; *iv)* $BrCH_2CCH$, NaH, THF, room temperature, 2h; *v)* $Co_2(CO)_8$, THF, room temperature, 2h.

**General procedures**

**General procedure for the preparation of 1,5-diarylpyrroles 11a-d** and **19**.

Compounds **11a-d** were obtained according to Paal-Knorr condensation conditions. 1,4-pentandiones **10a-c** (2.28 mmol), obtained as previously reported [3,4], were dissolved in ethanol (50 mL), then the suitable aniline (2.50 mmol) and *p*-toluenesulfonic acid (0.17 mmol) were added in sequence. The mixture was refluxed for 3 h and was then cooled down and concentrated under reduced pressure. Thereafter, the crude material was purified on silica gel using a mixture of petroleum ether/ethyl acetate 3:1 (v/v) (compounds **11a-b**) or dichloromethane (DCM)/methanol 2% (v/v) (compounds **11c-d**), giving the desired products in very good yields (60-83%).

**1-(3-fluorophenyl)-2-methyl-5-(4-(methylsulfonyl)phenyl)-1H-pyrrole (11a)**. Physicochemical, spectroscopic, and analytical data are consistent with those reported in the literature [4].

**1-(4-fluorophenyl)-2-methyl-5-(4-(methylsulfonyl)phenyl)-1H-pyrrole (11b).** Physicochemical, spectroscopic, and analytical data are consistent with those reported in the literature [4].

**4-(2-(3,4-difluorophenyl)-5-methyl-1*H*-pyrrol-1-yl)benzenesulfonamide (11c)**. White powder, 80% yield. $^1$H NMR (400 MHz, $CDCl_3$): δ ppm= 7.70 (d, 2H, *J*= 8.5 Hz), 7.30-7.26 (m, 1 H), 7.18 (d, 2H, *J*= 8.5 Hz), 7.06-7.02 (m, 1H), 6.97-6.93 (m, 1H), 6.40 (d, 1H, *J* = 3.4 Hz), 6.19 (d, 1H, *J* = 3.4 Hz), 4.92 (s broad, 2H), 2.10 (s, 3H).

**4-(2-methyl-5-(*p*-tolyl)-1*H*-pyrrol-1-yl)benzenesulfonamide (11d)**. White powder, 83% yield. $^1$H NMR (400 MHz, $CDCl_3$): δ ppm= 7.91 (d, 2H, *J* = 8.4 Hz), 7.27 (d, 2H, *J* = 8.4 Hz), 6.97 (d, 2H, *J* = 8.0 Hz), 6.91 (d, 2H, *J* = 8.0 Hz), 6.32 (d, 1H, *J* = 3.3 Hz), 6.12 (d, 1H, *J* = 3.3 Hz), 4.92 (s broad, 2H), 2.27 (s, 3H), 2.16 (s, 3H).

**4-(2-methyl-5-(*p*-tolyl)-1*H*-pyrrol-1-yl)benzoic acid (19)**: white powder, 60% yield. $^1$H NMR ($CDCl_3$) δ ppm: 8.21 (d, 2H, *J*= 8.3 Hz), 7.63 (d, 2H, *J*= 8.3 Hz), 7.13 (d, 2H, *J*= 8.1 Hz), 7.07 (d, 2H, *J*= 8.1 Hz), 6.32 (d, 1H, *J*= 3.3 Hz), 6.20 (d, 1H, *J*= 3.3 Hz), 2.34 (s, 3H), 2.20 (s, 3H).

**General procedure for the preparation of 1,5-diarylpyrrole-3-glyoxylic esters 12a-e**.

To a solution of the appropriate pyrrole (**11a-e**) (9 mmol) in anhydrous DCM (20 mL), ethoxalyl chloride (0.38 mL) and $TiCl_4$ (0.34 mL) were added at 0 °C under a nitrogen flow. The resulting purple mixture was left to react at room temperature for 4 h and was then diluted with water, stirred for an additional 30 minutes, and extracted with DCM. The organic layers were washed with brine and dried over $Na_2SO_4$. After filtration and removal of the solvent under vacuum, the crude residue was purified by column chromatography on silica gel using a mixture of petroleum ether/ethyl acetate (3:1 (v/v)) to afford compounds **12a-e** as pale-yellow solids.

**Ethyl 2-(1-(3-fluorophenyl)-2-methyl-5-(4-(methylsulfonyl)phenyl)-1H-pyrrol-3-yl)-2-oxoacetate (12a).** Physicochemical, spectroscopic, and analytical data are consistent with those reported in the literature [4].

**Ethyl 2-(1-(4-fluorophenyl)-2-methyl-5-(4-(methylsulfonyl)phenyl)-1H-pyrrol-3-yl)-2-oxoacetate (12b).** Physicochemical, spectroscopic, and analytical data are consistent with those reported in the literature [4].

**Ethyl 2-(5-(3,4-difluorophenyl)-2-methyl-1-(4-sulfamoylphenyl)-1*H*-pyrrol-3-yl)-2-oxoacetate** (**12c**). Pale-yellow powder, 50% yield. $^1$H NMR (400 MHz, $CDCl_3$): δ ppm= 7.78 (d, 2H, *J*= 8.5 Hz), 7.32-7.27 (m, 1 H), 7.24 (d, 2H, *J*= 8.5 Hz), 7.10 (s, 1H), 7.06-7.02 (m, 1H), 6.97-6.93 (m, 1H), 4.43 (q, 1H, *J*= 7.1 Hz), 3.04 (s, 3H), 2.47 (s, 3H), 1.43 (t, 2H, *J*= 7.1 Hz).

**Ethyl 2-(2-methyl-1-(4-sulfamoylphenyl)-5-(*p*-tolyl)-1*H*-pyrrol-3-yl)-2-oxoacetate** (**12d**). Pale-yellow powder, 55% yield. $^1$H NMR (400 MHz, $CDCl_3$): δ ppm= 7.97 (d, 2H, *J*= 8.5 Hz), 7.28 (d, 2H, *J*= 8.5 Hz), 6.99 (d, 2H, *J*= 8.0Hz), 6.91-6.88 (m, 3H), 4.92 (s broad, 2H), 4.42 (q, 2H, *J*= 7.1Hz), 2.47 (s, 3H), 2.28 (s, 3H), 1.43 (t, 3H, *J*= 7.1 Hz).

**Ethyl 2-(1-(3-fluorophenyl)-2-methyl-5-(4-sulfamoylphenyl)-1H-pyrrol-3-yl)-2-oxoacetate (12e)**. Physicochemical, spectroscopic, and analytical data are consistent with those reported in the literature [1].

**General procedure for the synthesis of ethyl 1,5-diarylpyrrole-3-acetic esters 13a-e**.

To a solution of the suitable glyoxylic derivative (**12a-e**) (2.3 mmol) in TFA (9 mL), triethylsilane (0.75 mL) was slowly added at 0 °C and under a nitrogen atmosphere. The mixture was stirred for 2 h at room temperature and then the reaction was quenched with 40% aqueous ammonia (10 mL) and extracted with DCM. The organic layers were then washed with brine, dried over $Na_2SO_4$, filtered, and concentrated under vacuum. The resulting residue was purified on silica gel using a mixture of petroleum ether/ethyl acetate (2:1 (v/v)) as the mobile phase and giving compounds **13a-e** as yellowish solids.

**Ethyl 2-(1-(3-fluorophenyl)-2-methyl-5-(4-(methylsulfonyl)phenyl)-1H-pyrrol-3-yl)acetate (13a)** Physicochemical, spectroscopic, and analytical data are consistent with those reported in the literature [4].

**Ethyl 2-(1-(4-fluorophenyl)-2-methyl-5-(4-(methylsulfonyl)phenyl)-1H-pyrrol-3-yl)acetate (13b)** Physicochemical, spectroscopic, and analytical data are consistent with those reported in the literature [4].

**Ethyl 2-(5-(3,4-difluorophenyl)-2-methyl-1-(4-sulfamoylphenyl)-1*H*-pyrrol-3-yl)acetate** (**13c**). Pale-yellow powder, 40% yield. $^1$H NMR (400 MHz, DMSO-$d_6$): δ ppm= 7.87 (d, 2H, *J*= 8.5 Hz), 7.50 (s broad, 2H), 7.41 (d, 2H, *J*= 8.5 Hz), 7.30-7.23 (m, 1H), 7.05-7.00 (m, 1H), 6.80-6.77 (m, 1H), 6.39 (s, 1H), 4.10 (q, 2H, *J* = 7.1 Hz), 3.49 (s, 2H), 2.01 (s, 3H), 1.21 (t, 2H, *J* = 7.1 Hz).

**Ethyl 2-(2-methyl-1-(4-sulfamoylphenyl)-5-(*p*-tolyl)-1*H*-pyrrol-3-yl)acetate** (**13d**). Pale-yellow powder, 45% yield. $^1$H NMR (400 MHz, $CDCl_3$) δ ppm: 7.90 (d, 2H, *J*= 8.6 Hz), 7.25 (d, 2H, *J*= 8.6 Hz), 6.96 (d, 2H, *J*= 8.1 Hz), 6.89 (d, 2H, *J*= 8.1 Hz), 6.33 (s, 1H), 4.86 (s broad, 2H), 4.19 (q, 2H, *J* = 7.1 Hz), 3.50 (s, 2H), 2.26 (s, 3H), 2.10 (s, 3H), 1.30 (t, 2H, *J* = 7.1 Hz).

**Ethyl 2-(1-(4-fluorophenyl)-2-methyl-5-(4-(sulfamoylphenyl)-1H-pyrrol-3-yl)acetate (13e)**. Physicochemical, spectroscopic, and analytical data are consistent with those reported in the literature [1].

**General procedure for the preparation of 1,5-diarylpyrrole-3-acetic acids 14a-e.**

The appropriate 1,5-diarylpyrrole-3-acetic ester (**13a-e**) (2.2 mmol) was dissolved in ethanol (15 mL) and 1N NaOH (15 mL) was slowly added to the solution. The mixture was refluxed for 2 h and then cooled down to room temperature and concentrated under vacuum. The residue was dissolved in water and acidified with 37% HCl. The so obtained precipitate was filtered off affording the acids **14a-e** in very good yields (75-90%).

**2-(1-(3-fluorophenyl)-2-methyl-5-(4-(methylsulfonyl)phenyl)-1H-pyrrol-3-yl)acetic acid (14a).** Physicochemical, spectroscopic, and analytical data are consistent with those reported in the literature [5].

**2-(1-(4-fluorophenyl)-2-methyl-5-(4-(methylsulfonyl)phenyl)-1H-pyrrol-3-yl)acetic acid (14b).** Physicochemical, spectroscopic, and analytical data are consistent with those reported in the literature [5].

**2-(5-(3,4-difluorophenyl)-2-methyl-1-(4-sulfamoylphenyl)-1*H*-pyrrol-3-yl)acetic acid** (**14c**). White powder, 75% yield. $^1$H NMR (400 MHz, DMSO-$d_6$): δ ppm= 12.20 (s broad, 1H), 7.87 (d, 2H, *J*= 8.5 Hz), 7.49 (s broad, 2H), 7.41 (d, 2H, *J*= 8.5 Hz), 7.30-7.23 (m, 1H), 7.04-6.99 (m, 1H), 6.80-6.77 (m, 1H), 6.39 (s, 1H), 3.40 (s, 2H), 2.01 (s, 3H).

**2-(2-methyl-1-(4-sulfamoylphenyl)-5-(*p*-tolyl)-1*H*-pyrrol-3-yl)acetic acid** (**14d**). White powder, 70% yield. $^1$H NMR (400 MHz, DMSO-$d_6$): δ ppm= 12.12 (s broad, 1H), 7.84 (d, 2H, *J*= 8.5 Hz), 7.47 (s broad, 2H), 7.37 (d, 2H, *J*= 8.5 Hz), 6.99 (d, *J* = 8.1 Hz, 2H), 6.89 (d, *J* = 8.1 Hz, 2H), 6.25 (s, 1H), 3.39 (s, 2H), 2.21 (s, 3H), 2.01 (s, 3H).

**2-(1-(3-fluorophenyl)-2-methyl-5-(4-sulfamoylphenyl)-1H-pyrrol-3-yl)acetic acid (14e).** Physicochemical, spectroscopic, and analytical data are consistent with those reported in the literature [1].

**General procedure for the preparation of propargylic esters 15a-b, 18 and 20.**

To a solution of the appropriate acid (**14a-b**, **17** and **19**) (0.77 mmol) in *N*,*N*-dimethylformamide (DMF) (3 mL), potassium carbonate (0.18 g) and propargyl bromide 80% solution in toluene (0.2

mL) were added at room temperature under a nitrogen atmosphere. The mixture was then heated at 40 °C and stirred for 1 h. After removal of the solvent under vacuum, the mixture was diluted with water and extracted with ethyl acetate. The organic phases were then washed with 1N HCl, brine and dried over $Na_2SO_4$. After filtration and concentration under reduced pressure, the crude product was purified on silica gel using a mixture of cyclohexane/ethyl acetate (3:1 (v/v)) as eluent to afford derivatives **15a-b, 18** and **20** in good yields (37-90%).

**Prop-2-yn-1-yl 2-(1-(3-fluorophenyl)-2-methyl-5-(4-(methylsulfonyl)phenyl)-1*H*-pyrrol-3-yl)acetate** (**15a**). Yellow powder, 80% yield. $^1$H NMR ($CDCl_3$): δ ppm= 7.68 (d, 2H, *J*= 8.6 Hz), 7.41-7.35 (m, 1H), 7.17 (d, 2H, *J*= 8.6 Hz), 7.13-7.08 (m, 1H), 6.96-6.94 (m, 1H), 6.92-6.89 (m, 1H), 6.52 (s, 1H), 4.74 (d, 2H, *J*= 2.5 Hz), 3.57 (s, 2H), 3.01 (s, 3H), 2.50 (t, 1H, *J*= 2.5 Hz), 2.09 (s, 3H).
**Prop-2-yn-1-yl 2-(1-(4-fluorophenyl)-2-methyl-5-(4-(methylsulfonyl)phenyl)-1*H*-pyrrol-3-yl)acetate** (**15b**). Yellow powder, 92% yield. $^1$H NMR ($CDCl_3$): δ ppm= 7.67 (d, 2H, *J*= 8.5 Hz), 7.17-7.08 (m, 6H), 6.52 (s, 1H), 4.74 (d, 2H, *J*= 2.5 Hz), 3.57 (s, 2H), 3.02 (s, 3H), 2.50 (t, 1H, *J*= 2.5 Hz), 2.07 (s, 3H).
**Prop-2-yn-1-yl 1-(4-fluorophenyl)-5-(4-(methylsulfonyl)phenyl)-1*H*-pyrrole-2-carboxylate** (**18**). Yellow powder, 37% yield. $^1$H NMR (400 MHz, $CDCl_3$): δ ppm= 7.76 (d, 2H, *J*= 8.5 Hz), 7.28-7.25 (m, 3H), 7.20-7.17 (m, 2H), 7.09-7.05 (m, 2H), 6.55 (d, 1 H, *J* = 4.1 Hz), 4.73 (d, 2H, *J* = 2.5 Hz), 3.02 (s, 3H), 2.46 (t, 1H, *J* = 2.5 Hz).
**Prop-2-yn-1-yl 4-(2-methyl-5-(*p*-tolyl)-1*H*-pyrrol-1-yl)benzoate** (**20**). Yellow powder, 90% yield. $^1$H NMR ($CDCl_3$): δ ppm= 8.06 (d, 2H, *J*= 8.3 Hz), 7.22 (d, 2H, *J*= 8.3 Hz), 6.95 (d, 2H, *J*= 8.1 Hz), 6.91 (d, 2H, *J*= 8.1 Hz), 6.32 (d, 1H, *J*= 3.3 Hz), 6.11 (d, 1H, *J*= 3.3 Hz), 4.93 (d, 2H, *J*= 2.2 Hz), 2.53 (t, 1H, *J*= 2.5 Hz), 2.26 (s, 3H), 2.16 (s, 3H).

**General procedure for the preparation of propargylic esters 15c-e.**

To a solution of the appropriate acid (**14c-e**) (1 mmol) in *N*,*N*-dimethylformamide (DMF) (3 mL), TEA (1.2 mmol), DMAP (1.2 mmol) and EDCI (1.2 mmol) were added in sequence under a nitrogen atmosphere. The mixture was stirred for 1 h at room temperature, then propargyl alcohol (4 mmol) was added. After 15 h the reaction was quenched with water (10 mL) and extracted with DCM. The organic layers were then washed with 1N HCl, brine and dried over $Na_2SO_4$. After filtration and evaporation under vacuum, the crude product was purified on silica gel using a mixture of cyclohexane/ethyl acetate (1:1 (v/v)) as eluent to afford derivatives **15c-e** as yellowish solids.

**Prop-2-yn-1-yl 2-(5-(3,4-difluorophenyl)-2-methyl-1-(4-sulfamoylphenyl)-1*H*-pyrrol-3-yl)acetate** (**15c**). Yellow powder, 25% yield. $^1$H NMR (400 MHz, $CDCl_3$): δ ppm= 7.95 (d, 2H, *J*= 8.5 Hz), 7.26 (d, 2H, *J*= 8.5 Hz), 6.97-6.90 (m, 1H), 6.81-6.78 (m, 1H), 6.69-6.67 (m, 1H), 6.35 (s, 1H), 5.05 (s broad, 2H), 4.73 (d, 2H, *J* = 2.3 Hz), 3.55 (s, 2H), 2.49 (t, 1H, *J* = 2.3 Hz), 2.08 (s, 3H).
**Prop-2-yn-1-yl 2-(2-methyl-1-(4-sulfamoylphenyl)-5-(*p*-tolyl)-1*H*-pyrrol-3-yl)acetate** (**15d**): yellow powder, 25% yield. $^1$H NMR (400 MHz, $CDCl_3$) δ ppm: 7.89 (d, 2H, *J*= 8.6 Hz), 7.25 (d, 2H, *J*= 8.6 Hz), 6.95 (d, 2H, *J* = 8.1 Hz), 6.88 (d, 2H, *J* = 8.1 Hz), 6.33 (s, 1H), 5.00 (s broad, 2H), 4.73 (d, 2H, *J* = 2.5 Hz), 3.56 (s, 2H), 2.48 (t, 1H, *J* = 2.5 Hz), 2.25 (s, 3H), 2.09 (s, 3H).
**Prop-2-yn-1-yl 2-(1-(3-fluorophenyl)-2-methyl-5-(4-sulfamoylphenyl)-1*H*-pyrrol-3-yl)acetate (15e): yellow powder**, 26% yield. $^1$H NMR (400 MHz, $CDCl_3$) δ ppm: 7.67 (d, 2H, *J*= 8.5 Hz), 7.40-7.35 (m, 1H), 7.14-7.08 (m, 3H), 6.96-6.88 (m, 2H), 6.50 (s, 1H), 4.80 (s, 2H), 4.75-4.73 (m, 4H), 3.57 (s, 2H), 2.50 (t, 1H, *J* = 2.5 Hz), 2.09 (s, 3H).

**General procedure for the synthesis of 1-(3-fluorophenyl)-2-methyl-5-(4-((3-(trimethylsilyl)propyl)sulfonyl)phenyl)-1H-pyrrole (16).**

Compound **16** was prepared according to the same procedure outlined previously [Consalvi2015]. Lithium diisopropylamide (LDA) was prepared *in situ* by adding dropwise 3.9 mL of butyllithium solution (2.5 M in hexane) to a solution of diisopropylamine (DIPA) (1.75 mL) in dry THF (13 mL) at 0 °C and under nitrogen atmosphere. After 30 minutes stirring, the reaction was cooled down to -78 °C and a solution of the pyrrole **11a** (8 mmol) in dry THF (23 mL) was slowly added. The mixture was stirred for 1.5 h. 2.58 mL of iodomethyltrimethylsilane were then added dropwise and the reaction was allowed to warm to room temperature. After 15h, the reaction was quenched with water and the pH was adjusted (pH= 2) with 1N HCl. The so obtained mixture was extracted with ethyl acetate and the organic layers were washed with brine and dried over $Na_2SO_4$. After evaporation under vacuum, the crude material was purified on silica gel using a mixture of cyclohexane/ethyl acetate 15:1 (v/v) to afford **16** as a white powder.

**1-(3-fluorophenyl)-2-methyl-5-(4-((3-(trimethylsilyl)propyl)sulfonyl)phenyl)-1H-pyrrole (16).**
Physicochemical, spectroscopic, and analytical data are consistent with those reported in the literature [1].

**General procedure for the preparation of 4-(1-(3-fluorophenyl)-5-methyl-1*H*-pyrrol-2-yl)benzenesulfonamide (11e)**

A solution of tetrabutylammonium fluoride (5 mL, 1M in THF) was added to a solution of compound **16** (1.5 mmol) in dry THF (12 mL) under a nitrogen flow and refluxed for 1.5 h. After cooling down to room temperature, a solution of sodium acetate (1.3 g) and hydroxylamine-*O*-sulfonic acid (1.8 g) in water (5 mL) was added, and the reaction was stirred for 1 h. The mixture was then diluted with water and extracted with ethyl acetate. The organic layers were washed with $NaHCO_3$ saturated solution, brine and dried over $Na_2SO_4$. After filtration and removal of the solvent under vacuum, the crude product was purified on silica gel with a mixture of cyclohexane/ethyl acetate 2:1 (v/v) as eluent. Recrystallization from diethyl ether yielded **11e** as a white powder.

**4-(1-(3-fluorophenyl)-5-methyl-1*H*-pyrrol-2-yl)benzenesulfonamide (11e).** Physicochemical, spectroscopic, and analytical data are consistent with those reported in the literature [1].

**General procedure for the preparation of lithium salts 23a-b**.

A solution of lithium bis(trimethylsilyl)amide (12.3 mmol) in 30 mL of anhydrous THF was cooled to -78°C. Afterwards, a solution of the appropriate acetophenone **21a-b** in 3 ml of anhydrous THF was added dropwise and the mixture was stirred for 1h. Diethyl oxalate was then added over 5 minutes and the resulting dark orange solution was warmed to room temperature over 4 h. After 18 h stirring, the precipitate was filtered off and washed with diethyl ether affording lithium salts **23a-b** in 80% yield.

**Lithium (*Z*)-1-ethoxy-4-(4-isopropylphenyl)-1,4-dioxobut-2-en-2-olate (23a).** Physicochemical, spectroscopic, and analytical data are consistent with those reported in the literature [2].

**Lithium (*Z*)-1-ethoxy-1,4-dioxo-4-(4-(trifluoromethyl)phenyl)but-2-en-2-olate (23b).** Physicochemical, spectroscopic, and analytical data are consistent with those reported in the literature [2].

**General procedure for the preparation of carboxylates 24a-b**

4-fluorophenylhydrazine hydrochloride (2.12 mmol) was added to a solution of the suitable lithium salt **23a-b** (2.12 mmol) in 12 mL of ethanol. The reaction mixture was heated at 90°C for 5 h and then cooled down to room temperature. After removal of the solvent under vacuum, the mixture was extracted with ethyl acetate and the organic layers were washed with brine, dried over $Na_2SO_4$ and evaporated *in vacuo*. The crude product was purified by column chromatography (cyclohexane/ethyl acetate 2/1 (v/v)) to yield carboxylates **24a-b** in good yields (65-70%).

**Ethyl 1-(4-fluorophenyl)-5-(4-isopropylphenyl)-1*H*-pyrazole-3-carboxylate (24a).** Physicochemical, spectroscopic, and analytical data are consistent with those reported in the literature [2].

**Ethyl 1-(4-fluorophenyl)-5-(4-(trifluoromethyl)phenyl)-1*H*-pyrazole-3-carboxylate (24b).** Physicochemical, spectroscopic, and analytical data are consistent with those reported in the literature [2].

**General procedure for the preparation of alcohols 25a-b**

The appropriate carboxylate **24a-b** (0.41 mmol) was dissolved in THF and cooled down to 0°C, then $LiAlH_4$ was added dropwise under a nitrogen flow (0.49 mL, 1 M in THF). At the end, the reaction was cooled down to 0°C and quenched with 0.18 mL of ethyl acetate, 0.08 mL of water and 0.1 mL of NaOH 2N. After 30 minutes stirring, the precipitate was filtered off and the filtrate was dried over $Na_2SO_4$ and concentrated *in vacuo*. The resulting crude product was purified by column chromatography (cyclohexane/ethyl acetate 1/1 (v/v)) to afford alcohols **25a-b** in good yields (63-91%).

**(1-(4-Fluorophenyl)-5-(4-isopropylphenyl)-1*H*-pyrazol-3-yl)methanol (25a).** Physicochemical, spectroscopic, and analytical data are consistent with those reported in the literature [2].

**(1-(4-Fluorophenyl)-5-(4-(trifluoromethyl)phenyl)-1*H*-pyrazol-3-yl)methanol (25b).** Physicochemical, spectroscopic, and analytical data are consistent with those reported in the literature [2].

**General procedure for the preparation of propargylic ethers 26a-b**

A solution of the appropriate alcohol **25a-b** (0.22 mmol) in THF (2 mL) was added dropwise at 0°C to a suspension of NaH 60% (0.22 mmol) in mineral oil under a nitrogen atmosphere. After stirring for 10 min, the mixture was allowed to warm at room temperature, and an 80% solution of propargyl bromide in toluene (0.66 mmol) was added. After 24 h, the reaction was cooled down to 0 °C, quenched with water (10 mL) and stirred for 30 minutes. The resulting mixture was extracted with ethyl acetate and the organic layers were washed with a $NaHCO_3$ saturated solution, brine and dried over $Na_2SO_4$. After filtration and removal of the solvent under vacuum, the solid residue was purified on silica gel using a mixture of petroleum ether/ethyl acetate (10:1 (v/v)) as eluent to afford the desired products **26a-b** in good yields (65-70%).

**1-(4-fluorophenyl)-5-(4-isopropylphenyl)-3-((prop-2-yn-1-yloxy)methyl)-1*H*-pyrazole** (**26a**). Colorless oil, 65% yield. $^1$H NMR ($CDCl_3$): δ ppm= 7.29-7.26 (m, 2H), 7.17-7.11 (m, 4H), 7.04-7.00 (m, 2H), 6.53 (s, 1H), 4.70 (s, 2H), 4.29 (d, 2H, *J*= 2.4 Hz), 2.89 (sept, 1H, *J*= 6.9 Hz), 2.48 (t, 1H, *J*= 2.4 Hz), 1.24 (d, 6H, *J*= 6.9 Hz).

**1-(4-fluorophenyl)-3-((prop-2-yn-1-yloxy)methyl)-5-(4-(trifluoromethyl)phenyl)-1*H*-pyrazole** (**26b**). Colorless oil, 70% yield. $^1$H NMR ($CDCl_3$) δ ppm: 7.57 (d, 2H, *J*= 8.3 Hz), 7.33 (d, 2H, *J*= 8.3 Hz), 7.27-7.04 (m, 2H), 7.08-7.04 (m, 2H), 6.63 (s, 1H), 4.72 (s, 2H), 4.30 (d, 2H, *J*= 2.3 Hz), 2.49 (t, 1H, *J*= 2.3 Hz).

**General procedure for the synthesis of (dicobalthexacarbonyl)derivatives 1-9**

To a solution of the appropriate propargyl derivative (**15a-e**, **18**, **20** and **26a-b**) (0.62 mmol) dissolved in the least volume of THF, dicobalt octacarbonyl (0.68 mmol) was added under a nitrogen atmosphere at room temperature. The resulting black mixture was left stirring for 2 h and the solvent was removed under reduced pressure. The so obtained black crude product was filtered on celite and then thoroughly washed with DCM. The filtrate was concentrated *in vacuo* and the black residue was purified on silica gel with a mixture of cyclohexane/ethyl acetate (20:1 (v/v)) or a mixture of DCM/ethyl acetate (15:1 (v/v)) as the mobile phase to obtain final products **1-9** as red solids.

**Prop-2-yn-1-yl 2-(1-(4-fluorophenyl)-2-methyl-5-(4-(methylsulfonyl)phenyl)-1*H*-pyrrol-3-yl)acetate hexacarbonyldicobalt** (**1**). Red powder, 80% yield. $^1$H NMR (400 MHz, $CDCl_3$): δ ppm= 7.60 (d, *J* = 8.1 Hz, 2H), 7.16-7.12 (m, 6H), 6.52 (s, 1H), 6.08 (s, 1H), 5.34 (s, 2H), 3.60 (s, 2H), 3.01 (s, 3H), 2.06 (s, 3H). $^{13}$C NMR (100 MHz, $CDCl_3$): δ ppm= 202.3, 171.7, 164.28, 161.53,138.30,

136.88, 134.88, 134.32, 130.07, 129.59, 121.07, 120.47, 116.56, 113.37, 110.08, 87.99, 71.76, 65.24, 44.48, 31.91, 10.92.

**Prop-2-yn-1-yl 2-(1-(3-fluorophenyl)-2-methyl-5-(4-(methylsulfonyl)phenyl)-1*H*-pyrrol-3-yl)acetate hexacarbonyldicobalt** (**2**). Red powder, 80% yield. $^{1}$H NMR (400 MHz, $CDCl_3$): δ ppm= 7.68 (d, 2H, *J* = 8.1 Hz), 7.41-7.35 (m, 1H), 7.17 (d, 2H, *J* = 8.1 Hz), 7.14-7.10 (m, 1H), 6.96-6.88 (m, 2H), 6.53 (s, 1H), 6.08 (s, 1H), 5.34 (s, 2H), 3.60 (s, 2H), 3.01 (s, 3H), 2.09 (s, 3H). $^{13}$C NMR (100 MHz, $CDCl_3$): δ ppm= 199.21, 171.60, 164.04, 161.53, 140.40, 140.37, 140.29, 138.14, 137.01, 131.62, 131.37, 130.67, 130.61, 127.38, 124.40, 116.07, 115.55, 115.23, 113.75, 112.79, 88.80, 72.05, 65.27, 44.20, 31.88, 10.95.

**Prop-2-yn-1-yl 2-(5-(3,4-difluorophenyl)-2-methyl-1-(4-sulfamoylphenyl)-1H-pyrrol-3-yl)acetate hexacarbonyldicobalt** (**3**). Red powder, 10% yield. $^{1}$H NMR (400 MHz, DMSO-$d_6$): δ ppm= 7.87 (d, *J* = 8.1 Hz, 2H), 7.50 (s broad, 2H), 7.40 (d, *J* = 8.1 Hz, 2H), 7.30-7.23 (m, 1H), 7.02-6.97 (m, 1H), 6.80-6.78 (m, 2H), 6.38 (s, 1H), 5.39 (s, 2H), 3.57 (s, 2H), 2.01 (s, 3H). $^{13}$C NMR (100 MHz, $CDCl_3$) δ ppm: 201.57, 171.22, 152.88, 151.24, 147.97, 142.74, 141.08, 131.35, 129.01, 127.60, 123.98, 123.88, 117.26, 117.09, 116.79, 116.61, 113.53, 111.84, 89.52, 75.06, 65.42, 32.01, 11.16.

**Prop-2-yn-1-yl 2-(2-methyl-1-(4-sulfamoylphenyl)-5-(*p*-tolyl)-1*H*-pyrrol-3-yl)acetate hexacarbonyldicobalt** (**4**). Red powder, 40% yield. $^{1}$H NMR (400 MHz, DMSO-$d_6$): δ ppm= 7.84 (d, 2H, *J* = 8.2 Hz), 7.49 (s broad, 2H), 7.36 (d, 2 H, *J* = 8.2 Hz), 7.00 (d, 2H, *J* = 8 Hz), 6.88 (d, 2H, *J* = 8 Hz), 6.79 (s, 1H), 6.25 (s, 1H), 5.39 (s, 2H), 3.56 (s, 2H), 2.21 (s, 3H), 2.01 (s, 3H). $^{13}$C NMR (100 MHz, $CDCl_3$); δ ppm= 201.37, 171.38, 143.35, 140.46, 136.08, 133.59, 129.63, 129.07, 128.99, 128.54, 127.96, 127.33, 113.26, 110.80, 89.02, 75.00, 62.29, 32.16, 21.06, 11.22.

**Prop-2-yn-1-yl 2-(1-(3-fluorophenyl)-2-methyl-5-(4-sulfamoylphenyl)-1*H*-pyrrol-3-yl)acetate hexacarbonyldicobalt** (**5**). Red powder, 40% yield. $^{1}$H NMR (400 MHz, DMSO-$d_6$): δ ppm= 7.60 (d, 2H, *J* = 8.1 Hz), 7.53–7.47 (m, 1H), 7.32–7.20 (m, 4H), 7.14 (d, 2H, *J* = 8.1 Hz), 7.04-7.02 (m, 1H), 6.79 (s, 1H), 6.47 (s, 1H), 5.39 (s, 2H), 3.58 (s, 2H), 2.03 (s, 3H). $^{13}$C NMR (100 MHz, $CDCl_3$): δ ppm= 200.05, 171.26, 163.07, 160.56, 138.47, 137.16, 131.46, 131.32, 130.66, 127.35, 126.41, 124.41, 116.02, 115.80, 115.22, 113.42, 112.59, 88.63, 75.09, 65.37, 32.03, 11.08.

**Prop-2-yn-1-yl 1-(4-fluorophenyl)-5-(4-(methylsulfonyl)phenyl)-1*H*-pyrrole-2-carboxylate hexacarbonyldicobalt (6)**. Red powder, 90% yield. $^{1}$H NMR (400 MHz, $CDCl_3$): δ ppm= 7.76 (d, 2H, *J*= 8.1 Hz), 7.28-7.25 (m, 3H), 7.20-7.17 (m, 2H), 7.10-7.06 (m, 2H), 6.55 (d, 1 H, *J* = 3.7 Hz), 6.08 (s, 1H), 5.31 (s, 2H), 3.02 (s, 3H). $^{13}$C NMR (100 MHz, $CDCl_3$) δ ppm: 201.7, 170.4, 163.02, 160.13, 140.31, 138.99, 135.23, 135.01, 130.12, 128.59, 128.33, 127.01, 122.98, 121.14, 117.01, 112.35, 88.43, 76.17, 56.24, 43.98.

**Prop-2-yn-1-yl 4-(2-methyl-5-(*p*-tolyl)-1*H*-pyrrol-1-yl)benzoate hexacarbonyldicobalt** (**7**). Red powder, 70% yield. $^{1}$H NMR (400 MHz, $CDCl_3$): δ ppm= 8.09 (d, 2H, *J*= 8.5 Hz), 7.21 (d, 2H, *J*= 8.5 Hz), 6.95-6.89 (m, 4H), 6.32 (d, 1H, *J*= 3.2 Hz), 6.13 (s, 1H), 6.10 (d, 1H, *J*= 3.2 Hz), 5.53 (s, 2H), 2.26 (s, 3H), 2.16 (s, 3H). $^{13}$C NMR (100 MHz, $CDCl_3$): δ ppm= 199.97, 170.13, 141.52, 139.11, 134.00, 130.11, 127.73, 127.64, 127.02, 126.83, 126.34, 122.16, 112.83, 111.96, 89.75, 78.06, 56.28, 21.47, 12.01.

**1-(4-fluorophenyl)-5-(4-isopropylphenyl)-3-((prop-2-yn-1-yloxy)methyl)-1*H*-pyrazole hexacarbonyldicobalt (8)**. Red powder, 70% yield. $^{1}$H NMR (400 MHz, $CDCl_3$): δ ppm= 7.27–7.23 (m, 2H), 7.17–7.09 (m, 4H), 7.04-7.00 (m, 2H), 6.54 (s, 1H), 6.09 (s, 1H), 4.78 (m, 4H), 2.90 (sept, 1H, *J* = 7.0 Hz), 1.24 (d, 6H, *J* = 7.0 Hz). $^{13}$C NMR (100 MHz, $CDCl_3$): δ ppm= 200.12, 162.12, 159.04, 149.25, 145.03, 136.27, 130.11, 128.82, 127.54, 127.35, 126.01, 115.92, 115.69, 106.76, 89.16, 76.80, 65.13, 58.09, 33.81, 23.45.

**1-(4-fluorophenyl)-3-((prop-2-yn-1-yloxy)methyl)-5-(4-(trifluoromethyl)phenyl)-1H-pyrazole hexacarbonyldicobalt (9)**: Red powder, 63% yield. $^{1}$H NMR (400 MHz, $CDCl_3$): δ ppm= 7.57 (d, 2H, *J* = 8.2 Hz), 7.29 (d, 2H, *J* = 8.2 Hz), 7.25–7.22 (m, 2H), 7.08-7.04 (m, 2H), 6.63 (s, 1H), 6.10 (s, 1H), 4.80 (m, 4H). $^{13}$C NMR (100 MHz, $CDCl_3$): δ ppm= 200.03, 163.01, 160.46, 147.98, 142.03, 136.30, 135.82, 130.78, 130.51, 130.21, 130.01, 128.78, 127.26, 123.58, 123.19, 121.64, 116.48, 116.20, 108.13, 89.88, 77.20, 65.50, 59.03.

**References**

1. Consalvi, S.; Alfonso, S.; Di Capua, A.; Poce, G.; Pirolli, A.; Sabatino, M.; Ragno, R.; Anzini, M.; Sartini, S.; La Motta, C.; et al. Synthesis, Biological Evaluation and Docking Analysis of a New Series of Methylsulfonyl and Sulfamoyl Acetamides and Ethyl Acetates as Potent COX-2 Inhibitors. *Bioorg Med Chem* **2015**, *23*, 810–820, doi:10.1016/j.bmc.2014.12.041.
2. Poce, G.; Consalvi, S.; Venditti, G.; Alfonso, S.; Desideri, N.; Fernandez-Menendez, R.; Bates, R.H.; Ballell, L.; Barros Aguirre, D.; Rullas, J.; et al. Novel Pyrazole-Containing Compounds Active against Mycobacterium Tuberculosis. *ACS Med Chem Lett* **2019**, *10*, 1423–1429, doi:10.1021/acsmedchemlett.9b00204.
3. Biava, M.; Porretta, G.C.; Poce, G.; Supino, S.; Deidda, D.; Pompei, R.; Molicotti, P.; Manetti, F.; Botta, M. Antimycobacterial Agents. Novel Diarylpyrrole Derivatives of BM212 Endowed with High Activity toward Mycobacterium Tuberculosis and Low Cytotoxicity. *J Med Chem* **2006**, *49*, 4946–4952, doi:10.1021/jm0602662.
4. Biava, M.; Porretta, G.C.; Poce, G.; Supino, S.; Forli, S.; Rovini, M.; Cappelli, A.; Manetti, F.; Botta, M.; Sautebin, L.; et al. Cyclooxygenase-2 Inhibitors. 1,5-Diarylpyrrol-3-Acetic Esters with Enhanced Inhibitory Activity toward Cyclooxygenase-2 and Improved Cyclooxygenase-2/Cyclooxygenase-1 Selectivity. *J Med Chem* **2007**, *50*, 5403–5411, doi:10.1021/jm0707525.
5. Biava, M.; Porretta, G.C.; Poce, G.; Battilocchio, C.; Manetti, F.; Botta, M.; Forli, S.; Sautebin, L.; Rossi, A.; Pergola, C.; et al. Novel Ester and Acid Derivatives of the 1,5-Diarylpyrrole Scaffold as Anti-Inflammatory and Analgesic Agents. Synthesis and in Vitro and in Vivo Biological Evaluation. *J Med Chem* **2010**, *53*, 723–733, doi:10.1021/jm901269y.

# Chapter 3 – Malaria: Current Status and Key Interventions to Block Transmission

## 3.1 Malaria

The threat of malaria has existed for ages. Historical medical documents reporting typical ill health, malarial fevers and other malarial-related symptoms occur from around 2700 BC from early civilizations based in China and then also in India, Mesopotamia and Greece. In the Middle Ages the word *malaria* was coined from the Italian words *mal*, "bad", and *aria* ,"air", since it was associated with marshes and swamps. However, it was only established at the end of the 19th century that this disease is caused by a protozoan parasite, identified as *Plasmodium*, and transmitted by *Anopheles* mosquitoes to humans. The full understanding of the cycle of *Plasmodium* parasites comes from different research occurred throughout the 20th century.[1,2]

Human malaria is caused by five different *Plasmodium* species: *P. falciparum*, *P. vivax*, *P. ovale*, *P. malariae* and *P.knowlesi.* The first four are specific for humans, while *P. knowlesi* is naturally maintained in macaque monkeys. *P. falciparum* is most common in sub-Saharan Africa and is responsible for the majority of the severe illness and deaths brought on by malaria. *P. vivax* contributes between 25% and 40% of the global malaria burden and is mostly found in South and Southeast Asia and some regions of Central and South America.[3] Anti-malarial research focuses for the major part on *P. falciparum* not only because is the most dangerous species, but also because *in vitro* culture techniques of *P. vivax* are not yet available and the evaluation of therapy outcomes in vivax malaria are more complex to interpret.[4]

The clinical manifestations of malaria vary with parasite species, epidemiology, immunity, and age. Typically, it results in a severe illness with a high fever and shivering chills, but in more extreme cases, it can result in serious health issues such seizures, brain damage, difficulty in breathing, organ failure, and death.[5,6]

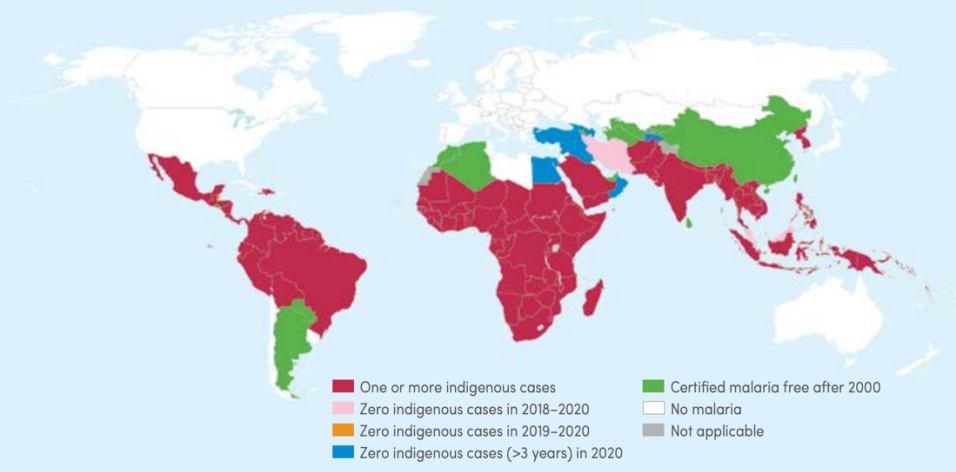


**Figure 3.1.** Global distribution of malaria in 2020. The status of countries with indigenous malaria cases in 2000 (figure from World Health Organization, 2021).[6]

The eradication of malaria in the US (1951) was possible thanks to actions like the widespread spraying of DDT and the use of chloroquine, inspired the creation of the Centers for Disease Control and Prevention (CDC) and global campaigns against malaria. Thus, in 1955 The World Health Organization (WHO) launched the Global Malaria Eradication Program (GMEP) to eradicate malaria also in the rest of the world. While malaria was successfully eradicated in Europe and North America and in the large part of Asia, in the undeveloped Sub-Saharan Africa regions malaria was not much affected. The struggle to reach complete malaria elimination in Sub-Saharan Africa was related not only to the more favorable climate conditions for the spread of the disease, but also to different economical and social settings that hamper the international cooperation between various countries and communities. Thus, research and development activities for malaria eradication turned into malaria control. Only after several decades, the global fight against malaria resuscitated interest with the African Summit on Roll Back Malaria (2000) and the initiation of a Global Fund in 2002. Ever since, new effective strategies for malaria surveillance, prevention, diagnosis and treatment of malaria were deployed and huge progress has been made in decreasing the burden of this life-threatening disease.[7–10]

Nevertheless, since 2015 the incidence of malaria cases and deaths is seeing a "flat-line" over the years due to the high impact of emerging parasite and vector resistance to the current treatments.[1,6,11] The latter include the use of anti-malarial drugs for human prevention and

treatment and the use of mosquito nets, insect repellents, insecticide spraying, and draining standing water for mosquito control.[6] In response to this deceleration in progress, in 2015 the first world's malaria vaccine was approved by the European Medicines Agency (EMA) for the use in children in Africa and in October 2021 it was recommended for broad use by WHO.[6,12]

Despite substantial progress in the field, malaria remains a global health issue accounting for 241 million cases and more than 600.000 deaths in 2020, especially among young children and in Sub-Saharan Africa (93% global deaths), to be one of the deadliest infectious diseases in the world.[6] These numbers are predicted to increase due to evolving resistance to the current malaria control and elimination strategies. Furthermore, the recent coronavirus disease 2019 (COVID-19) may threaten malaria control in multiple ways.[13] Therefore, there is an urgent need to tackle down the spreading of the diseases with novel tools and treatments that can be added to the existing interventions to reach the targets of Global technical strategy (GTS) (e.g., reduction of malaria mortality and case incidence by at least 90% withing 2030).[6]

## 3.2 *Plasmodium* Biology and Malaria Life Cycle

The genus *Plasmodium* is a member of Apicomplexa, a wider group of protozoans, and particularly belongs to the order Haemosporida and family Plasmodiidae. As all Apicomplexa *Plasmodium* is an obligate intracellular organism, and its life cycle is complex involving two hosts (Figure 3.2). So far *Plasmodium* has been identified in more than 200 species and as previously mentioned, only five of them can infect humans.[3]

*Plasmodium* parasites are haploid throughout their life cycle, with the exception of a brief diploid phase that occurs after fertilization in the midgut of the mosquito. As other eukaryotic cells, the endoplasmic reticulum (ER) is connected to the nucleus and proteins are transported to the Golgi apparatus, which in apicomplexans is often just one membrane-bound compartment.[14] Besides a plasma membrane, *Plasmodium* parasites possess a distinctive inner membrane complex (IMC), which is crucial for preserving the parasite's shape and controlling movement and the microtubules are attached to it. The IMC is

contained in the invasive or mobile stages of all *Plasmodium*, including the merozoites, ookinetes, and sporozoites, as well as in the male gametocytes of human pathogens.[15] A single large organelle, the mitochondrion, with the function of producing ATP is necessary in mosquito stages while is not during the growth in red blood cells. A second unique organelle is the apicoplast, derived from a photosynthetic red alga during a second endosymbiotic event of a plastid into a *Plasmodium* ancestor. However, all the photosynthetic skills were lost and the apicoplast is known to play a vital role for lipid metabolism but has a role also in other important prokaryotic metabolic processes such as synthesis of isoprenoids, iron-sulfur clusters, and elements of the heme biosynthesis.[16] Both organelles contain one copy of their own genome that is accurately inherited by daughter cells during cell division. Adaptations to the intra-erythrocytic cycle created the food vacuole (FV), which contains proteases and aminopeptidases essential for hemoglobin degradation.[17] The latter is essential for the intra-erythrocytic parasite survival since hemoglobin is the major source of amino acids. A nontoxic crystalline byproduct called hemozoin derived from this process, becomes a distinct feature of intra-erythrocytic parasites at late stages.[18] The apical end of *Plasmodium* parasites contains the organelles needed for adhesion to host-cell surface and invasion, including the bulbous rhoptries and micronemes. Secretory vesicles known as dense granules, which are dispersed throughout the parasite, contain parasite proteins involved in altering the membrane that separates the parasite from the host and is known as the parasitophorous vacuole.[19] The general structure of a *Plasmodium* parasite is depicted in Figure 3.2.

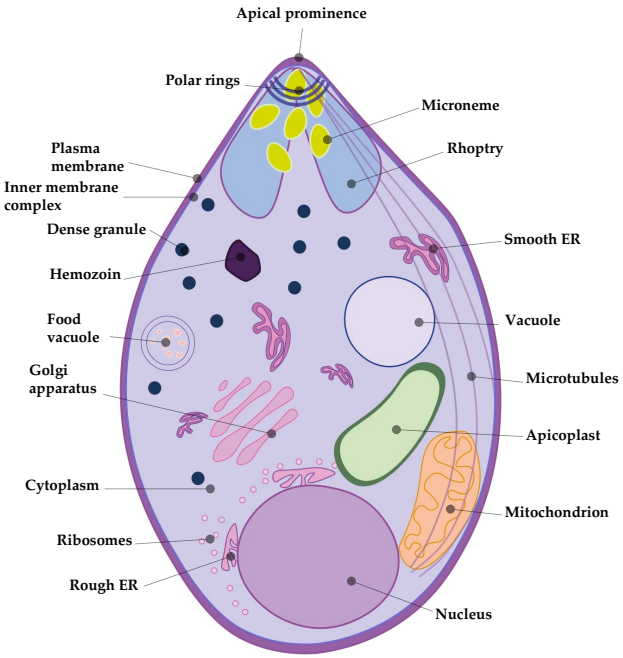


**Figure 3.2.** General cellular structure of *Plasmodium* parasites. Adapted from Bannister et al.[20]

During a bite of an infected female mosquito *Anopheles*, anticoagulants and spindle-shaped parasites known as sporozoites are injected from the salivary glands of the mosquito into the human dermis, from where they migrate through the blood stream to the liver. Sporozoites enter the hepatocytes by breaking through Kupffer cells and sinusoidal cell membrane and then evolve into erythrocyte-invasive forms in 7-10 days. The mechanism of invasion is not completely understood, but Pinzon-Ortiz et al.[21] found that circumsporozoite protein (CSP) plays a function in attachment, thrombospondin-related adhesive protein (TRAP) plays a role in internalization, and apical membrane antigen-1 (AMA-1) plays a role in invasion to promote hepatocyte invasion.[22] The contact between CSP and TRAP is again mediated by HSPGs on the surface of hepatocytes, allowing for binding and internalization.[19] Breakdown of the IMC of the sporozoite also occurs after internalization.[15] The liver infection is asymptomatic in humans, and it is also known as pre-erythrocytic schizogony, where sporozoites undergo nuclear division without cell division that culminates in the production of schizonts containing tens of thousands invasive exoerythrocytic merozoites from a single invading sporozoite. In parallel with nuclear replication, other organelles like mitochondrion and apicoplast start to grow and will divide

in the process of cellular invagination to release daughter merozoites.[23] This replication takes place within a parasitophorous vacuole (PV) which is a structure formed from the host cell membrane upon invasion and will be lost during the egress of daughter cells.[24] It was demonstrated that many host factors are critical during this development phase and migrate from the host cell to the parasite through the PV to ensure survival and replication of the parasite. For example, in *P. berghei*, a common murine malaria species, the host scavenger receptor B1 (SR-B1) was identified as a crucial factor for parasite invasion and development within hepatocytes.[25] Recently, Raphemot et al.[26] performed a genetic screen to study the role of human genes in *P. berghei* infection of Hep2 cells and found COPB2 and GGA1 to be vital protein trafficking modulators for parasite development.

The merozoites are then released into the blood stream, where they invade red blood cells (RBCs) and initiate the asexual life cycle of the parasite also known as erythrocytic schizogony. In the case of *P. vivax* and *P. ovale* some of the sporozoites may enter a latent stage known as the hypnozoite instead of immediately beginning asexual replication. Hypnozoites appear to have an intrinsic "reactivation clock" and can reactivate after months resulting in malaria disease relapses.[27] During RBCs invasion, merozoites attach their apical end to the RBC's membrane, which pushed by the merozoite actomyosin motor contort their membrane around the parasites to form a nascent PV.[19] At a molecular level, merozoite orientation to the apical end is mediated by proteins secreted by rhoptries and micronemes including, merozoite surface proteins (MSPs) which trigger the expression of erythrocyte-binding-like (EBL) adhesins, reticulocyte-binding-like (RBL) adhesins, and AMA-1.[19] After a subsequent recoil phase (RBC's membrane deformation), AMA-1 interacts with rhoptry neck protein 2 (RON2) to give a "tight junction" that along with the actomyosin motor activity leads to merozoite internalization and PV formation.[19]

In the erythrocytic schizogony phase, the parasite undergoes to rapid growth and replication cycle (approximately 24 hours for *P.knowlesi*, 48 hours for *P. falciparum*, *P. ovale* and *P. vivax* and 72 hours for *P. malariae*)[28,29] to develop from early rings to schizont stages which, depending on the parasite species, may contain between 16 and 32 merozoites that ultimately will egress the RBC to invade nascent RBCs. This asexual erythrocytic stage

accounts for the clinical malarial symptoms and pathology.[30] As in the liver stage, the blood stage's merozoite egress is regulated by the calcium signaling regulated by the cGMP-dependent protein kinase (PKG) and involves the quick rupture of the PV, then the host cell membrane rupturing.[31]

Triggered by a combination of genetic, epigenetic and environmental factors, a small fraction of schizonts diverts from asexual multiplication and a combination of differentiates them into sexual gametocytes.[32] While not responsible for symptom onset, this parasite stage is the only transmissible form and ensures transmission of the disease. The fundamental biology of gametocyte development still raises unanswered problems, despite the fact that crucial pathways of gametogenesis and fertilization are becoming increasingly known. Generally, when the transcription factor AP2-G is expressed, gametocyte formation is triggered and the new forming parasites go through five developmental stages (I-V),[32,33] where they grow and gradually elongate occupying the erythrocyte. In asexual parasites AP2-G expression is suppressed by heterochromatin protein 1 (HP1) and histone deacetylase 2 (HDA2) but can be activated by the perinuclear protein gametocyte development 1 (GDV1) which interacts with HP1 leading to sexual commitment in a fraction of schizonts.[34] Noteworthy, HDP1 controls also the expression of IMC genes which are activated in the early gametocyte stages in *P. falciparum*.[35] Immature gametocytes (stage I-IV) are sequestered in tissues, (i.e., the bone marrow) and mature stage V male and female gametocytes are released into the blood stream, where they are taken up by the mosquito through a blood meal.[36,37]

Stage V gametocytes are metabolically inactive in humans and are “reawaken” by the mosquito midgut environment, where they emerge from erythrocytes and develop into haploid female and male gametes. Environmental triggers that cause the activation of gametocytes in mosquitoes include a reduction in temperature (to around 20–25 °C), an increase in pH to 13, and the presence of the metabolic intermediary xanthurenic acid (XA), which activates guanylyl cyclize and phospholipase C (PLC) to initiate DNA replication in male gametes.[38] Then, male gametes become motile during exflagellation due to the egress of basal bodies from the main cellular body, so that they can mate with activated round-

shaped female gametes. Gametes fuse to form a diploid zygote, which during meiosis elongates into a tetraploid ookinete within ~24 hours.[39] Protein kinases NIMA (never-in-mitosis gene A)-related kinase 2 (NEK2) and NEK4 and the potentially the metallo-dependent protein phosphatase PPM2 play a key role in ookinete differentiation. Ookinete development occurs in six morphologically distinct stages and progress into oocysts (~48 hours) by penetrating the midgut wall.[40] The interaction of P25/28, CTRP, and SOAP with laminin appears to be important for triggering oocyst differentiation.[41] Oocyst is attached to the basal lamina of the midgut and replicates its genome for the next 6-12 days to develops hundreds of sporozoites inside the cellular membrane (sporogony). Next, following the actions of putative cysteine protease egress cysteine protease 1 (ECP1) and CSP, sporozoites will be released in the mosquito hemocoel to migrate to the lumen of mosquito's salivary glands, where phenotypic changes render mosquitoes infectious and ready to initiate another life cycle.[42]

Only 50 to 100 of the thousands of gametocytes ingested by the mosquito will mature into ookinetes and only 10% of them will fully mature into oocysts, and at least the 80% of ookinetes are eliminated.[43,44] The longest stage of the life cycle is oocyst maturation, which lasts around 14 days and results in the release of adult sporozoites that penetrate the salivary glands of mosquitoes after 21 days and continue to be infectious through the lifespan of the mosquito ready for transmission during the next blood meal.[42]

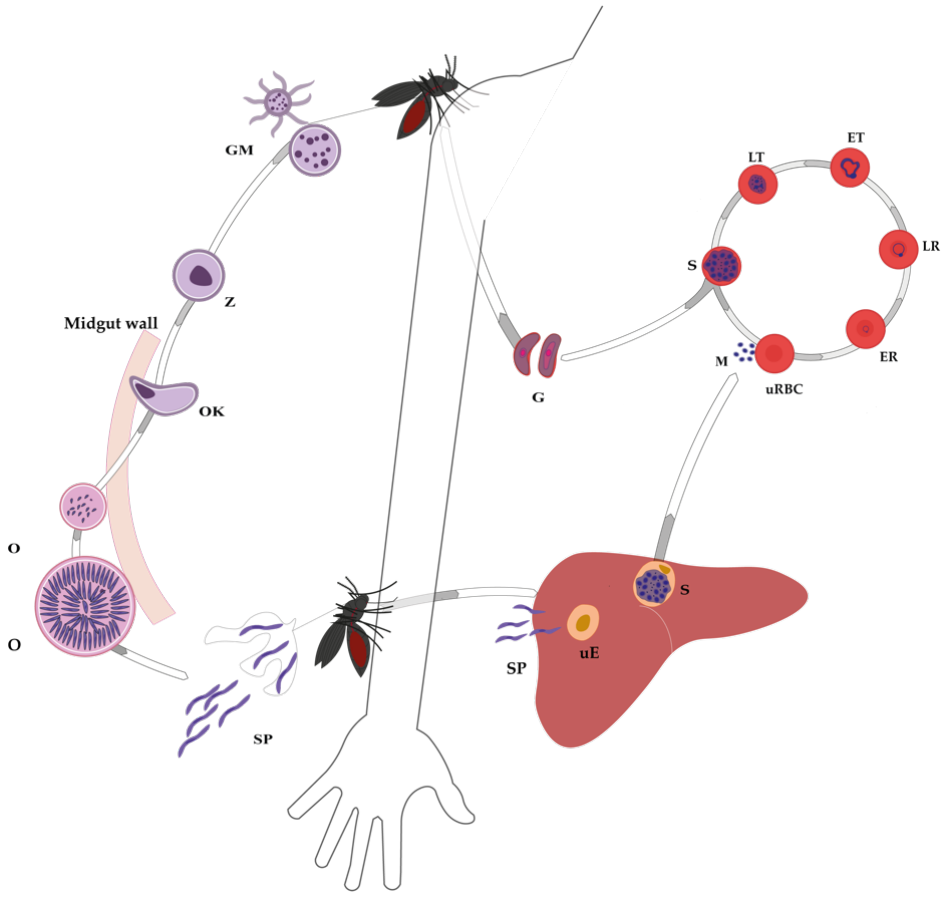


**Figure 3.3.** Malaria parasite life cycle. Plasmodium sporozoites are injected into the human host's dermis during an Anopheles mosquito bloodmeal before making their way to the liver. Hepatic schizogony begins when a sporozoite invades a hepatocyte, and the resultant merozoites enter the bloodstream to start the symptomatic asexual blood stages (ABS). A small percentage of asexual parasites engage in gametocytogenesis, producing adult male and female gametocytes that can be transmitted to Anopheles mosquitoes that are feeding on them. The midgut of the mosquito activates gametogenesis, which is followed by fertilization and further development in the mosquito. The cycle is restarted when sporozoites develop and go to the salivary glands to infect another host. SP: sporozoites; uE: uninfected hepatocytes; S: schizont; M: merozoites; uRBC: uninfected red blood cell; ER: early ring; LR: late ring; ET: early trophozoite; LT: late trophozoite; G: gametocytes; GM: gametes; Z: zygote; OK: ookinete; O: oocyst.

## 3.3 Current Malaria Control - Elimination Strategies and Challenges

Globally, long-lasting insecticide-treated bed nets (LLINs), indoor residual spraying (IRS), early diagnosis, treatment with artemisinin-based combination therapies (ACTs), chemotherapy prophylaxis in young children and pregnant women and the new WHO approved vaccine are the major methods used to combat malaria.[6]

Chloroquine acts by interfering with the digestion of hemoglobin in the blood stages of the malaria life cycle and it has been used in the standard therapy for uncomplicated malaria for more than 40 years, until *P. falciparum* drug resistance to this drug significantly increased cases of clinical failure.[45] To fight an increase of malaria cases the WHO recommended the use of ACTs and between 2001 and 2004 it was launched in 20 African countries and between 2000 and 2015 it is estimated that ACTs prevented around 21% of malaria cases.[8] ACTs consists of a combination of drugs with different mechanism of action active against malaria parasites, where at least one belongs to the class of artemisinin antimalarials (Figure 3.4). The latter exhibit its antimalarial activity inside the erythrocytes by forming free radical via a peroxide linkage causing protein damage. However, due to the complex structure (Figure 3.4), artemisinin drugs can interact with a large number of targets and further research is needed to fully elucidate the mechanism of action.[46]

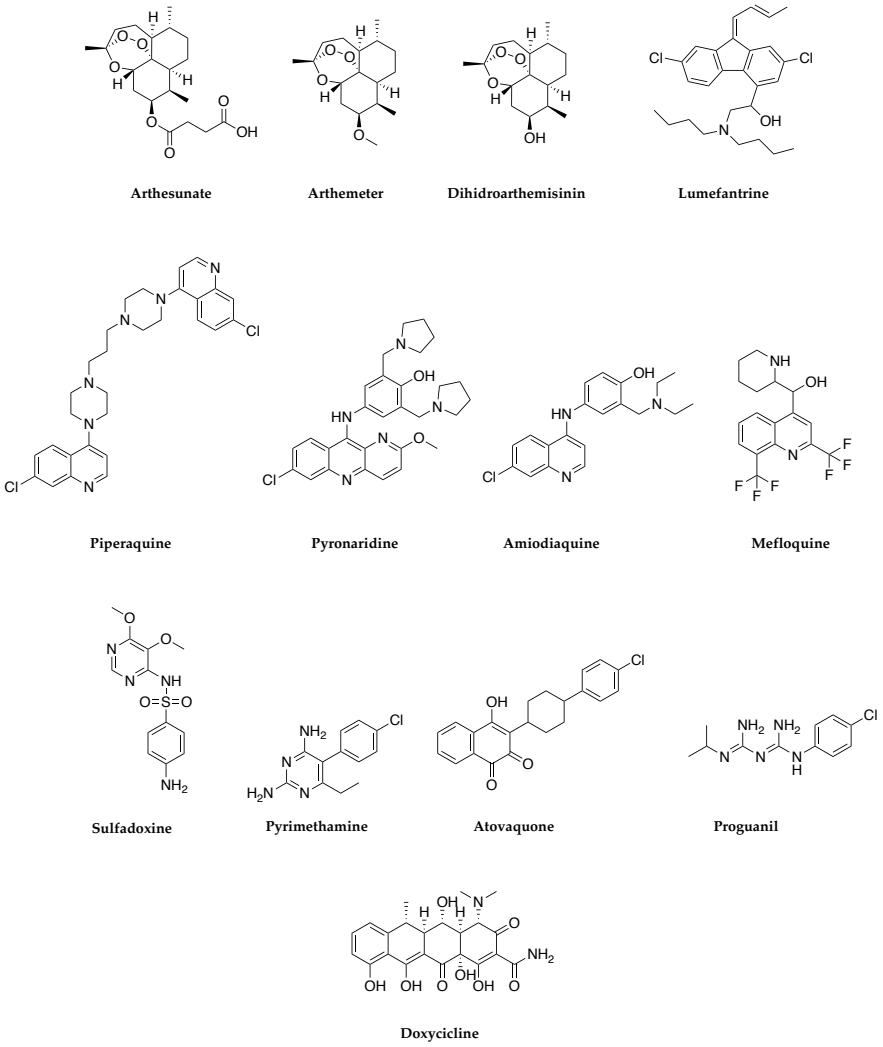


**Figure 3.4.** Chemical structure of antimalaria drugs used in therapy.

Such combinations include the use of strong, short-acting artemisinin derivatives such as pro-drugs artemether, artesunate or the active drug dihydroartemisin (DHA) together with less potent, longer-acting medications such as lumefantrine, amodiaquine, mefloquine, piperaquine, pyronaridine and sulfadoxine–pyrimethamine (SP) (Figure 3.4). Artemether-lumefantrine and artesunate-amodiaquine are frequently employed for the treatment of *P. falciparum* and *P. vivax*, respectively.[47,48] Although ACT is meant to treat malaria, it has also proven to be effective at preventing transmission.[49] ACT have played a crucial role in controlling malaria over the past 20 years and also today it is widely acknowledged that ACTs are the most effective cures for mild falciparum malaria. However, there are several characteristics that could be improved such as clarification of mechanisms of action, improvement of pharmacokinetic properties, and identifying a new generation of drugs

against artemisinin-resistant *Plasmodium* strains, which are present in Asia[50] and recent evidence suggest being emerging also in some African regions.[51]

Vulnerable people living in malaria endemic regions and travelers require the administration of drugs with prophylactic activity. Generally, for pregnant women and children SP is used, while atovaquone-proguanil, doxycycline, and mefloquine (Figure 3.4) are the antimalarial medications most frequently recommended to travelers.[52,53]

Light microscopy of stained blood films using Giemsa is the gold standard technique for diagnosing malaria.[54] Although highly effective, novel diagnostic methods for controlling the malaria public health burden are available and among these malaria rapid diagnostic tests (RDTs) are currently advised by WHO as the first test of choice in all parts of the world where malaria is prevalent.[6,55]

Indeed, due to its simplicity, speed, and lack of expensive equipment, RDT is the most practical diagnostic test, despite its rising false-negative rate (i.e., should be always confirmed by light microscopy of Giemsa stains). RDT is a immunochromatographic test that detect the presence of parasite antigens and it may be carried out without the use of any electrical apparatus or any specialized knowledge or abilities.[9]

Malaria control heavily relies on the use of vector-based interventions, and it is predicted that between 2000 and 2015 the increased usage of LLINs and IRS prevented around 75% (68% LLINs alone) of malaria infections in Africa.[56]

IRS kills malaria vectors by spraying a long-lasting residual insecticide on surfaces inside and outside of a home where they could congregate and rest. LLINs are insecticide-treated mosquito bed nets (ITNs) that have already been impregnated at the production facility and they can maintain their effectiveness against mosquito vectors for at least three years.[6,57,58]

For these two treatments, insecticides from four different families are used: pyrethroids, carbamates, organophosphates, and organochlorines, such as DDT.[59] Despite the high efficacy and wide-spread vector control, the use of these insecticide encountered limitations because the emergence and spread of resistance from mosquito vectors, particularly against pyrethroids.[6,59]

Insects can become resistant through enhanced metabolic detoxification, mutation in the insecticide target site (voltage-gated sodium channel) or by increasing the thickness of the cuticles.[60,61]

For decades, several vaccination initiatives aimed at targeting various parasite phases have been undertaken. While the majority of them showed poor efficacy in clinical trials, only recently the RTS,S/AS01 vaccine (Mosquirix) was recommended by the WHO as the first vaccination against human malaria. [6,12] The RTS,S/AS01 is a hybrid recombinant protein that consists of a fragment of the CSP fused to the hepatitis B surface antigen. As such, it induces antibodies against CSP and immobilizes the sporozoites, thereby preventing liver infection in humans. Thus, it is given before the erythrocytic stage to prevent the infection. Nevertheless, this vaccine is only accessible to infants and children and showed an efficacy rate of 36% in phase III clinical trials. So far, more than 2.3 million doses of the vaccine have been successfully delivered in endemic regions in Africa, meanwhile more than 30 vaccines, including whole sporozoite, blood-stage, and transmission-blocking vaccines, with promising activity are being tested in clinical trials.[62]

## 3.4 Antimalarial Drug Resistance and New Target Candidate Profiles

Antimalarial drug resistance is described as "the ability of a parasite strain to survive and/or multiply despite the administration and absorption of a drug in doses equal to or higher than those usually recommended but within the limits of tolerance of the subject".[63] The current rise in malaria-related mortality, notably in Africa, is due to resistance that has developed to all kinds of antimalarial medications including artemisinin derivatives. Our capacity to fight malaria with ACTs against *P. falciparum* has led to a significant reduction of the global malaria burden over the last two decades, but with the emerging of parasites less susceptible also to this treatment in the Greater Mekong Region,[64] the global public health is in danger and intensive containment efforts have therefore been initiated. In this context, understanding the causes of emerging resistance of malaria parasites (particularly *P. falciparum*) is a primary interest to develop novel “resistance proof” antimalarial medications.

Similar to those discovered in other microorganisms, the resistance mechanisms in malaria parasites are a result of an evolutionary reaction to the selection pressure induced by antimalarial drugs, therefore high-transmission regions are more prone to experience *de novo* mutations.[65] Emergence and/or spread of parasite-resistant strains are mostly caused by the lack of a fixed individual drug dosage.[66] Moreover, the enormous magnitude of pathogen populations ($10^{11}$ haploid parasites in acute infections of *P. falciparum*) and their rapid growth rates increase the likeness of mutations.[67] Antimalarial drug resistance may arise in the drug target or in putative drug transporters leading to faster drug expelling from the digestive vacuole, a decrease in the drug's ability to bind to its target, or a rise in the number of gene copies (copy number variations (CNVs)).[68] Drug target mutations are well represented by the case of pyrimethamine and cycloguanil, where point mutations (single nucleotide variations (SNVs)) in the dihydrofolate reductase genes (*PfDHFR*) of *P. falciparum* are associated with loss of binding affinity and then resistance to these antifolate drugs.[69] The *P. falciparum* chloroquine resistance transporter (*PfCRT*) gene and the *P. falciparum* multidrug resistance protein 1 (*PfMDR1*) gene polymorphisms are examples of drug transporters mutations, and they affect the malaria parasite's sensitivity to most of the available antimalarial medications.[70,71] Point mutations in *P. falciparum* of the Kelch protein 13 gene (*Pfk13*) were shown to be the primary cause of resistance for ART and its derivatives. This modification prolongs the time that the parasite spends in early ring stages, which is less susceptible to ART activity and the drug is rapidly cleared.[72] All these available genetic alterations can be detected with various techniques (e.g., in real-time PCR) and serve as molecular markers for clinical resistance, yet challenges related to the technique sensitivity and multiclonal parasite infections limit the outcome.[73,74]

The fast spreading of resistant parasite strains may also complicate the front-line therapy of ACTs, thus there is a need of new as antimalarial medications that tend to be resistant to the development of resistance. Recently, the leading product development partnership in antimalarial drug research Medicines for Malaria Venture (MMV) updated the target product profiles (TPPs) and target candidate profiles (TCPs), defined first in 2013,[75] which

outline the required indications for the development of new antimalarial medications and single compound, respectively.[76]

Two subcategories of TPPs have been described (Table 3.1):

- TPP1 defines a medication to treat the active disease. Antimalarial medications (ideally combinations of different compounds) that fall into this category should be used for acute and uncomplicated malaria in adults and children and should have TCP1 (i.e., clearance of the ABS of *P. falciparum* and all resistant strains), TCP5 (i.e., transmission-blocking activity by targeting gametocytes) and TCP3 (anti-relapse activity by targeting *P. vivax* hypnozoites) features. This will be likely accomplished by creating new products with a novel mode of action, avoiding any potential for field resistance that may already exist.
- TPP2 defines new chemopreventing drugs. Chemoprevention and chemoprotection should be reached after a single exposure of the medications (currently, a three-day course of three doses is advised for preventative therapy) with protection lasting at least a week. Ideal chemopreventing medications have a combination of TCP1 and TCP4 (activity against liver stages, hepatic schizonts) features.

Another approach taken into account for future drug formulations is the use of compounds able to kill the mosquito vector upon a blood meal (TCP6). Ivermectin has been suggested for this type of therapy, however due to the short-life, delayed effect in mosquitoes and side-effects in pregnant women, new compounds with improved endectocide profile are required.

**Table 3.1.** Target candidate profiles (TCPs) description and their combination for obtaining ideal target product profiles (TPPs). TCP2 has been retired. Adapted from Hooft et al. [77]

| | Description | TPP1: medication for the active disease | TPP2: single-dose chemopreventing medications |
|---|---|---|---|
| TCP1 | Fast clearance (ideally as fast as artesunate) of erythrocytic parasite stages including all resistant strains | X | X |

| | | | |
|---|---|---|---|
| TCP3 | Safe anti-relapse agents with activity against hypnozoites | X | |
| TCP4 | Liver stage activity (hepatic schizonts) | | X |
| TCP5 | Transmission-blocking agents by acting on gametocytes at low doses | X | |
| TCP6 | Transmission-blocking agents by functioning as endectocides | | |

The development of new antimalarial medicines that take into considerations all these parameters requires time and economic efforts. Furthermore, other major factors should be contemplated in drug development stages such as improved pharmacokinetic parameters and high efficacy in oral administration, synergistic mode of action and collateral sensitivity (resistant parasites of one drug in the combination are more sensitive to the partner drug) and the accessible price (required lower or equal to the ACTs currently in use).[76,77]

## 3.5 Transmission-Blocking Compounds

In response to the increasing drug resistance, scientists are studying new methodologies that aim to stop the spread of malaria by targeting the bottlenecks of the *Plasmodium* life cycle.[77–80]

From a thousand of gametocytes that are consumed by a mosquito during a blood meal, only 50 to 100 (~1% of asexual parasites) of them are thought to escape the immune factors and mature into ookinetes, which leads to fewer than five parasites per mosquito in the oocyst stage. Moreover, a significant number of sporozoites are lost on the way from the skin to the human liver.[81,82] Thus, by targeting gametocytes and other parasitic stages/events that occur in mosquitoes (gamete formation, fecundation and zygote formation, ookinete maturation) with the use of transmission-blocking tools, would prevent a mosquito from infecting a human and vice versa.

Transmission-blocking strategies can either target the vector (insecticides or endectocides) or the parasite life cycle. The latter include transmission-blocking vaccines (TBVs), transmission-blocking endosymbionts (e.g., *Wolbachia*) and transmission-blocking drugs.[78,83,84] While the first two subcategories are more difficult to implement in the field and require long processes, the development of transmission-blocking drugs, also known as transmission-blockers, seems more feasible at the moment bypassing some ethical and technical issues of the other two strategies.[83,85]

Using transmission-blockers, the chance of emerging resistant in a reduced size number of parasites would be largely decreased and could synergize with anti-asexual agents to prevent the escape of resistant mutants and slow down the evolution of drug-resistant parasites.[78,86] To date, primaquine (PQ) is the only medicine approved by WHO for transmission blocking purposes, and it can be used in conjunction with artemisinin in low to moderate transmission settings.[86] Nevertheless, this strategy is not extensively utilized because of the toxicity issues emerging in G6PD deficient individuals.[87] Furthermore, PQ is a dual-active drug that inhibit the same target in both asexual and sexual stages of parasites, thus may promote the spread of any resistance that could emerge against the ABS and the transmission-blocking efficacy is impaired.[78] As PQ, some clinical candidates (e.g., cipargimin; see section below) show equipotent activity against ABS and immature and/or mature gametocytes.[88] The key problem of a dual-active substance is that, in the great majority of instances, it will inhibit the same target in both the asexual (TCP1) and sexual stages (TCP5) of parasites, promoting the spread of any resistance that may emerge against the earlier stages. If that is the case, these drugs need to be combined with one or two ABS targeting drugs preferentially active also on early gametocytes, as demonstrated by PQ with artemisinins, whose gametocytocidal activity was previously reported. The development of transmission-blockers active on a single transmission stage will necessarily be combined with anti-asexual drugs. On the other hand, the chance of resistance development is significantly lower if dual-active medicines have distinct targets in sexual and asexual parasites.[78]

The most common target for transmission-blocking drugs are late-stage gametocytes, which seem more amenable to therapeutic intervention as they can be easily targeted within the human blood compartment.[89] Unlike anti-asexual drugs, these transmission-blocking agents not only target gametocytes in symptomatic carriers, but also gametocytes carried by asymptomatic individuals, who are responsible for up to 84% of persistent malaria transmission. Therefore, mass-drug administration irrespective of the symptoms is required and this strategy will need to face ethical and compliance hurdles before faking action in the field.[86]

Yet, there is a significant population bottleneck in the vector midgut, supporting the fact that sporogonic stages (gametes, zygotes, ookynetes and oocysts) are even more valuable targets for innovative strategies to block transmission.[40,43] The development of drugs targeting sporogonic stages has been hampered by the insufficiency of knowledge around these stages and technical obstacles. Targeting sporogonic stages via blood uptake or impairing vital functions of gametocytes for developments in mosquitoes require drugs with long half-lives since *P. falciparum* mature gametocytes may circulate in human blood up to 7 days. In addition, along with the lack of standardized methods for studying pharmacokinetics and pharmacodynamics of the drugs inside the mosquitoes there are no *in vitro* drug screenings targeting *P. falciparum* post-gamete formation stages.[89,90] Atovaquone (ATQ) and the chemoprophylactic combination ATQ - proguanil (namely Malarone) have been shown to reduce mosquito infectivity and thereby malaria transmission by suppressing ookinete production and oocyst maturation.[91,92] Recently, to overcome the difficulty to deliver transmission-blocking drugs in mosquitoes, Paton *et al.*[93] patented an innovative strategy that exploit the xenobiotic tarsal absorption of mosquitoes. They demonstrated that, similarly to insecticides, antimalarial compounds spread on surfaces (e.g., bed nets) can be delivered to mosquitoes in a short-time exposure. Most strikingly, ATQ (100 umol/$m^2$) alone could completely block the parasite transmission just after 6 minutes of exposure. However, using an approved antimalarial drug to reduce mosquito vectorial capacity and block transmission could further increase the risk of developing resistance to antimalarial drugs and compromising their efficacies.[94,95] Thus,

such a strategy overcomes the mechanism of vector-resistance (mosquito fitness is not affected) and the difficulties related to the indirect delivery of drugs into mosquitoes. Yet, it is essential to find new transmission-blocking compounds targeting sporogonic stages of the parasites with novel mechanism of action and a more complete understanding of post-transmission biology will aid in releasing such a strategy.

Finally, each transmission-blocking approach will require reliable models to quantify and model their efficacy and epidemiological impact along with the frontline interventions before administration.[93]

## 3.6 The Global Antimalarial Pipeline

In the last decade, the process of drug development to treat malaria and transition to clinical trials has seen a drastic acceleration. This contributed to the developments of several new or optimized chemotypes and discovery of new drug candidates against both known and new therapeutic targets. The development of new open partnership (e.g., MMV with its partners) played a major role in widening the pipeline of antimalarial candidates. Currently, preclinical and clinical research are presently being conducted to examine various medications and pharmacological combinations (Table 3.2).[96] The frontrunner is the spiroindolone KAE609 (Cipargamin),[97] but there are several other leading compounds advanced to translational sciences and product development, and some of them are potential transmission-blocking compounds (Figure 3.5).

Noteworthy, it is not clear whether these compounds affect the same target during the asexual and sexual stages, something that is typically only determined in retrospect.

The leading compounds having transmission-blocking activity that are currently progressing in development are target gametocytes (TCP5) and at least another parasite stage or act as endectocides (TCP6), and they are here addressed.

### 3.6.1 KAE609

KAE609 (Figure 3.5), also known as Cipargamin, is a synthetic molecule belonging to the spiroindolone class and developed at the Novartis Institute for Tropical Diseases in

Singapore, through a partnership with the Genomics Institute of the Novartis Research Foundation (GNF), the Biomedical Primate Research Centre and the Swiss Tropical Institute.[98] Among the lead compounds of the malaria drug pipeline, this molecule is the most advanced in Phase II and recruiting is ongoing to be tested against severe malaria caused by *P. falciparum* (NCT04675931).[99] It has both TCP-1 and TCP-5 features since has potent activity against ABS of *P. falciparum* and *P.vivax* and targets both early and late stages gametocytes and resistant strains.[88] Given its modest half-life (21 hours), a medication with a longer half-life would need to be combined with it. KAE609 disrupts the parasite's $Na^+$ homeostasis by acting as $Na^+/H^+$ antiporter on PfATP4, an ATP-dependent $Na^+$ channel. This mechanism eventually causes parasite swelling, consistent with the phenotypic effect of other drugs targeting ATP4. [100]

### 3.6.2 KAF156

KAF156 (Figure 3.5), also known as Ganaplacide, belongs to the class of the imadozolopiperazines and it is another synthetic drug developed by Novartis with multi-stage activity.[101] Indeed, KAF156 showed activity against both *P. vivax* and *P. falciparum*, has potent activity against ABS (TCP1), liver stages (TCP4) and gametocytes (TCP5) and all resistant strains.[102,103] As with KAE609 and the majority of antimalarial agents with half-life < 3 days, due to its moderate half-life (44 hours), it is expected that KAF156 will be given in combination regimen for the treatment of malaria.[104] KAF156 is now undergoing Phase IIb clinical trials in combination with lumefantrine (NCT04546633).[105] This drug promotes enlargement of the endoplasmic reticulum (ER) in parasites and inhibits protein trafficking, but the mechanism of action is unclear.[106] Mutations in the *P. falciparum* acetyl-CoA transporter, the UDP-galactose transporter, and PfCARL, all confer resistance, however none of them are believed to be the putative targets.[101] The TCP4 profile of this drug is promising as previously investigated in healthy subjects in phase I trial (NCT04072302).[107]

### 3.6.3 M5717

The collaboration between MMV and the Drug Discovery Unit at the University of Dundee in Scotland led to the discovery of M5717 (formerly DDD498, Figure 3.5) that is now being developed in partnership with Merck KGaA.[108] M5717 is a quinoline carboxamide derivative with pan-activity toward the human stages of malaria lifecycle (TCP1, TCP4 and TCP5) and previously identified as the most attractive transmission-blocking candidate.[109] The highly potent anti-malarial activity is associated to the novel mechanism of action and its high selectivity. Indeed, M5717 inhibits the cytosolic protein synthesis of elongation factor 2 (PeEF2) in different *Plasmodium* species showing no cross-reactivity to its human isoform.[110] In 2018, the drug successfully finished its phase 1a human safety clinical studies and, astonishingly, the slow half-life of this molecule (146-193 h at doses ≥ 200 mg)[108] enables single-dose cure of malaria in infected mice. This feature along with liver stage activity make M5717 a perfect candidate for the use as a chemoprophylactic agent, offering long-lasting protection.[75,76,111] Phase I clinical trials (NCT03261401 and NCT04250363) have been completed but no results are available.

### 3.6.4 Methylene Blue

Methylene Blue (MB, Figure 3.5) is a synthetic dye with a thiazine-based structure and used for different medical purposes. Already used in the 19$^{th}$ century to treat malaria before the discovery of chloroquine but with undesirable side effects (urine color and sclera change to blue),[112] today MB is mostly used as a control compound in gametocytes drug assays. Yet, it has been repurposed as a drug to treat malaria due to its low price and also because it is considered a promising alternative to primaquine by blocking all gametocyte stages (TCP5) though with ranging $IC_{50}$ values (e.g., 12– 490 nM), including transmission to anopheline mosquitoes.[113] Additionally, but of less significance, MB is active in ABS of malaria (TCP1).[114] Clinical studies are thus now focusing to find an appropriate combination of MB with a partner drug and also investigating the safety dosage in G6PD-deficient individuals.[112,115,116] Weakly known, but potentially complex, the mechanism of action of MB against malarial parasites raised different hypotheses. One potential mechanism is the competitive inhibition

of glutathione reductase, which makes the parasite more susceptible to the effects of other antimalarials like chloroquine. Other theories for how MB works also center on its capacity to alter the cellular redox equilibrium producing toxic products in both erythrocytic and gametocytes stages.[112,117]

### 3.6.5 BRD7929

The bicyclic azetidines derivative BRD7929 (Figure 3.5) was for the first time synthesized at the Broad Institute and then identified from a phenotypic screening as an emerging lead candidate due to its multi-stage activity (TCP1, TCP4, TCP5) both *in vitro* and *in vivo* at nanomolar concentrations.[118,119] Strikingly, BRD7929 is able to stop the transmission of parasites to the mosquito vector (late-stage gametocytocidal activity) at the same degree of exposure achieved in a single-dose cure in the ABS in rodent malaria models.[118,120] With a 32-hour half-life and rapid action on site, BRD7929 allows for single-dose therapy. BRD7929 and similar bicyclic azetidines share the same mechanism of action by inhibiting the parasite cytosolic phenylalanine tRNA-synthetase (PfcFRS and PvcFRS) and in a recent co-crystallization work it was elucidated the specific drug-target interactions.[119]
Along with further preclinical studies, a program for structure-based medication design is currently running particularly to improve some cytotoxicity features previously emerged.[119]

### 3.6.6 MMV609

MMV609 (Figure 3.5) is an ATP4 inhibitor that functions similarly to cipargamin in terms of its mode of action. It has been demonstrated to be effective against the ABS, the liver stage, and the sexual stages (TCP1, TCP4, TCP5). This compound is developed by MMV in partnership with the University of Kentucky (Kentucky, UK) and to our knowledge preclinical data results are not yet available. Currently, one of the main focuses is to find a faster and cheaper rput to synthesize this complex molecule.[121]

### 3.6.7 MMV183

The pantothenamide (PanAm) MMV183 (Figure 3.5) is a clinical development antimalarial candidate discovered by TropIQ (Netherlands) in partnership with MMV. Together with a potent and rapid (< 24 hours) anti-asexual activity against all ABS of both *P. falciparum* and *P. vivax* (TCP1), this compound has also nanomolar potency ($IC_{50}$: 12 nM) against *P. falciparum* female gametocytes determining the interesting transmission-blocking profile (TCP5). In addition, it was shown that MM183 keeps the nanomolar activity against artemisinin-resistant *P. falciparum*. Rapid action, favorable pharmacokinetic and minor toxicity properties suggest a safe single-dose malaria treatment in humans and further preclinical studies are ongoing.[122]

The mechanism of action of PanAms, including MMV183, has been elucidated and supported by a variety of biochemical assays such as *in vitro* assays such as evolution and whole-genome analysis (IVIEWGA), CRISPR-Cas9, conditional knockdown and cellular thermal shift assay (CETSA). Upon metabolization by three enzymes of the CoA biosynthesis pathway, PanAms form analog products of Coenzyme-A (CoA) that inhibit acetyl-CoA synthetase (AcAS) and block the formation of acetyl-CoA.[122]

### 3.6.8 Isoxazolines (endocticides-TCP6)

To find a solution to the limits in the use of ivermectin as endocticide (short half-life, slow action in mosquitoes) new insecticides are being tested in preclinical stage. Isoxazoline molecules (Figure 3.5) (lotilaner, fluralaenl, afoxolaner) act as insecticides by blocking native and expressed insect GABA-gated chloride channels with nanomolar potency. They are used as veterinary drugs to control ticks and fleas and have been recently considered as promising candidates since are well tolerated in these animals and may provide protection after a single oral dose because of their longer half-life (up to 48 days).

Analysis of mosquitocidal data suggest that also these isooxazoline derivatives have a slow onset of action but, interestingly, sub-lethal doses of afoxolaner significantly reduced the reproductive potential of surviving for *An. albimanus* and *An. Stephensi* mosquitoes. It

should be noted that human data are not available and these compounds are still subjected to preclinical studies.[123,124]

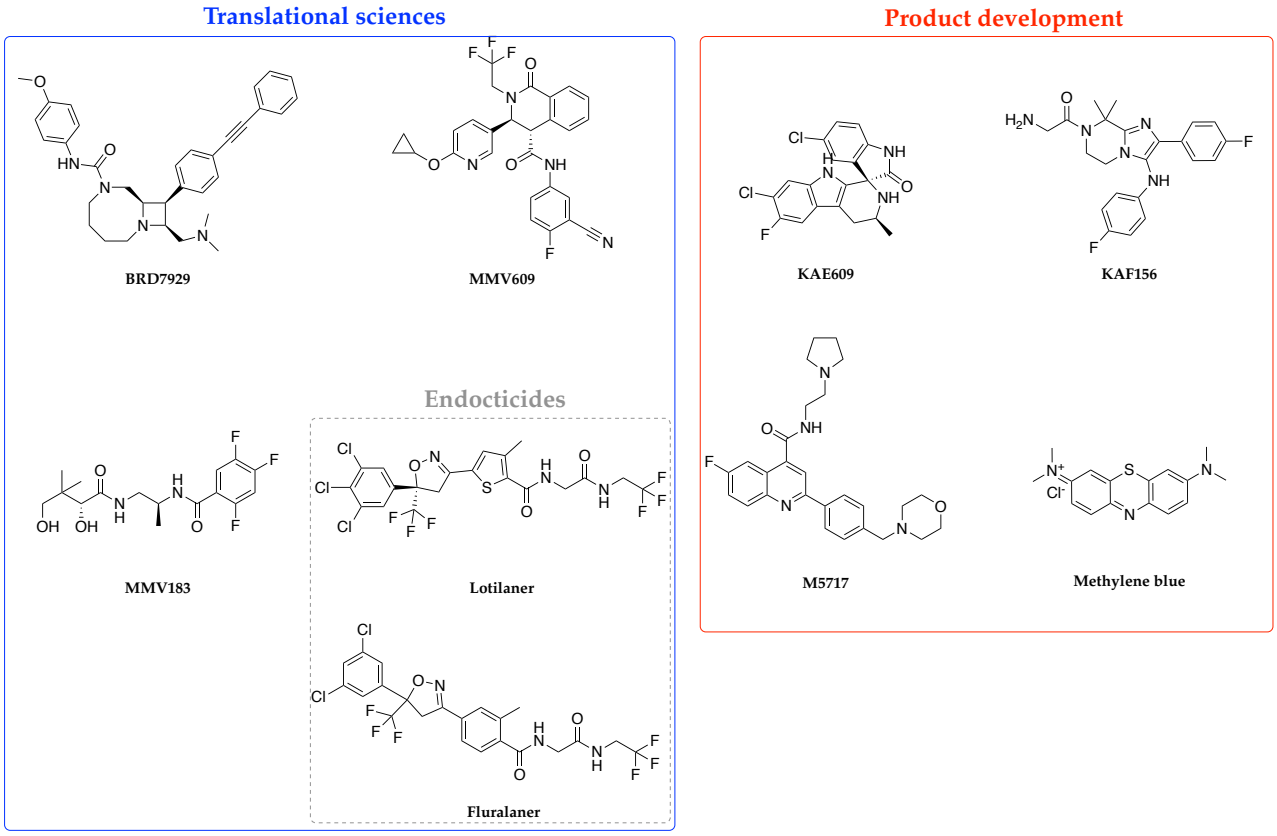


**Figure 3.5.** Chemical structures of compounds with transmission-blocking activity in translational and product development phases. Fluralaner and Lotilaner are example of isoxanoline-derived compound that together with other isoxanoline derivatives are being tested in preclinical studies.

## 3.7 The Transmission-blocking Screening Landscape

The majority of screens for new antimalarial compounds are focused on blood-stage parasites cultured *in vitro* (commonly fluorescence-based assays measuring cell proliferation) and they have been for long used as a primary filter to identify and prioritize novel hits.[125–127] Since transmission-blocking drugs have been a priority area of investigation, a race has begun to develop effective and rapid screening methods against the other phases of the parasite lifecycle to use in parallel with asexual *in vitro* screenings. Such improvement would remove the selection bias associated with ABS cell-proliferative screening and thus

would cover a broader chemical space for the identification of novel hits with transmission-blocking potential.[128–130] Today, the search of compound with transmission blocking activity prioritizes drugs able to prevent infections by blocking parasite transmission from infected individuals to the mosquito vectors (TCP5) since they are more amenable for medium-/high-throughput screening. Indeed, no *in vitro* standardized assays evaluating the activity of drugs against *P. falciparum* sporogonic cycle have been yet reported and only rodent malaria parasite *P. berghei* can provide tests for investigating the activity of compounds towards these stages.[131]

### 3.7.1 Gametocytocidal assays

Gametocytocidal assays are usually performed in *P. falciparum* NF54 (clone of 3D7) for both immature and mature gametocytes stages as the strain that generates the maximum gametocytemia and has good repeatability.[132,133]

Since gametocytes are non-replicative embryonic stages, gametocytocidal activity is assessed by a range of assays that use colorimetric readouts or reporter lines as measurement of metabolic activity (viability marker). Typical controls in these tests include methylene blue.[112,130]

Colorimetric assays include the use of indicator dyes sensitive to oxidation–reduction (Alamar Blue and Presto Blue assays) to the parasite lactate dehydrogenase (*Pf*LDH) levels, a crucial enzyme in anaerobic carbohydrate metabolism for ATP synthesis in *Plasmodium* parasites.[129,134] These methods are cheaper, faster, and easier to perform but unspecific interactions and challenges with purity of gametocyte culture would decrease the signal-to-noise ratio and interfere with the analysis.[134,135] More expensive alternatives measure the intensity of the bioluminescence or fluorescence signal that is proportional to gametocytes metabolic activity. These include gametocytes stained with a fluorescent dye (e.g., MitoTracker Red), reagents measuring ATP levels (e.g., BacTiter-Glo) or transgenic parasite line expressing a specific fluorescent reporter gene, such as GFP or GFP-luciferase.[134] It is also important to mention two recent large-scale screenings, Saponin-lysis Sexual Stage Assay (SaLSSA) developed by the University of California San Diego School of Medicine

and the use of acridine orange (AO) to measure gametocytemia and rounding-up post-activation as a marker of viability developed by researchers at the Istituto Superiore di Sanita' (ISS) in Rome.[136,137]

All these assays offer high sensitivity and can be adapted for medium/high throughput assays; however, results variability is common and thus is recommended to perform more than one of them to better assess compounds gametocytocidal activity.[129,135] Moreover, they do not reveal the actual ability of gametocytes to infect a mosquito, which is interrogated in a second screening cascade through membrane feeding assays (see below).

### 3.7.2 Dual Gamete Formation Assay

A mosquito must ingest at least one mature stage gametocyte from each sex to get infected.[138] Drug selectivity towards male or female has not been investigated in gametocytocidal assays until recently gametocidal assays made it possible, offering a way to improve transmission-blocking effectiveness. Gametocidal assays evaluate the transmission-blocking activity of compounds based on their capacity to inhibit mature female and/or male gametocytes to produce gametes (gametogenesis). Among these, the DGFA was the most successful and thus recently advanced to the 384-well format.[139] Briefly, mature gametocytes are exposed to test compounds and after the set incubation time and at the appropriate conditions, gametogenesis is induced. The development of "exflagellation centers" is a marker of male gamete production, whereas immunostaining of a surface protein expressed at the gamete surface upon egress (Pfs25) allows for the detection of female gamete production.[140]

The strong evidence of a linear link between DGFA and the standard membrane feeding assay (SMFA) has demonstrated to be a potent high-throughput indicator for transmission-blocking potential of tested compounds.[139,141]

### 3.7.3 Standard Membrane Feeding Assay (SMFA)

To date, all hits from transmission-blocking screenings need to be validated through the SMFA, that is considered the gold standard assay to evaluate compound transmission-

blocking activity.[142,143] This test commonly involves the infection of *Anopheles* mosquito by using an artificial membrane covering a vessel containing blood infected with mature gametocytes, which were previously exposed to transmission-blocking candidates. The parasite viability is then evaluated 7-10 days post infected-blood meal (pIBM) by counting the number of oocyst developed on mosquitoes' midguts.[142,144]

Variants of this assay, indirect washout SMFA (the candidate compounds are washed out the infectious blood meal before blood feeding) and a 'direct' SMFA (gametocytes are exposed to candidate compounds just before mosquito blood feeding) are used to give additional information to the selectivity of the tested hits.[135] The major drawback of SMFA is the low-throughput and research is advancing towards the improvement of transmission-blocking assays that can predict SMFA results. Among these, DGFA holds promise as a future gold-standard for transmission-blocking activity of compounds targeting gametocytes, but further investigations to validate its efficiency are needed.[128,140]

### 3.7.4 Sporogonic Development Assays using *P. berghei*

The ookinete development assay (ODA) was first described by Delves et al.[131] to allow the evaluation of the effect of compounds on the early sporogonic development (between gametogenesis and ookinete maturation) and of parasites in mosquitoes in a screening format. In this assay, GFP-expressing *P. berghei* gametocytes from an infected mouse are exposed to the compound and induced to form gametes simultaneously in a medium that simulates the mosquito midgut environment. By the time when mature ookinete should be formed (22-24 h), high-content imaging microscopy is used to evaluate the killing rate of the compound by counting GFP-expressing parasites.

More recently, Azevedo et al.[6,90] reported drug assays to using *P. berghei* to test the activity towards the oocyst formation and maturation. Oocyst formation is evaluated by treating purified ookinetes test compounds for 72 hours, while evaluation of oocyst development inhibition is achieved after an incubation of 12 days of early oocyst with the test compounds.

Despite these screening methods can be operated in a 384-well format, it does not detect compounds with *P. falciparum* specific activity and adapting to *P. falciparum* still remains a top priority.

## 3.8 Conclusions and Objectives of Our Study

In the last two decades significant decreases in the worldwide burden of malaria have been achieved as a result of very successful ACTs, preventative medications (e.g., PQ) and mosquito vector control strategies (LLINs and IRS). However, due to the growing prevalence of drug-resistant strains and insecticide-resistant *Anopheles* mosquitoes, the number of cases and deaths began to stall in 2015, and today malaria continues to be a worldwide health hazard with an estimated 241 million cases and more than 600.000 deaths in 2020.[6]

To further advance the malaria elimination agenda, the antimalarial community has moved the focus of malaria interventions from reducing the acquisition of infection (LLINs and IRS) and the clinical impact in the human host (ACTs), to block the host-vector parasite transmission. Transmission-blocking interventions act either by depleting the gametocyte reservoir in the human host or by preventing the growth of malaria parasites inside the mosquito vector and they are now considered critical for malaria eradication.[78–80]

The search of new transmission-blocking drugs besides PQ (limited clinical use), has provided novel clinical candidates that act on multiple-stages and has also advanced HTS platforms to identify compounds with gametocytocidal activity, but less has been achieved in the discovery of stage-selective compounds or compounds active in sporogonic stages.[98,108,119,122,145]

A recent study by Reader et al.[130] used parallel high-throughput screening to identify new transmission-blocking agents to provide proof of concept that parallel screenings can bring to the discovery of new selective compounds beyond asexual stages. They identified **MMV1580843** as a promising selective transmission-blocker.

Paton et al.[93,145] invented a novel transmission-blocking approach that overcome the limitations of current mosquito-targeted interventions demonstrating that *P. falciparum* transmission can be completely stopped when *Anopheles gambiae* are treated with the antimalarial ATQ (known to have anti-sporogonic activity) by tarsal contact, a manner of insecticide exposure similar to that used on insecticide-treated bed nets. Such a strategy lays the groundwork for the discovery of novel chemotypes acting against parasites in mosquitoes.

Therefore, we decided to look for additional compounds to validate **MMV1580843** activity, give a rational structure-activity relationship (SAR) and improve the drug likeness. In parallel, we aimed to find new compounds with antimalarial properties that could be adopted in control strategies by targeting the parasites in mosquitoes.

## References


(1) Talapko; Škrlec; Alebić; Jukić; Včev. Malaria: The Past and the Present. *Microorganisms* **2019**, *7* (6), 179. https://doi.org/10.3390/microorganisms7060179.

(2) Boualam, M. A.; Pradines, B.; Drancourt, M.; Barbieri, R. Malaria in Europe: A Historical Perspective. *Front Med (Lausanne)* **2021**, *8*. https://doi.org/10.3389/fmed.2021.691095.

(3) Sato, S. Plasmodium—a Brief Introduction to the Parasites Causing Human Malaria and Their Basic Biology. *J Physiol Anthropol* **2021**, *40* (1), 1. https://doi.org/10.1186/s40101-020-00251-9.

(4) Thomson-Luque, R.; Shaw Saliba, K.; Kocken, C. H. M.; Pasini, E. M. A Continuous, Long-Term Plasmodium Vivax In Vitro Blood-Stage Culture: What Are We Missing? *Trends Parasitol* **2017**, *33* (12), 921–924. https://doi.org/10.1016/j.pt.2017.07.001.

(5) Trampuz, A.; Jereb, M.; Muzlovic, I.; Prabhu, R. M. Clinical Review: Severe Malaria. *Crit Care* **2003**, *7* (4), 315. https://doi.org/10.1186/cc2183.

(6) WHO. World Malaria Report 2021.

(7) Nahlen BL, L.-B. D. *Collective Impact: The Global Fund Support for Measuring Reduction in the Burden of Malaria*, 6th ed.; Breman JG, A. M. W. N., Ed.; American Society of tropical medicine; Vol. 77.

(8) Cibulskis, R. E.; Alonso, P.; Aponte, J.; Aregawi, M.; Barrette, A.; Bergeron, L.; Fergus, C. A.; Knox, T.; Lynch, M.; Patouillard, E.; Schwarte, S.; Stewart, S.; Williams, R. Malaria: Global Progress 2000 – 2015 and Future Challenges. *Infect Dis Poverty* **2016**, *5* (1), 61. https://doi.org/10.1186/s40249-016-0151-8.

(9) Bhatt, S.; Weiss, D. J.; Cameron, E.; Bisanzio, D.; Mappin, B.; Dalrymple, U.; Battle, K. E.; Moyes, C. L.; Henry, A.; Eckhoff, P. A.; Wenger, E. A.; Briët, O.; Penny, M. A.; Smith, T. A.; Bennett, A.; Yukich, J.; Eisele, T. P.; Griffin, J. T.; Fergus, C. A.; Lynch, M.; Lindgren, F.; Cohen, J. M.; Murray, C. L. J.; Smith, D. L.; Hay, S. I.; Cibulskis, R. E.; Gething, P. W. The Effect of Malaria Control on Plasmodium Falciparum in Africa between 2000 and 2015. *Nature* **2015**, *526* (7572), 207–211. https://doi.org/10.1038/nature15535.

(10) Nahlen, B. L.; Low-Beer, D. Building to Collective Impact: The Global Fund Support for Measuring Reduction in the Burden of Malaria. *Am J Trop Med Hyg* **2007**, *77* (6 Suppl), 321–327.

(11) Lindsay, S. W.; Thomas, M. B.; Kleinschmidt, I. Threats to the Effectiveness of Insecticide-Treated Bednets for Malaria Control: Thinking beyond Insecticide Resistance. *Lancet Glob Health* **2021**, *9* (9), e1325–e1331. https://doi.org/10.1016/S2214-109X(21)00216-3.

(12) Nadeem, A. Y.; Shehzad, A.; Islam, S. U.; Al-Suhaimi, E. A.; Lee, Y. S. Mosquirix™ RTS, S/AS01 Vaccine Development, Immunogenicity, and Efficacy. *Vaccines (Basel)* **2022**, *10* (5), 713. https://doi.org/10.3390/vaccines10050713.

(13) Aborode, A. T.; David, K. B.; Uwishema, O.; Nathaniel, A. L.; Imisioluwa, J. O.; Onigbinde, S. B.; Farooq, F. Fighting COVID-19 at the Expense of Malaria in Africa: The Consequences and Policy Options. *Am J Trop Med Hyg* **2021**, *104* (1), 26–29. https://doi.org/10.4269/ajtmh.20-1181.

(14) Nacer, A.; Berry, L.; Slomianny, C.; Mattei, D. Plasmodium Falciparum Signal Sequences: Simply Sequences or Special Signals? *Int J Parasitol* **2001**, *31* (12), 1371–1379. https://doi.org/10.1016/S0020-7519(01)00253-3.

(15) Ferreira, J. L.; Heincke, D.; Wichers, J. S.; Liffner, B.; Wilson, D. W.; Gilberger, T.-W. The Dynamic Roles of the Inner Membrane Complex in the Multiple Stages of the Malaria Parasite. *Front Cell Infect Microbiol* **2021**, *10*. https://doi.org/10.3389/fcimb.2020.611801.

(16) Kobayashi, T.; Sato, S.; Takamiya, S.; Komaki-Yasuda, K.; Yano, K.; Hirata, A.; Onitsuka, I.; Hata, M.; Mi-ichi, F.; Tanaka, T.; Hase, T.; Miyajima, A.; Kawazu, S.; Watanabe, Y.; Kita, K. Mitochondria and Apicoplast of Plasmodium Falciparum: Behaviour on Subcellular Fractionation and the Implication. *Mitochondrion* **2007**, *7* (1–2), 125–132. https://doi.org/10.1016/j.mito.2006.11.021.

(17) Lamarque, M.; Tastet, C.; Poncet, J.; Demettre, E.; Jouin, P.; Vial, H.; Dubremetz, J.-F. Food Vacuole Proteome of the Malarial Parasite Plasmodium Falciparum. *Proteomics Clin Appl* **2008**, *2* (9), 1361–1374. https://doi.org/10.1002/prca.200700112.

(18) Chugh, M.; Sundararaman, V.; Kumar, S.; Reddy, V. S.; Siddiqui, W. A.; Stuart, K. D.; Malhotra, P. Protein Complex Directs Hemoglobin-to-Hemozoin Formation in *Plasmodium*

*Falciparum*. *Proceedings of the National Academy of Sciences* **2013**, *110* (14), 5392–5397. https://doi.org/10.1073/pnas.1218412110.

(19) Groomes, P. v.; Kanjee, U.; Duraisingh, M. T. RBC Membrane Biomechanics and Plasmodium Falciparum Invasion: Probing beyond Ligand–Receptor Interactions. *Trends Parasitol* **2022**, *38* (4), 302–315. https://doi.org/10.1016/j.pt.2021.12.005.

(20) Bannister, L. H.; Hopkins, J. M.; Fowler, R. E.; Krishna, S.; Mitchell, G. H. A Brief Illustrated Guide to the Ultrastructure of Plasmodium Falciparum Asexual Blood Stages. *Parasitology Today* **2000**, *16* (10), 427–433. https://doi.org/10.1016/S0169-4758(00)01755-5.

(21) Pinzon-Ortiz, C.; Friedman, J.; Esko, J.; Sinnis, P. The Binding of the Circumsporozoite Protein to Cell Surface Heparan Sulfate Proteoglycans Is Required for PlasmodiumSporozoite Attachment to Target Cells. *Journal of Biological Chemistry* **2001**, *276* (29), 26784–26791. https://doi.org/10.1074/jbc.M104038200.

(22) Silvie, O.; Franetich, J.-F.; Charrin, S.; Mueller, M. S.; Siau, A.; Bodescot, M.; Rubinstein, E.; Hannoun, L.; Charoenvit, Y.; Kocken, C. H.; Thomas, A. W.; van Gemert, G.-J.; Sauerwein, R. W.; Blackman, M. J.; Anders, R. F.; Pluschke, G.; Mazier, D. A Role for Apical Membrane Antigen 1 during Invasion of Hepatocytes by Plasmodium Falciparum Sporozoites. *Journal of Biological Chemistry* **2004**, *279* (10), 9490–9496. https://doi.org/10.1074/jbc.M311331200.

(23) Loubens, M.; Vincensini, L.; Fernandes, P.; Briquet, S.; Marinach, C.; Silvie, O. Plasmodium Sporozoites on the Move: Switching from Cell Traversal to Productive Invasion of Hepatocytes. *Mol Microbiol* **2021**, *115* (5), 870–881. https://doi.org/10.1111/mmi.14645.

(24) Nyboer, B.; Heiss, K.; Mueller, A.-K.; Ingmundson, A. The Plasmodium Liver-Stage Parasitophorous Vacuole: A Front-Line of Communication between Parasite and Host. *International Journal of Medical Microbiology* **2018**, *308* (1), 107–117. https://doi.org/10.1016/j.ijmm.2017.09.008.

(25) Rodrigues, C. D.; Hannus, M.; Prudêncio, M.; Martin, C.; Gonçalves, L. A.; Portugal, S.; Epiphanio, S.; Akinc, A.; Hadwiger, P.; Jahn-Hofmann, K.; Röhl, I.; van Gemert, G.-J.; Franetich, J.-F.; Luty, A. J. F.; Sauerwein, R.; Mazier, D.; Koteliansky, V.; Vornlocher, H.-P.; Echeverri, C. J.; Mota, M. M. Host Scavenger Receptor SR-BI Plays a Dual Role in the

Establishment of Malaria Parasite Liver Infection. *Cell Host Microbe* **2008**, *4* (3), 271–282. https://doi.org/10.1016/j.chom.2008.07.012.

(26) Raphemot, R.; Toro-Moreno, M.; Lu, K.-Y.; Posfai, D.; Derbyshire, E. R. Discovery of Druggable Host Factors Critical to Plasmodium Liver-Stage Infection. *Cell Chem Biol* **2019**, *26* (9), 1253-1262.e5. https://doi.org/10.1016/j.chembiol.2019.05.011.

(27) Markus, M. B. Do Hypnozoites Cause Relapse in Malaria? *Trends Parasitol* **2015**, *31* (6), 239–245. https://doi.org/10.1016/j.pt.2015.02.003.

(28) Ahmed, M. A.; Cox-Singh, J. Plasmodium Knowlesi - an Emerging Pathogen. *ISBT Sci Ser* **2015**, *10* (S1), 134–140. https://doi.org/10.1111/voxs.12115.

(29) Garnham, P. C. C. W. H. W. I. A. M. Malaria Parasites of Man: Life-Cycles and Morphology (Excluding Ultrastructure). *W.H. Wernsdorfer and I.* **1988**.

(30) Yazdani, S.; Mukherjee, P.; Chauhan, V.; Chitnis, C. Immune Responses to Asexual Blood-Stages of Malaria Parasites. *Curr Mol Med* **2006**, *6* (2), 187–203. https://doi.org/10.2174/156652406776055212.

(31) Collins, C. R.; Hackett, F.; Strath, M.; Penzo, M.; Withers-Martinez, C.; Baker, D. A.; Blackman, M. J. Malaria Parasite CGMP-Dependent Protein Kinase Regulates Blood Stage Merozoite Secretory Organelle Discharge and Egress. *PLoS Pathog* **2013**, *9* (5), e1003344. https://doi.org/10.1371/journal.ppat.1003344.

(32) Chawla, J.; Oberstaller, J.; Adams, J. H. Targeting Gametocytes of the Malaria Parasite Plasmodium Falciparum in a Functional Genomics Era: Next Steps. *Pathogens* **2021**, *10* (3), 346. https://doi.org/10.3390/pathogens10030346.

(33) Dantzler, K. W.; Ravel, D. B.; Brancucci, N. M.; Marti, M. Ensuring Transmission through Dynamic Host Environments: Host–Pathogen Interactions in Plasmodium Sexual Development. *Curr Opin Microbiol* **2015**, *26*, 17–23. https://doi.org/10.1016/j.mib.2015.03.005.

(34) Josling, G. A.; Russell, T. J.; Venezia, J.; Orchard, L.; van Biljon, R.; Painter, H. J.; Llinás, M. Dissecting the Role of PfAP2-G in Malaria Gametocytogenesis. *Nat Commun* **2020**, *11* (1), 1503. https://doi.org/10.1038/s41467-020-15026-0.

(35) Campelo Morillo, R. A.; Tong, X.; Xie, W.; Abel, S.; Orchard, L. M.; Daher, W.; Patel, D. J.; Llinás, M.; le Roch, K. G.; Kafsack, B. F. C. The Transcriptional Regulator HDP1 Controls

Expansion of the Inner Membrane Complex during Early Sexual Differentiation of Malaria Parasites. *Nat Microbiol* **2022**, *7* (2), 289–299. https://doi.org/10.1038/s41564-021-01045-0.

(36) de Niz, M.; Meibalan, E.; Mejia, P.; Ma, S.; Brancucci, N. M. B.; Agop-Nersesian, C.; Mandt, R.; Ngotho, P.; Hughes, K. R.; Waters, A. P.; Huttenhower, C.; Mitchell, J. R.; Martinelli, R.; Frischknecht, F.; Seydel, K. B.; Taylor, T.; Milner, D.; Heussler, V. T.; Marti, M. Plasmodium Gametocytes Display Homing and Vascular Transmigration in the Host Bone Marrow. *Sci Adv* **2018**, *4* (5). https://doi.org/10.1126/sciadv.aat3775.

(37) Donald L. Gardiner, K. R. T. Plasmodium Falciparum Gametocytes: Playing Hide and Seek. *Ann Transl Med* **2015**.

(38) Kuehn, A.; Pradel, G. The Coming-Out of Malaria Gametocytes. *J Biomed Biotechnol* **2010**, *2010*, 1–11. https://doi.org/10.1155/2010/976827.

(39) Bennink, S.; Kiesow, M. J.; Pradel, G. The Development of Malaria Parasites in the Mosquito Midgut. *Cell Microbiol* **2016**, *18* (7), 905–918. https://doi.org/10.1111/cmi.12604.

(40) Shaw, W. R.; Marcenac, P.; Catteruccia, F. Plasmodium Development in Anopheles: A Tale of Shared Resources. *Trends Parasitol* **2022**, *38* (2), 124–135. https://doi.org/10.1016/j.pt.2021.08.009.

(41) Arrighi, R. B. G.; Lycett, G.; Mahairaki, V.; Siden-Kiamos, I.; Louis, C. Laminin and the Malaria Parasite's Journey through the Mosquito Midgut. *Journal of Experimental Biology* **2005**, *208* (13), 2497–2502. https://doi.org/10.1242/jeb.01664.

(42) Kojin, B. B.; Adelman, Z. N. The Sporozoite's Journey Through the Mosquito: A Critical Examination of Host and Parasite Factors Required for Salivary Gland Invasion. *Front Ecol Evol* **2019**, *7*. https://doi.org/10.3389/fevo.2019.00284.

(43) Smith, R. C.; Vega-Rodríguez, J.; Jacobs-Lorena, M. The Plasmodium Bottleneck: Malaria Parasite Losses in the Mosquito Vector. *Mem Inst Oswaldo Cruz* **2014**, *109* (5), 644–661. https://doi.org/10.1590/0074-0276130597.

(44) Munro, B. A.; McMorran, B. J. Antimalarial Drug Strategies to Target Plasmodium Gametocytes. *Parasitologia* **2022**, *2* (2), 101–124. https://doi.org/10.3390/parasitologia2020011.

(45) Wellems, T. E.; Plowe, C. V. Chloroquine-Resistant Malaria. *J Infect Dis* **2001**, *184* (6), 770–776. https://doi.org/10.1086/322858.

(46) O'Neill, P. M.; Posner, G. H. A Medicinal Chemistry Perspective on Artemisinin and Related Endoperoxides. *J Med Chem* **2004**, *47* (12), 2945–2964. https://doi.org/10.1021/jm030571c.

(47) Marwa, K.; Kapesa, A.; Baraka, V.; Konje, E.; Kidenya, B.; Mukonzo, J.; Kamugisha, E.; Swedberg, G. Therapeutic Efficacy of Artemether-Lumefantrine, Artesunate-Amodiaquine and Dihydroartemisinin-Piperaquine in the Treatment of Uncomplicated Plasmodium Falciparum Malaria in Sub-Saharan Africa: A Systematic Review and Meta-Analysis. *PLoS One* **2022**, *17* (3), e0264339. https://doi.org/10.1371/journal.pone.0264339.

(48) Diarra, Y.; Koné, O.; Sangaré, L.; Doumbia, L.; Haidara, D. B. ben; Diallo, M.; Maiga, A.; Sango, H. A.; Sidibé, H.; Mihigo, J.; Nace, D.; Ljolje, D.; Talundzic, E.; Udhayakumar, V.; Eckert, E.; Woodfill, C. J.; Moriarty, L. F.; Lim, P.; Krogstad, D. J.; Halsey, E. S.; Lucchi, N. W.; Koita, O. A. Therapeutic Efficacy of Artemether–Lumefantrine and Artesunate–Amodiaquine for the Treatment of Uncomplicated Plasmodium Falciparum Malaria in Mali, 2015–2016. *Malar J* **2021**, *20* (1), 235. https://doi.org/10.1186/s12936-021-03760-9.

(49) Price, R. N. Potential of Artemisinin-Based Combination Therapies to Block Malaria Transmission. *J Infect Dis* **2013**, *207* (11), 1627–1629. https://doi.org/10.1093/infdis/jit079.

(50) Hassett, M. R.; Roepe, P. D. Origin and Spread of Evolving Artemisinin-Resistant Plasmodium Falciparum Malarial Parasites in Southeast Asia. *Am J Trop Med Hyg* **2019**, *101* (6), 1204–1211. https://doi.org/10.4269/ajtmh.19-0379.

(51) Balikagala, B.; Fukuda, N.; Ikeda, M.; Katuro, O. T.; Tachibana, S.-I.; Yamauchi, M.; Opio, W.; Emoto, S.; Anywar, D. A.; Kimura, E.; Palacpac, N. M. Q.; Odongo-Aginya, E. I.; Ogwang, M.; Horii, T.; Mita, T. Evidence of Artemisinin-Resistant Malaria in Africa. *New England Journal of Medicine* **2021**, *385* (13), 1163–1171. https://doi.org/10.1056/NEJMoa2101746.

(52) Saito, M.; Gilder, M. E.; McGready, R.; Nosten, F. Antimalarial Drugs for Treating and Preventing Malaria in Pregnant and Lactating Women. *Expert Opin Drug Saf* **2018**, *17* (11), 1129–1144. https://doi.org/10.1080/14740338.2018.1535593.

(53) del Prete, V.; Mateo-Urdiales, A.; Bueno-Cavanillas, A.; Ferrara, P. Malaria Prevention in the Older Traveller: A Systematic Review. *J Travel Med* **2019**, *26* (7). https://doi.org/10.1093/jtm/taz067.

(54) Gitta, B.; Kilian, N. Diagnosis of Malaria Parasites Plasmodium Spp. in Endemic Areas: Current Strategies for an Ancient Disease. *BioEssays* **2020**, *42* (1), 1900138. https://doi.org/10.1002/bies.201900138.

(55) Cunningham, J.; Jones, S.; Gatton, M. L.; Barnwell, J. W.; Cheng, Q.; Chiodini, P. L.; Glenn, J.; Incardona, S.; Kosack, C.; Luchavez, J.; Menard, D.; Nhem, S.; Oyibo, W.; Rees-Channer, R. R.; Gonzalez, I.; Bell, D. A Review of the WHO Malaria Rapid Diagnostic Test Product Testing Programme (2008–2018): Performance, Procurement and Policy. *Malar J* **2019**, *18* (1), 387. https://doi.org/10.1186/s12936-019-3028-z.

(56) Kenea, O.; Balkew, M.; Tekie, H.; Deressa, W.; Loha, E.; Lindtjørn, B.; Overgaard, H. J. Impact of Combining Indoor Residual Spraying and Long-Lasting Insecticidal Nets on Anopheles Arabiensis in Ethiopia: Results from a Cluster Randomized Controlled Trial. *Malar J* **2019**, *18* (1), 182. https://doi.org/10.1186/s12936-019-2811-1.

(57) Ng'ang'a, P. N.; Aduogo, P.; Mutero, C. M. Long Lasting Insecticidal Mosquito Nets (LLINs) Ownership, Use and Coverage Following Mass Distribution Campaign in Lake Victoria Basin, Western Kenya. *BMC Public Health* **2021**, *21* (1), 1046. https://doi.org/10.1186/s12889-021-11062-7.

(58) Killeen, G. F.; Masalu, J. P.; Chinula, D.; Fotakis, E. A.; Kavishe, D. R.; Malone, D.; Okumu, F. Control of Malaria Vector Mosquitoes by Insecticide-Treated Combinations of Window Screens and Eave Baffles. *Emerg Infect Dis* **2017**, *23* (5), 782–789. https://doi.org/10.3201/eid2305.160662.

(59) Toé, K. H.; Jones, C. M.; N'Fale, S.; Ismail, H. M.; Dabiré, R. K.; Ranson, H. Increased Pyrethroid Resistance in Malaria Vectors and Decreased Bed Net Effectiveness, Burkina Faso. *Emerg Infect Dis* **2014**, *20* (10). https://doi.org/10.3201/eid2010.140619.

(60) Balabanidou, V.; Grigoraki, L.; Vontas, J. Insect Cuticle: A Critical Determinant of Insecticide Resistance. *Curr Opin Insect Sci* **2018**, *27*, 68–74. https://doi.org/10.1016/j.cois.2018.03.001.

(61) Minetti, C.; Ingham, V. A.; Ranson, H. Effects of Insecticide Resistance and Exposure on Plasmodium Development in Anopheles Mosquitoes. *Curr Opin Insect Sci* **2020**, *39*, 42–49. https://doi.org/10.1016/j.cois.2019.12.001.

(62) Jagannathan, P.; Kakuru, A. Malaria in 2022: Increasing Challenges, Cautious Optimism. *Nat Commun* **2022**, *13* (1), 2678. https://doi.org/10.1038/s41467-022-30133-w.

(63) WHO. *Chemotherapy of Malaria : Report of a WHO Scientific Group*; 1967.

(64) Imwong, M.; Suwannasin, K.; Srisutham, S.; Vongpromek, R.; Promnarate, C.; Saejeng, A.; Phyo, A. P.; Proux, S.; Pongvongsa, T.; Chea, N.; Miotto, O.; Tripura, R.; Nguyen Hoang, C.; Dysoley, L.; Ho Dang Trung, N.; Peto, T. J.; Callery, J. J.; van der Pluijm, R. W.; Amaratunga, C.; Mukaka, M.; von Seidlein, L.; Mayxay, M.; Thuy-Nhien, N. T.; Newton, P. N.; Day, N. P. J.; Ashley, E. A.; Nosten, F. H.; Smithuis, F. M.; Dhorda, M.; White, N. J.; Dondorp, A. M. Evolution of Multidrug Resistance in Plasmodium Falciparum: A Longitudinal Study of Genetic Resistance Markers in the Greater Mekong Subregion. *Antimicrob Agents Chemother* **2021**, *65* (12). https://doi.org/10.1128/AAC.01121-21.

(65) Takala-Harrison, S.; Laufer, M. K. Antimalarial Drug Resistance in Africa: Key Lessons for the Future. *Ann N Y Acad Sci* **2015**, *1342* (1), 62–67. https://doi.org/10.1111/nyas.12766.

(66) Wells, T. N. C.; van Huijsduijnen, R. H.; van Voorhis, W. C. Malaria Medicines: A Glass Half Full? *Nat Rev Drug Discov* **2015**, *14* (6), 424–442. https://doi.org/10.1038/nrd4573.

(67) Ross, L. S.; Fidock, D. A. Elucidating Mechanisms of Drug-Resistant Plasmodium Falciparum. *Cell Host Microbe* **2019**, *26* (1), 35–47. https://doi.org/10.1016/j.chom.2019.06.001.

(68) Haldar, K.; Bhattacharjee, S.; Safeukui, I. Drug Resistance in Plasmodium. *Nat Rev Microbiol* **2018**, *16* (3), 156–170. https://doi.org/10.1038/nrmicro.2017.161.

(69) Sirawaraporn, W.; Sathitkul, T.; Sirawaraporn, R.; Yuthavong, Y.; Santi, D. V. Antifolate-Resistant Mutants of Plasmodium Falciparum Dihydrofolate Reductase. *Proceedings of the National Academy of Sciences* **1997**, *94* (4), 1124–1129. https://doi.org/10.1073/pnas.94.4.1124.

(70) Bray, P. G.; Martin, R. E.; Tilley, L.; Ward, S. A.; Kirk, K.; Fidock, D. A. Defining the Role of PfCRT in Plasmodium Falciparum Chloroquine Resistance. *Mol Microbiol* **2005**, *56* (2), 323–333. https://doi.org/10.1111/j.1365-2958.2005.04556.x.

(71) Babiker, H. A.; Pringle, S. J.; Abdel-Muhsin, A.; Mackinnon, M.; Hunt, P.; Walliker, D. High-Level Chloroquine Resistance in Sudanese Isolates of *Plasmodium Falciparum* Is Associated with Mutations in the Chloroquine Resistance Transporter Gene *Pfcrt* and the Multidrug Resistance Gene *Pfmdr1*. *J Infect Dis* **2001**, *183* (10), 1535–1538. https://doi.org/10.1086/320195.

(72) Ndwiga, L.; Kimenyi, K. M.; Wamae, K.; Osoti, V.; Akinyi, M.; Omedo, I.; Ishengoma, D. S.; Duah-Quashie, N.; Andagalu, B.; Ghansah, A.; Amambua-Ngwa, A.; Tukwasibwe, S.; Tessema, S. K.; Karema, C.; Djimde, A. A.; Dondorp, A. M.; Raman, J.; Snow, R. W.; Bejon, P.; Ochola-Oyier, L. I. A Review of the Frequencies of Plasmodium Falciparum Kelch 13 Artemisinin Resistance Mutations in Africa. *Int J Parasitol Drugs Drug Resist* **2021**, *16*, 155–161. https://doi.org/10.1016/j.ijpddr.2021.06.001.

(73) Berzosa, P.; de Lucio, A.; Romay-Barja, M.; Herrador, Z.; González, V.; García, L.; Fernández-Martínez, A.; Santana-Morales, M.; Ncogo, P.; Valladares, B.; Riloha, M.; Benito, A. Comparison of Three Diagnostic Methods (Microscopy, RDT, and PCR) for the Detection of Malaria Parasites in Representative Samples from Equatorial Guinea. *Malar J* **2018**, *17* (1), 333. https://doi.org/10.1186/s12936-018-2481-4.

(74) Zhong, D.; Koepfli, C.; Cui, L.; Yan, G. Molecular Approaches to Determine the Multiplicity of Plasmodium Infections. *Malar J* **2018**, *17* (1), 172. https://doi.org/10.1186/s12936-018-2322-5.

(75) Burrows, J. N.; Hooft van Huijsduijnen, R.; Möhrle, J. J.; Oeuvray, C.; Wells, T. N. Designing the next Generation of Medicines for Malaria Control and Eradication. *Malar J* **2013**, *12* (1), 187. https://doi.org/10.1186/1475-2875-12-187.

(76) Burrows, J. N.; Duparc, S.; Gutteridge, W. E.; Hooft van Huijsduijnen, R.; Kaszubska, W.; Macintyre, F.; Mazzuri, S.; Möhrle, J. J.; Wells, T. N. C. New Developments in Anti-Malarial Target Candidate and Product Profiles. *Malar J* **2017**, *16* (1), 26. https://doi.org/10.1186/s12936-016-1675-x.

(77) Hooft van Huijsduijnen, R.; Wells, T. N. The Antimalarial Pipeline. *Curr Opin Pharmacol* **2018**, *42*, 1–6. https://doi.org/10.1016/j.coph.2018.05.006.

(78) Birkholtz, L.-M.; Alano, P.; Leroy, D. Transmission-Blocking Drugs for Malaria Elimination. *Trends Parasitol* **2022**, *38* (5), 390–403. https://doi.org/10.1016/j.pt.2022.01.011.

(79) van der Watt, M. E.; Reader, J.; Birkholtz, L.-M. Adapt or Die: Targeting Unique Transmission-Stage Biology for Malaria Elimination. *Front Cell Infect Microbiol* **2022**, *12*. https://doi.org/10.3389/fcimb.2022.901971.

(80) Gonçalves, D.; Hunziker, P. Transmission-Blocking Strategies: The Roadmap from Laboratory Bench to the Community. *Malar J* **2016**, *15* (1), 95. https://doi.org/10.1186/s12936-016-1163-3.

(81) Smith, R. C.; Vega-Rodríguez, J.; Jacobs-Lorena, M. The Plasmodium Bottleneck: Malaria Parasite Losses in the Mosquito Vector. *Mem Inst Oswaldo Cruz* **2014**, *109* (5), 644–661. https://doi.org/10.1590/0074-0276130597.

(82) Kehrer, J.; Formaglio, P.; Muthinja, J. M.; Weber, S.; Baltissen, D.; Lance, C.; Ripp, J.; Grech, J.; Meissner, M.; Funaya, C.; Amino, R.; Frischknecht, F. Plasmodium Sporozoite Disintegration during Skin Passage Limits Malaria Parasite Transmission. *EMBO Rep* **2022**, *23* (7). https://doi.org/10.15252/embr.202254719.

(83) Duffy, P. E. Transmission-Blocking Vaccines: Harnessing Herd Immunity for Malaria Elimination. *Expert Rev Vaccines* **2021**, *20* (2), 185–198. https://doi.org/10.1080/14760584.2021.1878028.

(84) Caragata, E. P.; Dutra, H. L. C.; Sucupira, P. H. F.; Ferreira, A. G. A.; Moreira, L. A. Wolbachia as Translational Science: Controlling Mosquito-Borne Pathogens. *Trends Parasitol* **2021**, *37* (12), 1050–1067. https://doi.org/10.1016/j.pt.2021.06.007.

(85) Mishra, N.; Shrivastava, N. K.; Shivhare, D.; Singh, H. Wolbachia: An Evolutionary Way to Combat Mosquito Borne Disease and the Challenges in Success of the Strategy. *Int J Mosq Res* **2022**, *9* (2), 65–68. https://doi.org/10.22271/23487941.2022.v9.i2a.603.

(86) Consalvi, S.; Tammaro, C.; Appetecchia, F.; Biava, M.; Poce, G. Malaria Transmission Blocking Compounds: A Patent Review. *Expert Opin Ther Pat* **2022**, *32* (6), 649–666. https://doi.org/10.1080/13543776.2022.2049239.

(87) Bancone, G.; Chu, C. S. G6PD Variants and Haemolytic Sensitivity to Primaquine and Other Drugs. *Front Pharmacol* **2021**, *12*. https://doi.org/10.3389/fphar.2021.638885.

(88) Yipsirimetee, A.; Chiewpoo, P.; Tripura, R.; Lek, D.; Day, N. P. J.; Dondorp, A. M.; Pukrittayakamee, S.; White, N. J.; Chotivanich, K. Assessment In Vitro of the Antimalarial and Transmission-Blocking Activities of Cipargamin and Ganaplacide in Artemisinin-Resistant Plasmodium Falciparum. *Antimicrob Agents Chemother* **2022**, *66* (3). https://doi.org/10.1128/aac.01481-21.

(89) Birkholtz, L.-M.; Coetzer, T. L.; Mancama, D.; Leroy, D.; Alano, P. Discovering New Transmission-Blocking Antimalarial Compounds: Challenges and Opportunities. *Trends Parasitol* **2016**, *32* (9), 669–681. https://doi.org/10.1016/j.pt.2016.04.017.

(90) Azevedo, R.; Mendes, A. M.; Prudêncio, M. Inhibition of Plasmodium Sporogonic Stages by Ivermectin and Other Avermectins. *Parasit Vectors* **2019**, *12* (1), 549. https://doi.org/10.1186/s13071-019-3805-0.

(91) Butcher, G. A.; Mendoza, J.; Sinden, R. E. Inhibition of the Mosquito Transmission of Plasmodium Berghei by Malarone™ (Atovaquone-Proguanil). *Ann Trop Med Parasitol* **2000**, *94* (5), 429–436. https://doi.org/10.1080/00034983.2000.11813561.

(92) Goodman, C. D.; Buchanan, H. D.; McFadden, G. I. Is the Mitochondrion a Good Malaria Drug Target? *Trends Parasitol* **2017**, *33* (3), 185–193. https://doi.org/10.1016/j.pt.2016.10.002.

(93) Paton, D. G.; Childs, L. M.; Itoe, M. A.; Holmdahl, I. E.; Buckee, C. O.; Catteruccia, F. Exposing Anopheles Mosquitoes to Antimalarials Blocks Plasmodium Parasite Transmission. *Nature* **2019**, *567* (7747), 239–243. https://doi.org/10.1038/s41586-019-0973-1.

(94) Goodman, C. D.; Siregar, J. E.; Mollard, V.; Vega-Rodríguez, J.; Syafruddin, D.; Matsuoka, H.; Matsuzaki, M.; Toyama, T.; Sturm, A.; Cozijnsen, A.; Jacobs-Lorena, M.; Kita, K.; Marzuki, S.; McFadden, G. I. Parasites Resistant to the Antimalarial Atovaquone Fail to Transmit by Mosquitoes. *Science (1979)* **2016**, *352* (6283), 349–353. https://doi.org/10.1126/science.aad9279.

(95) Blake, L. D.; Johnson, M. E.; Siegel, S. v.; McQueen, A.; Iyamu, I. D.; Shaikh, A. K.; Shultis, M. W.; Manetsch, R.; Kyle, D. E. Menoctone Resistance in Malaria Parasites Is Conferred by M133I Mutations in Cytochrome *b* That Are Transmissible through Mosquitoes. *Antimicrob Agents Chemother* **2017**, *61* (8). https://doi.org/10.1128/AAC.00689-17.

(96) Medicine for Malaria Venture. *Global Portfolio of Antimalarial Medicines*. https://www.mmv.org/research-development/mmv-supported-projects.

(97) Guiguemde, W. A.; Shelat, A. A.; Bouck, D.; Duffy, S.; Crowther, G. J.; Davis, P. H.; Smithson, D. C.; Connelly, M.; Clark, J.; Zhu, F.; Jiménez-Díaz, M. B.; Martinez, M. S.; Wilson, E. B.; Tripathi, A. K.; Gut, J.; Sharlow, E. R.; Bathurst, I.; Mazouni, F. el; Fowble, J. W.; Forquer, I.; McGinley, P. L.; Castro, S.; Angulo-Barturen, I.; Ferrer, S.; Rosenthal, P. J.;

DeRisi, J. L.; Sullivan, D. J.; Lazo, J. S.; Roos, D. S.; Riscoe, M. K.; Phillips, M. A.; Rathod, P. K.; van Voorhis, W. C.; Avery, V. M.; Guy, R. K. Chemical Genetics of Plasmodium Falciparum. *Nature* **2010**, *465* (7296), 311–315. https://doi.org/10.1038/nature09099.

(98) Bouwman, S. AM.; Zoleko-Manego, R.; Renner, K. C.; Schmitt, E. K.; Mombo-Ngoma, G.; Grobusch, M. P. The Early Preclinical and Clinical Development of Cipargamin (KAE609), a Novel Antimalarial Compound. *Travel Med Infect Dis* **2020**, *36*, 101765. https://doi.org/10.1016/j.tmaid.2020.101765.

(99) NIH. *To Evaluate Efficacy, Safety, Tolerability and PK of Intravenous Cipargamin in Participants With Severe Plasmodium Falciparum Malaria*. ClinicalTrials.gov. https://clinicaltrials.gov/ct2/show/NCT04675931 (accessed 2022-09-06).

(100) Goldgof, G. M.; Durrant, J. D.; Ottilie, S.; Vigil, E.; Allen, K. E.; Gunawan, F.; Kostylev, M.; Henderson, K. A.; Yang, J.; Schenken, J.; LaMonte, G. M.; Manary, M. J.; Murao, A.; Nachon, M.; Stanhope, R.; Prescott, M.; McNamara, C. W.; Slayman, C. W.; Amaro, R. E.; Suzuki, Y.; Winzeler, E. A. Comparative Chemical Genomics Reveal That the Spiroindolone Antimalarial KAE609 (Cipargamin) Is a P-Type ATPase Inhibitor. *Sci Rep* **2016**, *6* (1), 27806. https://doi.org/10.1038/srep27806.

(101) Koller, R.; Mombo-Ngoma, G.; Grobusch, M. P. The Early Preclinical and Clinical Development of Ganaplacide (KAF156), a Novel Antimalarial Compound. *Expert Opin Investig Drugs* **2018**, *27* (10), 803–810. https://doi.org/10.1080/13543784.2018.1524871.

(102) White, N. J.; Duong, T. T.; Uthaisin, C.; Nosten, F.; Phyo, A. P.; Hanboonkunupakarn, B.; Pukrittayakamee, S.; Jittamala, P.; Chuthasmit, K.; Cheung, M. S.; Feng, Y.; Li, R.; Magnusson, B.; Sultan, M.; Wieser, D.; Xun, X.; Zhao, R.; Diagana, T. T.; Pertel, P.; Leong, F. J. Antimalarial Activity of KAF156 in Falciparum and Vivax Malaria. *New England Journal of Medicine* **2016**, *375* (12), 1152–1160. https://doi.org/10.1056/NEJMoa1602250.

(103) Kuhen, K. L.; Chatterjee, A. K.; Rottmann, M.; Gagaring, K.; Borboa, R.; Buenviaje, J.; Chen, Z.; Francek, C.; Wu, T.; Nagle, A.; Barnes, S. W.; Plouffe, D.; Lee, M. C. S.; Fidock, D. A.; Graumans, W.; van de Vegte-Bolmer, M.; van Gemert, G. J.; Wirjanata, G.; Sebayang, B.; Marfurt, J.; Russell, B.; Suwanarusk, R.; Price, R. N.; Nosten, F.; Tungtaeng, A.; Gettayacamin, M.; Sattabongkot, J.; Taylor, J.; Walker, J. R.; Tully, D.; Patra, K. P.; Flannery,

E. L.; Vinetz, J. M.; Renia, L.; Sauerwein, R. W.; Winzeler, E. A.; Glynne, R. J.; Diagana, T. T. KAF156 Is an Antimalarial Clinical Candidate with Potential for Use in Prophylaxis, Treatment, and Prevention of Disease Transmission. *Antimicrob Agents Chemother* **2014**, *58* (9), 5060–5067. https://doi.org/10.1128/AAC.02727-13.

(104) Ashton, T. D.; Devine, S. M.; Möhrle, J. J.; Laleu, B.; Burrows, J. N.; Charman, S. A.; Creek, D. J.; Sleebs, B. E. The Development Process for Discovery and Clinical Advancement of Modern Antimalarials. *J Med Chem* **2019**, *62* (23), 10526–10562. https://doi.org/10.1021/acs.jmedchem.9b00761.

(105) NIH. *Efficacy, Safety and Tolerability of KAF156 in Combination With Lumefantrine Solid Dispersion Formulation (LUM-SDF) in Pediatric Population With Uncomplicated Plasmodium Falciparum Malaria*. ClinicalTrials.gov. https://clinicaltrials.gov/ct2/show/NCT04546633 (accessed 2022-09-06).

(106) LaMonte, G. M.; Rocamora, F.; Marapana, D. S.; Gnädig, N. F.; Ottilie, S.; Luth, M. R.; Worgall, T. S.; Goldgof, G. M.; Mohunlal, R.; Santha Kumar, T. R.; Thompson, J. K.; Vigil, E.; Yang, J.; Hutson, D.; Johnson, T.; Huang, J.; Williams, R. M.; Zou, B. Y.; Cheung, A. L.; Kumar, P.; Egan, T. J.; Lee, M. C. S.; Siegel, D.; Cowman, A. F.; Fidock, D. A.; Winzeler, E. A. Pan-Active Imidazolopiperazine Antimalarials Target the Plasmodium Falciparum Intracellular Secretory Pathway. *Nat Commun* **2020**, *11* (1), 1780. https://doi.org/10.1038/s41467-020-15440-4.

(107) NIH. *Safety and Causal Prophylactic Efficacy of KAF156 in a Controlled Human Malaria Challenge Model*. ClinicalTrials.gov. https://clinicaltrials.gov/ct2/show/NCT04072302 (accessed 2022-09-06).

(108) McCarthy, J. S.; Yalkinoglu, Ö.; Odedra, A.; Webster, R.; Oeuvray, C.; Tappert, A.; Bezuidenhout, D.; Giddins, M. J.; Dhingra, S. K.; Fidock, D. A.; Marquart, L.; Webb, L.; Yin, X.; Khandelwal, A.; Bagchus, W. M. Safety, Pharmacokinetics, and Antimalarial Activity of the Novel Plasmodium Eukaryotic Translation Elongation Factor 2 Inhibitor M5717: A First-in-Human, Randomised, Placebo-Controlled, Double-Blind, Single Ascending Dose Study and Volunteer Infection Study. *Lancet Infect Dis* **2021**, *21* (12), 1713–1724. https://doi.org/10.1016/S1473-3099(21)00252-8.

(109) Dechering, K. J.; Duerr, H.-P.; Koolen, K. M. J.; Gemert, G.-J. van; Bousema, T.; Burrows, J.; Leroy, D.; Sauerwein, R. W. Modelling Mosquito Infection at Natural Parasite Densities Identifies Drugs Targeting EF2, PI4K or ATP4 as Key Candidates for Interrupting Malaria Transmission. *Sci Rep* **2017**, *7* (1), 17680. https://doi.org/10.1038/s41598-017-16671-0.

(110) Duffey, M.; Blasco, B.; Burrows, J. N.; Wells, T. N. C.; Fidock, D. A.; Leroy, D. Assessing Risks of Plasmodium Falciparum Resistance to Select Next-Generation Antimalarials. *Trends Parasitol* **2021**, *37* (8), 709–721. https://doi.org/10.1016/j.pt.2021.04.006.

(111) Baragaña, B.; Hallyburton, I.; Lee, M. C. S.; Norcross, N. R.; Grimaldi, R.; Otto, T. D.; Proto, W. R.; Blagborough, A. M.; Meister, S.; Wirjanata, G.; Ruecker, A.; Upton, L. M.; Abraham, T. S.; Almeida, M. J.; Pradhan, A.; Porzelle, A.; Martínez, M. S.; Bolscher, J. M.; Woodland, A.; Luksch, T.; Norval, S.; Zuccotto, F.; Thomas, J.; Simeons, F.; Stojanovski, L.; Osuna-Cabello, M.; Brock, P. M.; Churcher, T. S.; Sala, K. A.; Zakutansky, S. E.; Jiménez-Díaz, M. B.; Sanz, L. M.; Riley, J.; Basak, R.; Campbell, M.; Avery, V. M.; Sauerwein, R. W.; Dechering, K. J.; Noviyanti, R.; Campo, B.; Frearson, J. A.; Angulo-Barturen, I.; Ferrer-Bazaga, S.; Gamo, F. J.; Wyatt, P. G.; Leroy, D.; Siegl, P.; Delves, M. J.; Kyle, D. E.; Wittlin, S.; Marfurt, J.; Price, R. N.; Sinden, R. E.; Winzeler, E. A.; Charman, S. A.; Bebrevska, L.; Gray, D. W.; Campbell, S.; Fairlamb, A. H.; Willis, P. A.; Rayner, J. C.; Fidock, D. A.; Read, K. D.; Gilbert, I. H. A Novel Multiple-Stage Antimalarial Agent That Inhibits Protein Synthesis. *Nature* **2015**, *522* (7556), 315–320. https://doi.org/10.1038/nature14451.

(112) Lu, G.; Nagbanshi, M.; Goldau, N.; Mendes Jorge, M.; Meissner, P.; Jahn, A.; Mockenhaupt, F. P.; Müller, O. Efficacy and Safety of Methylene Blue in the Treatment of Malaria: A Systematic Review. *BMC Med* **2018**, *16* (1), 59. https://doi.org/10.1186/s12916-018-1045-3.

(113) Wadi, I.; Pillai, C. R.; Anvikar, A. R.; Sinha, A.; Nath, M.; Valecha, N. Methylene Blue Induced Morphological Deformations in Plasmodium Falciparum Gametocytes: Implications for Transmission-Blocking. *Malar J* **2018**, *17* (1), 11. https://doi.org/10.1186/s12936-017-2153-9.

(114) Bosson-Vanga, H.; Franetich, J.-F.; Soulard, V.; Sossau, D.; Tefit, M.; Kane, B.; Vaillant, J.-C.; Borrmann, S.; Müller, O.; Dereuddre-Bosquet, N.; le Grand, R.; Silvie, O.; Mazier, D.

Differential Activity of Methylene Blue against Erythrocytic and Hepatic Stages of Plasmodium. *Malar J* **2018**, *17* (1), 143. https://doi.org/10.1186/s12936-018-2300-y.

(115) Howes, R. E.; Piel, F. B.; Patil, A. P.; Nyangiri, O. A.; Gething, P. W.; Dewi, M.; Hogg, M. M.; Battle, K. E.; Padilla, C. D.; Baird, J. K.; Hay, S. I. G6PD Deficiency Prevalence and Estimates of Affected Populations in Malaria Endemic Countries: A Geostatistical Model-Based Map. *PLoS Med* **2012**, *9* (11), e1001339. https://doi.org/10.1371/journal.pmed.1001339.

(116) Mendes Jorge, M.; Ouermi, L.; Meissner, P.; Compaoré, G.; Coulibaly, B.; Nebie, E.; Krisam, J.; Klose, C.; Kieser, M.; Jahn, A.; Lu, G.; D`Alessandro, U.; Sié, A.; Mockenhaupt, F. P.; Müller, O. Safety and Efficacy of Artesunate-Amodiaquine Combined with Either Methylene Blue or Primaquine in Children with Falciparum Malaria in Burkina Faso: A Randomized Controlled Trial. *PLoS One* **2019**, *14* (10), e0222993. https://doi.org/10.1371/journal.pone.0222993.

(117) Kayabaşı, Y. Methylene Blue and Its Importance in Medicine. *Demiroglu Science University Florence Nightingale Journal of Medicine* **2020**, *6* (3), 136–145. https://doi.org/10.5606/fng.btd.2020.25035.

(118) Kato, N.; Comer, E.; Sakata-Kato, T.; Sharma, A.; Sharma, M.; Maetani, M.; Bastien, J.; Brancucci, N. M.; Bittker, J. A.; Corey, V.; Clarke, D.; Derbyshire, E. R.; Dornan, G. L.; Duffy, S.; Eckley, S.; Itoe, M. A.; Koolen, K. M. J.; Lewis, T. A.; Lui, P. S.; Lukens, A. K.; Lund, E.; March, S.; Meibalan, E.; Meier, B. C.; McPhail, J. A.; Mitasev, B.; Moss, E. L.; Sayes, M.; van Gessel, Y.; Wawer, M. J.; Yoshinaga, T.; Zeeman, A.-M.; Avery, V. M.; Bhatia, S. N.; Burke, J. E.; Catteruccia, F.; Clardy, J. C.; Clemons, P. A.; Dechering, K. J.; Duvall, J. R.; Foley, M. A.; Gusovsky, F.; Kocken, C. H. M.; Marti, M.; Morningstar, M. L.; Munoz, B.; Neafsey, D. E.; Sharma, A.; Winzeler, E. A.; Wirth, D. F.; Scherer, C. A.; Schreiber, S. L. Diversity-Oriented Synthesis Yields Novel Multistage Antimalarial Inhibitors. *Nature* **2016**, *538* (7625), 344–349. https://doi.org/10.1038/nature19804.

(119) Sharma, M.; Mutharasappan, N.; Manickam, Y.; Harlos, K.; Melillo, B.; Comer, E.; Tabassum, H.; Parvez, S.; Schreiber, S. L.; Sharma, A. Inhibition of Plasmodium Falciparum Phenylalanine TRNA Synthetase Provides Opportunity for Antimalarial Drug Development. *Structure* **2022**, *30* (7), 962-972.e3. https://doi.org/10.1016/j.str.2022.03.017.

(120) Okombo, J.; Chibale, K. Recent Updates in the Discovery and Development of Novel Antimalarial Drug Candidates. *Medchemcomm* **2018**, *9* (3), 437–453. https://doi.org/10.1039/C7MD00637C.

(121) Medicine for Malaria Venture. *MMV609 University of Kentucky*. https://www.mmv.org/research-development/project-portfolio/mmv609-university-kentucky (accessed 2022-09-06).

(122) de Vries, L. E.; Jansen, P. A. M.; Barcelo, C.; Munro, J.; Verhoef, J. M. J.; Pasaje, C. F. A.; Rubiano, K.; Striepen, J.; Abla, N.; Berning, L.; Bolscher, J. M.; Demarta-Gatsi, C.; Henderson, R. W. M.; Huijs, T.; Koolen, K. M. J.; Tumwebaze, P. K.; Yeo, T.; Aguiar, A. C. C.; Angulo-Barturen, I.; Churchyard, A.; Baum, J.; Fernández, B. C.; Fuchs, A.; Gamo, F.-J.; Guido, R. V. C.; Jiménez-Diaz, M. B.; Pereira, D. B.; Rochford, R.; Roesch, C.; Sanz, L. M.; Trevitt, G.; Witkowski, B.; Wittlin, S.; Cooper, R. A.; Rosenthal, P. J.; Sauerwein, R. W.; Schalkwijk, J.; Hermkens, P. H. H.; Bonnert, R. v.; Campo, B.; Fidock, D. A.; Llinás, M.; Niles, J. C.; Kooij, T. W. A.; Dechering, K. J. Preclinical Characterization and Target Validation of the Antimalarial Pantothenamide MMV693183. *Nat Commun* **2022**, *13* (1), 2158. https://doi.org/10.1038/s41467-022-29688-5.

(123) Dreyer, S. M.; Vaughan, J. A. Survival and Fecundity of Anopheles Stephensi and Anopheles Albimanus Mosquitoes (Diptera: Culicidae) After Ingesting Bovine Blood Containing Various Veterinary Systemic Parasiticides. *J Med Entomol* **2022**. https://doi.org/10.1093/jme/tjac103.

(124) Miglianico, M.; Eldering, M.; Slater, H.; Ferguson, N.; Ambrose, P.; Lees, R. S.; Koolen, K. M. J.; Pruzinova, K.; Jancarova, M.; Volf, P.; Koenraadt, C. J. M.; Duerr, H.-P.; Trevitt, G.; Yang, B.; Chatterjee, A. K.; Wisler, J.; Sturm, A.; Bousema, T.; Sauerwein, R. W.; Schultz, P. G.; Tremblay, M. S.; Dechering, K. J. Repurposing Isoxazoline Veterinary Drugs for Control of Vector-Borne Human Diseases. *Proceedings of the National Academy of Sciences* **2018**, *115* (29). https://doi.org/10.1073/pnas.1801338115.

(125) Burns, A. L.; Dans, M. G.; Balbin, J. M.; de Koning-Ward, T. F.; Gilson, P. R.; Beeson, J. G.; Boyle, M. J.; Wilson, D. W. Targeting Malaria Parasite Invasion of Red Blood Cells as an

Antimalarial Strategy. *FEMS Microbiol Rev* **2019**, *43* (3), 223–238. https://doi.org/10.1093/femsre/fuz005.

(126) Buchholz, K.; Burke, T. A.; Williamson, K. C.; Wiegand, R. C.; Wirth, D. F.; Marti, M. A High-Throughput Screen Targeting Malaria Transmission Stages Opens New Avenues for Drug Development. *J Infect Dis* **2011**, *203* (10), 1445–1453. https://doi.org/10.1093/infdis/jir037.

(127) Dechering, K. J.; Timmerman, M.; Rensen, K.; Koolen, K. M. J.; Honarnejad, S.; Vos, M. W.; Huijs, T.; Henderson, R. W. M.; Chenu, E.; Laleu, B.; Montefiore, B. C.; Segall, M. D.; Mills, J. E. J.; Guantai, E. M.; Duffy, J.; Duffey, M. Replenishing the Malaria Drug Discovery Pipeline: Screening and Hit Evaluation of the MMV Hit Generation Library 1 (HGL1) against Asexual Blood Stage Plasmodium Falciparum, Using a Nano Luciferase Reporter Read-Out. *SLAS Discovery* **2022**, *27* (6), 337–348. https://doi.org/10.1016/j.slasd.2022.07.002.

(128) Yahiya, S.; Rueda-Zubiaurre, A.; Delves, M. J.; Fuchter, M. J.; Baum, J. The Antimalarial Screening Landscape—Looking beyond the Asexual Blood Stage. *Curr Opin Chem Biol* **2019**, *50*, 1–9. https://doi.org/10.1016/j.cbpa.2019.01.029.

(129) Reader, J.; Botha, M.; Theron, A.; Lauterbach, S. B.; Rossouw, C.; Engelbrecht, D.; Wepener, M.; Smit, A.; Leroy, D.; Mancama, D.; Coetzer, T. L.; Birkholtz, L.-M. Nowhere to Hide: Interrogating Different Metabolic Parameters of Plasmodium Falciparum Gametocytes in a Transmission Blocking Drug Discovery Pipeline towards Malaria Elimination. *Malar J* **2015**, *14* (1), 213. https://doi.org/10.1186/s12936-015-0718-z.

(130) Reader, J.; van der Watt, M. E.; Taylor, D.; le Manach, C.; Mittal, N.; Ottilie, S.; Theron, A.; Moyo, P.; Erlank, E.; Nardini, L.; Venter, N.; Lauterbach, S.; Bezuidenhout, B.; Horatscheck, A.; van Heerden, A.; Spillman, N. J.; Cowell, A. N.; Connacher, J.; Opperman, D.; Orchard, L. M.; Llinás, M.; Istvan, E. S.; Goldberg, D. E.; Boyle, G. A.; Calvo, D.; Mancama, D.; Coetzer, T. L.; Winzeler, E. A.; Duffy, J.; Koekemoer, L. L.; Basarab, G.; Chibale, K.; Birkholtz, L.-M. Multistage and Transmission-Blocking Targeted Antimalarials Discovered from the Open-Source MMV Pandemic Response Box. *Nat Commun* **2021**, *12* (1), 269. https://doi.org/10.1038/s41467-020-20629-8.

(131) Delves, M. J.; Ramakrishnan, C.; Blagborough, A. M.; Leroy, D.; Wells, T. N. C.; Sinden, R. E. A High-Throughput Assay for the Identification of Malarial Transmission-Blocking

Drugs and Vaccines. *Int J Parasitol* **2012**, *42* (11), 999–1006. https://doi.org/10.1016/j.ijpara.2012.08.009.

(132) Gebru, T.; Lalremruata, A.; Kremsner, P. G.; Mordmüller, B.; Held, J. Life-Span of in Vitro Differentiated Plasmodium Falciparum Gametocytes. *Malar J* **2017**, *16* (1), 330. https://doi.org/10.1186/s12936-017-1986-6.

(133) Duffy, S.; Loganathan, S.; Holleran, J. P.; Avery, V. M. Large-Scale Production of Plasmodium Falciparum Gametocytes for Malaria Drug Discovery. *Nat Protoc* **2016**, *11* (5), 976–992. https://doi.org/10.1038/nprot.2016.056.

(134) Sykes, M. L.; Avery, V. M. Approaches to Protozoan Drug Discovery: Phenotypic Screening. *J Med Chem* **2013**, *56* (20), 7727–7740. https://doi.org/10.1021/jm4004279.

(135) Wadi, I.; Anvikar, A. R.; Nath, M.; Pillai, C. R.; Sinha, A.; Valecha, N. Critical Examination of Approaches Exploited to Assess the Effectiveness of Transmission-Blocking Drugs for Malaria. *Future Med Chem* **2018**, *10* (22), 2619–2639. https://doi.org/10.4155/fmc-2018-0169.

(136) Plouffe, D. M.; Wree, M.; Du, A. Y.; Meister, S.; Li, F.; Patra, K.; Lubar, A.; Okitsu, S. L.; Flannery, E. L.; Kato, N.; Tanaseichuk, O.; Comer, E.; Zhou, B.; Kuhen, K.; Zhou, Y.; Leroy, D.; Schreiber, S. L.; Scherer, C. A.; Vinetz, J.; Winzeler, E. A. High-Throughput Assay and Discovery of Small Molecules That Interrupt Malaria Transmission. *Cell Host Microbe* **2016**, *19* (1), 114–126. https://doi.org/10.1016/j.chom.2015.12.001.

(137) Lucantoni, L.; Silvestrini, F.; Signore, M.; Siciliano, G.; Eldering, M.; Dechering, K. J.; Avery, V. M.; Alano, P. A Simple and Predictive Phenotypic High Content Imaging Assay for Plasmodium Falciparum Mature Gametocytes to Identify Malaria Transmission Blocking Compounds. *Sci Rep* **2015**, *5* (1), 16414. https://doi.org/10.1038/srep16414.

(138) Shaw, W. R.; Marcenac, P.; Catteruccia, F. Plasmodium Development in Anopheles: A Tale of Shared Resources. *Trends Parasitol* **2022**, *38* (2), 124–135. https://doi.org/10.1016/j.pt.2021.08.009.

(139) Ruecker, A.; Mathias, D. K.; Straschil, U.; Churcher, T. S.; Dinglasan, R. R.; Leroy, D.; Sinden, R. E.; Delves, M. J. A Male and Female Gametocyte Functional Viability Assay To Identify Biologically Relevant Malaria Transmission-Blocking Drugs. *Antimicrob Agents Chemother* **2014**, *58* (12), 7292–7302. https://doi.org/10.1128/AAC.03666-14.

(140) Delves, M. J.; Miguel-Blanco, C.; Matthews, H.; Molina, I.; Ruecker, A.; Yahiya, S.; Straschil, U.; Abraham, M.; León, M. L.; Fischer, O. J.; Rueda-Zubiaurre, A.; Brandt, J. R.; Cortés, Á.; Barnard, A.; Fuchter, M. J.; Calderón, F.; Winzeler, E. A.; Sinden, R. E.; Herreros, E.; Gamo, F. J.; Baum, J. A High Throughput Screen for Next-Generation Leads Targeting Malaria Parasite Transmission. *Nat Commun* **2018**, *9* (1), 3805. https://doi.org/10.1038/s41467-018-05777-2.

(141) Delves, M.; Lafuente-Monasterio, M. J.; Upton, L.; Ruecker, A.; Leroy, D.; Gamo, F.-J.; Sinden, R. Fueling Open Innovation for Malaria Transmission-Blocking Drugs: Hundreds of Molecules Targeting Early Parasite Mosquito Stages. *Front Microbiol* **2019**, *10*. https://doi.org/10.3389/fmicb.2019.02134.

(142) Miura, K.; Stone, W. J. R.; Koolen, K. M.; Deng, B.; Zhou, L.; van Gemert, G.-J.; Locke, E.; Morin, M.; Bousema, T.; Sauerwein, R. W.; Long, C. A.; Dechering, K. J. An Inter-Laboratory Comparison of Standard Membrane-Feeding Assays for Evaluation of Malaria Transmission-Blocking Vaccines. *Malar J* **2016**, *15* (1), 463. https://doi.org/10.1186/s12936-016-1515-z.

(143) Miura, K.; Swihart, B. J.; Deng, B.; Zhou, L.; Pham, T. P.; Diouf, A.; Burton, T.; Fay, M. P.; Long, C. A. Transmission-Blocking Activity Is Determined by Transmission-Reducing Activity and Number of Control Oocysts in Plasmodium Falciparum Standard Membrane-Feeding Assay. *Vaccine* **2016**, *34* (35), 4145–4151. https://doi.org/10.1016/j.vaccine.2016.06.066.

(144) Churcher, T. S.; Blagborough, A. M.; Delves, M.; Ramakrishnan, C.; Kapulu, M. C.; Williams, A. R.; Biswas, S.; Da, D. F.; Cohuet, A.; Sinden, R. E. Measuring the Blockade of Malaria Transmission – An Analysis of the Standard Membrane Feeding Assay. *Int J Parasitol* **2012**, *42* (11), 1037–1044. https://doi.org/10.1016/j.ijpara.2012.09.002.

(145) Paton, D. G.; Probst, A. S.; Ma, E.; Adams, K. L.; Shaw, W. R.; Singh, N.; Bopp, S.; Volkman, S. K.; Hien, D. F. S.; Paré, P. S. L.; Yerbanga, R. S.; Diabaté, A.; Dabiré, R. K.; Lefèvre, T.; Wirth, D. F.; Catteruccia, F. Using an Antimalarial in Mosquitoes Overcomes Anopheles and Plasmodium Resistance to Malaria Control Strategies. *PLoS Pathog* **2022**, *18* (6), e1010609. https://doi.org/10.1371/journal.ppat.1010609.

# Chapter 4 - Discovery of Novel Pyrazole- and Pyrrole- Based Compounds as Potential Transmission-Blocking Compounds

## 4.1 Introduction

The development of new tools is of paramount importance to stay ahead resistance and to eventually eradicate malaria. Today, scientists prioritize the search of new antimalarial drugs carrying a new profile: transmission-blocking activity, selectivity against gametocytes and/or sporogonic stages, new mechanism of action (MoA), and no cross resistance with existing drugs.[1–4] The transmission blocking candidates present in the pipeline act on multiple stages, including asexual blood stages (ABS), thus none of them showed a selective activity towards the bottlenecks of malaria transmission, which contrary to drugs with multiple activity do not cause the selection of parasite resistant genotypes during asexual proliferation.[1,2,5,6] This is mainly due to the screening cascade that has for long time prioritized the activity against asexual parasites.[7–9]

To address this, a work from Reader et al.[5] recently described a parallel *de novo* screening of the Medicine for Malaria Venture (MMV) Pandemic Response Box (PRB) on *P. falciparum* avoiding any bias towards activity on any one life cycle stage. Interestingly, from an initial screening of 400 drug-like compounds, they identified novel chemotypes having multistage activity, ABS-specific activity, stage-specific activity against IV/V stage gametocytes (GC). Among these, the rimonabant-derivative **MMV1580843** (abbreviated as **MMV843**) showed potent selective activity against late-stage GC (Table 4.1), particularly towards the formation of male gametes, and thus an intriguing transmission-blocking profile. **MMV843** was initially discovered as an inhibitor of the lipid transporter mycobacterial membrane protein large 3 (Mmpl3) in *Mycobacterium tuberculosis*,[10] but since the are no direct homologues to this protein in the *P. falciparum* genome, the MoA of this compound cannot be predicted, and further analysis are needed. Moderate cytotoxicity and metabolic profile impede **MMV843** to progress as a clinical candidate for malaria transmission-blocking strategies,

yet it represents a good starting point for medicinal chemists in search of breakthrough antimalarial drugs.

**Table 4.1.** Activity of **MMV843** against asexual and late-stage GC of *P. falciparum* parasites and structure. [a] *Plasmodium falciparum*; [b] fold change of $IC_{50}$ ABS/ $IC_{50}$ stage IV/V GC; [c] transmission-reducing activity (reduction in oocyst intensity); [d] topological polar surface area; [e] predicted.

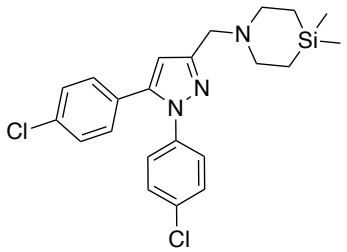


**MMV1580843**

| | |
|---|---|
| **Asexual $IC_{50}$ (μM) (FC[b])** | 1.79 (16) |
| **Pf[a] stages IV/V GC $IC_{50}$ (μM)** | 0.108 |
| **Pf[a] male gamete formation** | 58% |
| **Pf[a] female gamete formation** | 63.6% |
| **SMFA (% TRA[c])** | 80.2% |
| **Cytotoxicity (μM)** | 38.9 (HepG2) |
| **$LogD_{7.4}$** | 4.22[e] |
| **Solubility pH 6.5 (μM)** | 3.72[e] |
| **tPSA[d]** | 21.06[e] |

The recent discovery of Paton et al.[11] has recently built the foundation for a novel malaria control strategy based on incorporating antimalarial drugs into mosquito-targeting interventions, demonstrating that sporogonic stages of *P. falciparum* parasites, can be completely abrogated when *Anopheles gambiae* females are exposed tarsally to surfaces

coated with low concentrations of **ATQ** (Figure 4.1). This strategy lays the foundation for the search of new antimalarial compounds active against sporogonic stages, which have been hindered by the lack of knowledge of parasite-vector interaction and short availability of testing tools.[12] Indeed, as **ATQ** is used as a human therapeutic to treat malaria-infected people, it cannot be utilized in this strategy due to the risks of favoring the spread of parasite resistance.

These findings motivated our search for new transmission-blocking compounds. Due to the similarity between **MMV843** and potent anti-tubercular compounds previously discovered by us,[13] in collaboration with Birkholtz's research group at University of Pretoria (Department of Biochemistry Genetics and Microbiology) we started a research project to find new transmission-blocking compounds with improved physico-chemical features that retain the selective gametocytocidal activity and would help us to understand the structure activity relationships (SAR) around their scaffold.

In parallel to this, in collaboration with Catteruccia's research group at Harvard T.H. Chan School of Public Health (Department of Immunology and Infectious Diseases), we aim to discover new anti-malarial compounds active against sporogonic stages of *P. falciparum* to populate the chemical library to use in the aforementioned strategy. To this end, compounds of an in-house library were selected for phenotypic screenings.

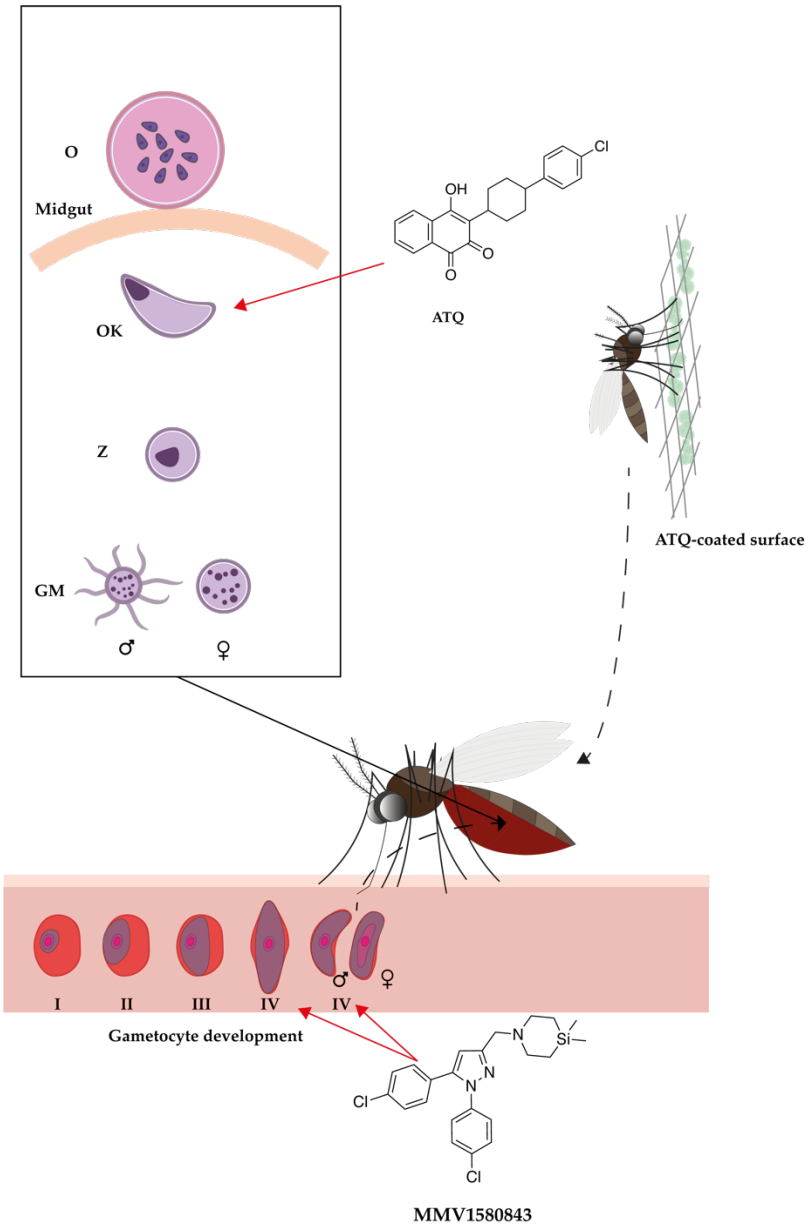


**Figure 4.1.** Schematic representation of transmission-blocking activity of **MMV843** and **ATQ**. **MMV843** targets late-stage GC (IV-V) with higher potency against male GC blocking their transition to male gametes. **ATQ** is absorbed through the cuticle of an uninfected mosquito upon tarsal exposure to an **ATQ**-coated surface. When the mosquito ingests GC, **ATQ** blocks the formation of mature ookinetes and thus the development of infectious sporozoites. GM: gametes; Z: zygote; OK: ookinete; O: oocyst.

## 4.2 Results

### 4.2.1 Selection of MMV843 Analogues

In order to explore which alterations are best tolerated and then the minimum requirements for activity, 14 synthetically accessible derivatives were selected with the best substituents resulting from our previous works.[13,14] (Figure Table 4.2). Changes to $R^1$ and $R^2$ of **MMV843** were first in priority and included changes of the chlorophenyl groups with other electron withdrawing groups (EWGs) (**1** - **4**, **7** - **10**, **12** - **15**) or electron donating groups (EDGs) (**5** - **7**, **11**, **14**), or replacement with aliphatic substituents (**1**, **2**, **4 - 6**, **9**, **11**, **13**). Changes to $R^3$ were second in priority and included the replacement of the azasilinane amine with other cyclic amines (**5** – **15**). The latter were particularly attractive considering the role of the silicon amine which previously showed to be responsible of high cytotoxicity together with high levels of human ether-a-go-go-related gene (hERG) activity, low water solubility, as well as low membrane permeability.[13]

**Table 4.2.** Chemical structures of compounds **1-15**. [a]Previously reported in outer source.[13]

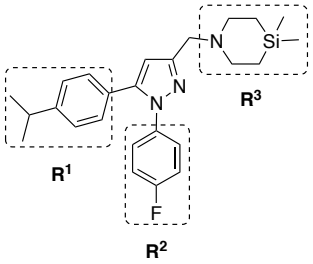


| Compound | $R^1$ | $R^2$ | $R^3$ |
|---|---|---|---|
| **1** | 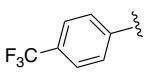 |  | 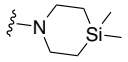 |
| **2**[a] | 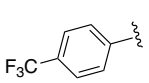 |  | 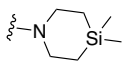 |
| **3** |  | 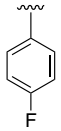 | 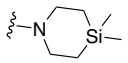 |
| **4**[a] | 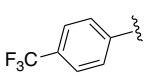 | 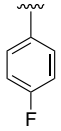 | 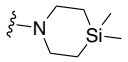 |

| | | | |
|---|---|---|---|
| **5** | 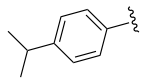 |  | 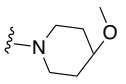 |
| **6** | 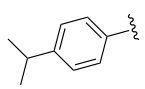 |  | 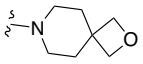 |
| **7** | 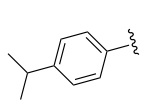 | 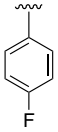 | 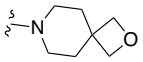 |
| **8** [a] | 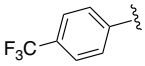 | 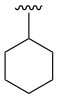 | 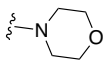 |
| **9** [a] | 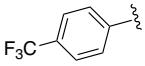 | 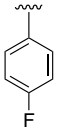 | 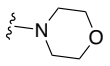 |
| **10** [a] | 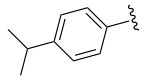 |  | 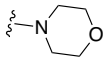 |
| **11** [a] | 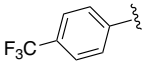 | 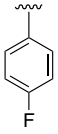 | 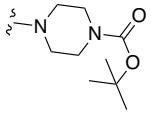 |
| **12** [a] | 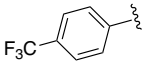 |  | 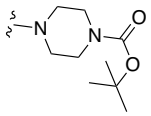 |
| **13** [a] | 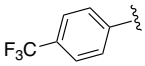 | 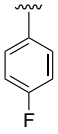 | 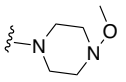 |
| **14** | 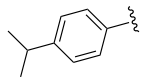 | 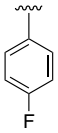 | 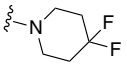 |
| **15** | 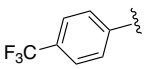 | 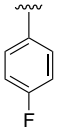 | 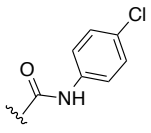 |

### 4.2.2 Activity and Cytotoxicity Studies of Selected Analogues for a preliminary Structure Activity Relationship (SAR)

To assess the activity of **1** - **15** against *P. falciparum,* compounds were screened in parallel against *Pf*NF54 asexual parasites and stage IV/V GC along with **MMV843**. Anti-asexual activity was determined after three independent experiments of SYBR Green I assay (72

hours cycle) and activity data against stage IV/V GC were orthogonally confirmed on three different gametocyte assays (PrestoBlue fluorescence assay, ATP bioluminescence assay, luciferase reporter assay). Safety of compounds with gametocytocidal activity lower than 1 μM was predicted by performing cytotoxicity counter-screening and HepG2 toxicity screenings.

All analogues showed moderate anti-asexual activity ($IC_{50}$ > 1 μM) but different substitutions around the pyrazole core determined a wider change of values of activity towards stage IV/V GC (Table 4.3). The azasilinane series (**1** – **4**) displayed submicromolar activity ($IC_{50}$ = 0.219 – 0.708 μM), with compound **1** to be the most potent one and characterized by the highest fold change (FC; $IC_{50}$ ABS/ $IC_{50}$ stage IV/V GC) of this series. Compounds **1** - **4** were particularly interesting since they suggest that the replacement of the aryl group at both positions $R^1$ or $R^2$ with an aliphatic group does not "switch off" the activity against late-stage GC, which is retained. Generally, such substitutions increased anti-asexual activity ($IC_{50}$ = 1.087 – 2.043) and decreased gametocytocidal activity with respect to **MMV843**. Consequently, FC is also decreased making compounds **2** (FC = 2.85) and **4** (FC = 1.68) not selective against late-stage GC according to TCP5 criteria.

Interestingly, all the structural modifications at position $R^3$ determined a loss of activity against late-stage GC except for compound **14** ($IC_{50}$ = 0.582 μM), which is characterized by a 4,4-difluoro piperidine at $R^3$, suggesting that that there is space for modifications also at this position. Moreover, compared to its activity against ABS parasites, activity towards stage IV/V GC was significantly lower with a FC = 7.18, that is closer to the one of **MMV843**. Compounds substituted with morpholine (**8** – **10**), *tert*-butyl piperazine-1-carboxylate (**11**, **12**), and 2-oxa-7-azaspiro[3.5]nonane (**6**, **7**) showed a complete loss of activity against late-stage GC ($IC_{50}$ > 10 μM) regardless whether carrying both aryl rings at $R^1$ and $R^2$ or aliphatic groups at one of the two positions. Notably, compounds **5** and **13** carry the same substituent at position $R^3$ (4-methoxypiperidine) but only compound **5** showed moderate activity against late-stage GC ($IC_{50}$ =1.1 μM) indicating that the 2-methylpropan-2-ol at position $R^2$ plays a role in recovering such activity. Loss of activity of these compounds does not

correlate with the activity against ABS, which is generally higher as in the case of compounds **6**, **7** and **15** ($IC_{50}$ = 1.39 – 3.975 μM).

Additionally, the replacement of the chlorophenyl group with the more potent EWG trifluoromethyl phenyl can lead to an increase of anti-asexual activity making compounds up to 10-fold orders of magnitude more active than **MMV843**.

Finally, on the basis of their gametocytocidal activities, and excellent solubility profile (solubility in PBS at pH 7.4 = 55 – 165 μM), compounds **1** - **5** were tested for microsomal stability and Hep2G cytotoxicity. Like **MMV843**, these compounds were not cytotoxic at concentrations > 25 μM, however previous studies reported in our recent work[13] revealed hERG toxicity (not yet tested in **MMV843**) in the case of compounds **2** and **4** that was correlated to the azasilinane group. Microsomal stability studies (not yet tested in **MMV843**) showed rapid clearance of the tested compounds that do not meet the TCP-5 criteria and could bring to a lack of efficacy *in vivo*.

**Table 4.3.** Activity against *Pf*NF54 ABS and late-stages of GC (IV/V), physico-chemical properties, cytotoxicity on HepG2 cells and hERG interactions of compounds **1** - **15** and **MMV843**, compared to TCP-5 hit/early lead criteria.

| Comp. | IV/V GC $IC_{50}$ (μM) | ABS $IC_{50}$ (μM) (FC) | Cytotoxicity Hep2 (μM) | Sol. pH 6.5[a] (μM) | Microsome EH (h/r/m) | MW (g/mol) | $logD_{7.4}$[a] | tPSA[a] | hERG $IC_{50}$ (μM) |
|---|---|---|---|---|---|---|---|---|---|
| **TCP-5 criteria** | **< 0.5/0.1 μM** | **> 5 (FC > 3/ >10)** | **> 100/1000 fold** | **> 10 (PBS)** | **< 0.5** | **< 500** | **< 3** | **< 75Å²** | **-** |
| **MMV843** | 0.112 | 1. 79 (16) | 38.9 | 3.72 | n/a | 430.40 | 5.5 | 21.06 | - |
| **1** | 0.219 | 1.813 (8) | > 25 | 165 | 0.88/0.74/0.72 | 407.55 | 3.0 | 21 | - |
| **2** | 0.382 | 1.087 (3) | > 25 | 120 | 0.90/0.89/0.94 | 435.60 | 3.2 | 21 | 2.5[b] |
| **3** | 0.526 | 2.043 (4) | > 25 | 170 | 0.92/0.90/0.89 | 385.59 | 2.5 | 18.84 | - |
| **4** | 0.708 | 1.191 (2) | > 25 | 55 | 0.87/0.88/0.63 | 447.54 | 3.6 | 21 | 1.26[b] |
| **5** | 1.1 | - | > 25 | - | - | 385.54 | 4.3 | 21 | - |
| **6** | > 10 | 1.39 (0.14) | 7% at 20 uM | 165 | - | 407.60 | 3.4 | 28.07 | - |

| | | | | | | | | | |
|---|---|---|---|---|---|---|---|---|---|
| **7** | > 10 | 3.975 (0.4) | 0.2% at 20 uM | 110 | - | 419.54 | 3.9 | 6 | - |
| **8** | > 10 | - | - | - | - | 393.45 | 4.4 | 28 | - |
| **9** | > 10 | - | - | - | - | 405.40 | 4.4 | 28 | - |
| **10** | > 10 | - | - | - | - | 327.47 | 3.8 | 28 | - |
| **11** | > 10 | - | - | - | - | 504.43 | 5.4 | 48.38 | - |
| **12** | > 10 | - | - | - | - | 492.59 | 5.4 | 48.38 | - |
| **13** | > 10 | - | - | - | - | 434.44 | 4.2 | 31 | - |
| **14** | 0.582 | 4.176 (7) | > 20 | < 5 | - | 413.49 | 4.3 | 21 | - |
| **15** | > 10 | 2.115 (0.2) | > 20 | < 5 | - | 459.83 | 5.6 | 47 | - |

[a] predicted; [b] data reported from outer source[13]; -: to be determined; h/r/m: human, rat, and mouse liver microsomes; Comp.: Compound.

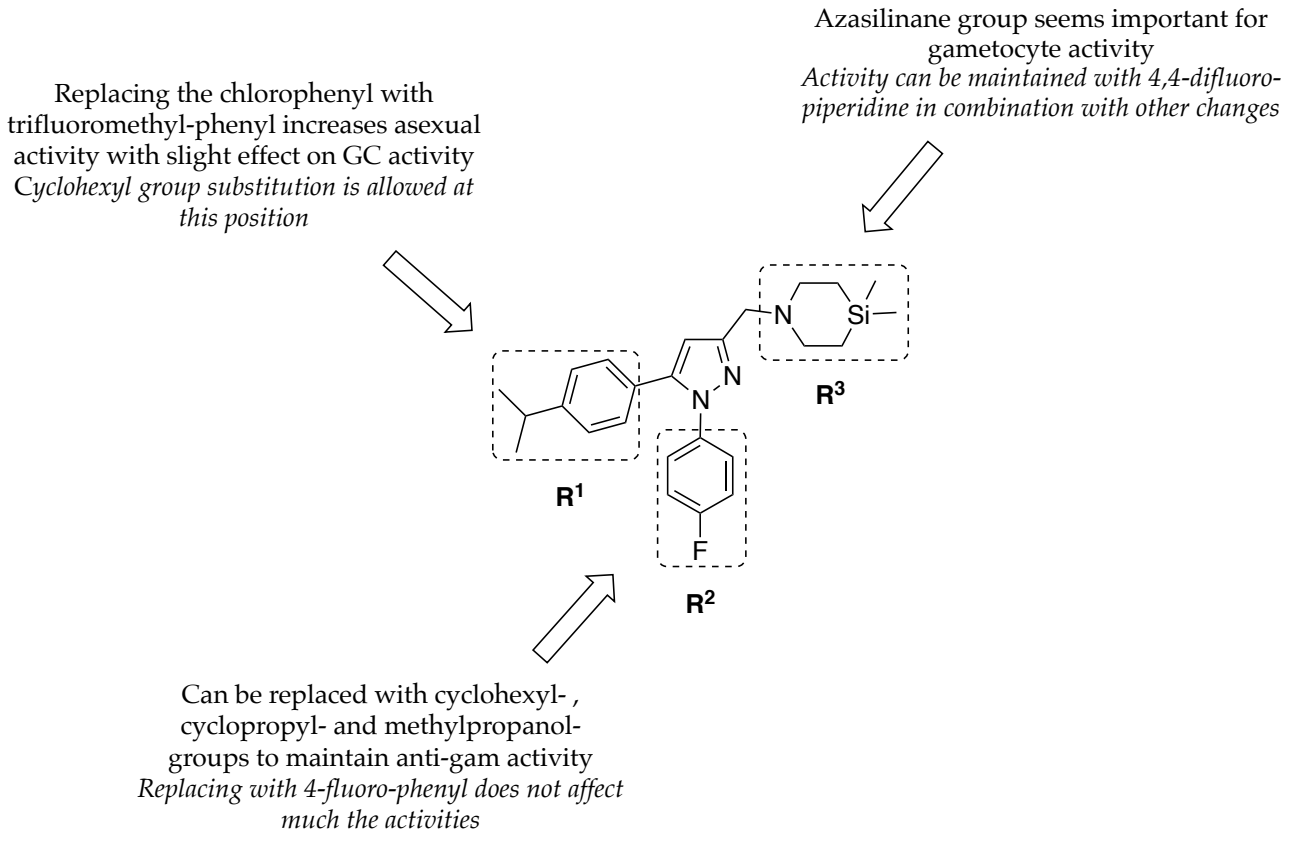


**Figure 4.2.** Preliminary SAR characterization around **MMV843**.

### 4.2.3 Compounds Selected for Screening Against Multiple-Stages of *P. falciparum*

For the purpose to find novel compounds to use as a transmission-blockers in mosquitoes through tarsal contact, 127 compounds were selected from our in-house library (1000

compounds) according three parameters, i) chemical diversity, ii) tPSA < 90 Å$^2$, iii) logP > 2. Of these 127 compounds, 86 were 1,5-diaryl pyrroles, 34 were pyrazoles and 7 were hydrazide derivatives of the 2-fluorobenzoic acid (Figure 4.3). Some of them demonstrated anti-tubercular activity in our previous works[13–17] and, while pyrroles and pyrazoles show structural similarity with **MMV843**, antiplasmodial activity of benzohydrazide chemotypes have not been yet reported.

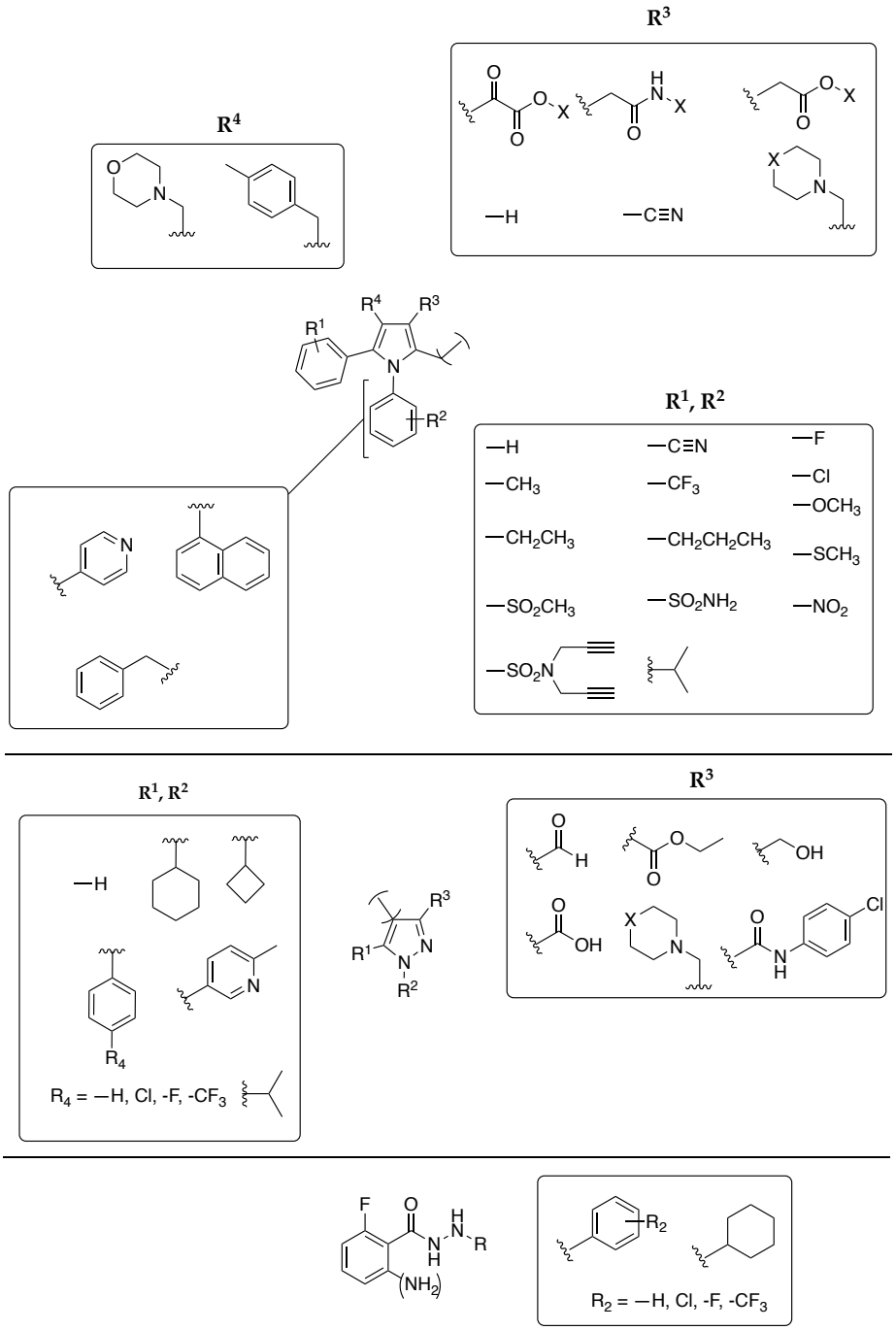


**Figure 4.3.** General structures of the 127 selected compounds. From the top to the bottom: 1,5 diaryl pyrroles, pyrazoles and 2-fluorobenzohydrazide derivatives. X = either a heteroatom or aliphatic substituent.

### 4.2.4 Anti-asexual Screening Data Analysis, Chemical Series Prioritization and Preliminary SAR Analysis

Hit selection of compounds was first performed in ABS of *Pf*NF54 by using SYBR Green I assay. The selected 127 compounds were first screened in three different concentrations (20 μM, 2 μM and 0.2 μM) on three independent experiments and hits were identified at 2 μM with a cut-off ≥ 30% of growth inhibition of asexual parasites. ABS activity of the hits was confirmed in a second round of screening by evaluating the $IC_{50}$ and ATQ was used as control for the reproducibility of the assay.

Following incubation of 72 hours, 12 hits of the 127 compounds proved to be active on ABS of *Pf*NF54, of which 6 were pyrroles and 6 were pyrazoles (Table 4.4). We assumed that these compounds were characterized by a good cell permeation profile since were characterized by a tPSA in a range between 6.46 and 49.85 $Å^2$, and $LogD_{7.4}$ between 4.2 and 6.2.

Since none of the fluorobenzohydrazide derivatives were active at 2 μM, they were not considered for further analysis. $IC_{50}$ values ranged from 0.74 to 3.70 μM and of the 12 hits, 4 compounds had $IC_{50}$ < 2 μM, with **18** ($IC_{50}$ = 1.26 μM) and **16** ($IC_{50}$ = 0.74 μM) to be the most potent of the pyrrole and pyrazole series, respectively. As reported above, also here compounds **3** ($IC_{50}$ = 2.60 μM), **6** ($IC_{50}$ = 2.78 μM), **11** ($IC_{50}$ = 3.70 μM) and **12** ($IC_{50}$ = 1.54 μM) (Table 4.2) were found to be active against asexual stages with similar potency, except for compound **6** ($IC_{50}$ = 2.78 μM), denoting 2-fold increase compared to the values observed in previous experiments (Table 4.2).

Screening data helped us to conduct preliminary SAR studies around these two chemical groups (Figure 4.4). They suggest that pyrazole and pyrroles are active against ABS of parasites when substituted at positions 1, 3 and 5. Generally, a basic non-aryl six membered saturated heterocycle at position three is important for the activity. The azasilinane group at position 3 is not essential for ABS activity and this position can be occupied by *tert*-butyl piperazine-1-carboxylate (**11**, **12**), 2-oxa-7-azaspiro[3.5]nonane (**6**) and 4,4-difluoro piperidine (**16**, **21**). Interestingly, none of the compounds carrying a morpholine at position 3 were active. Contrary, 5 hit compounds (**17**, **19**, **20**, **22**, **23**) carry thiomorpholine on that

position. Interestingly, **18** was the only exception, since it is substituted at $R^3$ by an ethyl-oxoacetate group, which might confer different target-molecule interaction due to electron-density and conformational differences with the other molecules.

Combinations of EDGs and EWGs on the aryl rings at both positions 1 and 5 modulate the potency of compounds and as previously seen, the presence of a trifluoromethylphenyl group seems to be favorable for increased anti-asexual activity. Pyrazoles containing one aryl ring and a cyclohexyl group on either position 1 or 5, showed increased potency compared to pyrazoles with two aryl rings. For instance, compound **12** showed $IC_{50}$ of 1.54 μM, while compound **11** $IC_{50}$ was 3.70 μM, and they differ only for the presence of a cyclohexyl group in position 1. 1-naphyl group in position one is allowed (**20**) and indicates that there is a wide space for chemical modifications in this position.

**Table 4.4.** Activity against *Pf*NF54 ABS, physico-chemical properties, **3**, **6**, **11**, **12**, and **19-23**.

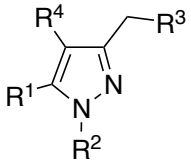


| Comp. | $R^1$ | $R^2$ | $R^3$ | $R^4$ | ABS $IC_{50}$ (μM) | MW (g/mol) | $logD_{7.4}$[a] | tPSA[a] |
|---|---|---|---|---|---|---|---|---|
| **3** |  | 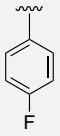 | 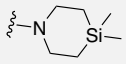 | -H | 2.60 | 385.59 | 2.5 | 18.84 |
| **6** | 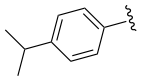 |  | 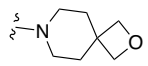 | -H | 2.78 | 407.60 | 3.4 | 28.07 |
| **11** | 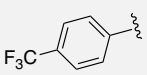 | 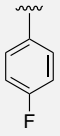 | 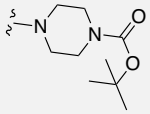 | -H | 3.70 | 504.43 | 5.4 | 48.38 |
| **12** | 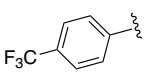 | 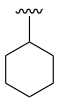 | 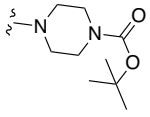 | -H | 1.54 | 492.59 | 5.4 | 48.38 |

| | | | | | | | | |
|---|---|---|---|---|---|---|---|---|
| **16** | 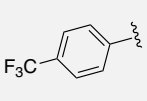 | 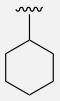 | 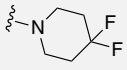 | -H | 0.74 | 427.46 | 5.6 | 18.84 |
| **17** | 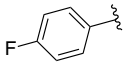 | 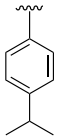 | 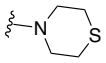 | -$CH_3$ | 3.37 | 409.57 | 5.7 | 18.84 |
| **ATQ** | | | | | $2.2 \times 10^{-4}$ | 366.84 | 5.8 | 54.37 |

[a] predicted; Comp. = Compound.

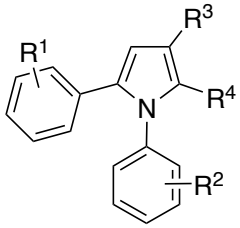


| Comp. | $R^1$ | $R^2$ | $R^3$ | $R^4$ | ABS $IC_{50}$ (μM) | MW (g/mol) | $logD_{7.4}$[a] | tPSA[a] |
|---|---|---|---|---|---|---|---|---|
| **18** | -4-Cl | -4-Cl | 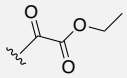 | -$CH_3$ | 1.26 | 402.27 | 6.16 | 46.61 |
| **19** | -4-*i*-propyl | -4-$OCH_3$ | 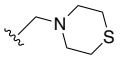 | -$CH_3$ | 1.28 | 420.62 | 4.99 | 15.71 |
| **20** | -2-Cl | Benzene | 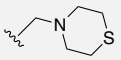 | -$CH_3$ | 2.24 | 433.01 | 5.46 | 6.48 |
| **21** | -4-*i*-propyl | -4-F | 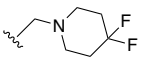 | -$CH_3$ | 3.19 | 426.53 | 2.1 | 49.85 |
| **22** | -4-$CH_2CH_3$ | -4-Cl | 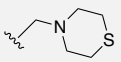 | -$CH_3$ | 2.93 | 411.00 | 5.46 | 6.48 |
| **23** | -2-F | -4-F | 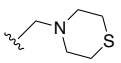 | -$CH_2CH_3$ | 3.69 | 398.52 | 4.8 | 6.48 |
| **ATQ** | | | | | $2.2 \times 10^{-4}$ | 366.84 | 5.8 | 54.37 |

[a] predicted; Comp. = Compound.; MW = molecular weight.

### 4.2.5 Pyrrole- and Pyrazole-based Compounds are Active Against the Early Stages of the Asexual Parasite Cycle and Prevent Schizont Rupture

To quantitatively assess the susceptibility of the distinct stages of *Pf*NF54 intra-erythrocytic development, we designed an *in vitro* stage-specific assay. For this experiment compounds **16** and **19** were chosen as representative of their pyrazole and pyrrole series, respectively. Highly synchronized parasites cultures (44 hours ABS cycle) were exposed to three concentrations (20 μM, 2 μM and 0.2 μM) of the test compounds during the early ring, late

ring, trophozoite, and schizont stages (Figure 4.5A). To validate the stage-specificity of activity, cultures were also exposed in parallel to test compounds for the standard 72 hours. We benchmarked the assay against the anti-malarial drug pyrimethamine due to its known stage-specific susceptibility profile, with peak activity on trophozoite and schizont stages.[18] After the time of exposure, cultures were continued to allow parasites to further develop in the absence of compounds, extending through to invasion of new RBCs and development until the trophozoite stage. The total assay duration was 77 h. Parasites were stained with SYBR green I and MitoTracker™ Orange CMTMRos and quantified by flow cytometry. Giemsa stains corresponding to the different developmental stages at the different periods of exposure were assessed by light microscopy to evaluate any phenotypical effect to the parasites.

As reported in Figure 4.5B, the pyrazole compound **19** displayed peak activity during the ring and trophozoite stages at both 20 (*Pf* survival < 10%) and 2 μM (*Pf* survival < 50%), and activity showed at least 2-fold decrease when only schizonts were exposed. Survival values at the peak activities were similar to the 72 hours exposure, suggesting that this compound might have good onset of action.

Similarly, the pyrrole derivative **16** was less active against schizonts stages at 2 μM (*Pf* survival = 68%) but showed peak activity against trophozoite stages (*Pf* survival = 11%) which was closer to the 72 hours exposure (*Pf* survival = 2.8%). Intermediate growth inhibition was seen at both early and late rings stages with *Pf* survival < 45% at 2 μM. Contrary to **19**, at a concentration of 20 μM, **16** displayed almost complete killing activity at all parasites intra-erythrocytic stages. This could be explained by the fact that the dose-response curve (Figure 4.5C) of **19** is steeper at higher concentrations than the dose-response curve of compound **16**. Finally, as expected, both compounds are inactive at a concentration of 0.2 μM.

These data suggest that pyrazole- and pyrrole- based compounds start to block the parasite growth already from early stages of the parasites, with peak activity on trophozoite stages. Such mode of action behavior is not common in antimalarial compounds, which are more selective for late stages of the asexual cycle.[19,20]

Through light microscopy we could assess the effect of compounds exposure (2 μM) to the cell structure of the parasites. As showed in Figure 4.5D, exposure of late rings or trophozoites, or continuous exposure to compound **16** lead to amorphous schizonts, which arrested their growth until cell death. Whereas exposure to early rings, slowed the parasite growth and merozoites egress occurred later than 44 hours. Similarly, exposure of later rings and trophozoites to **19** led to amorphous and compromised schizonts. However, continuous exposure to the compound or early rings exposure arrested the parasite growth to late ring and trophozoite stages, respectively. Interestingly, while schizonts exposures to **16** does not display any phenotypic effect, exposure to **19** can still arrest schizonts growth and merozoites egress of some parasites.

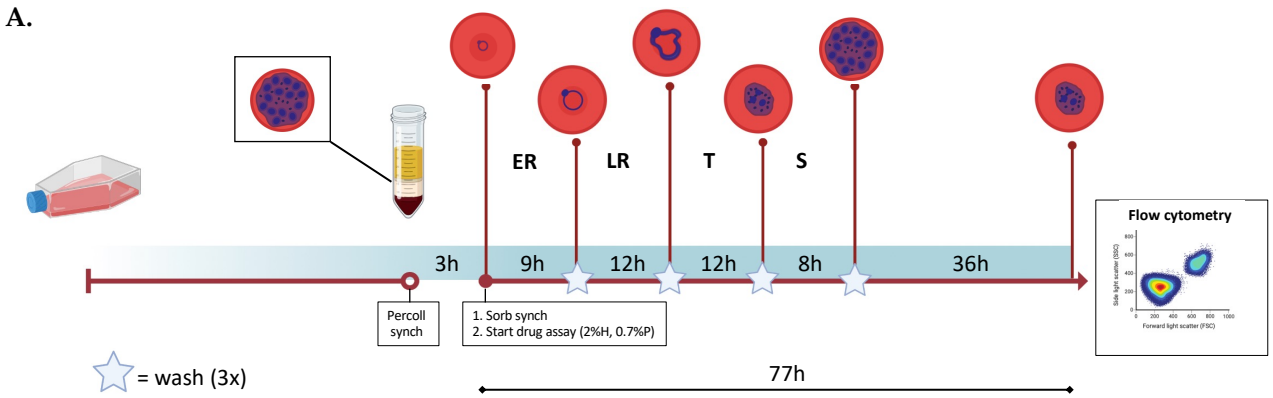
A.
ER
LR
T
S
3h
9h
12h
12h
8h
36h
Percoll synch
1. Sorb synch
2. Start drug assay (2%H, 0.7%P)
= wash (3x)
77h
Flow cytometry

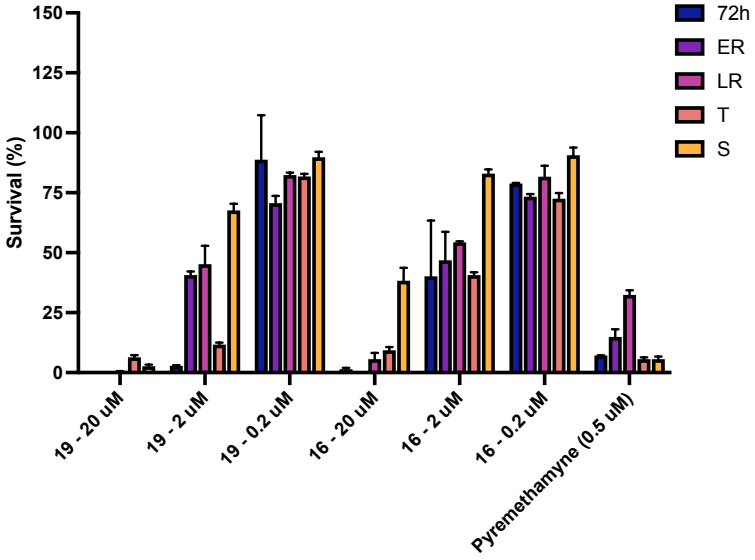
B.
Survival (%)
150
125
100
75
50
25
0
72h
ER
LR
T
S
19 - 20 uM
19 - 2 uM
19 - 0.2 uM
16 - 20 uM
16 - 2 uM
16 - 0.2 uM
Pyremethamyne (0.5 uM)

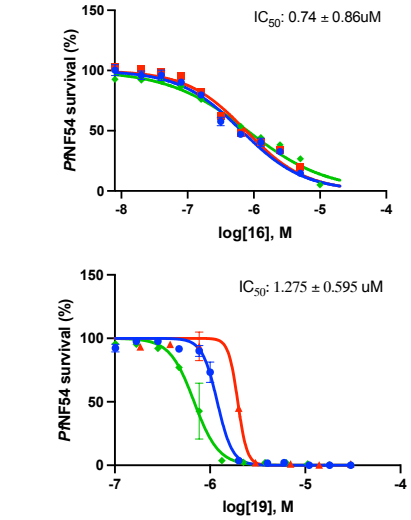
C.
IC50: 0.74 ± 0.86uM
PfNF54 survival (%)
log[16], M
IC50: 1.275 ± 0.595 uM
PfNF54 survival (%)
log[19], M

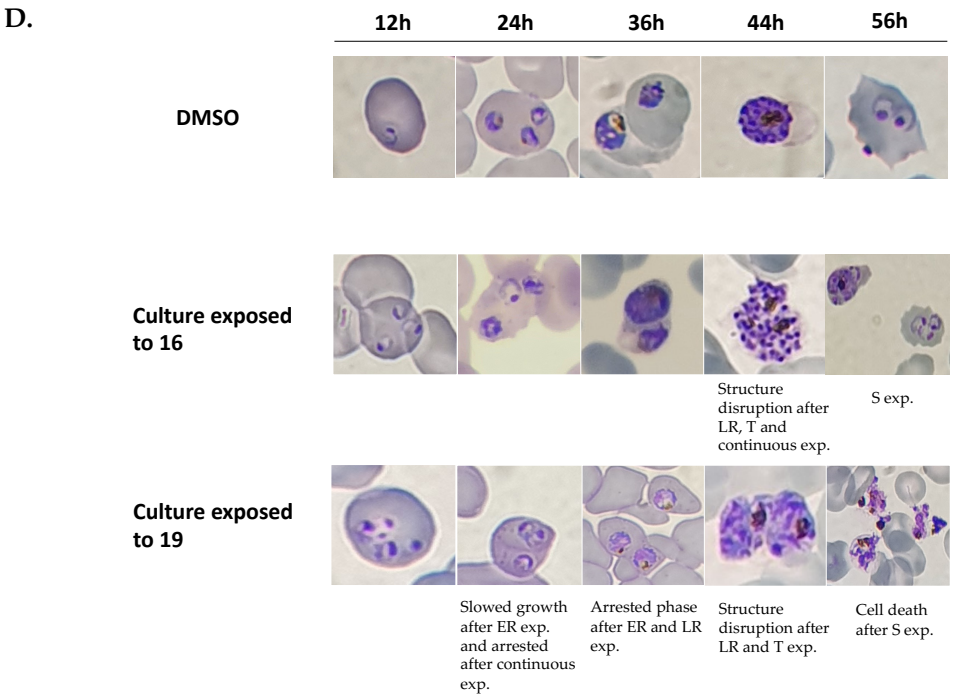
D.
12h
24h
36h
44h
56h
DMSO
Culture exposed to 16
Structure disruption after LR, T and continuous exp.
S exp.
Culture exposed to 19
Slowed growth after ER exp. and arrested after continuous exp.
Arrested phase after ER and LR exp.
Structure disruption after LR and T exp.
Cell death after S exp.

**Figure 4.5**. ABS-specificity assay of compounds **16** and **19**. **A)** Experimental design for the ABS specificity assay. Drug susceptibility of highly synchronized *P. falciparum* parasites was determined with flow cytometry at 77 hours after the first exposure. Parasites were exposed as early rings (ER) (9 hours), late rings (LR) (12 hours), trophozoites (T) (12 hours), schizonts (S) (8 hours) for 72 hours. Compounds were washed out three times after each exposure. **B)** Stage-specificity activity of **16**, **19** and Pyrimethamine (reference compound). Bar plots indicate the survival (%) of parasites when they were exposed only during the ER, LR, T, S stages or over the course of 72 hours. Error bars show the standard error of the mean based on at least three independent repeats. **C)** Dose response curves of **16** and **19**. The difference in steepness between the curves reflected the data of the assay at different concentrations of the two compounds. **D)** Comparison of the effects to the parasite cell morphologies between compound treated (**16** and **19**) and control parasites (DMSO treated). Both compounds slowed parasite growth and induced a visible schizonts structure damage after LR (**16**) or T exposure (**16** and **19**). Compounds **16** arrested parasites growth when applied on ER and LR stages.

### 4.2.6 The pyrazole 3 is the Only Hit Active in Indirect SMFA (iSMFA) but Does not Block Gametes Formation

Transmission-blocking activity of hit compounds was first tested in iSMFA to identify or validate compounds active against mature gametocytes. In this assay, 14-16 days old gametocytes were exposed to hit compounds (2 μM) for 48 hours and then compounds were washed out before feeding. The potent gametocytocidal drug methylene blue (MB) was used as a reference compound for this assay.

Analysis of *Anopheles gambiae* midguts 7 days post-infectious blood meal (pIBM) revealed a dramatic reduction in both terms of *Pf*NF54 oocysts intensity and prevalence in compound **3** relative to control (DMSO < 0.25%) (Figure 4.6), whereas all the other compounds did not display any significant difference. Even more relevant, a second set of experiment was performed at 24 hours of incubation with compound **3** and resulted again in a significant reduction of both oocyst intensity and prevalence. These data validate the activity of

compound **3** against late-stage gametocytes (Table 4.3) and the potential transmission-blocking use of this compound.

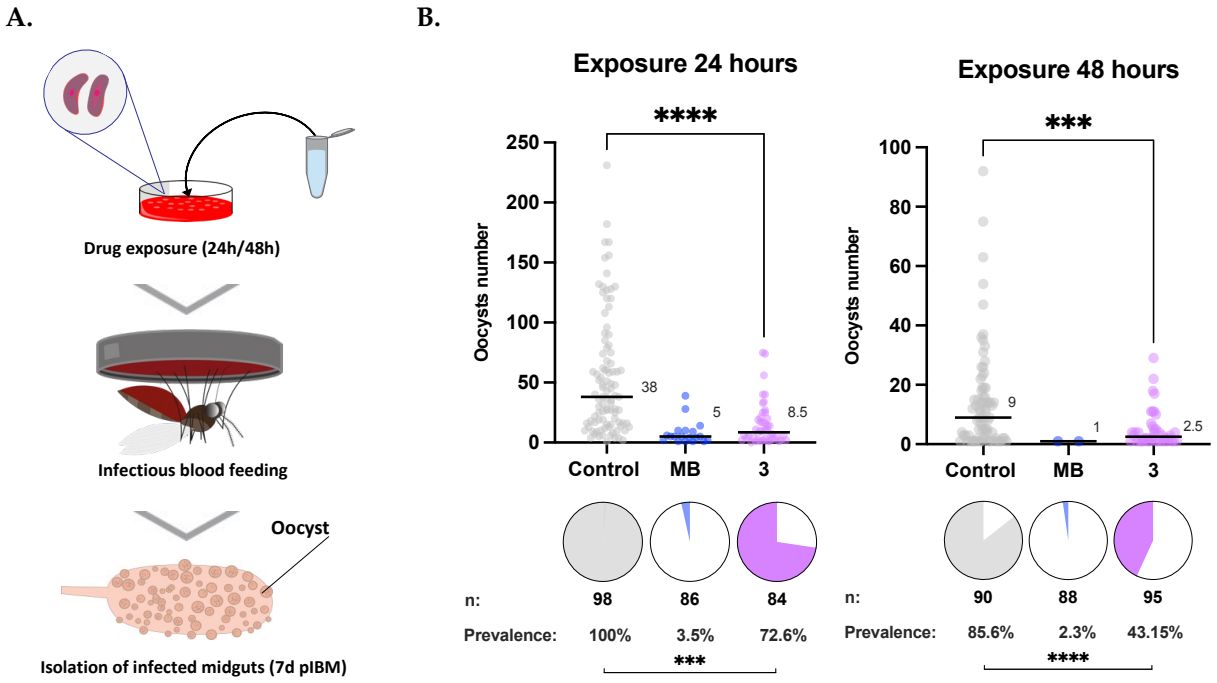


**Figure 4.6**. iSMFA using compound **3** with 24 and 48 hours of exposure. **A)** Experimental scheme. **B)** Both oocyst prevalence and oocyst intensity are significantly reduced after compound **3** exposure to mature gametocytes. Median lines and values are indicated, "n" indicates the number of independent samples. To isolate oocyst prevalence and oocyst intensity, midgut samples with zero oocysts have been excluded from intensity analysis. Statistical significance is indicated where relevant as follows: * = $p<0.05$, ** = $p<0.01$, *** = $p<0.001$, **** = $p<0.0001$. MB: methylene blue; Control: DMSO (< 0.25% v/v).

To further assess the transmission-blocking profile of compound **3**, the dual gamete formation assay (DGFA) at a "carry-over" format was performed at decreasing concentrations of the compound (20 – 0.1 μM). This assay assessed the ability of the test compound to block maturation of both male and female stage V gametocytes after 48 hours of exposure, providing a readout of functional viability.[21,22] Surprisingly, only modest activity was seen against male gametocytes at high concentrations (~42% inhibition at 20 μM) and no significant activity was seen in female gametocytes. Thus, no transmission-

blocking activity was observed, which was not predictive of the values observed *in vitro* gametocytocidal assays and in iSMFA.

### 4.2.7 Topical Exposure of Selected Hit Compounds and Analysis of Transmission-Blocking Activity

Anti-plasmodial activity in *An. gambiae* was assessed by topical application of hit compounds directly onto the dorsal thorax of the mosquitoes, which showed previously to be predictive of tarsal contact assays.[22,23] Compounds were dissolved in acetone (2mM), which is a volatile solvent that does not affect the mosquito fitness,[22] and then applied on anesthetized mosquitoes (0.5 μl, 1 nmol). At 7 days pIBM, the oocyst intensity and oocyst prevalence were measured as indication of the transmission-blocking activity of test compounds. Of the 12 compounds, **12** and **19** showed a significant decrease in terms of oocyst intensity (Figure 4.7B) in a total of three replicates. Although not statistically significant, a decreased in oocyst intensity was also obtained for compounds **16**, **18** and **20** (Figure 4.7B). These data suggest that sporogonic stages of parasites are also susceptible to pyrroles and pyrazoles surrogates. Except for **3**, **6** and **21**, compounds lipophilicities were close to the one of ATQ (Table 4.4), as well as tPSA were similar or lower. Therefore, we assumed a good compounds absorption in the mosquito cuticle, and overall compounds activities could correlate with their $IC_{50}$ against ABS. A preliminary SAR assessment confirmed that the copresence of aryl and cyclohexyl rings at positions $R^1$ and $R^2$, respectively, is favorable for higher activity in pyrazoles, whereas the matched compounds with two aryl rings showed smaller effects. Moreover, potency is increased with the trifluoromethyl group on the phenyl ring.

Metabolic liability at position $R^3$ could have lowered the performance of **16** and **18**, the two most potent compounds of their series in ABS, and that would need to be addressed in metabolic studies. For instance, the hydrolysis of carboxylic acid ester by carboxylesterase of compound **18** could form an inactive carboxylic derivative in the mosquito midgut.

Additionally, no reduction in oocyst intensity and prevalence was observed also for compound **3**, which showed to be active in iSMFA studies (Figure 4.6) but to minimally

affect the gamete development in DGFA. This indicates that its transmission-blocking potential in iSMFA is related to an impairment caused to gametocytes that blocks the development of the downstream sexual stages (i.e., zygote, ookinete and oocyst formations). To further probe the anti-sporogonic activity of these compounds, oocyst size at day 7 was evaluated compared to the control. No significant reduction in size was observed even for compounds **12** and **19** (Figure 4.7B), thus parasites could display susceptibility to these compounds at previous stages in mosquitoes.

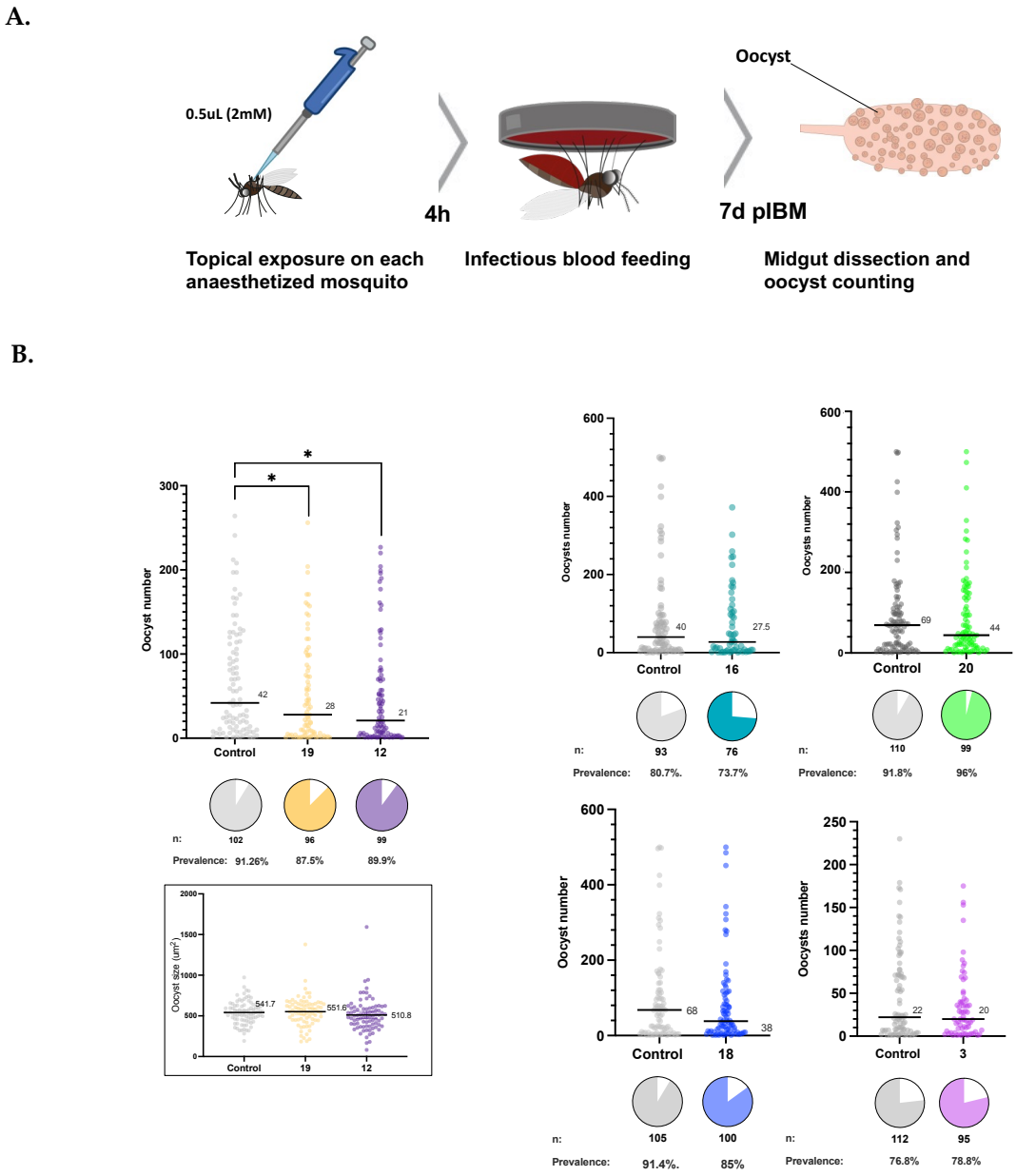


**Figure 4.7**. Topical exposure assay of compounds **3**, **12**, **16**, **18** – **20**. **A)** Schematic representation of the topical application on *An. Gambiae* mosquitoes. **B)** Compounds activity

indicated as oocyst intensity, oocyst prevalence and oocyst size (for compounds **19** and **12**). Median lines and values are indicated, "n" indicates the number of independent samples. Mean lines are indicated for oocyst size. To isolate oocyst prevalence and oocyst intensity, midgut samples with zero oocysts have been excluded from intensity analysis. Statistical significance is indicated where relevant as follows: * = $p<0.05$, ** = $p<0.01$, *** = $p<0.001$, **** = $p<0.0001$. Control: acetone or DMSO in acetone (0.5% v/v).

### 4.2.8 Resistant Parasites Selections

For target identification of our selected hits, we performed single-step selection studies to generate resistant parasite populations of *Pf*NF54 using sublethal concentrations of compound **16**, which was the most potent found in our ABS screening (Table 4.4). As illustrated in Figure 4.8A, drug pressure on parasites was performed at 9.6 μM (13 x $IC_{50}$) and 19.2 μM (26 x $IC_{50}$) over the period of three days and for each exposure the experiment was conducted on two separate replicates. After three days, all parasites were either dead or formed early gametocytes (phase I - III) due to the stressed induced by both drug concentrations and after 7 days all parasites were cleared. After 28 days resistant parasites emerged from bulk cultures and the resistance selections were repeated to increase the population of resistant parasites. Then, two weeks were enough to re-obtain resistant parasites in all flasks.

Bulk cultures showed for compound **16** a $IC_{50}$ shift of 2.5- to 7.4-fold compared to the parental line (Figure 4.8B). Interestingly, the same cultures showed also a marginal $IC_{50}$ shift (1.29- to 2-fold) for compound **19** (Figure 4.8B), suggesting that pyrazoles and pyrroles might have the same target. Alternatively, a multidrug resistance phenotype could have been generated from a copy number variation (CNV) in genes of transporter proteins as in the case of the multidrug resistance gene-1 (mdr1).[24–26] To address this, following-up studies are ongoing, and they include whole genome sequencing (WGS) of selected clones and cross-resistance of antimalarials with known target against selected clones.

**A.** **B.**

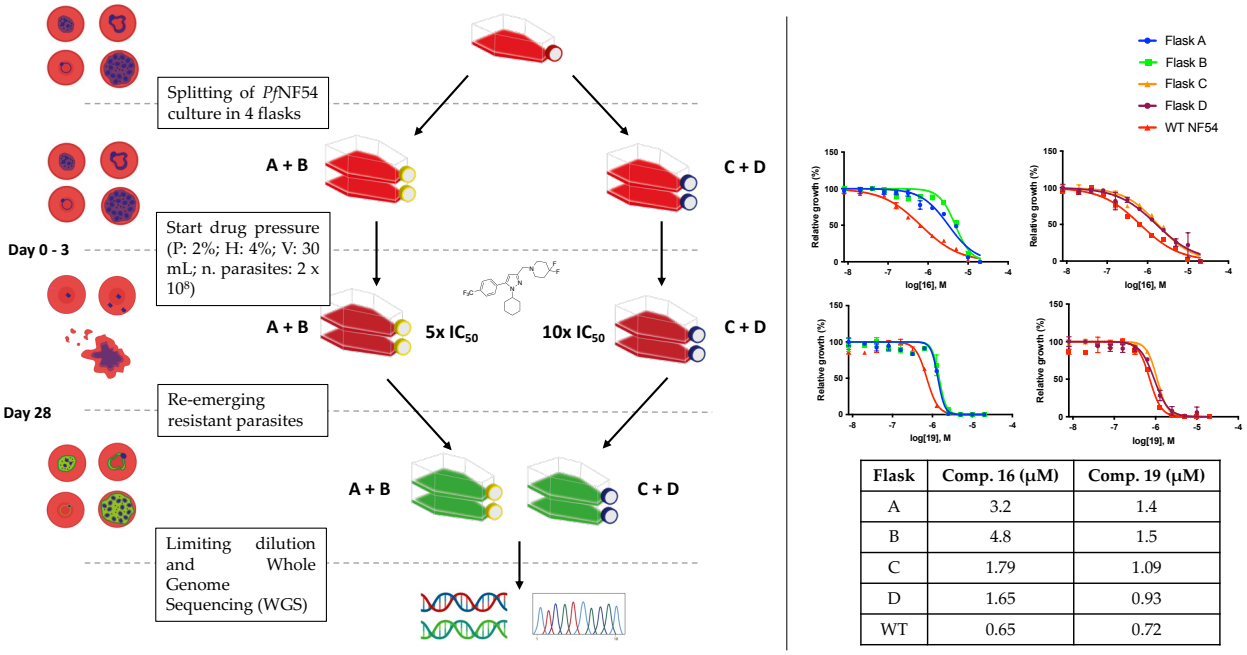


| Flask | Comp. 16 (μM) | Comp. 19 (μM) |
|---|---|---|
| A | 3.2 | 1.4 |
| B | 4.8 | 1.5 |
| C | 1.79 | 1.09 |
| D | 1.65 | 0.93 |
| WT | 0.65 | 0.72 |

**Figure 4.8**. Resistant parasite selections using compound **16**. **A)** Schematic representation of the resistant parasite single-step selections. **B)** $IC_{50}$ shifts of compounds **16** and **19** against bulk resistant cultures (flask A, B, C and D) compared to the parental line (flask WT).17

## 4.3 Discussion

Here, we sought to identify novel anti-malarial compounds to be potentially used in transmission-blocking interventions.

The pyrazole skeleton was originally present in **MMV843,** identified by an original HTS program to discover transmission-blocking compounds selective towards gametocytes.[5] We progressed the pyrazole series to conduct a hit-to-lead program around **MMV843** by elucidating the importance of substituents on the pyrazole core.

Systematic changes of functional groups at $R^1$, $R^2$, and $R^3$ were carried out to try to improve potency and physicochemical properties of compound **MMV843** (Table 4.2). We showed that selectivity towards gametocytes could be modulated with small drug-like modifications (e.g., $-CF_3$ increases anti-asexual activity) and the majority of them decrease the FC. Compound **1** was the most potent of the series with 2-fold increase in $IC_{50}$ ($IC_{50}$ = 0.219 μM) compared to **MMV843** and still selective towards gametocytes (FC = 8). Also

compounds **2-5** and **14** exhibited anti-gametocytocidal activity but were less selective towards gametocytes. Interestingly, positions $R^1$ and $R^2$ are amenable to aliphatic substitutions displaying favorable features in terms of lipophilicity, indexed by Log D, and of aqueous solubility, which considerably agreed with TCP-5 criteria thus improving the properties of **MMV843**. Despite the majority of substitutions at position $R^3$ led to a loss of activity against ABS and/or gametocytes, we showed that 4,4-difluoropiperidine could maintain the gametocytocidal activity of compounds as in the case of compound **14**. This provided the direct evidence that the azasilinane group in that position is not necessary for gametocytocidal activity. Compounds carrying the azasilinane group tend to be cytotoxic due to higher binding affinity to hERG channels,[13] therefore the discovery that it can be replaced by other groups is important for further chemical optimization studies. Generally, change in gametocytocidal activity of test compounds did not correlate with the activity against ABS. This might be the consequence of binding to two different targets between ABS and late-stage gametocytes, thus a potentially important hydrophobic interaction with the target is lost in gametocytes. Another explanation could come from structural features in mature gametocytes that are absent in ABS parasites that might affect compounds transport in the parasite.[27,28]

Overall, our initial SAR exploration has highlighted areas of the scaffold that can be subjected to modification to optimize activity and physicochemical properties and has shown that substantial improvements are possible. However, microsome assays of active compounds predict rapid clearance *in vivo*, which is not ideal for transmission-blocking interventions where compounds with long-lasting activity are a priority (TCP-5).[6,29] For a complete evaluation, ongoing research is determining missing data such as hERG bindings and metabolic stability for compound **MMV843**.

Further efforts will be required to identify compounds with improved potency and ADME properties that will support *in vivo* efficacy and eventual development. Following-up studies will focus on evaluating a new set of compounds carrying diverse substitutions and will also explore the importance of the pyrazole core by analyzing pyrroles-based

compounds. Furthermore, target identification and comprehensive mechanistic studies will be a priority to better understand the SAR needed for the development of a lead compound.

Following phenotypic screenings of our in-house library, we have also identified novel pyrazole- and pyrrole-based compounds active against early ABS and we have shown that their chemical scaffold could be potentially used in mosquito-targeted strategies to kill sporogonic stages of *P. falciparum*.

From our initial screening, we showed that of the three chemotypes, only pyrazoles and pyrroles were active *in vitro* against ABS of *P. falciparum*. Fluorobenzohydrazide derivatives were previously shown to inhibit tryptophan biosynthesis in *Mycobacterium tuberculosis*,[30] but here were inactive even at high concentrations (20 μM). Their inactivity is supported by the fact that *Plasmodium spp.* cannot biosynthesize amino acids *de novo* and need to acquire it from host cells or from blood plasma.[31,32] These results provided us the first insights for a preliminary SAR, which was similar between the two chemotypes indicating that they might share the same target. Generally, analogues bearing water-solubilizing such as -OH, -COOH, -CHO, and -NH, had loss inactivity. While, aryl rings at positions $R^1$ and/or $R^2$ favored lipophilic groups for higher activity, such as the -F, -Cl groups and -4-*i*-propyl groups. Consistently with previous results, pyrazoles allowed the presence of an aliphatic substituent at either position $R^1$ or $R^2$ with the trifluoromethyl analogue (**16**) showing the highest potency of these series against ABS ($IC_{50}$ = 0.74 μM). Although antiplasmodium activity was generally favored by substitution with EWGs, compound **19** carrying a 4-OMe group at $R^2$ produced the second highest activity of its series ($IC_{50}$ = 0.74 μM). The amine group at position $R^3$ in the majority of pyrrole and pyrazole surrogates, suggests the significance of the nitrogen basicity toward antiplasmodium activity. On the contrary, the most potent pyrrole of this series was **18** ($IC_{50}$ = 1.26 μM)**,** which carried a α-keto ester group at $R^3$. It is worth noting that the α-keto ester group presents itself as a unique and versatile functional group that differ from an amine group. The $sp^2$ hybridized carbons change the electron density and distortion in the structure and, the inductive effect of the adjacent ester enhances the electrophilicity of the compound that can readily react with nucleophiles or

can provide opportunities for chelation.[33] Therefore, we assumed that the activity of compound **18** might derive from an interaction with a different target.

By performing a stage-specificity assay, we demonstrated that pyrrole and pyrazole compounds target multiple stages in the asexual blood cycle leading to a membrane disruption of schizonts. Most notably, pyrazole **16** acts against rings and trophozoite stages in a similar manner, whereas pyrrole **19** showed peak of activity against trophozoites and > 50% activity on both early and late rings. The development of antimalarial compounds active on the early stages of the asexual blood cycle are highly desired since they prevent the formation of late trophozoites and schizonts, which are responsible for severe clinical pathology of the disease.[34] Moreover, only few antimalarial drugs are active on ring stages (e.g., artemisinins), while the majority of them only target trophozoites and/or schizonts due to their higher metabolic activity.[18,19] Targeting of ring stages is therefore attractive because could suggest that a new MOA is involved. A limitation of our stage-specificity assay need to be considered, which could affect the final readout of the assay. In this study mitochondrial dye (MitoTracker™ Orange CMTMRos) was used, which stains live parasites with functional mitochondria for obtaining reliable live parasite counts since it reflects metabolic activity and integrity. Thus, the readout of the assay could be compromised if our test compounds target mitochondria, as in the case of ATQ.[35]

Through iSMFA we established that selected compounds are not active against late-stage gametocytes except for compound **3**, which was previously identified as a potent anti-gametocytocidal compound ($IC_{50}$ = 0.526 μM) *in vitro* assays. However, we also showed in DGFA that mature gametocytes exposed to **3** are still able to transform into gametes suggesting that the compound exerts activity against gametocytes that permanently damage the parasites in such a manner that they are alive but cannot complete post-gametogenesis development. It is important to keep in mind that these outcomes were obtained from female mosquitoes that had only one blood meal, as opposed to the female mosquitoes in a mass drug administration (MDA) study who would have fed every two to three days, potentially increasing the blocking activity.[36,37]

Topical exposures on *An. gambiae* mosquitoes with compounds **19** and **12** reduced oocyst intensity, which implicates an upstream inhibition of plasmodium development in mosquitoes. Preliminary SAR seems to have a correlation with ABS activity but factors such as compounds absorption and metabolic liability could have affected compounds efficiency, rendering compounds **16** and **18** not significantly active. The inactivity of compound **3** validate the gametocyte-selective activity of this compound. These results are still far from what Paton et al.[11] reported with ATQ, which is considered the "gold-standard" compound to which aspire to since completely block oocyst intensity and prevalence at low doses. Moreover, while topical exposure assay is a good predictor of compounds activity in mosquitoes exposed tarsally,[22,23] they do not take into account the time of exposure to compounds, which in tarsal contact it affects the final results of the assay due to the positive correlation between exposure time and compound absorption. Despite this, these data tell us that mosquito stages of parasites are susceptible to the activity of pyrrole- and pyrazole-based compounds, which have a potential to be used in tarsal exposure assays, but most importantly to be developed as transmission-blockers. For unbiased analysis, dose-response studies are in plan and immunofluorescence assays will be considered to determine the stage of activity.[11,38] Furthermore, direct SMFA (compound/gametocytes mixture is immediately fed to female mosquitoes)[39,40] will be performed to validate these results. Further rounds of iterative SAR analysis will also help us to design more potent compounds with favorable absorption/elimination profile, which will be more achievable after target deconvolution studies and target-based assays.

Resistant selection assays with the most potent pyrazole **16** are underway. Resistant bulk cultures were tested against **16** and the representative pyrrole **19**, which uncovered an overlapping resistance behavior of the two compounds. This suggests that pyrroles and pyrazoles share the same target. However, the levels of shift of $IC_{50}$ values were still too low for progressing in WGS analysis and will be retested after selection of resistant clones by limiting dilution. For further validation analysis, the other hits will be also tested against resistant cultures, including compound **18** that might act through a different MOA as previously suggested. Common antimalarial drugs with known targets will also be tested

for cross-resistance studies to elucidate if it is the case of a multidrug resistance phenotype as seen in other works.[41,42]

In conclusion, our studies provide insights for the development of new antimalarial compounds to be potentially used in two different transmission-blocking strategies. **MMV843** analogues showed that the pyrazole chemical scaffold is amenable to a variety of structural modifications. This lays the groundwork for the progress of a hit-to-lead campaign toward equally potent and gametocyte-selective compounds with improved physicochemical characteristics in agreement with TCP-5 requirements.
Phenotypic screenings of our in-house library identified early-stage active pyrrole- and pyrazole-based compounds that showed potential activity against parasites also in *An. gambiae*, providing important starting points for the synthesis of more potent compounds that could completely block the sporogonic parasite development in the midgut.
For further progress in both approaches, target deconvolution and a better understanding of the MOA in gametocytes and asexual blood stages of *P. falciparum* are required.

## 4.4 Materials and Methods

### 4.4.1 Criteria of Selection of Compounds

#### 4.4.1.1 Selection of MMV158084 analogues

For hit validation and preliminary SAR studies, test compounds were chosen in order to investigate positions 1, 3 and 5, and based on the TCP-5 hit/early lead criteria. Compounds already tested and published previously from our group[13] were preferentially considered since cytotoxicity and physicochemical assays were already available in different settings.

#### 4.4.1.2 Selection of Compounds from In-House Library

Selection of test compounds from our in-house library was based on three parameters. Chemical diversity was considered in order to increase the likelihood of finding hits for

follow-up evaluation. tPSA < 90 Å$^2$ and logP > 2 were used as set of parameters to favor the discovery of hits with satisfactory absorption through the cuticle of the mosquito.

### 4.4.2 Chemistry

All hit compounds from screening were synthesized for further biological assays.

All chemicals used were obtained from commercial sources (Merck, Acros, Syngene, Enamine) and were used as supplied without further purification. For chromatographic purifications, Merck silica gel 60 (230-400 mesh) and, when specified, Merck aluminum oxide (activity II-III, according to Brockmann) were utilized with the specified solvents. Thin layer chromatography (TLC) plates of silica gel 60 (F 254) and aluminum oxide (F 254) were acquired by Merck and allowed the monitoring of reactions and column purifications of compounds by using UV light (254 and 365 nm) and/or staining with the appropriate reagent. $^{13}$C NMR and $^{1}$H NMR spectra were recorded on a Bruker Avance III NMR 400 and to tetramethylsilane (TMS) was used as a reference compound. Chemical shifts (δ) are given in ppm downfield, coupling constants, J, are recorded in hertz (Hz) and signal multiplicities reported as singlet (s), doublet (d), triplet (t), quadruplet (q) and multiplet (m). IUPAC names of compounds and chemical structures were generated by ChemDraw Professional 16.0. LodD and Solubility values were predicted using ACD/Labs software.

Compound MMV843 was already available for use in testing assays.

Compounds **1-14** and **16** were synthesized as reported in our recent work[13] (Scheme 4.1). First, lithium salts (**26a-c**) were produced through the reaction of the appropriate ketone (**24a-c**) with diethyloxalate (**25**) in the presence of lithium bis(trimethylsilyl)-amide. Next, the reaction between the substituted hydrazines (**27a-e**) and lithium salts (**26a-c**) gave the 1,3,5 substituted pyrazoles (**28a-h**). The ethyl ester function of pyrazoles (**28a-h**) was first reduced to primary alcohol (**29a-h**) by using lithium alumine hidride ($LiAlH_4$) and then oxidized to give the corresponding pyrazole- 3-carbaldehydes (**30a-h**). Finally, in the presence of the reductive agent $NaBH(CH_3COO)_3$, **30a-h** underwent reductive amination with the suitable amine to get the required final compounds **1-14** and **16**. Compound **15** was

obtained following hydrolysis with NaOH of **31** and then coupling reaction with the appropriate amine using dicyclohexylcarbodiimide (DCC) and 4-dimethylaminopyridine (DMAP). as a coupling reagents.

## Scheme 4.1.

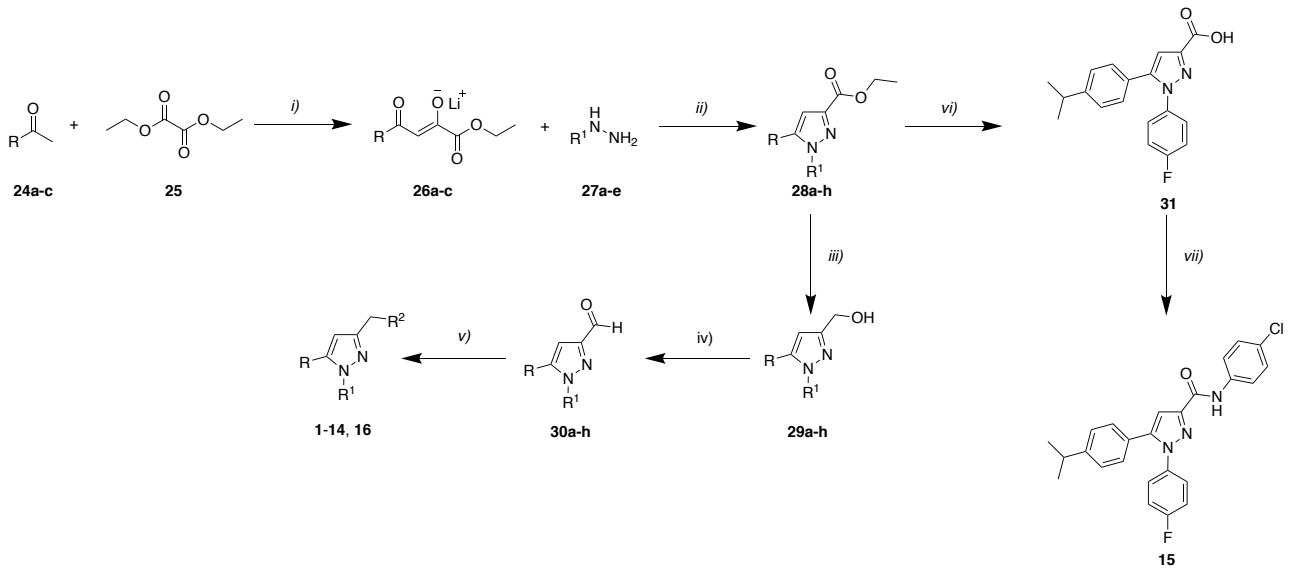


**Reagents and conditions**: i) $LiN(Si(CH_3)_3)_2$, THF, -78 °C and then room temperature, 24 h, yield: 80-83%; ii) EtOH, 90 °C, 5h, yield: 27.2-85%; iii) $LiAlH_4$, THF, 0 °C and then room temperature, 3h, yield: 63-91%; iv) Dess-Martin periodinane, DCM, room temperature, 30 min, yield: 59-86%; v) Amine, $CH_3COOH$, $NaBH(CH_3COO)_3$, DCE, room temperature, 2h, yield: 38-86%; vi); NaOH (1N), EtOH, reflux, 2h, yield: 90%; vii) *p*-chloroaniline, DCC, DMAP, DCM, rt, 3h, yield: 40%.

The synthesis of compound **17** (Scheme 4.2) was carried out as previously described.[13] Briefly, 4-isopropylaniline (**32**) was first transformed into the diazonium salt using HCl and $NaNO_2$ before being treated with ethyl 2-chloroacetoacetate (**33**) to get the corresponding hydrazone (**34**). **34** was converted into the ethyl ester pyrazole derivative (**36**) by reaction with morpholine enamine (**35**), synthesized beforehand from a reaction between 4'-fluoropropiophenone (**39**) and morpholine (**40**). As described above, a round of reduction

and oxidation gave the corresponding pyrazole-3-carbaldehyde (**38**), which was finally reacted with tiomorpholine to give the final product **17** via reductive amination.

## Scheme 4.2.

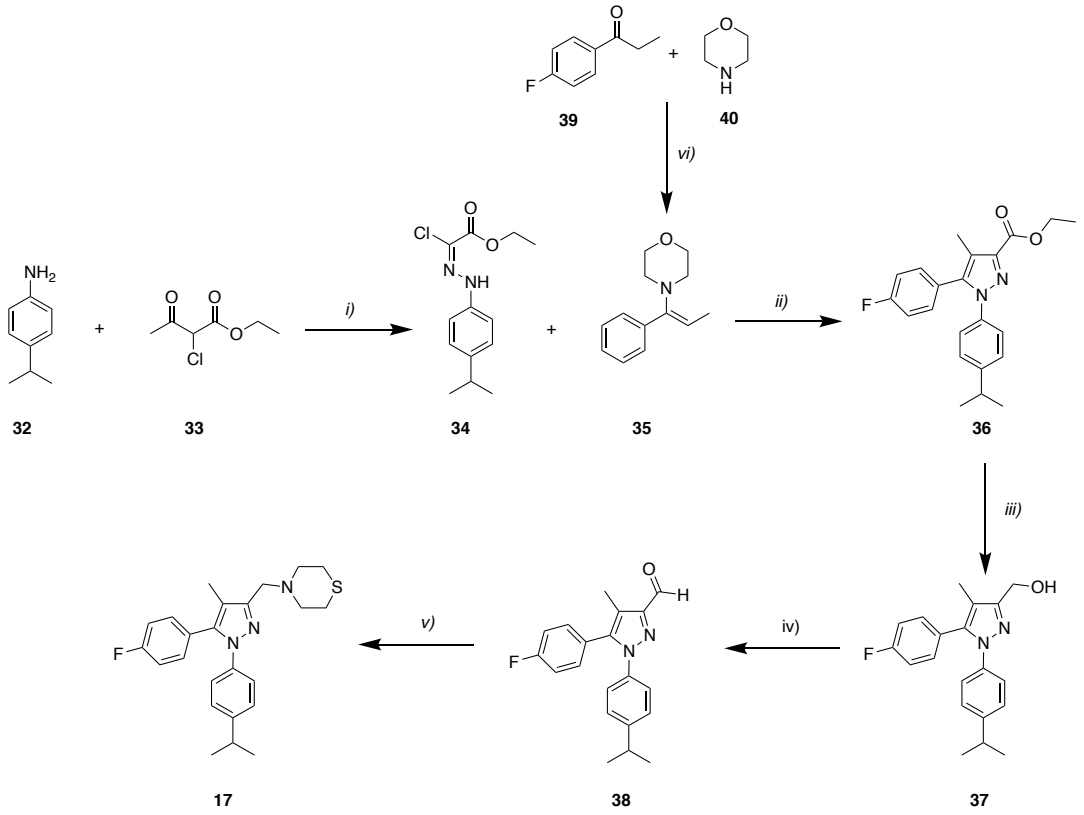


Reagents and conditions: i) 37% HCl, $NaNO_2$, AcONa, $H_2O$, EtOH, 0 °C and then room temperature, 22 h, yield: 80%; ii) DIPEA, EtOH, room temperature, 18h, yield: 30%; iii) $LiAlH_4$, THF, 0 °C and then room temperature, 3h, yield: 50%; iv) Dess-Martin periodinane, DCM, room temperature, 30 min, yield: 75%; v) $C_4H_9NS$, $CH_3COOH$, $NaBH(CH_3COO)_3$, DCE, room temperature, 2h, yield: 58%; vi) MgSO4, $TiCl_4$, DIPEA, toluene, room temperature and then 60 °C, 18 h, yield: 80%.

The synthesis of pyrroles **18-23** was carried out as previously reported[14–16,47] (Scheme 4.3). Briefly, the 1,4-diketones (**43a-g**) were obtained through a Stetter reaction between methyl vinyl ketone (**42**) and the suitable benzaldehyde (**41a-g**). Then, by cyclization of **43a-g** in the presence of the appropriate amine, the expected 1,5- diarylpyrroles (**44a-j**) were obtained. Compounds **19 - 22** were synthesized by reacting compounds **44a-j** with formaldehyde and

the suitable amine under Mannich reaction conditions. Compound **18** was obtained through a regioselective reaction with the appropriate pyrrole with ethoxalyl chloride and $TiCl_4$.

## Scheme 4.3.

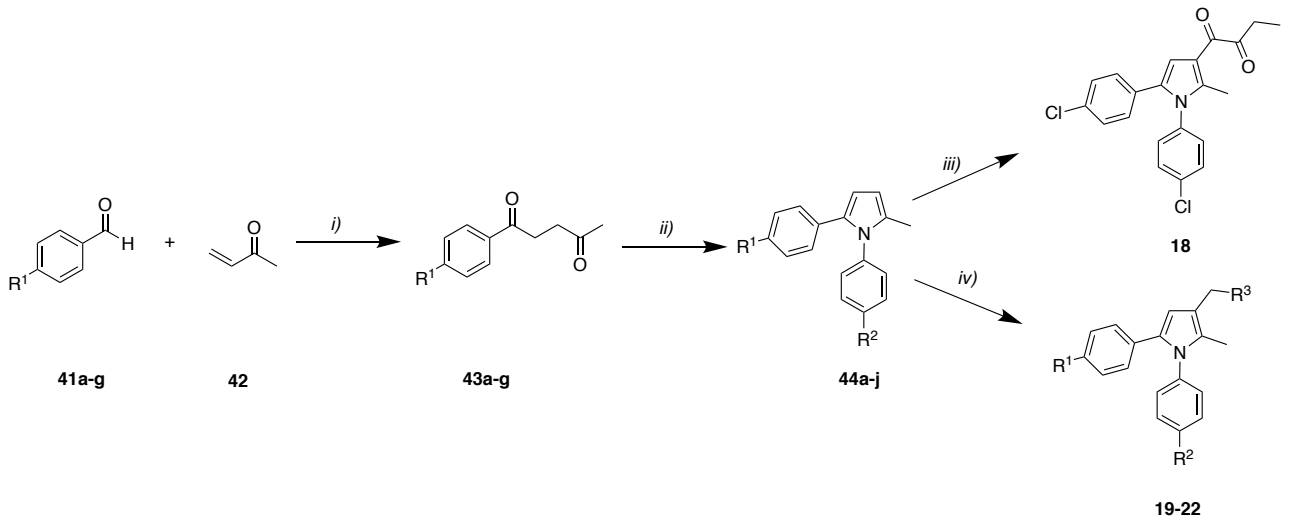


Reagents and conditions: i) 3-ethyl-5-(2-hydroxyethyl)-4-methylthiazolium bromide, TEA, 75°C, 5h, yield: 60-80%; ii) amine, *p*-toluensulfonic acid, EtOH, reflux, 5h, yield: 50-78%; *iii*) morpholine, $CH_3CN$, HCHO, $CH_3COOH$, room temperature, 1 h, yield: 40%; iv) $CH_3CH_2OCOCOCl$, $TiCl_4$, $CH_2Cl_2$, room temperature, 4h, yield: 39-62%.

The synthesis of compound **23** was carried out as reported in scheme 4.4. Following a Stetter reaction between ethyl vinyl ketone (**46**) and the suitable 2-fluorobenzaldehyde (**45**), the 1,4-diketone (**47**) was obtained. The latter was cyclized into the pyrrole **53** as described above and went into a Mannich reaction to give compound **23**.

## Scheme 4.4.

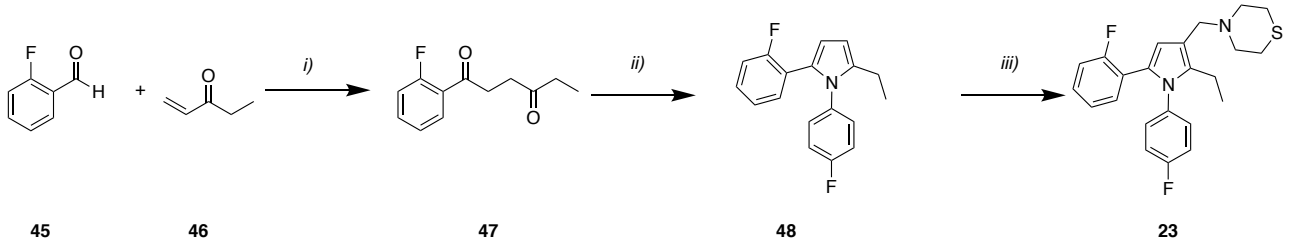

Reagents and conditions: i) 3-ethyl-5-(2-hydroxyethyl)-4-methylthiazolium bromide, TEA, 75°C, 5h, yield: 70%; ii) amine, *p*-toluensulfonic acid, EtOH, reflux, 5h; , yield: 50%; iii) tiomorpholine, $CH_3CN$, HCHO, $CH_3COOH$, room temperature, 1 h, yield: 37%.

#### 4.4.2.1 General procedure for the preparation of lithium salts 26a-c.

To a solution of lithium bis(trimethylsilyl)amide (12.3 mmol) in 30 ml of anhydrous THF, cooled down to -78 °C, a solution of the appropriate acetophenone **24a-c** in 3 ml of anhydrous THF was added dropwise and the mixture was mixt for at least 1 hour. Diethyl oxalate was then added over 5 minutes to form a dark solution, which was brought to room temperature over 4 hours. After 18 hours, THF was dried out *in vacuum* and lithium salts **26a-c** were purified (60-80% yield) after two steps of filtration and washing with diethyl ether.

*Lithium (Z)-1-ethoxy-4-(4-isopropylphenyl)-1,4-dioxobut-2-en-2-olate* (**26a**). Physicochemical, spectroscopic, and analytical data are consistent with those reported in literature.[13]

*Lithium (Z)-1-ethoxy-1,4-dioxo-4-(4-(trifluoromethyl)phenyl)but-2-en-2-olate* (**26b**). Physicochemical, spectroscopic, and analytical data are consistent with those reported in literature.[13]

*Lithium (Z)-4-cyclohexyl-1-ethoxy-1,4-dioxobut-2-en-2-olate* (**26c**). Yellow solid, 83% yield. $^1$H NMR (400 MHz, DMSO) δ ppm= 5.68 (s, 1H), 4.09 (q, *J* = 7.1 Hz, 2H), 2.51 (p, *J* = 1.8 Hz, 2H), 2.05 (s, 1H), 1.78 – 1.57 (m, 5H), 1.37 – 1.09 (m, 6H).

#### 4.4.2.2 General procedure for the preparation of carboxylates 28a-h

The appropriate hydrazine **27a-e** (2.5-5 mmol) was added to a solution of the suitable lithium salt **26a-c** (2.5-5mmol) in ethanol (20mL). The reaction mixture was heated to 90 °C for at least 5 h and monitored using TLC. As the reaction was completed, the mixture was cooled down to room temperature and the solvent removed under *vacuum*. After purification using column chromatography (cyclohexane/ethyl acetate 2/1 v/v), the crude product produced the carboxylates **28a–h** with decent yields (40–75%).

*ethyl 1-cyclobutyl-5-(4-(trifluoromethyl)phenyl)-1H-pyrazole-3-carboxylate* (**28a**). Yellow oil, 65% yield. $^1$H NMR (400 MHz, $CDCl_3$) δ ppm= 7.67 (d, *J* = 8.0 Hz, 2H), 7.41 (d, *J* = 8.0 Hz, 2H), 6.77 (s, 1H), 4.73-4.64 (m, 1H), 4.36 (q, *J* = 7.1 Hz, 2H), 2.91 – 2.71 (m, 2H), 2.37 – 2.20 (m, 2H), 1.92 – 1.78 (m, 1H), 1.68-1.58 (m, 1H), 1.38-1.32 (m, 3H).

*ethyl 1-cyclohexyl-5-(4-(trifluoromethyl)phenyl)-1H-pyrazole-3-carboxylate* (**28b**). Physicochemical, spectroscopic, and analytical data are consistent with those reported in literature.[13]

*ethyl 5-cyclohexyl-1-(4-fluorophenyl)-1H-pyrazole-3-carboxylate* (**33c**). Yellow solid, 70% yield. $^1$H NMR (400 MHz, $CDCl_3$) δ ppm= 7.37 – 7.27 (m, 2H), 7.18 – 7.05 (m, 2H), 6.67 (s, 1H), 4.34 (q, *J* = 7.1 Hz, 2H), 2.47 (tt, *J* = 11.8, 3.4 Hz, 1H), 1.82 – 1.48 (m, 5H), 1.42 – 1.06 (m, 8H).

*ethyl 1-(4-fluorophenyl)-5-(4-(trifluoromethyl)phenyl)-1H-pyrazole-3-carboxylate* (**28d**). Physicochemical, spectroscopic, and analytical data are consistent with those reported in literature.[13]

*ethyl 1-(2-hydroxy-2-methylpropyl)-5-(4-isopropylphenyl)-1H-pyrazole-3-carboxylate* (**28e**). Yellow oil, 27.2%. $^1$H NMR (400 MHz, $CDCl_3$): δ ppm= 7.26 (d, J= 8.3 Hz 2H), 7.21 (d, J = 8.3 Hz 2H), 6.76 (s, 1H), 4.33 (q, J = 7.1 Hz 2H), 4.06 (s, 2H), 2.93-2.88 (m, 1H), 1.36-1.22 (m, 10H), 0.98 (s, 6H).

*ethyl 1-cyclohexyl-5-(4-isopropylphenyl)-1H-pyrazole-3-carboxylate* (**28f**). Physicochemical, spectroscopic, and analytical data are consistent with those reported in literature.[13]

*ethyl 1-(4-fluorophenyl)-5-(4-isopropylphenyl)-1H-pyrazole-3-carboxylate* (**28g**). Physicochemical, spectroscopic, and analytical data are consistent with those reported in literature.[13]

*ethyl 1-isopropyl-5-(4-isopropylphenyl)-1H-pyrazole-3-carboxylate* (**28h**). Physicochemical, spectroscopic, and analytical data are consistent with those reported in literature.[13]

#### 4.4.2.3 General procedure for the preparation of alcohols 29a-h and 37

To a solution of the appropriate carboxylate (**28a-h** or **36**) (0.35-1 mmol) in dry THF, 0.4-1.1 ml of $LiAlH_4$ (1M in THF) were added dropwise at 0 °C under a nitrogen flow. Then, the reaction was left stirring at room temperature for 1-2 hours. When the reaction was

completed, the mixture was cooled down to 0 °C and quenched with ethyl acetate (0.15-0.30 ml), water (0.05-0.13 ml) and NaOH 2N (0.05-0.17 ml). The precipitate was removed after 30 minutes of agitation, and the filtrate was then dried over $Na_2SO_4$ and concentrated *in vacuo*. Alcohols **29a-h** and **37** were obtained in good yields (70-94%) when the crude product was purified using column chromatography (cyclohexane/ethyl acetate 1/1 (v/v)).

*(1-cyclobutyl-5-(4-(trifluoromethyl)phenyl)-1H-pyrazol-3-yl)methanol* (**29a**). White solid, 65%. $^1$H NMR (400 MHz, $CDCl_3$) δ ppm= 7.65 (d, *J* = 8.1 Hz, 2H), 7.39 (d, *J* = 8.1 Hz, 2H), 6.24 (s, 1H), 4.71 – 4.56 (m, 3H), 2.77-2.66 (m, 2H), 2.28-2.21 (m, 2H), 2.07 (d, *J* = 73.7 Hz, 1H), 1.89 – 1.75 (m, 1H), 1.72-1.60 (m, 1H).

*(1-cyclohexyl-5-(4-(trifluoromethyl)phenyl)-1H-pyrazol-3-yl)methanol* (**29b**). Physicochemical, spectroscopic, and analytical data are consistent with those reported in literature.[13]

*(5-cyclohexyl-1-(4-fluorophenyl)-1H-pyrazol-3-yl)methanol* (**29c**). White solid, 70% yield. $^1$H NMR (400 MHz, $CDCl_3$) δ ppm= 10.01 (s, 1H), 7.35 (d, *J* = 8.2 Hz, 2H), 7.29 (d, *J* = 8.2 Hz, 2H), 6.82 (s, 1H), 4.44 (s, 1H), 4.15 (s, 2H), 2.98 (hept, *J* = 6.9 Hz, 1H), 1.30 (d, *J* = 6.9 Hz, 6H), 1.09 (s, 6H).

*(1-(4-fluorophenyl)-5-(4-(trifluoromethyl)phenyl)-1H-pyrazol-3-yl)methanol* (**29d**). Physicochemical, spectroscopic, and analytical data are consistent with those reported in literature.[13]

*1-(3-(hydroxymethyl)-5-(4-isopropylphenyl)-1H-pyrazol-1-yl)-2-methylpropan-2-ol* (**29e**). White solid, 66.5%. $^1$H NMR (400 MHz, $CDCl_3$): δ ppm= 7.32 (d, J = 8.1 Hz 2H), 7.27 (d, J = 8.0 Hz 2H), 6.31 (s, 1H), 4.73 (s, 2H), 4.02 (s, 2H), 3.00-2.95 (m, 1H), 1.93 (m, 2H), 1.31 (d, J = 4.0 6H), 1.05 (s, 6H).

*(1-cyclohexyl-5-(4-isopropylphenyl)-1H-pyrazol-3-yl)methanol* (**29f**). Physicochemical, spectroscopic, and analytical data are consistent with those reported in literature.[13]

*(1-(4-fluorophenyl)-5-(4-isopropylphenyl)-1H-pyrazol-3-yl)methanol* (**29g**). Physicochemical, spectroscopic, and analytical data are consistent with those reported in literature.[13]

*(1-isopropyl-5-(4-isopropylphenyl)-1H-pyrazol-3-yl)methanol* (**29h).** Physicochemical, spectroscopic, and analytical data are consistent with those reported in literature.[13]

*(5-(4-fluorophenyl)-1-(4-isopropylphenyl)-4-methyl-1H-pyrazol-3-yl)methanol* (**37**). Physicochemical, spectroscopic, and analytical data are consistent with those reported in literature.[13]

#### 4.4.2.4 General procedure for the preparation of pyrazole- 3-carbaldehydes 30a-h and 38

Under nitrogen flow, Dess-Martin periodinane (0.3-1 mmol) was added to a solution of the appropriate alcohol (**29a-h** or **37**) (0.25-0.81 mmol) in 5-10 ml of anhydrous DCM and let it react for 1h at room temperature. The reaction was then quenched with $NaHCO_3$ (4.1-13.3 ml) and a saturated solution of $Na_2S_2O_3$ (4.1-13.3 ml), and stirred for 30 min. Next, extraction of the mixture was carried out in DCM and the organic phase was washed with a saturated solution of $NaHCO_3$ and brine, and dried over $Na_2SO_4$. Purification by column chromatography (cyclohexane/ethyl acetate 5/1 (v/v)) gave carbaldehydes **30a-h** and **38** in good yields (44-95%).

*1-cyclobutyl-5-(4-(trifluoromethyl)phenyl)-1H-pyrazole-3-carbaldehyde* (**30a**). White solid, 79% yield. $^1$H NMR (400 MHz, $CDCl_3$) δ ppm= 9.97 (s, 1H), 7.57 (d, *J* = 8.2 Hz, 2H), 7.38 (d, *J* = 8.2 Hz, 2H), 6.75 (s, 1H), 4.78-4.69 (m, 1H), 2.82-2.71 (m, 2H), 2.37 – 2.25 (m, 2H), 1.94 – 1.84 (m, 1H), 1.79-1.67 (m, 1H).

*1-cyclohexyl-5-(4-(trifluoromethyl)phenyl)-1H-pyrazole-3-carbaldehyde* (**30b**). Physicochemical, spectroscopic, and analytical data are consistent with those reported in literature.[13]

*5-cyclohexyl-1-(4-fluorophenyl)-1H-pyrazole-3-carbaldehyde* (**30c**). White solid, 86% yield. $^1$H NMR (400 MHz, $CDCl_3$) δ ppm= 9.91 (s, 1H), 7.40 – 7.30 (m, 2H), 7.19 – 7.11 (m, 2H), 6.66 (s, 1H), 2-71-2.50 (m, 1H), 1.84 – 1.59 (m, 4H), 1.40 – 1.05 (m, 6H).

*1-(4-fluorophenyl)-5-(4-(trifluoromethyl)phenyl)-1H-pyrazole-3-carbaldehyde* (**30d**). Physicochemical, spectroscopic, and analytical data are consistent with those reported in literature.[13]

*1-(2-hydroxy-2-methylpropyl)-5-(4-isopropylphenyl)-1H-pyrazole-3-carbaldehyde* (**30e**). Colorless oil, 59%. $^1$H NMR (400 MHz, $CDCl_3$) δ ppm= 7.35 – 7.23 (m, 4H), 6.30 (s, 1H), 4.72 (s, 2H),

4.01 (s, 2H), 2.97 (hept, *J* = 6.9 Hz, 1H), 1.93 (s, 1H), 1.61 (s, 3H), 1.30 (d, *J* = 6.9 Hz, 6H), 1.04 (s, 6H).

*1-cyclohexyl-5-(4-isopropylphenyl)-1H-pyrazole-3-carbaldehyde* (**30f**). Physicochemical, spectroscopic, and analytical data are consistent with those reported in literature.[13]

*1-(4-fluorophenyl)-5-(4-isopropylphenyl)-1H-pyrazole-3-carbaldehyde* (**30g**). Physicochemical, spectroscopic, and analytical data are consistent with those reported in literature.[13]

*1-isopropyl-5-(4-isopropylphenyl)-1H-pyrazole-3-carbaldehyde* (**30h**). Physicochemical, spectroscopic, and analytical data are consistent with those reported in literature.[13]

*5-(4-fluorophenyl)-1-(4-isopropylphenyl)-4-methyl-1H-pyrazole-3-carbaldehyde* (**38**). Physicochemical, spectroscopic, and analytical data are consistent with those reported in literature.[13]

#### 4.4.2.5 General procedure for the preparation of final compounds 1-14, 16 and 17

To a solution of the appropriate carbaldehyde (**30a-h** and **28**) (0.1-0.72 mmol) in anhydrous DCE (5-13 ml) a drop of glacial acetic acid was added, and the mixture was stirred for 10 min. The suitable amine (0.1-0.72 mmol) was then added, followed by $NaBH(CH_3COO)_3$ (0.11-0.79 mmol) and the reaction mixture was stirred for 2 h. The mixture was then quenched with sat $NaHCO_3$ (5-13 ml) and extracted with DCM. The organic layers were dried over $Na_2SO_4$, concentrated *in vacuo* and purified by column chromatography (cyclohexane/ethyl acetate 1/1 (v/v)) to give compounds **1-14**, **16** and **17** in moderate-good yields (24-89%).

*1-((1-cyclobutyl-5-(4-(trifluoromethyl)phenyl)-1H-pyrazol-3-yl)methyl)-4,4-dimethyl-1,4-azasilinane* (**1**). White solid, 65% yield. $^1$H NMR (400 MHz, $CDCl_3$) δ ppm= 7.65 (d, *J* = 8.2 Hz, 2H), 7.43 (d, *J* = 8.2 Hz, 2H), 6.24 (s, 1H), 4.68-4.62 (m, 1H), 3.63 (s, 2H), 2.83 – 2.67 (m, 6H), 2.32 – 2.20 (m, 2H), 1.90 – 1.76 (m, 2H), 1.71-1.64 (m, 1H), 0.79 – 0.71 (m, 4H), 0.00 (s, 6H).$^{13}$C NMR (100 MHz, $CDCl_3$) δ ppm= 149.67, 142.11, 134.75, 130.44, 130.11, 129.14, 125.57, 106.33, 56.00, 52.72, 52.49, 30.66, 14.60, 13.73.

*1-((1-cyclohexyl-5-(4-(trifluoromethyl)phenyl)-1H-pyrazol-3-yl)methyl)-4,4-dimethyl-1,4 azasilinane* (**2**). Physicochemical, spectroscopic, and analytical data are consistent with those reported in literature.[13]

*1-((5-cyclohexyl-1-(4-fluorophenyl)-1H-pyrazol-3-yl)methyl)-4,4-dimethyl-1,4-azasilinane* (**3**). White solid, 55% yield. $^{1}$H NMR (400 MHz, $CDCl_3$) δ ppm= 7.69-7.63 (m, 2H), 7.61-7.53 (m, 2H), 6.47 (s, 1H), 3.79 (s, 2H), 2.83-2.55 (m, 4H), 1.92-1.70 (m, 6H), 1.41-1.29 (m, 5H), 0.85-0.79 (m, 4H), 0.00 (s, 6H). $^{13}$C NMR (100 MHz, $CDCl_3$) δ ppm= 162.52, 156.36, 151.68, 135.34, 124.60, 116.51, 109.38, 56.96, 51.73, 37.70, 31.68, 25.91, 25.14, 16.14, 6.76.

*1-((1-(4-fluorophenyl)-5-(4-(trifluoromethyl)phenyl)-1H-pyrazol-3-yl)methyl)-4,4-dimethyl-1,4-azasilinane* (**4**). Physicochemical, spectroscopic, and analytical data are consistent with those reported in literature.[13]

*1-(5-(4-isopropylphenyl)-3-((4-methoxypiperidin-1-yl)methyl)-1H-pyrazol-1-yl)-2-methylpropan-2-ol* (**5**). White solid, 65% yield. $^{1}$H NMR (400 MHz, $CDCl_3$) δ ppm= 7.36 – 7.24 (m, 4H), 6.26 (s, 1H), 5.33 (s, 1H), 4.01 (s, 2H), 3.59 (s, 2H), 3.33 (s, 3H), 3.24-3.17 (m, 1H), 2.96 (hept, *J* = 6.9 Hz, 1H), 2.88-2.80 (m, 2H), 2.24 (t, *J* = 10.0 Hz, 2H), 1.94-1.90 (m, 1H), 1.80 (s, 1H), 1.68 – 1.55 (m, 2H), 1.29 (d, *J* = 6.9 Hz, 6H), 1.01 (s, 6H). $^{13}$C NMR (100 MHz, $CDCl_3$) δ ppm= 149.11, 137.49, 134.31, 131.34, 128.07, 125.56, 123.74, 109.81, 77.92, 74.98, 55.94, 53.67, 36.16, 34.32, 34.30, 31.10, 29.70, 27.51, 23.93, 11.02.

*7-((1-cyclohexyl-5-(4-isopropylphenyl)-1H-pyrazol-3-yl)methyl)-2-oxa-7 azaspiro[3.5]nonane* (**6**). White solid, 41% yield. $^{1}$H NMR (400 MHz, $CDCl_3$): δ ppm= 7.32 – 7.29 (m, 4H), 6.18 (s, 1H), 4.43 (s, 4H), 4.15-4.09 (m, 1H), 3.57 (s, 2H), 2.99-2.97 (m, 1H), 2.45 (s, 4H), 2.07-2.02 (m, 2H), 1.92-1.83 (m, 8H), 1.68 (s,1H), 1.33 (d, J = 4.0 Hz 9H). $^{13}$C NMR (100 MHz, $CDCl_3$): δ ppm= 149.56, 149.21, 144.05, 133.34, 127.71, 126.73, 105.37, 79.48, 56.79, 53.07, 50.55, 39.49, 34.31, 31.47, 30.89, 25.83, 24.52, 23.93.

*7-((1-(4-fluorophenyl)-5-(4-isopropylphenyl)-1H-pyrazol-3-yl)methyl)-2-oxa-7-azaspiro[3.5]nonane* (**7**). White solid, 38% yield. $^{1}$H NMR (400 MHz, $CDCl_3$): δ ppm= 7.60 – 7.54 (m, 4H), 7.28 – 7.22 (m, 4H), 6.38 (t, *J* = 0.9 Hz, 1H), 4.64 (s, 4H), 3.74 – 3.70 (m, 2H), 2.90 – 2.75 (m, 5H), 1.64-1.47 (m, 4H), 1.25 (d, *J* = 6.7 Hz, 6H). $^{13}$C NMR (100 MHz, $CDCl_3$): δ ppm=

149.56, 149.21, 144.05, 133.34, 127.71, 126.73, 105.37, 79.48, 56.79, 53.07, 50.55, 39.49, 34.31, 31.47, 30.89, 25.83, 24.52, 23.93.

*4-((1-cyclohexyl-5-(4-(trifluoromethyl)phenyl)-1H-pyrazol-3-yl)methyl)morpholine* (**8**). Physicochemical, spectroscopic, and analytical data are consistent with those reported in literature. [13]

*4-((1-(4-fluorophenyl)-5-(4-(trifluoromethyl)phenyl)-1H-pyrazol-3-yl)methyl)morpholine* (**9**). Physicochemical, spectroscopic, and analytical data are consistent with those reported in literature.[13]

*4-((1-isopropyl-5-(4-isopropylphenyl)-1H-pyrazol-3-yl)methyl)morpholine* (**10**). Physicochemical, spectroscopic, and analytical data are consistent with those reported in literature.[13]

*tert-butyl 4-((1-(4-fluorophenyl)-5-(4-(trifluoromethyl)phenyl)-1H-pyrazol-3-yl)methyl)piperazine-1-carboxylate* (**11**). Physicochemical, spectroscopic, and analytical data are consistent with those reported in literature.[13]

*tert-butyl 4-((1-cyclohexyl-5-(4-(trifluoromethyl)phenyl)-1H-pyrazol-3-yl)methyl)piperazine-1-carboxylate* (**12**). Physicochemical, spectroscopic, and analytical data are consistent with those reported in literature.[13]

*1-((1-(4-fluorophenyl)-5-(4-(trifluoromethyl)phenyl)-1H-pyrazol-3-yl)methyl)-4-methoxypiperazine* (**13**). Physicochemical, spectroscopic, and analytical data are consistent with those reported in literature.[13]

*4,4-difluoro-1-((1-(4-fluorophenyl)-5-(4-isopropylphenyl)-1H-pyrazol-3-yl)methyl)piperidine* (**14**). White solid, 45 % yield. 1 H NMR (400 MHz, $CDCl_3$) δ ppm= 7.66 – 7.58 (m, 4H), 7.28 – 7.16 (m, 4H), 6.79 (s, 1H), 3.79 (s, 2H), 2.98 -2.95 (m, 4H), 2.90 – 2.78 (m, 1H), 2.26 - 2.15 (m, 4H), 1.25 (d, J = 6.7 Hz, 6H). 13 C NMR (101 MHz, $CDCl_3$) δ ppm= 163.09, 161.12, 149.73, 149.36, 143.96, 138.18, 138.15, 133.30, 128.57, 127.06, 124.98, 124.91, 121.35,
119.46, 117.56, 116.52, 116.34, 107.17, 53.04, 48.17, 48.13, 48.09, 34.31, 32.39, 32.20, 32.02, 23.93.

*1-((1-cyclohexyl-5-(4-(trifluoromethyl)phenyl)-1H-pyrazol-3-yl)methyl)-4,4-difluoropiperidine* (**16**). Colorless oil, 52% yield. 1 H NMR (400 MHz, $CDCl_3$) δ ppm= 7.65 (d, J = 8.1 Hz, 2H), 7.41 (d, J = 8.1 Hz, 2H), 6.16 (s, 1H), 3.97 - 3.89 (m,1H), 3.58 (s, 2H), 2.58 (t, J = 5.8 Hz, 4H), 2.04 – 1.88 (m, 6H), 1.86 – 1.72 (m, 4H), 1.26 – 1.10 (m, 3H). 13 C NMR (101 MHz, $CDCl_3$) δ

ppm= 142.06, 134.78, 130.58, 130.26, 129.24, 125.71, 122.63, 106.21, 57.98, 55.12, 49.88, 33.94, 33.31, 25.60, 25.01.

*4-((5-(4-fluorophenyl)-1-(4-isopropylphenyl)-4-methyl-1H-pyrazol-3-yl)methyl)thiomorpholine* (**17**). White solid, 58% yield. $^{1}$H NMR (400 MHz, $CDCl_3$) δ ppm= 7.26 – 7.03 (m, 8H), 3.66 (s, 2H), 2.87-2.72 (m, 8H), 2.07 (s, 3H), 0.87 (d, *J* = 8.2 Hz, 6H). $^{13}$C NMR (100 MHz, $CDCl_3$) δ ppm= 160.73, 151.62, 148.76, 144.88, 141.37, 131.12, 130.16, 129.55, 126.88, 119.74, 116.29.

#### 4.4.2.6 General procedure for the preparation of the pyrazole carboxylic derivative 31

To a solution of the appropriate carboxylate derivative (**28d**) (0.8 mmol) in EtOH (5.7 ml), a solution of NaOH 1N (5.7 ml) was added and the reaction kept stirring at reflux. After 2 hours, the mixture was concentrated *in vacuo*, followed by additions of $dH_2O$ and then HCl (12N in $ddH_2O$) until precipitation of a white solid (**31**). Thus, after filtration and rinsing with petroleum ether, purified compound **31** was obtained.

*1-(4-fluorophenyl)-5-(4-(trifluoromethyl)phenyl)-1H-pyrazole-3-carboxylic acid* (**31**). White solid, 90% yield. $^{1}$H NMR (400 MHz, $CDCl_3$): δ ppm= 12.20 (s, 1H), 7.84 – 7.82 (m, 4H), 7.65 – 7.58 (m, 2H), 7.53 (s, 1H), 7.27 – 7.19 (m, 2H).

#### 4.4.2.7 General procedure for the preparation of final compound 15

To a stirring solution of the pyrazole carboxylic derivative **31** (0.7mmol), *p*-chloroaniline (0.7 mmol) and DMAP (0.05 mmol), in DCM (4.8 ml) a solution of DCC (0.7 mmol) in DCM (3 ml) under ice-cooling was added. The mixture was stirred under ice-cooling and slowly warmed up to room temperature. After stirred for 3 h, the mixture was filtered through a pad of celite and the filtrate was evaporated to dryness. The residue was chromatographed on a silica gel (cyclohexane/ethyl acetate 1/1 (v/v)) to give compound **15** as a white solid.

*N-(4-chlorophenyl)-1-(4-fluorophenyl)-5-(4-(trifluoromethyl)phenyl)-1H-pyrazole-3-carboxamide* (**15**). White solid, 40% yield. $^{1}$H NMR (400 MHz, $CDCl_3$): δ ppm= 7.85 – 7.79 (m, 4H), 7.75 (d, *J* = 8.1 Hz, 2H), 7.56 (d, *J* = 8.1 Hz, 2H), 7.39 – 7.33 (m, 4H), 7.22 (s, 1H), 7.18 (s, 1H). $^{13}$C NMR

(100 MHz, $CDCl_3$): δ ppm= 163.12, 159.81, 144.62, 140.81, 136.47, 136.20, 135.28, 131.83, 129.97, 128.42, 127.19, 124.46, 124.22, 123.04, 116.40, 111.62.

### 4.4.2.8 Procedure for the preparation of the hydrazone 34

1 ml of 37% HCl was added to an ice-cooled solution of isopropylaniline (**32**) (7.4 mmol) in 2 ml of ethanol. After that, a cold sodium nitrite solution (8.1 mmol in 2.4 ml of water) was added dropwise, and the liquid for the reaction was stirred for 1 h while being watched to ensure that the temperature never exceeded 10 °C. Ethyl chloroacetate (**33**) (7.4 mmol) and sodium acetate (11.1 mmol) in ethanol-water (9:1, 20 ml) were added dropwise to the mixture and let the reaction happening at room temperature for 4 hours. The reaction was quenched with water and stirred for further 18 hours before filtration and concentration of the white solid product **34** (yield 70%).

*Ethyl-2-chloro-2-(2-(4-isopropylphenyl)hydrazono)acetate* (**34**). Physicochemical, spectroscopic, and analytical data are consistent with those reported in literature.[13]

### 4.4.2.9 Procedure for the preparation of the morpholine enamine 35

To a solution of morpholine (**40**) (40 mmol) in 6 ml of toluene, 0.44 g of $MgSO_4$ were added and giving a suspension that was stirred at room temperature for 10 min. The reaction was cooled down to 0 °C and $TiCl_4$ (5.17 mmol, 1M in toluene) was added dropwise to give a dark green suspension. Then the reaction was stirred in the presence of **39** for 18 h at 60 °C. When the reaction mixture had been cooled to room temperature, the solid was filtered out and concentrated *in vacuo* to give the enamine **35** (yield 80%).

*4-(1-(4-fluorophenyl)prop-1-en-1-yl)morpholine* (**35**). Physicochemical, spectroscopic, and analytical data are consistent with those reported in literature.[13]

### 4.4.2.10 Procedure for the preparation of the pyrazole carboxylate 36

To a stirred solution of **34** (9.72 mmol) and **35** (9.72 mmol) in 70 ml of ethanol, 5.1 ml of DIPEA were added. After being agitated at room temperature for 18 hours, the reaction mixture was concentrated *in vacuo* and then the crude material was directly purified by

column chromatography (cyclohexane/ethyl acetate 20/1 (v/v)) to give the desired product (**36**).

*ethyl 5-(4-fluorophenyl)-1-(4-isopropylphenyl)-4-methyl-1H-pyrazole-3-carboxylate* (**36**). Physicochemical, spectroscopic, and analytical data are consistent with those reported in literature.[13]

### 4.4.2.11 General procedure for the preparation 1,4 diketones 43a-g, 47

To the appropriate benzaldehyde derivative (**41a-g** or **45**) (0.02 mol), 3-ethyl-5-(2-hydroxyethyl)-4-methylthiazolium bromide (0.4 mmol), vinyl ketone (**42** or **46**) (0.02 mol) and TEA (1.98 ml) were added at 75 °C and the created mixture stirred for 5 h. Then, HCl (2N) was added to the reaction until pH= 2 and stirred for 30 min. The extraction was carried out in ethyl acetate washing with $NaHCO_3$. After drying over $Na_2SO_4$, the crude product was concentrated *in vacuo* and the desired diketones (**43a-g** and **47**) were obtained in two purification steps. First, column chromatography purification on aluminum oxide (cyclohexane/ethyl acetate, 3:1 v/v) gave light-yellow solids, and then recrystallization from cyclohexane gave the purified products.

*1-(4-isopropylphenyl)pentane-1,4-dione* (**43a**). Physicochemical, spectroscopic, and analytical data are consistent with those reported in literature.[15]

*1-(2-chlorophenyl)pentane-1,4-di*one (**43b**). Physicochemical, spectroscopic, and analytical data are consistent with those reported in literature.[16]

*1-(4-ethylphenyl)pentane-1,4-dione* (**43c**). Physicochemical, spectroscopic, and analytical data are consistent with those reported in literature.[47]

*1-phenylpentane-1,4-dione* (**43d**). Physicochemical, spectroscopic, and analytical data are consistent with those reported in literature.[48]

*1-(2-fluorophenyl)pentane-1,4-dione* (**43e**). Physicochemical, spectroscopic, and analytical data are consistent with those reported in literature.[15]

*1-(4-fluorophenyl)pentane-1,4-dione* (**43f**). Physicochemical, spectroscopic, and analytical data are consistent with those reported in literature.[15]

*1-(4-chlorophenyl)pentane-1,4-dione* (**43g**). Physicochemical, spectroscopic, and analytical data are consistent with those reported in literature.[17]

*1-(2-fluorophenyl)hexane-1,4-dione* (**47**). Physicochemical, spectroscopic, and analytical data are consistent with those reported in literature.[14]

### 4.4.2.12 General procedure for the preparation of 1,5-disubstituted pyrroles 44a-j, 48

The proper diketone (**43a-g** or **47**) (2.28 mmol) and the suitable amine (2.28 mmol) were dissolved in ethanol (50 mL) in the presence of *p*-toluenesulfonic acid (0.17 mmol) and solution was refluxed and stirred for at least 5 h. The reaction was then cooled down to room temperature and concentrated *in vacuo*. The purified products (**44a-j** and **48**) were obtained by column chromatography purification on aluminum oxide using only cyclohexane.

*2-(4-isopropylphenyl)-1-(4-methoxyphenyl)-5-methyl-1H-pyrrole* (**44a**). Physicochemical, spectroscopic, and analytical data are consistent with those reported in literature.[15]

*2-(2-chlorophenyl)-5-methyl-1-(naphthalen-1-yl)-1H-pyrrole* (**44b**). Physicochemical, spectroscopic, and analytical data are consistent with those reported in literature.[16]

*1-(4-fluorophenyl)-2-(4-isopropylphenyl)-5-methyl-1H-pyrrole* (**44c**). Physicochemical, spectroscopic, and analytical data are consistent with those reported in literature.[47]

*1-(4-chlorophenyl)-2-(4-ethylphenyl)-5-methyl-1H-pyrrole* (**44d**). Physicochemical, spectroscopic, and analytical data are consistent with those reported in literature.[47]

*1-(4-fluorophenyl)-2-methyl-5-phenyl-1H-pyrrole* (**44e**). Physicochemical, spectroscopic, and analytical data are consistent with those reported in literature.[49]

*2-(2-fluorophenyl)-1-(4-fluorophenyl)-5-methyl-1H-pyrrole* (**44f**). Physicochemical, spectroscopic, and analytical data are consistent with those reported in literature.[15]

*2-(4-fluorophenyl)-5-methyl-1-(p-tolyl)-1H-pyrrole* (**44g**). Physicochemical, spectroscopic, and analytical data are consistent with those reported in literature.[15]

*1,2-bis(4-chlorophenyl)-5-methyl-1H-pyrrole* (**44h**). Physicochemical, spectroscopic, and analytical data are consistent with those reported in literature.[17]

*2-(4-ethylphenyl)-1-(4-fluorophenyl)-5-methyl-1H-pyrrole* (**44i**). Physicochemical, spectroscopic, and analytical data are consistent with those reported in literature.[17]

*1,2-bis(2-fluorophenyl)-5-methyl-1H-pyrrole* (**44j**). Physicochemical, spectroscopic, and analytical data are consistent with those reported in literature.[16]

*2-ethyl-5-(2-fluorophenyl)-1-(4-fluorophenyl)-1H-pyrrole* (**48**). Physicochemical, spectroscopic, and analytical data are consistent with those reported in literature.[14]

#### 4.4.2.13 General procedure for the preparation of the final pyrrole compound 18

To a solution of the appropriate pyrrole (**44j**) (9 mmol) in anhydrous DCM (20 mL), ethoxalyl chloride (0.38 mL) and $TiCl_4$ (0.34 mL) were added at 0 °C under a nitrogen flow. The resultant dark suspension was agitated for 4 hours and then the reaction quenched with water at room temperature (30 min stirring), before being extracted with DCM. After being brine-washed, the organic layers were dried over $Na_2SO_4$ and concentrated *in vacuo*. The crude residue was purified by column chromatography (cyclohexane/ethyl acetate, 3:1 v/v) to yield compounds **17** as a pale-yellow powder.

*ethyl 2-(1,5-bis(4-chlorophenyl)-2-methyl-1H-pyrrol-3-yl)-2-oxoacetate* (**18**). White solid, 40% yield. $^1$H NMR (400 MHz, $CDCl_3$) δ ppm= 7.35 – 7.27 (m, 2H), 7.12 – 7.04 (m, 2H), 7.03 – 6.95 (m, 2H), 6.93 – 6.85 (m, 2H), 6.71 (s, 1H), 4.25 (q, *J* = 7.1 Hz, 2H), 2.32 (s, 3H), 1.30 (t, *J* = 7.1 Hz, 3H). $^{13}$C NMR (100 MHz, $CDCl_3$) δ ppm= 182.43, 162.44, 142.64, 140.46, 136.03, 135.99, 133.56, 131.09, 129.54, 129.53, 127.60, 127.18, 120.09, 114.69, 62.33, 13.77, 13.70.

#### 4.4.2.14 General procedure for the preparation of final pyrrole compounds 19-23

A Mannich reaction was performed to obtain compounds **19-23**. To the suitable pyrrole (**44a-j** or **48**) (5.6 mmol) solubilized in 20 ml of acetonitrile, a mixture of formaldehyde (5.6 mmol) (40% in water), appropriate amine (5.6 mmol), and glacial acetic acid (2 mL), was added dropwise over the course of 5 min at room temperature. When the reaction was completed

(1-5 h), a solution of NaOH (20%, w/v) was added to quench it for at least 30 minutes stirring. The reaction was then extracted in ethyl acetate, washed with brine, and dried over $Na_2SO_4$ for at least 10 min. After filtering off $Na_2SO_4$, the organic solution was put under vacuum to obtain the concentrated crude product, which was purified by column chromatography (cyclohexane/ethyl acetate, 3:1 v/v) to give purified compounds **19-23** in satisfactory yields.

*4-((5-(4-isopropylphenyl)-1-(4-methoxyphenyl)-2-methyl-1H-pyrrol-3-yl)methyl)thiomorpholine* (**19**). Physicochemical, spectroscopic, and analytical data are consistent with those reported in literature.[15]

*4-((5-(2-chlorophenyl)-2-methyl-1-(naphthalen-1-yl)-1H-pyrrol-3-yl)methyl)thiomorpholine* (**20**). Physicochemical, spectroscopic, and analytical data are consistent with those reported in literature.[16]

*4,4-difluoro-1-((1-(4-fluorophenyl)-5-(4-isopropylphenyl)-2-methyl-1H-pyrrol-3-yl)methyl)piperidine* (**21**). White solid, 62% yield. $^1$H NMR (400 MHz, $CDCl_3$): δ ppm= 7.66 – 7.58 (m, 1H), 7.28 – 7.16 (m, 1H), 3.79 (d, J = 1.0 Hz, 0H), 3.21-2.96 (m, 1H), 2.43-2.21 (m, 1H), 1.25 (d, J = 6.7 Hz, 2H). $^{13}$C NMR (100 MHz, $CDCl_3$): δ ppm= 163.09, 161.12, 149.73, 149.36, 143.96, 138.18, 138.15, 133.30, 128.57, 127.06, 124.98, 124.91, 121.35, 119.46, 117.56, 116.52, 116.34, 107.17, 53.04, 48.17, 48.13, 48.09, 34.31, 32.39, 32.20, 32.02, 23.93.

*4-((1-(4-chlorophenyl)-5-(4-ethylphenyl)-2-methyl-1H-pyrrol-3-yl)methyl)thiomorpholine* (**22**). Physicochemical, spectroscopic, and analytical data are consistent with those reported in literature.[47]

*4-((2-ethyl-5-(2-fluorophenyl)-1-(4-fluorophenyl)-1H-pyrrol-3-yl)methyl)thiomorpholine* (**23**). Physicochemical, spectroscopic, and analytical data are consistent with those reported in literature.[14]

### 4.4.3 Biology

ABS screening, *in vitro* GC assays and cytotoxicity assays were carried out in collaboration with Birkholtz's research group at University of Pretoria (Department of Biochemistry Genetics and Microbiology).

The biological assays for the analysis of the compounds belonging to our in-house library were carried out in collaboration with Catteruccia's research group at Harvard T.H. Chan School of Public Health (Department of Immunology and Infectious Diseases) and they include ABS screening, stage-specificity assay, DGFA, iSMFA, topical exposure assay, and resistance selection.

All graphs that report test compounds activities were plotted using Prism GraphPad version 9 (GraphPad Software, La Jolla, CA).

#### 4.4.3.1 Parasite Culturing

*P. falciparum* asexual parasites were cultured *in vitro* from drug-sensitive strain NF54 (*Pf*NF54). Cultures were maintained in an atmosphere of 5 % $CO_2$, 5 % $O_2$ and 90 % $N_2$, at 37 °C, without shaking, with daily media changes. Parasites were maintained in fresh human erythrocytes (O+) in Hepes buffered Rosewell Park Memorial Institute (RPMI) media containing 10% O+ human serum (heat inactivated and pooled), if needed for gametogenesis or 10% of 0.5% Albumax if needed for ABS screening assay.

For mosquito infection and infection assays, gametocytogenesis was induced at a 4-5% parasitemia (5% hematocrit) and then followed by daily media changes until mature GC (V) were seen (day14-16). When needed, gametes formation was triggered by addition of ookinete medium (RPMI1640 with 25mM HEPES, 50μg/mL hypoxanthine, 2g/L $NaHCO_3$, 100 μM xanthurenic acid) and by cooling the plate at 4 °C for 4 min and then a further 5 min at 28 °C.

For drug assays, gametocytogenesis was induced adapting the method from Carter et al.[43] to obtain synchronized parasite cultures. Briefly, parasitemia was increased up to 6-10% and culture then fed by a glucose-free medium (daily changes, same atmosphere and temperature conditions). Remaining asexual parasites were removed on days 6 through 9 by a continuous 50 mM N-acetyl glucosamine (NAG; Sigma-Aldrich) treatment, this time with 0.2% glucose. From day 10 on, glucose enrichment was maintained, and GC were regularly seen under a microscope until they were mostly stage V and were employed in *in vitro* drug assays.

#### 4.4.3.2 ABS Screening

The asexual drug assay was carried out using the SYBR Green I method as previously described.[44] Briefly, sorbitol synchronized rings (>80% of parasite population) were grown for 72 hours in the presence of different concentrations of drugs (DMSO stocks) previously dispensed by dispensed by a HP D300 Digital Dispenser (Hewlett Packard Palo Alto, CA) in 384-clear-bottom well plates (Corning). Parasites were grown in 1% hematocrit, 1% starting parasitemia and 40 μl of 0.5% Albumax culture media for 72 h (trophozoite stage), and then the SYBR Green I (Lonza, Visp, Switzerland) staining of parasite DNA was measured. After 24h incubation in a dark room of the plates at room temperature (RT), a SpectraMax M5 (Molecular Devices, Sunnyvale, CA) plate reader was used to measure fluorescence, and data were analyzed with GraphPad Prism version 9 (GraphPad Software, La Jolla, CA). $EC_{50}$ was calculated using nonlinear regression with the log(inhibitor) vs. response with a four-parameter variable slope curve-fitting equation. Parasite treated with DHA 25 μM and dimethyl sulfoxide (DMSO) were used as positive control and negative control, respectively.

To assess the anti-asexual activity of **MMV158084** analogues, the EnVision® Multilabel Reader (PerkinElmer) (485 nm excitation, 530 nm emission) was used and $IC_{50}$ values were determined in CDD vault (https://www.collaborativedrug.com/) normalized to maximum and minimum inhibition levels for the positive (artemisinin) and negative (DMSO) control wells.

All asexual blood stage assays were repeated on at least three independent occasions with three technical replicates.

#### 4.4.3.3 Gametocytocidal assays

On three separate assay platforms—the PrestoBlue fluorescence assay, the ATP bioluminescence assay, and the luciferase reporter assay— compounds were tested for gametocytocidal activity against *Pf*NF54 stage IV/V GC. Gametocytocidal assays were performed as previously described.[5]

#### 4.4.3.4 Stage-Specificity Assay

*Pf*NF54 parasites (44 hours to complete one life cycle) were first synchronized transferring them in 5% sorbitol to get parasites with 8h of difference. Schizonts were then isolated using the Percoll protocol[45] and, after allowing 3 hours for uRBC re-invasion, the parasite cultures were again sorbitol synchronized to obtain a pure ring-stage culture (time = 3 hours). *P. falciparum* drug assays were conducted in flat-bottom 96-well plates in a 200 μl culture volume, 2% hematocrit, and 1% starting parasitemia. Compounds **CL191** and **CL241** were plated at three different concentrations (0.2 μM, 2 μM, 20 μM) and then parasites cultures were added as early rings (3-12 hours), late rings (12-24 hours), trophozoites (24-36 hours) or schizonts (36-44 hours). After every exposure time, compounds were removed from the plates after three rounds of wash-off using incomplete drug media, and the parasites allowed to grow in complete media. Incubation times were therefore adjusted to the 44 hours asexual blood stage cycle of our *Pf*NF54 parasite line. DMSO and DHA 25 μM were used as negative and positive control, respectively. Pyrimethamine 0.5 μM was also used as a positive control since as a specific activity towards late-stages (trophozoites and schizonts).[46] Giemsa stains (GS) were evaluated at each time point by light microscopy. Relative growth inhibition was assessed using flow cytometry at 80 hours time point, at which parasite developed into the trophozoites stage after one life cycle. Prior to flow-cytometric analysis, samples were stained in MitoTracker™ Orange CMTMRos (ThermoFisher) and 10 x SYBR Green I (Lonza, Visp, Switzerland) in 1 x PBS for 30 minutes in the dark at 37°C. The staining solution was removed and cells were resuspended in PBS to reach 0.25% of hematocrit. FACS data acquisition was performed on a MACSQuant VYB (Milteni Biotec) with a 488 nm laser and a 525 nm filter and analyzed with FlowJo 2. RBCs were gated on the forward light scatter and side scatter and infected RBCs were detected in channel B1. At least 100,000 events were analyzed per sample. All asexual blood stage assays were repeated on at least three independent occasions with two technical replicates. The threshold for separating infected cells from healthy ones was determined using a matched sample of uninfected erythrocytes.

#### 4.4.3.5 DGFA

Compound **3** activity against gamete formation was assessed in the *Pf*DGFA in the carry-over assay format adapted from Ruecker et al.[21] Briefly, the capacity of exflagellation was first determined under light microscopy (x40 magnification) to check the maturity of the gametocyte cultures (> 0.3% of total RBCs; induced with ookinete medium in 1:1 ratio). Thereafter, the gametocyte cultures were diluted to 12.5 million cells/ml (including RBCs) and 35.5 µl (1.05 million cells) added to each well of glass-bottomed 18 well µ-slides (Ibidi, US) containing 37.5 µl of the test compound diluted in complete media in eight different concentrations (from 20 to 0.15625 µM), and negative (DMSO < 0.25% w/v) and positive (MB 25 µM) controls. After 24 hours of incubation (37°C, 5 % $CO_2$, 5 % $O_2$ and 90 % $N_2$) GC were induced to form gametes by dispensing 15 µL ookinete medium containing 0.5 µg $ml^{-1}$ anti-Pfs25 clone 4B7 (BEI Resources, cat. no. MRA-315) conjugated to the fluorophore CS568 at RT. Following incubation at 4°C for 4 minutes and then 5 minutes at 28°C, exflagellation was immediately recorded on using a Zeiss Observer.Z1 (Carl Zeiss Microscopy GmbH, Jena, Germany) with phase-contrast and 10-frame time lapse image over 2 seconds each well (x 4 magnification, x 1.5 zoom). The slides were then further incubated overnight (dark room, 28°C) and were read using Zeiss Observer.Z1 with single-image fluorescence microscopy (x4 magnification, x1.5 zoom). Comparing the inhibitory activity of the tested drug to that of the control wells allowed for the calculation of the percentage of inhibition. This assay was repeated on at least three independent occasions with three technical replicates.

#### 4.4.3.6 Mosquito rearing and Infection Assays

*An. gambiae* mosquitoes from the G3 strain, a highly lab-adapted, insecticide-susceptible strain competent for *P. falciparum* of African origin, were kept in a 27 °C insectary environment with 70-80% humidity and a 12 hours light - 12 hours dark cycle. For mosquito colonies, 2-liter plastic trays filled with 500 ml of distilled water ($dH_2O$) and containing Tetramin Baby Fish Food (Tetrawerke, Melle, Germany) were used for larvae cultivation

following an ideal density and feeding schedule. Pupae were separated from larvae at the beginning of pupation using a vacuum aspirator, collected in $dH_2O$, and housed in a cage of 30 x 30 x 30 cm (Bugdorm, Megaview Science Co, Ltd, Thailand). Adult mosquitoes were provided with of 10% glucose (Sigma Aldrich, US) *ab libitum* and $dH_2O$ after their emergence. An artificial membrane feeding system (Hemotek, UK) was used to give a blood meal of donated human blood to 5-7-day-old adult mosquitoes for colony maintenance.
Mosquito infections for drug assays were carried out to 4-5-day-old female adults, which were provided an *in vitro* culture of *Pf*NF54 mature GC through a specially designed, water-heated, glass membrane feeder. Females were moved to an infectious sealed and safe glovebox as soon as they were blood fed.

#### 4.4.3.7 iSMFA

Cultures of *Pf*NF54 mature stage V GC (14-16 days old, gametocytemia 1-2%) were treated with test compounds (2 μM) or DMSO (< 0.25% w/v) for 48 hours in a 12-well plate (2 mL/well of parasite culture). After the time of exposure, GC were mixed with uRBC and then pelleted. The blood pellet was resuspended in human serum and kept at 37°C vefore and during mosquito blood feeding. Females who did not fully engorge after 60 minutes were vacuum sucked out of their cages immediately into 80% ethanol container, placed at -20°C overnight and eventually thrown away. At 7 days pIBM, the remaining mosquitoes were vacuum aspirated into 80% ethanol, incubated for 10 minutes at 20°C, and then moved out of the safe feeding box into PBS on ice. Mosquitoes were dissected to isolate the midguts, which were stained in 0.2% w/v mercurochrome (in $ddH_2O$) and kept for 12-14 minutes. Next, midguts were transferred on microscope slides containing 0.02% w/v mercurochrome and oocyst counted under bright field illumination at x 40 magnification
on an inverted compound light microscope (Olympus Corporation, Waltham, MA). For infection analysis, oocyst prevalence (number of infected midguts/number of total midguts) and intensity (number of oocyst/midgut) were calculated. Data were plotted using GraphPad Prism 9 for statistical analysis (non-parametric T test (Mann–Whitney)).

#### 4.4.3.8 Topical Exposure Assay

The topical exposure assay was adapted from Lees et al.[22] Briefly, test compounds were solubilized in acetone to reach a concentration of 2mM. 1% w/v of DMSO in acetone was used as a negative control when 100 mM DMSO stocks of compounds were used to make the samples, otherwise only acetone was considered as negative control. Adult female mosquitoes (4-5 days-old) were anesthetized on ice for 15 minutes and then transferred on Petri dishes covered with filter paper (Whatman, Grade 1). 0.5 µL of test compounds and control sample were pipetted to the dorsal thorax of mosquitoes, which were immediately transferred to cages supplied with $dH_2O$. After complete recovery (4 hours), mosquitoes were provided of IBM and unfed females were discarded into 80% ethanol. After 7 days pIBM, mosquito dissection of midguts for oocyst counting was performed as described above.

#### 4.4.3.9 Selection of Drug-Resistant Parasites

*Pf*NF54 parasites were exposed to suboptimal concentrations of **CL241** to induce and select for drug-resistant parasites. Parasites were set at a 2.5-3% parasitemia ($10^8$ number of parasites) before exposure to 5x or 10x $IC_{50}$ of **CL241**. The assay was carried in at least three independent experiments. Parasites were exposed to **CL241** for 72 hours and the drug media was changed daily. Once the cultures were cleared, cultures were transferred to complete media which was changed every other day. Recrudescence was monitored with GS under light microscopy (100x magnification).

#### 4.4.3.10 *In vitro* cytotoxicity Assays

HepG2 toxicity screening was used to assess compound safety *in vitro* as previously reported.[5]

#### 4.4.3.11 *In vitro* Microsomal Metabolic Assay

This assay was performed in duplicate using a 96-well microtiter plate. Test compounds were incubated at 37 °C in rat, mouse and pooled human liver microsomes with a final protein concentration of 0.4 mg.ml-1; XenoTech, Lenexa, KS suspended in 0.1 M phosphate buffer at pH 7.4 for predetermined time points. This was in the presence and absence of cofactor-reduced nicotinamide adenine dinucleotide phosphate (NADPH, 1.0 mM). The reactions were quenched by adding ice-cold MeCN containing an internal standard (Carbamazepine, 0.0236 μg/mL). The samples were centrifuged, and the supernatant was analyzed via liquid chromatography-tandem mass spectrometry (LC–MS/MS) (Agilent Rapid Resolution HPLC, AB SCIEX 4500 MS). The relative loss of the parent compound with time was monitored, and plots were prepared for each compound of Ln% remaining versus time to determine the first-order rate constant for compound depletion. This was used to calculate the degradation half-life and subsequently to predict the in vitro intrinsic clearance (CLint) and in vitro hepatic extraction ratio (EH).

## References


(1) Paonessa, G.; Siciliano, G.; Graziani, R.; Lalli, C.; Cecchetti, O.; Alli, C.; la Valle, R.; Petrocchi, A.; Sferrazza, A.; Bisbocci, M.; Falchi, M.; Toniatti, C.; Bresciani, A.; Alano, P. Gametocyte-Specific and All-Blood-Stage Transmission-Blocking Chemotypes Discovered from High Throughput Screening on Plasmodium Falciparum Gametocytes. *Commun Biol* **2022**, *5* (1), 547. https://doi.org/10.1038/s42003-022-03510-w.

(2) Siciliano, G.; di Paolo, V.; Rotili, D.; Migale, R.; Pedini, F.; Casella, M.; Camerini, S.; Dalzoppo, D.; Henderson, R.; Huijs, T.; Dechering, K. J.; Mai, A.; Caccuri, A. M.; Lalle, M.; Quintieri, L.; Alano, P. The Nitrobenzoxadiazole Derivative NBDHEX Behaves as Plasmodium Falciparum Gametocyte Selective Inhibitor with Malaria Parasite Transmission Blocking Activity. *Pharmaceuticals* **2022**, *15* (2), 168. https://doi.org/10.3390/ph15020168.

(3) Malebo, H. M.; D'Alessandro, S.; Ebstie, Y. A.; Sorè, H.; Tenoh Guedoung, A. R.; Katani, S. J.; Parapini, S.; Taramelli, D.; Habluetzel, A. In Vitro Multistage Malaria Transmission Blocking Activity of Selected Malaria Box Compounds</P>. *Drug Des Devel Ther* **2020**, *Volume 14*, 1593–1607. https://doi.org/10.2147/DDDT.S242883.

(4) Azevedo, R.; Mendes, A. M.; Prudêncio, M. Inhibition of Plasmodium Sporogonic Stages by Ivermectin and Other Avermectins. *Parasit Vectors* **2019**, *12* (1), 549. https://doi.org/10.1186/s13071-019-3805-0.

(5) Reader, J.; van der Watt, M. E.; Taylor, D.; le Manach, C.; Mittal, N.; Ottilie, S.; Theron, A.; Moyo, P.; Erlank, E.; Nardini, L.; Venter, N.; Lauterbach, S.; Bezuidenhout, B.; Horatscheck, A.; van Heerden, A.; Spillman, N. J.; Cowell, A. N.; Connacher, J.; Opperman, D.; Orchard, L. M.; Llinás, M.; Istvan, E. S.; Goldberg, D. E.; Boyle, G. A.; Calvo, D.; Mancama, D.; Coetzer, T. L.; Winzeler, E. A.; Duffy, J.; Koekemoer, L. L.; Basarab, G.; Chibale, K.; Birkholtz, L.-M. Multistage and Transmission-Blocking Targeted Antimalarials Discovered from the Open-Source MMV Pandemic Response Box. *Nat Commun* **2021**, *12* (1), 269. https://doi.org/10.1038/s41467-020-20629-8.

(6) Birkholtz, L.-M.; Alano, P.; Leroy, D. Transmission-Blocking Drugs for Malaria Elimination. *Trends Parasitol* **2022**, *38* (5), 390–403. https://doi.org/10.1016/j.pt.2022.01.011.

(7) Avery, V. M.; Bashyam, S.; Burrows, J. N.; Duffy, S.; Papadatos, G.; Puthukkuti, S.; Sambandan, Y.; Singh, S.; Spangenberg, T.; Waterson, D.; Willis, P. Screening and Hit Evaluation of a Chemical Library against Blood-Stage Plasmodium Falciparum. *Malar J* **2014**, *13* (1), 190. https://doi.org/10.1186/1475-2875-13-190.

(8) Almela, M. J.; Lozano, S.; Lelièvre, J.; Colmenarejo, G.; Coterón, J. M.; Rodrigues, J.; Gonzalez, C.; Herreros, E. A New Set of Chemical Starting Points with Plasmodium Falciparum Transmission-Blocking Potential for Antimalarial Drug Discovery. *PLoS One* **2015**, *10* (8), e0135139. https://doi.org/10.1371/journal.pone.0135139.

(9) Subramanian, G.; Belekar, M. A.; Shukla, A.; Tong, J. X.; Sinha, A.; Chu, T. T. T.; Kulkarni, A. S.; Preiser, P. R.; Reddy, D. S.; Tan, K. S. W.; Shanmugam, D.; Chandramohanadas, R. Targeted Phenotypic Screening in Plasmodium Falciparum and Toxoplasma Gondii Reveals Novel Modes of Action of Medicines for Malaria Venture Malaria Box Molecules. *mSphere* **2018**, *3* (1). https://doi.org/10.1128/mSphere.00534-17.

(10) Ramesh, R.; Shingare, R. D.; Kumar, V.; Anand, A.; B, S.; Veeraraghavan, S.; Viswanadha, S.; Ummanni, R.; Gokhale, R.; Srinivasa Reddy, D. Repurposing of a Drug Scaffold: Identification of Novel Sila Analogues of Rimonabant as Potent Antitubercular Agents. *Eur J Med Chem* **2016**, *122*, 723–730. https://doi.org/10.1016/j.ejmech.2016.07.009.

(11) Paton, D. G.; Childs, L. M.; Itoe, M. A.; Holmdahl, I. E.; Buckee, C. O.; Catteruccia, F. Exposing Anopheles Mosquitoes to Antimalarials Blocks Plasmodium Parasite Transmission. *Nature* **2019**, *567* (7747), 239–243. https://doi.org/10.1038/s41586-019-0973-1.

(12) Oke, C. E.; Ingham, V. A.; Walling, C. A.; Reece, S. E. Vector Control: Agents of Selection on Malaria Parasites? *Trends Parasitol* **2022**, *38* (10), 890–903. https://doi.org/10.1016/j.pt.2022.07.006.

(13) Poce, G.; Consalvi, S.; Venditti, G.; Alfonso, S.; Desideri, N.; Fernandez-Menendez, R.; Bates, R. H.; Ballell, L.; Barros Aguirre, D.; Rullas, J.; de Logu, A.; Gardner, M.; Ioerger, T. R.; Rubin, E. J.; Biava, M. Novel Pyrazole-Containing Compounds Active against Mycobacterium Tuberculosis. *ACS Med Chem Lett* **2019**, *10* (10), 1423–1429. https://doi.org/10.1021/acsmedchemlett.9b00204.

(14) Biava, M.; Porretta, G. C.; Poce, G.; de Logu, A.; Meleddu, R.; de Rossi, E.; Manetti, F.; Botta, M. 1,5-Diaryl-2-Ethyl Pyrrole Derivatives as Antimycobacterial Agents: Design, Synthesis, and Microbiological Evaluation. *Eur J Med Chem* **2009**, *44* (11), 4734–4738. https://doi.org/10.1016/j.ejmech.2009.06.005.

(15) Biava, M.; Porretta, G. C.; Poce, G.; Battilocchio, C.; Alfonso, S.; Logu, A. de; Serra, N.; Manetti, F.; Botta, M. Identification of a Novel Pyrrole Derivative Endowed with Antimycobacterial Activity and Protection Index Comparable to That of the Current Antitubercular Drugs Streptomycin and Rifampin. *Bioorg Med Chem* **2010**, *18* (22), 8076–8084. https://doi.org/10.1016/j.bmc.2010.09.006.

(16) Biava, M.; Porretta, G. C.; Poce, G.; Deidda, D.; Pompei, R.; Tafi, A.; Manetti, F. Antimycobacterial Compounds. Optimization of the BM 212 Structure, the Lead Compound for a New Pyrrole Derivative Class. *Bioorg Med Chem* **2005**, *13* (4), 1221–1230. https://doi.org/10.1016/j.bmc.2004.11.018.

(17) Baiocco, P.; Poce, G.; Alfonso, S.; Cocozza, M.; Porretta, G. C.; Colotti, G.; Biava, M.; Moraca, F.; Botta, M.; Yardley, V.; Fiorillo, A.; Lantella, A.; Malatesta, F.; Ilari, A. Inhibition of Leishmania Infantum Trypanothione Reductase by Azole-Based Compounds: A Comparative Analysis with Its Physiological Substrate by X-Ray Crystallography. *ChemMedChem* **2013**, *8* (7), 1175–1183. https://doi.org/10.1002/cmdc.201300176.

(18) Murithi, J. M.; Owen, E. S.; Istvan, E. S.; Lee, M. C. S.; Ottilie, S.; Chibale, K.; Goldberg, D. E.; Winzeler, E. A.; Llinás, M.; Fidock, D. A.; Vanaerschot, M. Combining Stage Specificity and Metabolomic Profiling to Advance Antimalarial Drug Discovery. *Cell Chem Biol* **2020**, *27* (2), 158-171.e3. https://doi.org/10.1016/j.chembiol.2019.11.009.

(19) Wilson, D. W.; Langer, C.; Goodman, C. D.; McFadden, G. I.; Beeson, J. G. Defining the Timing of Action of Antimalarial Drugs against Plasmodium Falciparum. *Antimicrob Agents Chemother* **2013**, *57* (3), 1455–1467. https://doi.org/10.1128/AAC.01881-12.

(20) Delves, M. J.; Ramakrishnan, C.; Blagborough, A. M.; Leroy, D.; Wells, T. N. C.; Sinden, R. E. A High-Throughput Assay for the Identification of Malarial Transmission-Blocking Drugs and Vaccines. *Int J Parasitol* **2012**, *42* (11), 999–1006. https://doi.org/10.1016/j.ijpara.2012.08.009.

(21) Ruecker, A.; Mathias, D. K.; Straschil, U.; Churcher, T. S.; Dinglasan, R. R.; Leroy, D.; Sinden, R. E.; Delves, M. J. A Male and Female Gametocyte Functional Viability Assay To Identify Biologically Relevant Malaria Transmission-Blocking Drugs. *Antimicrob Agents Chemother* **2014**, *58* (12), 7292–7302. https://doi.org/10.1128/AAC.03666-14.

(22) Lees, R.; Praulins, G.; Davies, R.; Brown, F.; Parsons, G.; White, A.; Ranson, H.; Small, G.; Malone, D. A Testing Cascade to Identify Repurposed Insecticides for Next-Generation Vector Control Tools: Screening a Panel of Chemistries with Novel Modes of Action against a Malaria Vector. *Gates Open Res* **2019**, *3*, 1464. https://doi.org/10.12688/gatesopenres.12957.2.

(23) Brown, F.; Paton, D. G.; Catteruccia, F.; Ranson, H.; Ingham, V. A. A Steroid Hormone Agonist Reduces Female Fitness in Insecticide-Resistant Anopheles Populations. *Insect Biochem Mol Biol* **2020**, *121*, 103372. https://doi.org/10.1016/j.ibmb.2020.103372.

(24) Gil, J. P.; Krishna, S. Pfmdr1 (Plasmodium Falciparum Multidrug Drug Resistance Gene 1): A Pivotal Factor in Malaria Resistance to Artemisinin Combination Therapies. *Expert Rev Anti Infect Ther* **2017**, *15* (6), 527–543. https://doi.org/10.1080/14787210.2017.1313703.

(25) Shafik, S. H.; Richards, S. N.; Corry, B.; Martin, R. E. Mechanistic Basis for Multidrug Resistance and Collateral Drug Sensitivity Conferred to the Malaria Parasite by Polymorphisms in PfMDR1 and PfCRT. *PLoS Biol* **2022**, *20* (5), e3001616. https://doi.org/10.1371/journal.pbio.3001616.

(26) Koenderink, J. B.; Kavishe, R. A.; Rijpma, S. R.; Russel, F. G. M. The ABCs of Multidrug Resistance in Malaria. *Trends Parasitol* **2010**, *26* (9), 440–446. https://doi.org/10.1016/j.pt.2010.05.002.

(27) Ngotho, P.; Soares, A. B.; Hentzschel, F.; Achcar, F.; Bertuccini, L.; Marti, M. Revisiting Gametocyte Biology in Malaria Parasites. *FEMS Microbiol Rev* **2019**, *43* (4), 401–414. https://doi.org/10.1093/femsre/fuz010.

(28) van Biljon, R.; van Wyk, R.; Painter, H. J.; Orchard, L.; Reader, J.; Niemand, J.; Llinás, M.; Birkholtz, L.-M. Hierarchical Transcriptional Control Regulates Plasmodium Falciparum Sexual Differentiation. *BMC Genomics* **2019**, *20* (1), 920. https://doi.org/10.1186/s12864-019-6322-9.

(29) Munro, B. A.; McMorran, B. J. Antimalarial Drug Strategies to Target Plasmodium Gametocytes. *Parasitologia* **2022**, *2* (2), 101–124. https://doi.org/10.3390/parasitologia2020011.

(30) Consalvi, S.; Venditti, G.; Zhu, J.; Boshoff, H. I.; Arora, K.; de Logu, A.; Ioerger, T. R.; Rubin, E. J.; Biava, M.; Poce, G. 6-Fluorophenylbenzohydrazides Inhibit Mycobacterium Tuberculosis Growth through Alteration of Tryptophan Biosynthesis. *Eur J Med Chem* **2021**, *226*, 113843. https://doi.org/10.1016/j.ejmech.2021.113843.

(31) Krishnan, A.; Soldati-Favre, D. Amino Acid Metabolism in Apicomplexan Parasites. *Metabolites* **2021**, *11* (2), 61. https://doi.org/10.3390/metabo11020061.

(32) Spielmann, T.; Gras, S.; Sabitzki, R.; Meissner, M. Endocytosis in Plasmodium and Toxoplasma Parasites. *Trends Parasitol* **2020**, *36* (6), 520–532. https://doi.org/10.1016/j.pt.2020.03.010.

(33) Steward, K. M. Strategies for the Synthesis and Use of B-Stereogenic A-Keto Esters. *University of North Carolina at Chapel Hill* **2012**.

(34) Silamut, K.; White, N. J. Relation of the Stage of Parasite Development in the Peripheral Blood to Prognosis in Severe Falciparum Malaria. *Trans R Soc Trop Med Hyg* **1993**, *87* (4), 436–443. https://doi.org/10.1016/0035-9203(93)90028-O.

(35) Jogdand, P. S.; Singh, S. K.; Christiansen, M.; Dziegiel, M. H.; Singh, S.; Theisen, M. Flow Cytometric Readout Based on Mitotracker Red CMXRos Staining of Live

Asexual Blood Stage Malarial Parasites Reliably Assesses Antibody Dependent Cellular Inhibition. *Malar J* **2012**, *11* (1), 235. https://doi.org/10.1186/1475-2875-11-235.

(36) Kobylinski, K. C.; Jittamala, P.; Hanboonkunupakarn, B.; Pukrittayakamee, S.; Pantuwatana, K.; Phasomkusolsil, S.; Davidson, S. A.; Winterberg, M.; Hoglund, R. M.; Mukaka, M.; Pluijm, R. W.; Dondorp, A.; Day, N. P. J.; White, N. J.; Tarning, J. Safety, Pharmacokinetics, and Mosquito-Lethal Effects of Ivermectin in Combination With Dihydroartemisinin-Piperaquine and Primaquine in Healthy Adult Thai Subjects. *Clin Pharmacol Ther* **2020**, *107* (5), 1221–1230. https://doi.org/10.1002/cpt.1716.

(37) Kobylinski, K. C.; Deus, K. M.; Butters, M. P.; Hongyu, T.; Gray, M.; da Silva, I. M.; Sylla, M.; Foy, B. D. The Effect of Oral Anthelmintics on the Survivorship and Re-Feeding Frequency of Anthropophilic Mosquito Disease Vectors. *Acta Trop* **2010**, *116* (2), 119–126. https://doi.org/10.1016/j.actatropica.2010.06.001.

(38) Wang, P.; Jiang, X.; Bai, J.; Yang, F.; Yu, X.; Wu, Y.; Zheng, W.; Zhang, Y.; Cui, L.; Liu, F.; Zhu, X.; Cao, Y. Characterization of PSOP26 as an Ookinete Surface Antigen with Improved Transmission-Blocking Activity When Fused with PSOP25. *Parasit Vectors* **2022**, *15* (1), 175. https://doi.org/10.1186/s13071-022-05294-8.

(39) Miura, K.; Swihart, B. J.; Deng, B.; Zhou, L.; Pham, T. P.; Diouf, A.; Burton, T.; Fay, M. P.; Long, C. A. Transmission-Blocking Activity Is Determined by Transmission-Reducing Activity and Number of Control Oocysts in Plasmodium Falciparum Standard Membrane-Feeding Assay. *Vaccine* **2016**, *34* (35), 4145–4151. https://doi.org/10.1016/j.vaccine.2016.06.066.

(40) Wadi, I.; Anvikar, A. R.; Nath, M.; Pillai, C. R.; Sinha, A.; Valecha, N. Critical Examination of Approaches Exploited to Assess the Effectiveness of Transmission-Blocking Drugs for Malaria. *Future Med Chem* **2018**, *10* (22), 2619–2639. https://doi.org/10.4155/fmc-2018-0169.

(41) Cowman, A. F.; Galatis, D.; Thompson, J. K. Selection for Mefloquine Resistance in Plasmodium Falciparum Is Linked to Amplification of the Pfmdr1 Gene and Cross-Resistance to Halofantrine and Quinine. *Proceedings of the National Academy of Sciences* **1994**, *91* (3), 1143–1147. https://doi.org/10.1073/pnas.91.3.1143.

(42) Nzila, A.; Mwai, L. In Vitro Selection of Plasmodium Falciparum Drug-Resistant Parasite Lines. *Journal of Antimicrobial Chemotherapy* **2010**, *65* (3), 390–398. https://doi.org/10.1093/jac/dkp449.

(43) Carter, R.; Ranford-Cartwright, L.; Alano, P. The Culture and Preparation of Gametocytes of Plasmodium Falciparum for Immunochemical, Molecular, and Mosquito Infectivity Studies. In *Protocols in Molecular Parasitology*; Humana Press: New Jersey; pp 67–88. https://doi.org/10.1385/0-89603-239-6:67.

(44) Johnson, J. D.; Dennull, R. A.; Gerena, L.; Lopez-Sanchez, M.; Roncal, N. E.; Waters, N. C. Assessment and Continued Validation of the Malaria SYBR Green I-Based Fluorescence Assay for Use in Malaria Drug Screening. *Antimicrob Agents Chemother* **2007**, *51* (6), 1926–1933. https://doi.org/10.1128/AAC.01607-06.

(45) Radfar, A.; Méndez, D.; Moneriz, C.; Linares, M.; Marín-García, P.; Puyet, A.; Diez, A.; Bautista, J. M. Synchronous Culture of Plasmodium Falciparum at High Parasitemia Levels. *Nat Protoc* **2009**, *4* (12), 1899–1915. https://doi.org/10.1038/nprot.2009.198.

(46) Blasco, B.; Leroy, D.; Fidock, D. A. Antimalarial Drug Resistance: Linking Plasmodium Falciparum Parasite Biology to the Clinic. *Nat Med* **2017**, *23* (8), 917–928. https://doi.org/10.1038/nm.4381.

(47) Biava, M.; Porretta, G. C.; Poce, G.; de Logu, A.; Saddi, M.; Meleddu, R.; Manetti, F.; de Rossi, E.; Botta, M. 1,5-Diphenylpyrrole Derivatives as Antimycobacterial Agents. Probing the Influence on Antimycobacterial Activity of Lipophilic Substituents at the Phenyl Rings. *J Med Chem* **2008**, *51* (12), 3644–3648. https://doi.org/10.1021/jm701560p.

(48) Ryzhkov, I. O.; Andreev, I. A.; Belov, G. M.; Kurkin, A. v.; Yurovskaya, M. A. Preparation of Chiral Pyrrole Derivatives by the Paal-Knorr Reaction. *Chem Heterocycl Compd (N Y)* **2011**, *47* (2), 182–193. https://doi.org/10.1007/s10593-011-0739-7.

(49) Xu, C.; Han, Y.; Chen, S.; Xu, D.; Zhang, B.; Shan, Z.; Du, S.; Xu, L.; Gong, P. One-Pot Synthesis of 2-Methyl-1,5-Diaryl-1H-Pyrroles from Styrene, Acetone and Arylamines Using TBHP, Copper(II) Trifluoromethanesulfonate and Sulfamic Acid. *Tetrahedron Lett* **2018**, *59* (3), 260–263. https://doi.org/10.1016/j.tetlet.2017.12.031.

## Supplementary Materials

| | |
|---|---|
| Figure S1 | Dose-response curves of compounds **3**, **6**, **11**, **12**, **17**, **18**, **20-23**. |
| Figure S2 | iSMFA results of compounds **6**, **11**, **12**, **16-23** with 48h of exposure time. |
| Figure S3 | DGFA of compound **3.** |
| Figure S4 | Topical exposure results. |

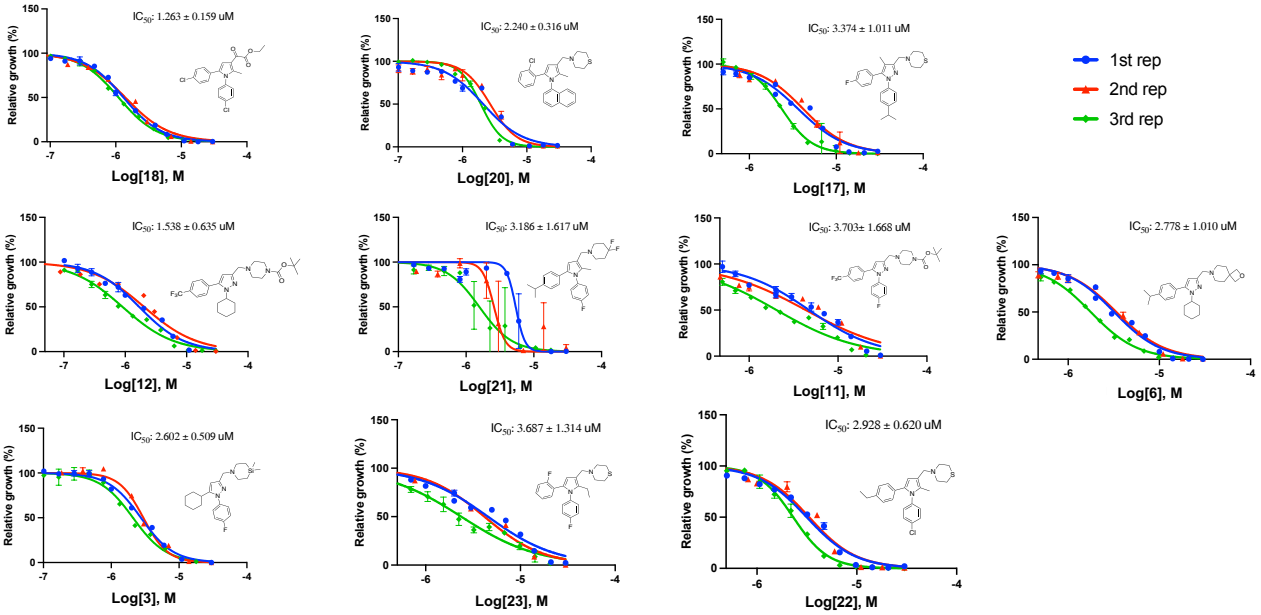


**Figure S1.** Dose-response curves of compounds **3**, **6**, **11**, **12**, **17**, **18**, **20-23**. $IC_{50}$ values and chemical structures of compounds and confidence interval are indicated.

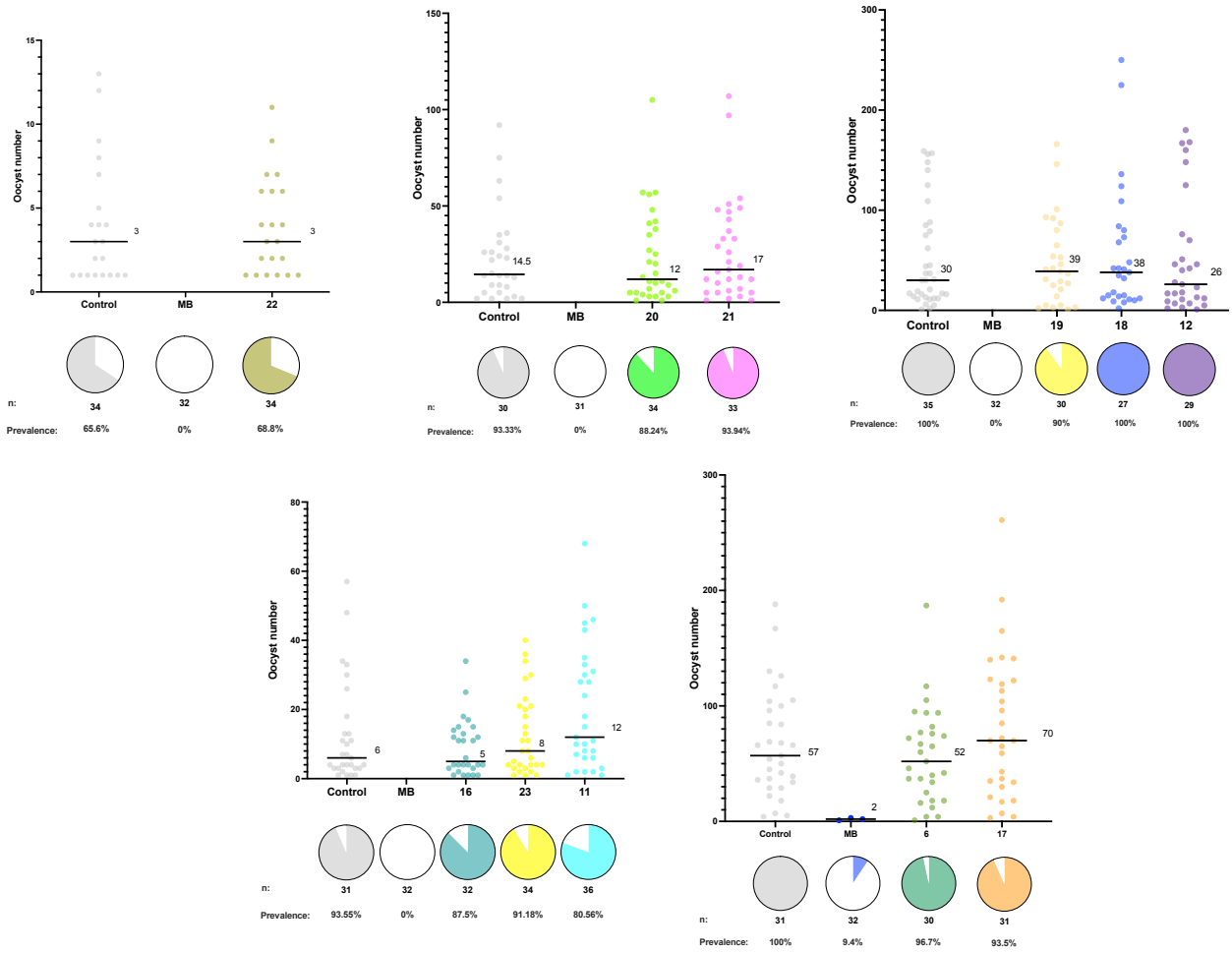

**Figure S2.** iSMFA results of compounds **6**, **11**, **12**, **16-23** with 48h of exposure time. Results were obtained after a single experiment and are reported as oocyst prevalence and oocyst intensity. Median lines and values are indicated, "n" indicates the number of independent samples. To isolate oocyst prevalence and oocyst intensity, midgut samples with zero oocysts have been excluded from intensity analysis. Statistical significance is indicated where relevant as follows: * = p<0.05, ** = p<0.01, *** = p<0.001, **** = p<0.0001. MB: methylene blue; Control: DMSO (< 0.25% v/v).

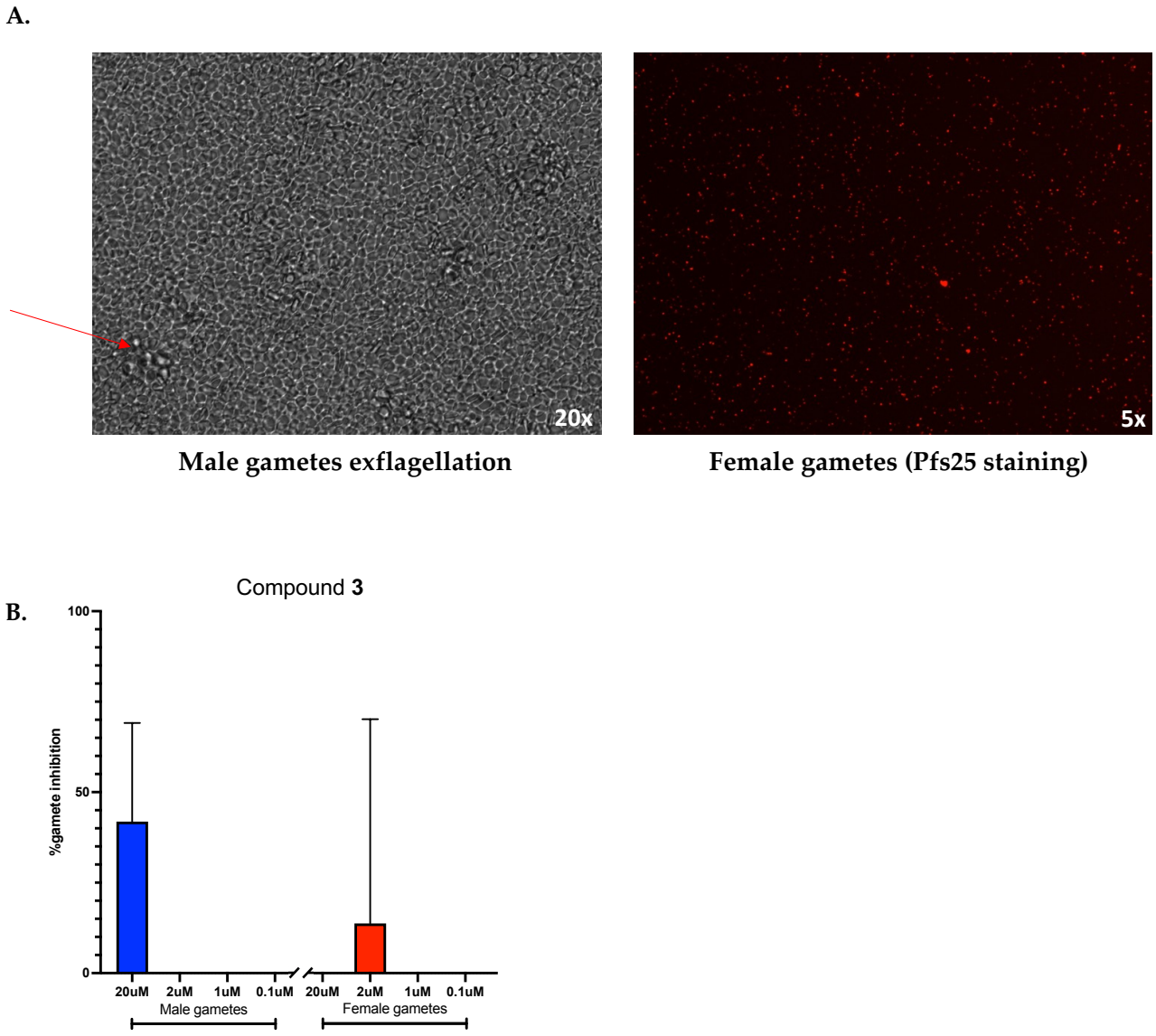


**Figure S3.** DGFA of compound **3. A**) Screenshots of male gamete exflagellation points and female gametes stained with Pfs25. **B**) Bar plots indicate the male (blue) and female (red)

gamete inhibition (%) after 48h of exposure of mature gametocytes to compound **3**. Error bars show the standard error of the mean based on at least three independent repeats.

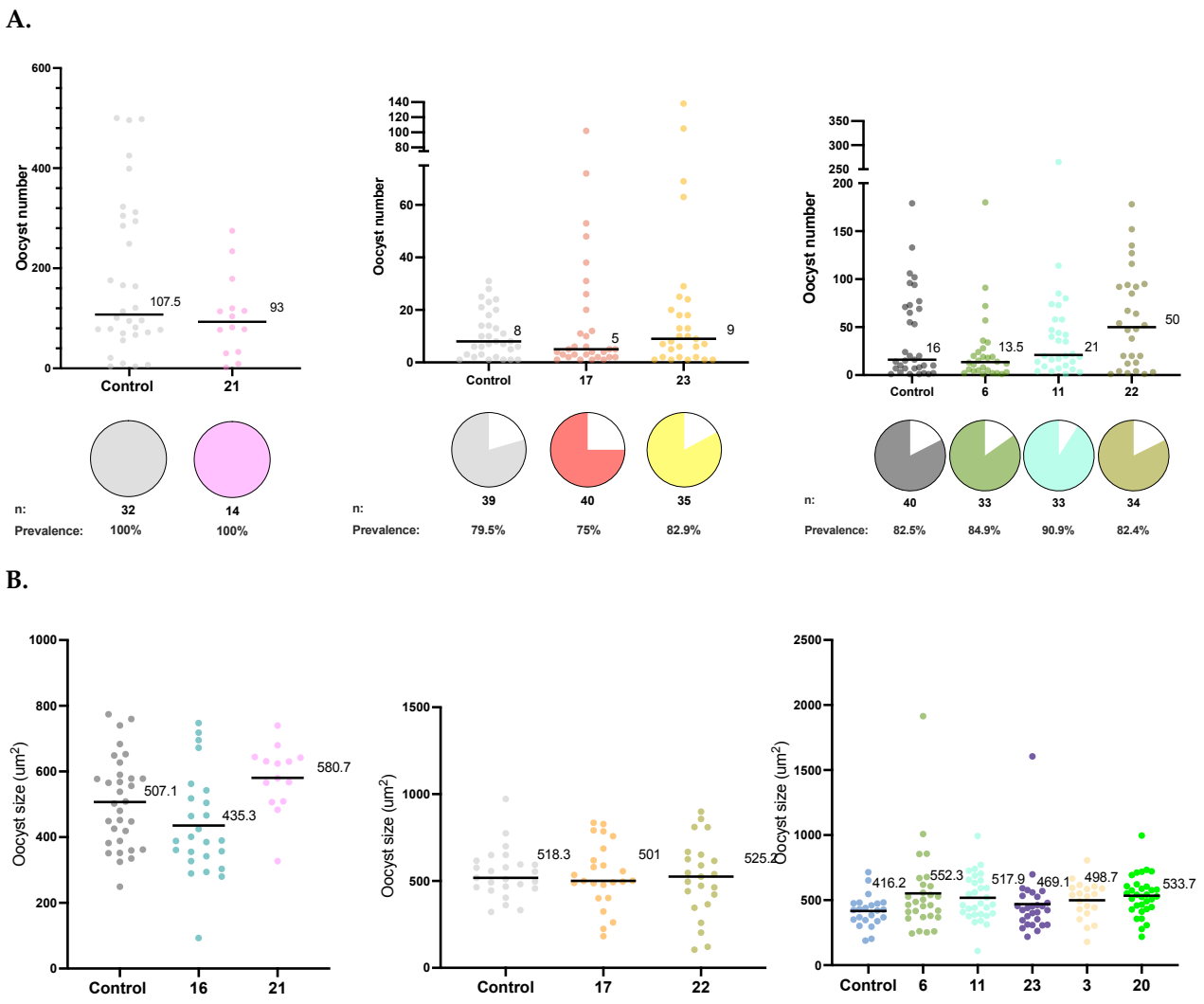


**Figure S4.** Topical exposure results. Compounds activity indicated as oocyst intensity (**A**), oocyst prevalence (**B**) for compounds **6**, **11**, **17**, **21-23** and oocyst size (**B**) for compounds **3**, **6**, **11**, **16**, **17, 20-23** after one single experiment. Median lines and values are indicated, "n" indicates the number of independent samples. Mean lines are indicated for oocyst size. To isolate oocyst prevalence and oocyst intensity, midgut samples with zero oocysts have been excluded from intensity analysis. Statistical significance is indicated where relevant as follows: * = p<0.05, ** = p<0.01, *** = p<0.001, **** = p<0.0001. Control: acetone or DMSO in acetone (0.5% v/v).

# LIST OF PUBLICATIONS AND CONFERENCES

Works published during PhD candidature, relating to this thesis:

1. Consalvi, S.; Tammaro, C.; **Appetecchia, F.**; Biava, M.; Poce, G. Malaria Transmission Blocking Compounds: A Patent Review. *Expert Opinion on Therapeutic Patents* **2022**, 32 (6), 649–666. https://doi.org/10.1080/13543776.2022.2049239.
2. **Appetecchia, F.**; Consalvi, S.; Berrino, E.; Gallorini, M.; Granese, A.; Campestre, C.; Carradori, S.; Biava, M.; Poce, G. A Novel Class of Dual-Acting DCH-Corms Counteracts Oxidative Stress-Induced Inflammation in Human Primary Tenocytes. *Antioxidants* **2021**, 10 (11), 1828. https://doi.org/10.3390/antiox10111828.

Works published or submitted during PhD candidature, unrelated to this thesis:

1. **Appetecchia, F.**; Consalvi, S.; Scarpecci, C.; Biava, M.; Poce, G. SAR Analysis of Small Molecules Interfering with Energy-Metabolism in Mycobacterium Tuberculosis. *Pharmaceuticals* **2020**, 13 (9), 227. https://doi.org/10.3390/ph13090227.
2. **Appetecchia, F.**; Biava, M.; Poce, G. Natural Flavonoid and Chalcone Scaffolds as Leads for Synthetic Antitubercular Agents; *Medicinal Chemistry: Lessons from Nature*; submitted in Medicinal Chemistry Lessons from Nature; Vol. 1.

Conferences actively attended during PhD candidature:

- Poster:

  **Appetecchia**, **F.**; Paton, D.; Probst, A; De Vries, L; Tammaro, C; Consalvi, S; Wirth, F. D.; Catteruccia, F; Poce, G. Novel pyrazole- and pyrrole- based compounds active against multiple stages of *P.falciparum*. Poster presentation presented at *3rd MMCS: Shaping Medicinal Chemistry for the New Decade*; July **2022**; Rome, Italy.

- Presentation:

**Appetecchia, F.** Development of targeted transmission-blocking agents against malaria. Presented at *Terzo workshop sulla Ricerca*; June **2022**; Dip. Chimica e Tecnologie del Farmaco - La Sapienza Università di Roma; Rome, Italy.